

**QUANTITATIVE CHEMICAL HYPERSPECTRAL NEAR-INFRARED IMAGING
OF HISTORICAL CELLULOSIC MATERIALS**

Hend MAHGOUB

A thesis submitted in partial fulfilment
of the requirements for the degree of
Doctor of Philosophy
of
University College London

UCL Institute for Sustainable Heritage
University College London

30th September 2019

I, *Hend Mahgoub*, confirm that the work presented in this thesis is my own. Where information has been derived from other sources, I confirm that this has been indicated in the thesis.

ACKNOWLEDGEMENTS

Firstly, I would like to thank God for his blessings and exceptional love and for giving me the strength and knowledge, especially during challenging moments to undertake this research and complete the thesis.

I am indebted to so many individuals for being part of my PhD journey. Without their inspiration and support, it would not be possible to achieve such a moment. Thus, I would like to thank all of those wonderful people.

My sincerest thanks and deepest gratitude are extended to my principal supervisor and mentor, Professor Matija Strlič (UCL Institute for Sustainable Heritage), for the great experience he gave to me during the research time. Without his encouragement, invaluable support, continuous guidance and enthusiasm, this research would not be completed. I am also hugely appreciative to Professor Tom Fearn (UCL Department of Statistical Science), not only for being dedicated to his role as my secondary supervisor, but also for his exceptional support, sharing his time and expertise in statistics so willingly.

The Engineering and Physical Sciences Research Council (EPSRC) and the H2020 European project 'NanoRestART' are acknowledged for their financial support and investment in the research. UCL Institute for Sustainable Heritage (ISH) and EPSRC Centre for Doctoral Training in Science and Engineering in Arts, Heritage and Archaeology (SEAHA) are also acknowledged for their administrative support, easing all the logistics and promptly responding to all requests.

I also want to express my gratitude to all my heritage and industrial partners and the individuals that were involved in the supervision of this PhD: Dr. Marta Oriola Folch (Faculty of fine Arts, University of Barcelona, Spain), Dr. Katrien Keune (the Rijksmuseum, Amsterdam), Dr. Manfred Anders (ZFB GmbH – Zentrum für Bucherhaltung GmbH, Germany), and Dr. John R. Gilchrist (Camlin Photonics Ltd., UK). It was really great meeting and working with you and being in receipt of your invaluable contributions during my PhD research.

Special mention goes to Dr. Irena Cigić (Faculty of Chemistry and Chemical Technology, University of Ljubljana) for her great contribution and help in all the accelerated degradation experiments done during the research.

Thanks also go to Dr. Fenella France (Library of Congress, Washington, D.C.) for her interest and valuable feedback on the research during my upgrade. In addition to her help in the degradation experiments.

My gratitude goes to Gildden Photonics Ltd., University of Barcelona (Faculty of fine Arts, Department of Arts, Conservation and Restoration), and the Rijksmuesum teams for their support and great hospitality during the time I spent there for either training or field work.

I am also grateful to Museu Nacional d'Art de Catalunya for giving me the opportunity to access the reference collection of canvas samples that were lent from University of Barcelona.

I would like to show my appreciation to all 'NanoRestART' project partners for sharing their expertise, and for providing valuable information throughout this research.

I express my warmest gratitude to Stefania Signorello from the Wellcome Collection in London and her team for their collaboration and making it possible to access the Wellcome collection and carry out the Islamic paper survey which has been a valuable input for this thesis.

Similarly, I am thankful to Maria Ragan and Louise Bascombe from the UCL Petrie museum for giving me the opportunity to access the papyri collection and conducting my papyri study that has immensely influenced this research.

It is a pleasure to thank all my colleagues, visiting students and staff (Katherine Curran, Josep Grau-Bove, Miriam Wright and Mark Underhill) at the Heritage Science laboratory, UCL for their friendship and support and for the cordial working environment, positive experience gained and wonderful time spent during the thesis work.

I am deeply thankful for the friends and people I met and got to know in London who gave me a great time and the necessary support making my stay in London memorable.

I cannot begin to express my gratitude to my family and friends everywhere for all of the love, support, encouragement and prayers they have sent my way along this journey. To all of them, thank you for believing in me and providing help whenever needed, I hope that I have made you proud. To my lovely daughter Aalyah and my charming son Ali, it was great having you during the time of my PhD, you are my inspiration to achieve greatness.

Finally, I would like to thank my husband and life partner, Ibrahim El-Rifai for being there for me at the end of the day. Your love and patience is what has gotten me through when I wanted to give up. Without you, I would not be where I am today. I am forever thankful to you and I dedicate this thesis to you.

ABSTRACT

Hyperspectral imaging in the visible and near infrared (VNIR) regions is slowly becoming routine process in the documentation and characterization of historic surfaces. The VNIR spectral region contains colour information and limited chemical information. Conversely, the spectral region further in the NIR (short-wavelength IR, SWIR) is much less explored although suitable hyperspectral cameras exist. The first quantitative application in heritage science was published in 2011. Due to the complexity of NIR data hypercubes where the spectra holds thousands of C-H, O-H and N-H molecular bonds representing the chemical and physical features of the investigated object in addition to their spatial distribution, multivariate data analysis methods are required to extract qualitative and quantitative information such as acidity and molecular weight from a historical object e.g. document or canvas, which are important indicators of its state (condition). Using imaging to document the spatial distribution of an object's chemical composition and condition is therefore possible, however, significant research work is still necessary to understand how the measurement conditions (lighting spectral distribution and intensity, concentrations of the imaged component, calibration) as well as the stability of calibrations over time, affect the analytical outcome.

This project will explore analytical robustness of quantitative chemical imaging as well as studying two specific areas of application from the historical cellulosic materials: Islamic paper (distribution of sizing and polishing components, acidity, and cellulose degree of polymerization - DP) and painting canvases (distribution of acidity and cellulose DP). This aims to provide a better understanding of degradation processes and provide a measure of change in collections through imaging which will reflect on the management and preservation plans of collections. Another area of application from the historical cellulosic materials: Papyri will also be explored by investigating the effect of imaging through glass on the accuracy of the acquired data from the spatial and spectral perspectives in addition to the extraction of chemical information that could be used to enrich our scientific knowledge about papyri.

Moreover, the degradation behaviour of the historical materials under investigation, exploring their degradation rate and study their stability is investigated with the aid of accelerated degradation in controlled conditions allowing for the study of different scenarios of storage environment conditions leading to better preservation decisions.

The PhD project is a collaboration between researchers with a strong experience in collections research; University College London, Rijksmuseum, University of Barcelona, ZFB GmbH, and Gilden Photonics Ltd, in addition to being a part of the H2020 Nanorestart project.

IMPACT STATEMENT

The research aims to have significant impact on heritage institutions housing cellulosic collections and on heritage scientists interested in applying new techniques in the field of cultural heritage by providing new knowledge and its interpretation from the conservation perspective.

One of the impacts of this research lies in a deeper understanding of the material properties of Islamic paper and its effect on the paper stability compared to the European paper. This was the first experimental systematic study on Islamic paper showing the need for more materials science research as the available literature abounds with inconsistencies and our knowledge of the history of papermaking in Islamic countries is based on assumptions and little to no evidence. The results of the study show the potential of the use of NIR spectroscopy and quantitative imaging to study and survey Islamic paper collections and emphasize the role of scientific analysis and non-destructive methods to complement historical and textual analysis. Such comprehensive investigations of the paper materials largely advanced the research in heritage materials.

Moreover, the research provides a new condition assessment tool for the investigation of painting canvas through NIR quantitative imaging, resulting in chemical and lifetime maps for canvases for the first time visualizing the variability of its material state. Also, it provides a new knowledge about the degradation behaviour of historical painting canvases allowing for the study of different scenarios of storage environment conditions thus better preservation decisions. As part of the H2020 European project 'NanoRestART' with more than 27 partners investigating Nano-materials for the restoration of artworks, the new gained knowledge about canvases and the developed assessment tool were fed directly in one of the work packages of the project to aid in the evaluation of the efficiency of the new developed de-acidification treatments.

Another impact lies in the proposed study of papyri which opens new opportunities to study papyri collections that never have been subject to scholarly or scientific study (maybe due to their state of preservation or accessibility) by exploring the potential of spectral imaging through glass and prediction modelling for the purpose of enhanced conservation and research.

The research is also opening new horizons and challenges for quantitative imaging in heritage science by studying the metrology of quantitative chemical mapping based on hyperspectral imaging which is already an active area of research. Exploring the benefits and limitations of the technique and its analytical robustness of cellulosic heritage materials focusing on study the effect of measurement parameters, will encourage heritage and imaging scientists to extend the use the technique in the field and conduct further investigations to solve any issues highlighted by the research.

The collaboration conducted through the research with the three heritage institutions: The Wellcome Collection, the Petrie Museum and the Rijksmuseum demonstrates the research's direct impact where the developed methodologies and techniques were applied to heritage collections in situ. Moreover, the new gained knowledge about the different materials and their degradation behaviour was communicated with the researchers and conservators in addition to the potential and capabilities of the quantitative hyperspectral imaging in the short wavelength region as a new technology in the field of cultural heritage.

TABLE OF CONTENTS

LIST OF TABLES	15
LIST OF FIGURES.....	18
LIST OF ABBREVIATIONS	27
1. INTRODUCTION	29
2. CELLULOSIC MATERIALS: Background and Development	35
2.1 Islamic Paper	36
2.2 Painting Canvas.....	41
2.3 Papyrus.....	43
2.4 Classical Characterization Methods	45
2.4.1 Sizing Characterization of Islamic Paper	45
2.4.2 Surface Characterization of Islamic Paper.....	46
2.4.3 Acidity	46
2.4.4 Degree of Polymerization	47
2.5 Degradation Processes in Cellulosic Materials.....	48
3. HYPERSPECTRAL IMAGING: Characterization and Robustness	55
3.1 Background.....	55
3.2 Hyperspectral Imaging (HSI) System: Current System.....	61
3.3 Near-Infrared Spectroscopy	65
3.4 Data Analysis Techniques.....	66
3.4.1 Classification Models.....	66
3.4.2 Regression Models.....	67
3.5 System Performance and Calibration: HSI Robustness	67
3.5.1 Detector Dead Pixels.....	68
3.5.2 Radiometric Reflectance Calibration.....	69
3.5.3 Spatial Performance.....	70
3.5.4 Spectral Performance.....	73
3.5.5 Illumination	80
3.6 Discussion	84
4. HISTORIC ISLAMIC PAPER.....	87
4.1 Islamic Paper Survey	88
4.1.1 Characterization of the Reference Collection.....	88
4.1.1.1 Morphology	89
4.1.1.2 Sizing	91
4.1.1.3 Surface Characterization: Polishing.....	91
4.1.1.4 Fibre Furnish.....	94

4.1.1.5	Acidity and Degree of Polymerization	94
4.1.2	Discussion and Conclusions of the Survey	96
4.2	Effect of Starch Sizing	98
4.3	Non-Destructive Characterization Methodology	101
4.3.1	Handheld Portable VIS-NIR Spectroscopy Analysis.....	103
4.3.1.1	Presence of Starch and Polishing	103
4.3.1.2	Determination of pH and DP	104
4.3.1.3	Wellcome Collection Survey	106
4.3.1.3.1.	Wellcome Collection Objects.....	106
4.3.1.3.2.	Spectral Data	106
4.3.1.3.3.	Survey Results.....	107
4.3.1.3.4.	Conclusions of the Survey	113
4.3.2	HSI Spectral Analysis	113
4.3.2.1	Sample Selection.....	116
4.3.2.2	Data Analysis: Calibration Models	117
4.3.2.3	Quantitative Near-Infrared Chemical Mapping	121
4.4	Evaluation Methodology: Effect of Acquisition Parameters on Calibration	125
4.5	Degradation Study.....	128
4.6	Summary.....	137
5.	PAINTING CANVAS.....	139
5.1	Reference Collection	140
5.2	Spectral Analysis: Condition Assessment Tool.....	141
5.2.1	Spot Analysis: NIR Regression Models.....	141
5.2.1.1	Acidity (pH).....	141
5.2.1.2	Degree of Polymerization (DP)	143
5.2.1.3	Predictions for Real Paintings.....	144
5.2.2	HSI Analysis: NIR Regression Models	145
5.2.2.1	Sample Selection.....	145
5.2.2.2	Calibration models: pH and DP.....	146
5.2.3	Near-Infrared Chemical Mapping	148
5.3	Canvas Degradation Study.....	152
5.4	Summary of Results	159
6.	PAPYRI	161

6.1	Scanning through Glass.....	161
6.2	Qualitative Evaluation	166
6.3	Quantitative Aspect (A Trial Study)	174
6.4	Summary of Results.....	184
7.	CONCLUSIONS	187
7.1	Research Questions and Contribution to New Knowledge	187
7.2	Future Work	191
7.3	Dissemination	192
	REFERENCES.....	193
	APPENDICES.....	211
	<i>Appendix I: Islamic Paper Reference Collection: Calibration Target / ISH Collection</i>	211
	<i>Appendix II: Painting Canvases Reference Collection: Calibration Target.....</i>	217
	<i>Appendix III: HSI Penetration Experiment.....</i>	221
	<i>Appendix IV: UCL-ISH Painting Canvases Collection (10 Oil Paintings)</i>	223

LIST OF TABLES

Table 2-1. The 105 Islamic paper calibration target samples, showing the distribution of samples containing starch (samples with yellow cells). Grey slots are without samples. 40	
Table 2-2. Results from the characterization of UCL-ISH painting samples showing the fibres, pH and cellulose DP values of the 10 paintings.....42	42
Table 2-3. The different conditions of the accelerated degradation experiments applied to Islamic paper and canvases samples. The table showing combinations of temperature and relative humidity conditions, the total experiment duration for each material and sampling rate. In addition to experiments' locations and chamber types information.....53	53
Table 3-1. Main specifications of the used HSI system provided by the manufacturer. ..62	62
Table 3-2. Hyperspectral imaging system acquisition parameters used in the research. 62	62
Table 3-3. Main characteristic peaks in two wavelength standard targets (Spectralon and Zenith) provided by the manufacturer. The peaks are shown in nm.76	76
Table 3-4. The main peaks from the average spectra of the Spectralon standard collected using the HSI system and NIR LabSpec-5000 spectrometer corresponding to the provided data from the manufacturer.....78	78
Table 3-5. Acquisition parameters of HSI system used in the experiments of this section.80	80
Table 3-6. Lux measurements collected using GL Spectis 1.0 Touch from 9 positions over the HSI scanning stage. M1, M2 and M3 represent three measurements per position. Average (Avg), standard deviation (SD) and relative standard deviation (RSD) are calculated for each position and overall the stage.....82	82
Table 3-7. Distribution of the average lux values per each position on the HSI scanning stage in addition to the average lux over the white tile (appears in blue).....83	83
Table 4-1. Summary of the characterization techniques used in the Islamic paper survey, with the corresponding number of samples. The numbers differ for each technique for different reasons; no enough samples for DP determination analysis (as it requires big amount of samples ~ 20-30 mg) or available data is enough for calibration to support a hypothesis as in the case of pH analysis. All of the available samples were analysed for the presence of starch and polishing.....89	89
Table 4-2. The frequency of sheet-forming techniques for paper samples in the ref-collection.....91	91
Table 4-3. List of 15 samples from the ref-collection and their properties (starch-sized, polished surface, written text and type of paper (identified visually based on mould features and alignment of the fibres (Cornell University Library 2005)) that were selected randomly for the fibre furnish analysis.94	94
Table 4-4. Validation matrices for LDA models for identification of starch and polishing. 138 and 74 samples were used for calibration, respectively.....104	104

Table 4-5. Specifications (calibration and validation parameters) of PLS regression models for pH and DP using NIR spectra obtained with the PHAZIR hand-held spectrometer; <i>n</i> – number of samples.	104
Table 4-6. Estimated properties of the surveyed papers from the Wellcome Islamic collection: probability of the presence of starch (%starch), probability of the presence of polished surfaces (%polishing), predicted average degree of polymerization (DP) and predicted average pH with the standard deviation (\pm). Colour shading indicates a positive ID for starch and polishing. If both are present, the paper has been classified as Islamic paper.	109
Table 4-7. Specifications of the PLS models for dating; <i>n</i> – number of samples, RMSEC – calibration error, RMSECV – validation error, and R^2 – correlation coefficient.	112
Table 4-8. Acquisition parameters of HSI system used in the experiments of this section.	114
Table 4-9. Validation matrices for PCDA and PLSDA models for identification of starch and polishing using leave-one-out cross validation (LOOCV) method. Cross validated (CV) success rate for the different classes and the total are shown.	119
Table 4-10. PLS regression model results for determination of DP using spectral measurements of the IP target collected by the HSI system with two different backgrounds (99% diffuse reflectance Spectralon and Whatman paper) and without any backgrounds (plastic stage). The calculations were done using different pre-treatment methods for the collected spectra in the range 1450 – 2350 nm to avoid noisy edges.	126
Table 4-11. PCDA model results for identification of starch presence using HSI data of IP target collected by two different lenses (30 and 56 mm). The calculations were done based on an average spectrum of two different ROI sizes (3x3 and 5x5 pixels) from each sample in the target. Measurements were collected in the range 1450 – 2350 nm with Whatman paper as background and pre-treated using SNV method.	127
Table 4-12. Different conditions of the accelerated degradation experiments conducted using Islamic paper samples to assess its degradation behaviour. The table shows the selected samples for each experiment with its properties (pH, DP) and whether the sample is starched or polished.	128
Table 4-13. Rate constants ($k - \text{day}^{-1}$) for the degraded samples and the corresponding correlation coefficients (R^2) of linear fit for the paper samples used in the study. The samples are categorized by colour representing: starched and polished (orange), neither starched nor polished (red), starched but not polished (green) and not starched but polished (blue).	134
Table 5-1. Specifications of PLS regression models for determination of pH and DP of cellulose in canvases based on spectral measurements of ~ 70 historic samples using HSI system.	147

Table 5-2. Calculated Rate constant ($k - \text{day}^{-1}$) of the accelerated degraded samples (90 °C - 70% RH, 70 °C - 30% RH and 50 °C - 50% RH) and the corresponding correlation coefficients (R^2) values of linear fit of the Ekenstam equation on 10 historic painting canvases from UCL-ISH collection.....	154
Table 6-1. Acquisition parameters of the scanning experiment.	162
Table 6-2. Root mean square errors of cross-validation (RMSECV) resulting from the developed PLS models for the determination of DP of cellulose in paper. The Leave-one-out cross-validation method was used. The models were developed based on the spectral data of the HSI scans of IP calibration target without and with glass (~ 2 mm thickness) taking into account its involvement in the calibration process while scanning. Different pre-processing methods were used to clean the spectra from any noise. The table also shows the correlation and number of factors selected to generate the optimal results for each model.....	165
Table 6-3. Prediction errors and its correlation resulted from validating the developed regression PLS model for determination of cellulose DP in paper. The model is based on the spectral data of IP target samples without glass. Spectral data of same samples but scanned with glass were used as a validation set.	166
Table 6-4. Details of 62 objects from the papyrus collection of Petrie museum showing the ID, dimensions, language and date for each object.....	166
Table 6-5. Hyperspectral imaging system acquisition parameters used in the survey. .	169
Table 6-6. Specifications of two PLS regression models developed for the determination of cellulose DP in Islamic paper based on the spectral data of the Islamic paper calibration target samples collected by HSI system.....	177

LIST OF FIGURES

Figure 2-1. Application of sizing (left and middle) and polishing (right) techniques on paper. © (left) http://precious-piece.com/?page_id=2358 , © (right and middle) http://www.hussainpapers.co.in/gallery.htm	37
Figure 2-2. Two objects in the historic reference material collection at UCL-ISH (<i>Left</i> : AP 85, <i>right</i> : AP 53)	38
Figure 2-3. Calibration target with 105 characterized samples of Islamic paper (Front and back sides).	40
Figure 2-4. Structure of an easel painting. © Dominguez Rubio, 2014.....	41
Figure 2-5. Reference collection samples from a prior study conducted in 2011 (Oriola et al., 2011; Oriola, 2011) (left) and one object (P10) from UCL-ISH painting collection (right).	43
Figure 2-6. Calibration target with 72 well-characterized samples of painting canvases (16 th – 20 th C.).....	43
Figure 2-7. Some objects from the collection at the Petrie museum that were examined in the research.	45
Figure 2-8. pH meter during calibration and measurement processes.	47
Figure 2-9. DP measurement experiment of canvas samples, showing the special preparation process needed for the samples due to the heavy glue and paints.	48
Figure 2-10. Some of the Islamic paper and canvases samples during one of the accelerated degradation experiments.	53
Figure 3-1. Gilden Photonics hyperspectral imaging system (Translational setup); Top: HSI system in situ and its components; 1: SWIR Camera, 2: Mirror system, 3: Halogen Light source, 4: Spectralon 99% calibration standard, 5: Scanning stage, 6: PC. Bottom: Diagram of the HSI system showing the scanning pipeline and system components.....	63
Figure 3-2. Diagram shows the different acquisition parameters required to calculate the scanning speed of the HSI system.	64
Figure 3-3. Sensor frame image (left) and same image after applying a threshold (right) identify some dead pixels. The image size is 320 (scan line) x 256 (bands).	69
Figure 3-4. Reflectance spectra collected in the column 303 out of 320 of the scanning line demonstrating the effect of the dead pixel on spectra. The spike at around 2077 nm (band number 183) represents the position of the detected dead pixel. The figure shows the spectra before (blue) and after (red) removal of the dead pixel response by replacing it with the average response from its surrounding neighbours.	69
Figure 3-5. The painted test panel target from Vitorino's work (2014) showing the line patterns used as resolution target.....	71
Figure 3-6. A grey image at 1486 nm for part of the test panel (resolution target from Vitorino's work (2014)) scanned with the HSI system using the 56 mm lens.....	72

Figure 3-7. Visual assessment of how well the details of the line patterns of the resolution target (Vitorino’s test panel (2014)) can be resolved to assess the spatial resolution of the HSI system. The figure shows two grey images at 1240 nm scanned using the HSI system by 30 mm lens (top) and 56 mm lens (bottom). The green and red rectangles represent selected areas of a scale of 2 mm of the watercolour line patterns.72

Figure 3-8. Plots of vertical profiles of watercolor lines (2 mm) from the resolution target (Vitorino’s test panel (2014) – red and green rectangles in Figure 3-7) to assess the spatial resolution of the HSI system using two lenses 30 mm (top) and 56 mm (bottom).73

Figure 3-9. A grey image (1404 nm) for the wavelength standard targets (Spectralon (top left) and Zenith (bottom)) scanned with the HSI system using the 56-mm lens. The 99% diffuse reflectance Fluorilon standard from Avian Technologies LLC (top right) was scanned as well.76

Figure 3-10. The average spectra of the two wavelength standard targets; Zenith (top) and Spectralon (bottom) scanned with the HSI system demonstrating the main characteristic peaks in both spectra. The red boxes show the characteristic relative to the provided manufacturer peaks shown in Table 3-3.77

Figure 3-11. Comparison between an average reflectance spectrum of Zenith standard scanned with the HSI system (Gilden in blue) and the provided spectra from the manufacturer (in orange).78

Figure 3-12. Comparison between average reflectance spectra of Spectralon target collected by the NIR LabSpec-5000 spectrometer and the HSI system.78

Figure 3-13. Three mean reflectance spectra of data collected from the IP calibration target using the HSI system in addition to their standard deviation to visualize any variability in the measurements.79

Figure 3-14. Average reflectance spectra and its difference, collected from the Islamic paper target using HSI scanner using different acquisition parameters; two illumination intensities: 250 and 500 W to spot any differences.81

Figure 3-15. Design of the scanning Stage divided into 9 positions using A3 paper (right) and scanning of the Spectralon multi-component wavelength standard in position 5 (left).82

Figure 3-16. Collection of lux measurements using a light meter (GL Spectics 1.0 Touch) over the HSI scanning stage from different positions (right). Live view from the HSI software showing the meter sensor to verify its location on the stage (right).82

Figure 3-17. Comparison between 9 average reflectance spectra of Spectralon multi-component wavelength target collected using the HSI system after placing it in 9 different positions over the scanning stage. The standard deviation (SD) shows the variations between the spectra from one position to another.84

Figure 4-1. Example of Zig-zag indentation (AP 37) in diagonal lines from the sheet’s head to tail. Visible image (left), back-lighting image (middle) with the indentation illustration, selected area (right).....	90
Figure 4-2. Example of the strengthening technique observed in two samples (AP 44, AP 97) from the ref-collection involving two sheets being glued together on their unpolished sides (known as Waṣṣālī method).	90
Figure 4-3. Example of the triple-crescent watermark found in the samples, that was used for papers exported from European paper mills to Islamic countries.	90
Figure 4-4. Box plot of 20 values of the specular vs. diffuse reflectance ratio at 457 nm calculated from the spectral measurements collected from Islamic paper samples using LabSpec-5000 spectrometer. The “Polished” and “Unpolished” categories were determined visually. Each box shows the distribution of the measurements based on the median, 1 st and 3 rd quartile. The whiskers represent minimum and maximum values.	92
Figure 4-5. SEM images (×100) of an unpolished sample (left, AP 127-1) and a polished sample (right, AP 110).....	93
Figure 4-6. Frequency plots for pH ($n = 70$) and DP ($n = 60$) of Islamic paper samples in the ref-collection.	96
Figure 4-7. Boxplots for pH ($n = 70$) and DP ($n = 60$) showing the 1 st and 3 rd quartile, the median and minimum and maximum values (whiskers) for categories with identified polishing (P), starch (S) or not (0).....	96
Figure 4-8. Two biplots from the correlation analysis using PCA of four paper characteristics for 40 samples from the Islamic paper ref-collection to study the effect of the different techniques on paper stability. The left and bottom axes are of the PCA plot showing the scores of the samples (dots) while the top and right axes belong to the loadings plot which shows how strongly each characteristic (vectors) affect the principle components. On the right, the biplot shows the analysis of the initial values of DP and pH with the starch-presence and polishing characteristics. On the left, the biplot shows the correlation between pH, polished surfaces, starch-presence and % DP loss characteristics. % DP Loss is calculated from the initial DP values and the DP measured after ageing the samples (at 80 °C and 65% RH for two weeks). The two figures show the PCA scores of PC1 vs PC2 categorized according to starch-sizing property (Starched samples in blue and unstarched samples in red).	99
Figure 4-9. Scatter plot representing the DP measurements of Whatman samples (1 st X-axis on top) before (0 days) and after degradation at 80 °C and 65% RH for 3 weeks (21 days) and 2 months (60 days). A correction factor for the sample mass due to the addition of starch was used. The full square points show the standard deviation per degradation period (2 nd X-axis on bottom), taking the average value of DP for all the samples (after correction) degraded for 21 and 60 days.	101

Figure 4-10. Degradation rates of the reference sample with no starch and sample no. 1 with the least amount of starch (1 immersion). The error bars represent standard deviations for duplicate DP determinations. 101

Figure 4-11. Comparisons of predicted and actual pH and DP values obtained with models developed specifically for Islamic paper (IP, above) and with models developed for European paper (SurveNIR, below). Hollow squares samples with starch, black squares no starch. R^2 was calculated for each set of data. 105

Figure 4-12. Collection of spectral data using PHAZIR handheld NIR instrument (Polychromix) in the interval 1600 – 2400 nm from the Wellcome Library Islamic collection. 107

Figure 4-13. Boxplots of the distribution of the pH (left) and DP (right) values predicted for samples (43 objects) of the Wellcome Islamic collection as a measure of stability using a non-destructive characterization methodology based on NIR spectroscopy. Values are grouped according to the two main characteristics of Islamic papermaking; starch-sizing and surface polishing which have been also estimated using same methodology. (0) means samples with no starch/unpolished, (S) means samples are starch-sized and (P) means samples are polished. Each box shows the distribution of the measurements based on the median, 1st and 3rd quartile. The whiskers represent minimum and maximum values. 111

Figure 4-14. Validation of two dating models developed based on spectral data collected from Wellcome Collection samples using NIR spectroscopy (Table 4-6). The blue dots in both plots represent paper samples with (right) and without starch (left). The figure shows the correlation coefficient between the actual and predicted date for both models. 113

Figure 4-15. Distributions of pH (left) and DP (right) of the Islamic paper target samples. 115

Figure 4-16. Pixel selection process: left: the area from where samples are extracted; middle: average image of the calibration target calculated over the spectral dimension for each pixel, following which a threshold was applied (default 0.4); right: minimum average value (black) assigned to the holder pixels, maximum values (white) representing the sample pixels, and the position of selected ROI (3x3 pixels) of each sample (blue). 116

Figure 4-17. Reflectance spectra of 105 samples collected by the HSI system in the spectral range 1000 – 2500 nm from the calibration target. These samples were for subsequent calibration. 117

Figure 4-18. Weighted PCA loading vectors based on LDA coefficients, indicating the wavelengths with the highest contribution (1600–1950 nm) to the starch discrimination model developed for Islamic paper using HSI system. 118

Figure 4-19. The results of the developed PLS regression model for the determination of pH using spectral measurements of 68 samples scanned by the HSI system. 120

Figure 4-20. The results of the developed PLS regression model for the determination of DP of cellulose in paper using 57 Islamic paper samples with an RMSECV= 285 DP units and correlation coefficient $R_{cv}=0.77$ using 13 factors. The plot correlates predicted with actual DP measurements.	121
Figure 4-21. Chemical maps of the distribution of DP and pH values of selected area of some examples of Islamic paper samples from the ref-collection (Islamic paper survey) (AP 44, AP 35, AP 57, AP 127-1), estimated based on the developed calibration models of HSI system. The figure shows the visible image with the selected area (red rectangle) and that area at 1932.7 nm. In addition to the average image with ink pixels excluded and the actual and average estimated DP and pH values for each sample.	124
Figure 4-22. Average reflectance spectra and its difference, collected from the IP target by the HSI scanner using different lenses: 30 and 56 mm to visualize the variability in the measurements.....	127
Figure 4-23. Linear fits as per the Ekenstam equation, for Islamic paper samples degraded at different conditions as follows (90 °C - 70% RH, 80 °C - 50% RH, 70 °C - 30% RH, 60 °C - 70% RH and 50 °C - 50% RH for 4, 8, 12, 8 weeks and 8 months respectively). DP_0 is the initial degree of polymerization of cellulose and DP_t is at time t.	133
Figure 4-24. Comparison of degradation rates as measured and as predicted for Islamic paper samples and paper samples as reported by Strlič et al. (2015), represented by empty symbols. $\ln(k)$ is the natural logarithm of the degradation rate. In the bottom figure, the solid symbols are coloured according to Islamic paper properties (starch-sizing and polishing); starched and polished (orange), neither starched nor polished (red), starched but not polished (green) and not starched but polished (blue).	135
Figure 4-25. Demographic plots for the surveyed Wellcome collection objects at the standard environmental conditions (18 °C, 56% RH) (left) as well as another hypothetic scenario at 35 °C, 56% RH (right).....	136
Figure 5-1. Hyperspectral Imaging Scanner	140
Figure 5-2. Reflectance spectra of 142 historic canvas samples collected by LabSpec-5000 Spectrometer in the spectral range 1000 – 2500 nm. Samples were used to develop PLS regression model to determine pH of unknown canvases. Blue shades lines show the spectra of calibration dataset while red lines represent validation dataset.	142
Figure 5-3. The results of the developed PLS regression model; calibration (Left) and validation (Right) for the determination of pH in painting canvas using spectral measurements of 142 historic samples collected by LabSpec-5000 spectrometer. The plot correlates predicted with actual pH measurements.....	143
Figure 5-4. The results of the developed PLS regression model; calibration (Left) and validation (Right) for the determination of DP of cellulose in painting canvas using ~90 historic samples based on their spectral measurements from the Spectrometer. The plot correlates predicted with actual DP measurements.	143

Figure 5-5. Absorbance spectra of 89 historic canvas samples collected by LabSpec-5000 Spectrometer in the spectral range 1000 – 2500 nm. Samples were used to develop PLS regression model to determine DP of cellulose in canvases. Blue shades lines show the spectra of calibration dataset while red lines represent validation dataset..... 144

Figure 5-6. The results of the pH and DP predictions for two painting canvases; P8 (left, bottom) and P9 (right, bottom) from the UCL-ISH collection based on the developed regression calibration models. Yellow dots representing the different selected positions for the spectral measurements. The top row shows the front side of the two paintings; P8 (left, top) and P9 (right, top)..... 145

Figure 5-7. Reflectance spectra measurements of two paintings (P8 and P9) with and without background (BG) collected by LabSpec-5000 spectrometer to investigate its effect on the spectra. 145

Figure 5-8. An image at 1932 nm resulting from a scan of the canvas calibration target using the HSI system. The red points are showing the manually selected position from each sample to collect average representative spectra (3x3 ROI) from the historic samples to build the quantitative calibration models to determine pH and DP of cellulose in canvas. 146

Figure 5-9. Reflectance spectra of 72 historic canvas samples collected by HSI system in the spectral range 1000 – 2500 nm. Samples were used to develop PLS regression models to determine cellulose DP and pH of unknown canvases. Blue shades lines show the spectra of calibration dataset while red lines represent validation dataset..... 147

Figure 5-10. The results of the developed PLS regression models for the determination of DP of cellulose (bottom) and pH (top) using spectral measurements of ~ 70 canvas samples scanned by the HSI system. The plot correlates predicted with actual values. 148

Figure 5-11. Chemical maps of the distribution of DP and pH values of selected areas of some examples of historic canvas paintings from the UCL-ISH collection (P6, P7), estimated based on the developed calibration models of HSI system. The figure shows the front and back sides of each painting with the selected area (red rectangle) and the actual and average estimated DP and pH values for each painting. 151

Figure 5-12. Scatterplots of the correlation between estimated DP and pH values for the two paintings (P6 – left and P7 – right). The figure also shows the correlation coefficient (R^2) for each painting. 151

Figure 5-13. Linear fit of the Ekenstam equation (change of $1/DP$ as a function of time) on canvases samples (from 10 historic paintings labelled as P1, P2, ...etc.) degraded at three different conditions (90 °C - 70% (top), 70 °C - 30% (middle) and 50 °C - 50% (bottom) for 2, 8 and 16 weeks respectively). DP_0 is the initial degree of polymerization of cellulose and DP_t is the one at time t. 154

Figure 5-14. Comparison of rates of degradation as measured and as predicted of 10 real painting canvases samples from UCL-ISH collection and paper samples using the dose-response function as reported in Strlič et al. (2015). Solid circles represent the rate constants at different degradation conditions; 90 °C - 70% (green), 70 °C - 30% (blue) and 50 °C - 50% (red). Empty symbols represent rate constants of paper samples from earlier studies (Zou et al., 1996; Strlič & Kolar 2005; Strlič et al., 2015)..... 155

Figure 5-15. Lifetime maps of selected area of two examples of historic canvas paintings from UCL-ISH collection (P6, P7), estimated using the pH and DP maps generated based on the developed calibration models of HSI system and relative to 'standard' values of storage environment where T = 20 °C and RH = 50% and Canvas DP threshold=600 DP units. The figure shows the back side of the selected area from each painting and that area at 1970 nm. In addition to the maps of calculated lifetime (expected remaining time of a canvas until it is not fit for use) for each painting with the average in years. 158

Figure 5-16. Scatterplots of correlation between estimated pH and DP and calculated lifetime maps of selected area of two canvas paintings (P7 - top, P6 - bottom). The figure shows the correlation coefficient (R^2) for each painting..... 159

Figure 6-1. Scanning of the Islamic paper target using the HSI system showing the different positions of one of the glass samples; Without a glass frame (left), over the white calibration tile and the IP target (middle) and only over the IP target (right). The red rectangle represents the glass frame. The orange squares represent the area used to calculate the average spectra..... 162

Figure 6-2. Average reflectance spectra of Spectralon multi-component wavelength standard (top) and Islamic paper calibration target (bottom) from different scans using HSI. Scans show the effect of scanning with and without glass using different frames with various thicknesses. Also, the figure shows the effect of including the glass frame in the calibration process..... 163

Figure 6-3. Scatter plots show the reflectance correlation between scans of Islamic paper calibration target with and without glass in the two scenarios; when the glass is used in calibration (left) and when it only covers the tested object (right). 164

Figure 6-4. A papyrus sample (ID=32781) from the papyri collection of Petrie museum. 168

Figure 6-5. Scanning of a papyrus object from the Petrie museum collection using the HSI system..... 169

Figure 6-6. Results of the analysis of spectral image of two papyri (ID = 32069 and 32070- blue cells in Table 6-4) from the Petrie museum collection acquired by the HSI system in the spectral range 1000-2500 nm. In the first row, the figure shows a visible image of the two papyri. Then, the results of PCA and K-means clustering are shown where the distribution of the values of the spectral image based on the K-means clusters on the top and the score image of the first principal component (PC1) with the scatter plot of PCA

scores for the first and third PCs are in the bottom part. On the last row, the spectra of 20 pixels (top) selected randomly by the software from the spectral image after pre-processing by Savitzky-Golay (SG) derivation filter and SNV methods, in addition to color maps of the spectral image at two bands (@1393 nm, @1879 nm) that can be used to characterize the two papyri.172

Figure 6-7. The results of the analysis of spectral images of two papyri (blue cells in Table 6-4) collected using the HSI system to investigate the type of used ink. On the left side, visible images and grey images at 1750 nm are shown where object 32778 with carbon-based ink is shown at the top and object 71073 with iron-based ink is at the bottom. The right side shows the scatter plot of PCA scores (top) for the first two PCs where the different types of materials of the spectral image separated from each other as indicated. The score images of PC1 and PC2 are shown in the lower part where the first emphasizes the papyrus support and the other separates the ink.174

Figure 6-8. Papyri samples (4 historic (naturally aged) and 1 new) (top) with its corresponding spectra collected by HSI system in spectral interval 1000 – 2500 nm (bottom). Red rectangles highlight the samples after ageing at 80° C and 65% RH for 2 weeks.175

Figure 6-9. Results of PCA analysis of spectral image of 5 papyri samples (4 historic (naturally aged-old) and 1 new) before and after artificial ageing. Grey image at band 2046 nm (top left), score image of PC 2 (top right) masked with colors in relation to the scatter plot (bottom) for PC 2 and PC 3 for the papyri samples which highlights spatial locations with similar spectral signatures.176

Figure 6-10. Predictions of cellulose DP of papyri samples before and after ageing based on the PLS regression model developed for determination of DP of cellulose in Islamic paper. The predictions are classified into more or less degraded state based on their predicted DP regardless of the numerical information. Colored bars represent the old samples before (green - naturally aged) and after ageing (blue – naturally/artificially aged) in addition to the new sample before (red – new) and after ageing (cyan – new/artificially aged) as well.177

Figure 6-11. Predictions of DP of papyri samples before and after ageing based on two different PLS regression models developed for determination of DP of cellulose in Islamic paper. The predictions classify samples into more and less degraded based on their predicted DP regardless of the numerical information. Colored bars represent the historic samples before (green-naturally aged) and after degradation (blue – naturally/artificially aged) in addition to the new sample before (red) and after degradation (cyan – new/artificially aged) as well.....179

Figure 6-12. Four average reflectance spectra of a papyrus sample (P9) from different scans pre-processed by 2nd order Savitzky-Golay (SG) derivation over specific range 1450

– 2350 nm. Spectra were collected from different scans. The red square highlights the area with the most variations between spectra. 180

Figure 6-13. A grey image at 1750 nm of Islamic paper calibration target and 5 papyri samples before and after ageing scanned together using HSI system..... 180

Figure 6-14. Three average reflectance spectra of a papyri sample located in different positions on the stage (changing vertically from top to down) collected using the HSI system in the same scanning time/session for the purpose of exploring the effect of sample position on the spectra. The spectra are pre-processed by 2nd order Savitzky-Golay (SG) derivation over specific range 1400 – 2500 nm..... 181

Figure 6-15. Semi-quantitative chemical map of the distribution of estimated DP values of a papyri object (ID=55861-blue cell in Table 6-4) from the Petrie museum collection, estimated based on the PLS regression model developed using the HSI spectral data of Islamic paper calibration target. The map visualizes the DP values according to the degradation state, from less (red pixels) to more (blue pixels) degraded. The figure shows the visible image of the object with a grey image at band 1586 nm in addition to an average image with a threshold to exclude inks and background. 182

Figure 6-16. Semi-quantitative chemical maps of the distribution of estimated DP values of a papyri object (front and back sides) (ID=55898-blue cell in Table 6-4) from the Petrie museum collection, estimated based on the PLS regression model developed using the HSI spectral data of Islamic paper calibration target. The maps visualize the DP values according to the degradation state, from less (red pixels) to more (blue pixels) degraded. The figure shows the visible images of the object with grey images at band 1492 nm in addition to average images with a threshold to exclude inks and background. 183

Figure 6-17. Semi-quantitative chemical maps of the distribution of estimated DP values of two papyri objects (ID=32069 (bottom) and 32070 (top) -blue cell in Table 6-4) from the Petrie museum collection, estimated based on the PLS regression model developed using the HSI spectral data of Islamic paper calibration target. The maps visualize the DP values according to the degradation state, from less (red pixels) to more (blue pixels) degraded. The figure shows the grey images of the two objects at band 2120 nm in addition to average images with a threshold to exclude inks and background. Visible image of the two objects can be seen in an earlier figure (Figure 6-6)..... 184

LIST OF ABBREVIATIONS

AP	Arabic Paper
ATR	Attenuated Total Reflectance
Avg.	Average
B.C.E.	Before the Common/Christian Era
C	Calibration or Century in some Chapters
CED	Copper (II) Ethylenediamine
CV	Cross Validation
CoV	Coefficient of Variance
D	Camera Dark Current
DP	Degree of Polymerization
DSLR	Digital Signal Lens Reflex
E_a	Activation Energy
FPA s	Focal Plane Arrays
fps	Frame per Second
FTIR	Fourier Transform Infrared
GU	Gloss Units
[H⁺]	Concentration of Hydrogen Ions
[H₂O]	Water Content
H₂SO₄	Sulfuric Acid
HgAr	Mercury Argon
HSI	Hyperspectral Imaging
I	RAW Image or A/D Counts
I₂	Iodine
InGaAs	Indium Gallium Arsenide
IP	Islamic Paper
IR	Infrared
ISH	Institute for Sustainable Heritage
K	Rate Constant
KI	Potassium Iodide
LCTF	Liquid Crystal Tunable Filter
LDA	Linear Discriminant Analysis
ln	Natural Logarithm
LOOCV	Leave-One-Out Cross Validation
MCT	Mercury Cadmium Telluride (HgCdTe)
MSC	Multiplicative Scatter Correction
MSI	Multispectral Imaging
MTF	Modulation Transfer Function
MVA	Multivariate Data Analysis
MWIR	Mid-Wave Infrared
N	Number of Samples
NIR	Near Infrared
NO₂	Nitrogen Dioxide
[O₂]	Oxygen Concentration
P	Samples with Polished Surfaces
PC	Principal Component

PCA	Principal Component Analysis
PCDA	Principal Component Discriminant Analysis
PGP	Prism-Grating-Prisms
pH	Acidity Scale
PLS	Partial Least Squares
PLSDA	Partial Least Squares Discriminant Analysis
R	Relative Diffuse Reflectance or Gas constant in Chapter 5
R²	Correlation Coefficient of Determination
R_a	Roughness Parameter
R_{cv} / R²_{cv}	Correlation Coefficient of Cross Validation
RH	Relative Humidity
RMSE	Root Mean Square Error
RMSEC	Root Mean Square Error of Calibration
RMSECV	Root Mean Square Error of Cross-Validation
RMSEP	Root Mean Square Error of Prediction
ROC curve	Receiver Operating Characteristic curve
ROI	Region of Interest
R_p/R²_p	Correlation Coefficient of Prediction
RSD	Relative Standard Deviation
S	Samples containing Starch
SD	Standard Deviation
SEE	Standard Estimation Error
SEM	Scanning Electron Microscopy
SG filter	Savitzky-Golay filter
SNR or S/N	Signal to Noise Ratio
SNV	Standard Normal Variate
SWIR	Short-Wave Infrared
T	Temperature or Time in some chapters
UB	University of Barcelona
UCL	University College London
UV	Ultraviolet
V	Validation
Var	Variance
VIS	Visible
VNIR	Visible and Near-Infrared
W	99% Diffuse Reflectance (White) Standard or Watt as a measurement unit in some chapters
0	Samples with No Starch and Unpolished

1. INTRODUCTION

The preservation of heritage objects is a vital matter for humankind to be able to pass cultural heritage to the next generations and keep connections with the past. Heritage objects, based on cellulose -in particular- such as paper, canvases and papyri are the most important carrier of information about our cultures and history. As cellulose is an organic polymer easily affected by environmental degrading agents such as heat, humidity, pollution and light, degradation of cellulosic objects is an inevitable process. This is why understanding material properties of such valuable heritage objects is indispensable for their effective preservation. Many studies have been carried out to characterize cellulosic materials such as European paper (Papyrus 2001-2004, PaperTreat 2005-2008, SurveNIR 2005-2008), Chinese paper (Brown et al., 2017) and painting canvas (Oriola et al., 2011, Oriola, 2011) using different classical analytical techniques aiming to explore the characteristics of the materials and the main factors affecting its state. However, scientific understanding of Islamic paper and papyri is almost entirely lacking which is important for the development of better sustainable preservation plans (Strlič & Kolar, 2005).

Due to the materials and processes employed in their production, heritage objects are well-known for their compositional inhomogeneity. Regardless of extensive research to date, spatially resolved chemical analysis of heritage materials based on cellulose is not straightforward (Strlič & Kolar, 2005; Oriola et al., 2014).

Numerous investigations have been successfully performed to study cellulosic collections utilizing near infrared (NIR) spectroscopy as a non-destructive analytical technique combining multivariate data analysis (chemometrics) techniques for the purpose of material characterization, and many have been used for collection surveys (Oriola et al., 2014; Mahgoub et al., 2016; SurveNIR).

Although NIR spectroscopy has received considerable attention, such investigations have so far focused on point analyses, whilst processes of degradation advance in a heterogeneous way with possibly significant local variations due to the utilization of various materials and added substances, such as the priming and painting layers on canvases and the sizing and finishing layers in the papermaking process (Trafela et al., 2007; Oriola et al., 2014).

Thus, the development of a methodology that enables us to map the distribution of chemical composition of a whole artwork is of great importance (Wang & Paliwal, 2007; Kubik, 2007; ElMasry & Sun, 2010).

Spectral imaging techniques including hyperspectral imaging (HSI) and multispectral imaging (MSI) overcome the limits of spectroscopic techniques, rather than collecting a single spectrum at one spot on a sample, hyperspectral imaging simultaneously records spatial and spectral information for each pixel in the sample.

Since its invention around 50 years ago, spectral imaging technology has dramatically developed and is widely used in remote sensing, medicine, forensics and food engineering fields. With the evolution of detectors and sensors, it became a fast growing technology, providing promising results which encouraged researchers to adopt the technique in the field of heritage conservation (Lu & Chen, 1999; Fischer & Kakoulli, 2006; Chang, 2007; Kubik, 2007; ElMasry & Sun, 2010; Liang, 2012).

Spectral imaging technology has expanded imaging and material characterization possibilities (Fischer & Kakoulli, 2006) through building chemical images or maps, which has the potential to improve knowledge of distribution of material properties while investigating an entire object (Lu & Chen, 1999; Wang & Paliwal, 2007; Liang, 2012; Dooley et al., 2013).

Due to the complexity of the objects and the lack of standard calibration materials, most applications of spectral imaging in the field of cultural heritage have focused on qualitative research, such as the identification, comparison and mapping of materials on the surface of objects especially in studying paintings and manuscripts (Fischer & Kakoulli, 2006; Delaney et al., 2005). It was also widely used to examine or document object's condition, monitor and evaluate conservation treatments in addition to the enhancement and detection of underdrawings and faded texts and colour reproduction (Fischer & Kakoulli, 2006; Cséfalvayová et al., 2011; Liang, 2012). The three-dimensional dataset (hypercube or datacube) resulting from HSI contains two spatial dimensions and one spectral dimension, which can be used to study physical characteristics as well as chemical composition, thus condition of an object, especially in the NIR region (Lawrence et al., 2003; ElMasry & Sun, 2010; Yao & Lewis, 2010).

Multivariate regression is a necessity to analyse the outcomes of such systems because of the complexity of the data to extract quantitative information from this spectral region (ElMasry & Sun, 2010; Dooley et al., 2013). A 2D quantitative chemical map of iron gall ink on paper was developed in 2011 for the first time to visualize degradation and material properties (Cséfalvayová et al., 2011); however, the need remains to study the effect of different measurement conditions and calibration parameters e.g. the lighting spectral distribution and its intensity, or surface morphology, as well as to ascertain calibration stability. In other words, we need to focus on the metrology of quantitative chemical mapping based on hyperspectral imaging. This is an active research area that requires further studies (Fischer & Kakoulli, 2006; Dooley et al., 2013).

The overall aim of the research project is to explore the benefits and limitations of quantitative chemical imaging and its analytical robustness of cellulosic heritage materials with a focus on studying the effect of measurement parameters. The study will focus on mapping the chemical composition and condition of Islamic paper and painting canvases

in particular. Acidity and cellulose degree of polymerization (DP) of both materials will be studied due to its significant roles in degradation process, in addition to two main characteristic components of Islamic paper; starch sizing and polishing (Mahgoub et al., 2016). Together, these parameters provide a better understanding of the material and provide a measure of change in collections through imaging. For the quantitative study, special calibration targets need to be developed based on well-characterized reference collections for both cellulosic materials under study.

Another aim of the project is to explore the potential of the use of hyperspectral imaging technique in the SWIR region to deduce new knowledge about Papyri improving their conservation, especially as most of the papyri collections are embedded in glass frames.

The degradation of cellulose-based collections is an inevitable process. There is a strong relationship between the durability of paper and the materials and techniques used in its production. Many studies have been extensively conducted over the past few decades to investigate cellulose degradation mechanisms and its kinetics analysis, especially for western paper (Zou et al., 1996; Strlič & Kolar, 2005; Zervos, 2010; Menart et al., 2011; Strlič et al., 2015-III). Degradation study was carried out as part of the research project trying to understand the degradation behaviour and stability of the cellulosic materials under investigation: Islamic paper and painting canvas towards prolonging their lifetime. In addition to that, the applicability of the kinetic models developed for western paper on the investigated materials is also explored for the first time, which is very useful for simulating different scenarios of storage conditions and potential risks based on that for better evidence based preservation plans.

This research was a collaboration of different organizations from academia, heritage and industry. Camlin Photonics Ltd, specialized in developing hyperspectral imaging systems and ZFB GmbH who are experts in the field of interventive conservation. In addition, University of Barcelona (UB) and the Rijksmuseum who provide access to collections and conservation expertise.

Research questions

- Can the spatial distribution of chemical properties (pH and cellulose DP) in cellulosic materials (Canvases and Islamic papers) be imaged?
- Do the measurement parameters (calibration, illuminant intensity and stability, material surface structure) affect the quantitative image data?
- Can further case studies be developed for other cellulosic materials such as papyri, contributing to their more successful conservation?
- What information of value to conservators, curators and scholars can be obtained using NIR hyperspectral imaging technique and accelerated degradation to study degradation behaviour of cellulosic materials?

Thesis Structure

This thesis divides into seven chapters;

Chapter 1 has discussed the narratives of the entire PhD research project, describing the main aims and questions of the research.

Chapter 2 describes the nature and material properties of the three cellulosic materials under investigation: Islamic paper, painting canvas and papyri as well as the details of the reference collections and the classical analytical characterization methods that were used in the research. It also includes a background about the common degradation mechanisms of cellulose in paper and canvas with experimental details of a degradation study conducted using reference samples of Islamic paper and painting canvas in order to study their degradation behaviour and stability. The results of the degradation studies are described later in Chapter 4 and 5.

Chapter 3 reviews the Hyperspectral imaging system in terms of the background of the technique, its instrumentation, data acquisition parameters, important metrics, calibration, data analysis methods and usage in the field of heritage conservation in addition to a discussion about the robustness of the system through a series of evaluation tests. The chapter also includes a description about the specifications of an NIR spectroscopic technique used through the research for comparison with the HSI system in terms of performance, calibration and data analysis.

Chapter 4 focusses on historic Islamic paper exploring its material properties and the effect of some of these properties on its stability. It also describes the experimental details, data analysis and results of the development of non-destructive characterization methodology for the determination of four characteristics: starch sizing, polishing, pH and cellulose DP using NIR spectroscopy and HSI in addition to the validation of the developed methodology using real historic collection. Moreover, the details of the development of quantitative chemical maps for Islamic paper showing its advantages and limitations are described. The experimental details and results of an experiment to study the degradation rate and behaviour of Islamic paper are also included in the chapter.

Chapter 5 explores painting canvas describing the details and results of the development of an assessment tool for its condition (pH and DP properties) using NIR spectroscopy and HSI in addition to the validation of the tool using real paintings. Moreover, the development of quantitative NIR chemical maps of canvases and the study of their degradation behaviour and stability are also discussed in the chapter.

Chapter 6 focusses on the application of near infrared (NIR) hyperspectral imaging (HSI) on ancient papyri, exploring the potential of imaging through glass and its effect on the spatial and spectral accuracy of the collected information.

Chapter 7 collects the findings and conclusions of different chapters obtained for the entire PhD research explaining how the different aims and questions of the research have been covered. Interesting future avenues for research that have been identified during the research are also described, in addition to the different dissemination aspects of the research.

For each chapter, a brief introduction is included in the beginning together with the structure of each chapter. In addition to Chapter -, the conclusions and findings for each material under investigation are summarised at the end of Chapters 4, 5 and 6.

2. CELLULOSIC MATERIALS: Background and Development

Cellulose is the main constituent of many cultural heritage objects especially written heritage and paintings. It can be found in most fibres as it is considered the most abundant organic compound (Mills & White, 1987). As a linear polymer and due to its complex morphological structure, it can be exposed to many degradation reactions such as hydrolytic, oxidative and thermal (Porck, 2000; Strlič & Kolar, 2005).

Since the focus of this research is to study cellulosic materials, it is of great importance to be aware of cellulose degradation mechanisms for better preservation and management of heritage objects and collections. To be able to achieve that, firstly, we need to know about the nature and morphology of each object/material under study and how it was produced then investigate the factors and degradation processes influencing its lifetime.

The research will explore three different examples of cellulosic materials with different characteristics; Islamic paper, painting canvas, and papyrus. Islamic paper was chosen specifically as no previous systematic scientific study was conducted on it resulting in a scientific gap in understanding such historic material. Although painting canvas was investigated in earlier study enriching our scientific knowledge about this material, it was a good example to pick as another cellulose-based material with more heterogeneous nature than paper. On the other hand, papyri as the oldest writing material is another complicated material which were rarely investigated due to the inaccessibility of collections and/or lacking of information about its original manufacturing techniques.

This chapter is divided into 5 sections. The first three sections (2.1, 2.2 and 2.3) describe the nature and material properties constituting the three cellulosic materials under investigation in detail together with their development through history. The sections will also include description about the reference collections that were used in the research for each material.

Section 2.4 describes all the experimental details of classical analytical methods that were carried out through the research to characterize the cellulosic materials under investigation. The analysis of the results collected from the characterization methods are discussed later in Chapter 4 and 5 to be in context.

The last section (2.5) describes the common degradation mechanisms of cellulose in paper and canvas. The section also shows the experimental details of a degradation study conducted using reference samples of Islamic paper and painting canvas in order to study their degradation behaviour and stability. The results of the degradation studies are described in context with their relative data in Chapter 4 and 5.

2.1 Islamic Paper

As an information carrier, paper has a significant role in history and culture (Hunter, 1947; Bloom, 2001). Yet, although the craft originated in China (105 AD), the focus of much of recent research has been on Western papermaking (Papyrus 2001-2004, PaperTreat 2005-2008, SurveNIR 2005-2008). Such studies explored the characteristics of the European paper and the main factors affecting its material state such as using alum-rosin and gelatine for sizing. Also, a recent study on the 19th and 20th century Chinese paper (Brown et al., 2017) revealed the differences in the characteristics of the paper compared to European paper from the same period such as the low grammage and inhomogeneity of the paper. Material properties of paper changed as the knowledge of its production travelled from China through central Asia (751 AD) until it reached the West (1151 AD) then continued the development (Hunter, 1947; Pedersen, 1984; Bloom, 2001; Loveday, 2001). It is well known that Islamic papermakers utilized techniques and processes not often used elsewhere to cope with the different cultural environments, such as surface polishing, starch sizing or dyeing and decoration, which appear to make Islamic paper distinct from Indic, Sino-Asian or European (Baker, 1989; Baker, 1991; Bloom, 2001; Loveday, 2001; Karabacek, 2001; Déroche, 2005). However, it is as yet unknown how geographically distinct and widespread these techniques were and whether they affect paper stability.

For the purpose of this research, 'Islamic paper' is defined as paper that has been produced in the Islamic cultural realm, i.e. in Arab, Persian or Turkic territories. There could be regional differences in the history and techniques of papermaking; however, there is currently insufficient knowledge to distinguish them. There is a significant gap in the knowledge of what Islamic paper is, as provenancing can only be achieved by historical, palaeographical and codicological research (Déroche, 2005), and scientific understanding of Islamic paper is almost entirely lacking. We also know little about what proportion of Islamic paper constitutes manuscripts in Islamic library collections, especially since intensive trade led to significant imports of European paper into Islamic countries from the 17th century on (Baker, 1991; Bloom, 2001; Loveday, 2001; Déroche, 2005).

There is a strong relationship between the durability of paper and the materials and techniques used in its production, e.g. the effect of alum-rosin on European paper (Hubbe, 2004; Strlič & Kolar, 2005) widely used as a sizing material since the second half of the 19th century (Barrow, 1974; Au & Thorn, 1995). Gaining such knowledge would help custodians of Islamic paper collections to understand the materials and develop more sustainable preservation plans (Strlič & Kolar, 2005).

The main characteristics of Islamic paper are still considered controversial. Although some of the Islamic papermaking techniques were not often used in the European countries such as starch sizing, polished surfaces and dyeing paper, it should be taken into consideration that starch was used in Chinese papermaking and in the production of the early Western

paper as well (Garlick, 1986; Déroche, 2005). Also, dyed papers can be found in China from the 7th century AD (Déroche, 2005). In addition to that, it is possible that polishing, as a finishing technique, was applied separately from the original paper production process and in different locations and times (Loveday, 2001).

Paper fibres can be a conclusive characterization parameter, as was shown, e.g. for Tibetan paper (Helman-Ważny & Van-Schaik, 2012). However, we currently have no knowledge of, or historical information on, the use of particular fibres in Islamic papermaking, although bast and cotton have been used, as was the case of European papermaking (Loveday, 2001; Karabacek, 2001; Al-Sāmarrā'ī, 2001; Déroche, 2005; Al-Hassan, 2001).

All of that makes the characterization of Islamic paper difficult and multidisciplinary studies are required: palaeography for the identification of date and place of paper use, codicology for the identification of morphological characteristics and production techniques and scientific analysis for the identification of papermaking materials and state of degradation. Despite not being unique, starch sizing and polishing are used in this research as two representative characteristics of paper with a potential to be of Islamic origin due to their widespread use. Originally, the application of the two finishing techniques was done manually (Figure 2-1) using different techniques, which may lead to local differences in terms of surface degradation. A variety of starch sources were used for sizing of Islamic paper e.g. wheat and rice (Baker, 1991; Loveday, 2001). Polishing was also applied using tools e.g. glass stone either with or without additives acting as a coating layer such as egg white or gum tragacanth (Ibn Bādīs, 1025; Levey, 1962; Loveday, 2001; Karabacek, 2001; Al-Sāmarrā'ī, 2001) which resulted in different levels of quality and shine of paper (Baker, 1991; Loveday, 2001; Karabacek, 2001; Déroche, 2005).



Figure 2-1. Application of sizing (left and middle) and polishing (right) techniques on paper. © (left) http://precious-piece.com/?page_id=2358, © (right and middle) <http://www.hussainpapers.co.in/gallery.htm>.

Reference Collection

A collection of Islamic paper samples (228) was collected (Figure 2-2) from different sources in Central Asia, Near East and North Africa covering the period from 15th to 19th century. The substantial collection is part of the UCL Institute for Sustainable Heritage (UCL-ISH) Historic Reference Material Collection gathered before the time of this research. All of the samples in the collection have no historical or any value and were purchased from authentic galleries in the form of single sheets and once out of context so it was decided that it is suitable for destructive sampling for the purpose of material

analysis and scientific research based on ICON guidance (Quye & Strlič, 2019) and after an internal assessment.

Samples are single sheets with text mostly on both sides which are written in several languages e.g. Coptic, Persian and Turkic but mostly in Arabic (168). 31 samples are from Samarqand (Uzbekistan).

Unfortunately, the production dates of more than a half of the samples (133) are unknown, while ~90 samples are from 18th -19th century and older. In general, no clear information is available about the provenance, date or history of the storage environment for these samples. Such information is of great importance to be able to assure the scientific conclusions resulted from the analysis of the collection. For that reason, the reference collection was well-characterized and chemically analysed following the standard classical techniques used for paper to collect as many information as possible about its material state. In addition to that, the degradation rate and behaviour of the samples were also investigated with the aid of accelerated degradation.

The collection was visually examined and digitally documented before any sampling or further analysis. A reference database was constructed to record all measurements, observations and images using catalogue number (Arabic paper—AP) and unique ID, consisting of “AP” followed by an incremental number for each sample. Sub-samples such as AP 1-1 and AP 1-2 were given to sheets from the same bound volume.

Then the collection was characterized using chemical analytical methods to identify two main properties of Islamic paper: starch and surface polishing, and to explore the average material state of the samples by the determination of pH and degree of polymerization of cellulose in paper. Analytical methods are described later in this chapter (Section 2.4).

88 % of the samples either contain starch or are polished, or both. The majority of papers are neutral to mildly acidic, which is in contrast to their DP values where ~69 % have DP < 1000 which indicate their extensive degradation. The characterization of the collection in addition to the investigation of the possibility of any relationship between polishing and starch sizing characteristics with the measured values of pH and DP will be discussed later in Chapter 4 .



Figure 2-2. Two objects in the historic reference material collection at UCL-ISH (*Left*: AP 85, *right*: AP 53)

Islamic Paper Calibration Target

Due to the lack of standard materials for calibration representing the complexity of the real objects under study, qualitative applications were more common for the HSI analysis. Thus, a special calibration target was prepared using the well-characterized reference collection of Islamic paper described earlier. The target was involved in the development of quantitative calibration models (discrimination and regression) with the aid of multivariate data analysis techniques. The target was also used to test the robustness and stability of the scanning system as it allows for scanning the samples keeping the same position and order in each scan.

The Islamic paper calibration target (Figure 2-3) was devised using 105 samples (Table 2-1) from the well-characterized reference collection of Islamic paper (228 samples) (see Appendix I). The target was scanned, analysed and used to build calibration models using multivariate data analysis methods using both HSI system and Labspec-5000 spectrometer. Different samples from the same reference collection were also used to validate the models and to build quantitative chemical maps of different material characteristics of Islamic paper. Four material properties were of interest; starch sizing, surface polishing, pH and cellulose degree of polymerization (DP).

The design of the target permits the use of different backgrounds while taking spectral measurements as seen in Figure 2-3. the target was also used to explore the performance of the HSI system and its robustness as explained later in Section 4.4.

Regarding target samples properties, Starch was identified in 45 samples versus 60 samples without starch. 43 out of the 105 samples are categorized as polished. pH values were available for ~ 70 samples which ranges from 4.5 to 7.5. Also, DP measurements were conducted for only 57 samples as the other samples contained lignin, which cannot be measured using the traditional analytical method. The average DP of all the samples is 848 with a standard deviation of 427.

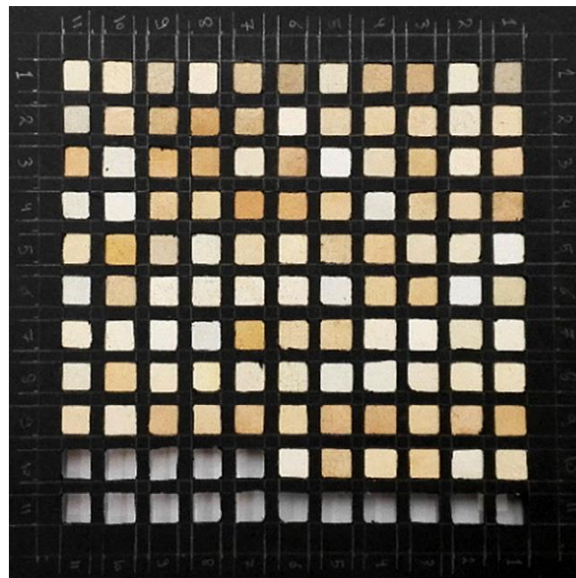


Figure 2-3. Calibration target with 105 characterized samples of Islamic paper (Front and back sides).

Table 2-1. The 105 Islamic paper calibration target samples, showing the distribution of samples containing starch (samples with yellow cells). Grey slots are without samples.

	11	10	9	8	7	6	5	4	3	2	1	
1	56-3	55	45-3	42	36	26	6	5	3	56-1	45-2	1
2	131	125-1	121	114	108	97	91	85	84	83	74	2
3	43	18	10	9	8	29-2	127-2	133-2	17	44	125-2	3
4	126	116	115-1	113	107	100	98	72-4	69	49	29-1	4
5	2	129-2	129-1	16-1	25	35	37	115-3	133-1	128	127-1	5
6	109	38	39	40	41	47	48	63	65	75-T1	76	6
7	34	33	89	110	111	117	118	123	124	130	120	7
8	75-1	27-1	72-2	101	96	82-1	73-2	53	57	50	46	8
9	95	72-1	62-1	52	31	30-1	28-2	23	11-1	4	62-2	9
10						72-3	24	132	106	104	103	10
11												11

2.2 Painting Canvas

Paintings are complex cultural heritage objects. They have layered structures (Figure 2-4) with different materials and compounds such as wood, glue, canvas, metal and pigments that can easily migrate from one layer to another (Boon et al., 2007).

Canvas support is one of the important layers of easel paintings as it holds the paint layers therefore the aesthetic value, for that reason its preservation is very important. The investigation and condition assessment of canvases sometimes require destructive sampling, which is rarely permitted for valuable objects, such as assessing the strength of a canvas using mechanical tests e.g. stress/strain curves of a canvas or maximum load before failure which require large samples and repetitions or measuring the degree of polymerization (DP) and acidity of the canvas to assess the degradation state of a canvas thus developing a non-destructive assessment method would be both required and welcomed.

Traditionally, the most often used fibres for painting canvases were linen, cotton, hemp, jute and ramie (Villers, 1981; Oriola, 2011). Since canvas is traditionally a cellulose-based material, it is affected by degrading agents such as heat, humidity, light, pollution and biological agents (Strlič & Kolar, 2005; Boersma et al., 2007).

The main consequence of canvas degradation is the loss of its mechanical strength making it fragile (Garside & Wyeth, 2006). Since the mechanical strength and degree of polymerization (DP) of cellulose in canvas are related (Zou et al., 1996; Oriola, 2011) and most mechanical tests require large amount of sacrificial samples in comparison to the viscometric method of DP determination, viscometry can be used to assess the condition of the canvases. On the other hand, acidity is also known to be an important parameter for cellulose-based materials and could accelerate the degradation processes (Strlič & Kolar, 2005). Application of primer, glue and some paint in addition to the acidic gases from the environment increases the acidity of canvases (Villers, 1981; Hackney & Hedley, 1993; Anonymous, 1997; Zervos & Moropoulou, 2005). Thus, gathering information about both material properties provides information to assess the material state of canvases. Also, the distribution of these properties across a painting canvas can be very heterogeneous leading to possible local differences during degradation.



Figure 2-4. Structure of an easel painting. © Dominguez Rubio, 2014

Reference Samples

The reference database of painting canvas samples used in this research was built based on two different sources; ~150 historic canvas samples from the reference collection of a prior study conducted in 2011 (Oriola et al., 2011; Oriola, 2011) and 10 historical oil paintings belonging to UCL-ISH Reference Collection (Figure 2-5) (see Appendix IV). The reference collection from the study at 2011 is well characterized so the DP, pH and fibres are known (with expected changes in the measurements and condition of the samples since the study time). Most of the samples were collected from paintings and linings from Museu Nacional d'Art de Catalunya (Barcelona). The samples are dated from the 16th century to 19th /20th century. There is a large variation in the fibres and types of the samples. The description of the collection in addition to its characterization can be found in the original study (Oriola et al., 2011; Oriola, 2011).

Regarding UCL-ISH samples, most of the paintings are from the 20th century and only 2 are from the 19th century. Similar to the Islamic paper reference samples and under the ICON guidance, Paintings are suitable for destructive analysis as they were purchased from authentic galleries on an individual basis and each has no historical, aesthetic or any values so it can be used to validate the developed calibration models acting as real cases. Samples were characterized (Table 2-2) similar to Islamic paper samples in terms of acidity, cellulose DP and fibre furnish analysis (done with the aid of University of Barcelona). Most of the samples are made of linen fibres with only two cotton samples. pH of the samples ranges from 4.5 to 6.4 while cellulose DP values ranges from 880 to 3800.

Table 2-2. Results from the characterization of UCL-ISH painting samples showing the fibres, pH and cellulose DP values of the 10 paintings.

	Fibres	DP	pH
P1	Linen	1229	4.9
P2	Linen	3289	6.0
P3	Linen	1207	4.9
P4	Cotton	1834	6.4
P5	Linen	888	4.5
P6	Linen	1032	5.0
P7	Linen	1397	5.4
P8	Linen	899	4.9
P9	Linen	3826	5.8
P10	Cotton (Probably mercerized)	1166	4.7



Figure 2-5. Reference collection samples from a prior study conducted in 2011 (Oriola et al., 2011; Oriola, 2011) (left) and one object (P10) from UCL-ISH painting collection (right).

Canvas Calibration Target

Similar to the Islamic paper calibration target, around 70 samples were selected from the Canvases Reference collection to build the quantitative calibration models (Figure 2-6) (see Appendix II). Spectral measurements were collected from the samples in the target using the Labspec spectrometer and HSI system with different acquisition parameters. Whatman filter paper sheets were used as a measurement background. Cellulose DP and pH regression models were developed for both instruments and the results were compared. In addition, the models were evaluated using the real paintings from UCL-ISH collection. The selected canvases were non-destructively scanned with the HSI system and pH and DP values were predicted using the developed models then compared to the real measurements. Quantitative chemical maps of the two properties were also generated to enable a visualisation way of the distribution of material properties and its chemical state.



Figure 2-6. Calibration target with 72 well-characterized samples of painting canvases (16th – 20th C.).

2.3 Papyrus

Papyrus is one of the oldest writing materials used to transfer information (Grasselli, 1983). It has a particular place in history due to its unique historic significance, information content, durability and structure. However, little scientific research focused on papyrus conservation, preservation and material characterization as well as on the writing materials and pigments used (Frösén, 2012). This may be due to the difficulty of accessing

collections and the less well-known ancient manufacturing process of papyrus (Grasselli, 1983; Bülow-Jacobsen, 2012) and its writing and decoration in addition to the complex structure of the support itself.

Papyrus as a writing support has a unique layered structure. It consists mostly of cellulose, hemi-cellulose and lignin in addition to few proteinaceous materials (Leach & Tait, 2000). It has a rough surface as sheets are woven from ribbons cut directly from plant stems (Elnaggar et al., 2015). Similarly, as any cellulose-based organic material it is prone to degradation affected by different parameters in the environment, however, this is still underexplored as it would require access to and analysis of reference collections which is unavailable, particularly with respect to the nature and rate of the degradation processes and to assessment of its mechanical stability.

Inks used on papyri if well explored could reveal useful information about the development of the writing materials through the history of papyri as it links Egyptian, Roman and modern civilizations. It is known that carbon is the oldest ink material used in Egypt before the beginning of the 1st dynasty (3400 B.C.E.) and is mostly made of soot (Lucas & Harris, 1962). Romans and Greeks used carbon ink as well, while Romans also made ink from sepia. Some evidence of the use of oak galls in the production of ink was found as well starting from 2nd - 3rd century AD onward (Lucas, 1922; Mitchell & Hepworth, 1937; Lucas & Harris, 1962; Bülow-Jacobsen, 2012). Few literatures mentioned the detection of iron ink around the third century B.C.E. (Lucas, 1922; Bülow-Jacobsen, 2012) but further investigation supported with scientific evidence is needed to verify such information.

Different pigments were also used such as red lead, red and yellow ochre, verdigris, orpiment, malachite, lapis lazuli, and Egyptian blue. Black ink was mainly used for writing while red ink was used for titles, headings and notes. The other colours were used for illustrated scenes and decoration (Montague, 1890; Lucas, 1922; Mitchell & Hepworth, 1937; Lucas & Harris, 1962). More research is needed to study the pigment palette used through this period.

More applications using scientific techniques especially non-destructive and portable ones need to be developed to be able to access and systematically study collections and to explore and verify the chronology of the development of the writing materials in addition to study the degradation nature and damaging effect of it on the support. A scientific trial was done on 2001 (Françoise & Delange, 2001) to study papyri trying to answer some important conservation questions about the source of the papyrus, the existence of glue between its layers and the impact of time on it. The authors used some analytical techniques such as proton-induced X-ray emission (PIXE) for the mineral analysis, optical microscopy to detect starch presence, mechanical strength (zero-span tensile strength), acidification (pH) and oxidation in addition to accelerated degradation under the presence of the agents causing chemical and physical degradation: heat, humidity, light and pollution to study the behaviour of papyrus.

Moreover, some research on papyrus conservation has been developed recently e.g. evaluation of using laser cleaning to remove burial encrustation on papyrus (Elnaggar et al., 2015) and investigation of using advanced imaging techniques to identify and characterize the writing on papyrus which is beneath the surface of ancient Egyptian mummy cartonnage (Gibson et al., 2018) that demonstrates the potential and need for such tools to study this complex material (Françoise & Delange, 2001).

Papyri Collection

Around 60 samples (Figure 2-7) from the collection at the Petrie museum covering the period from Middle Kingdom (2024 BC) to Islamic Period (1000 AD) were investigated. The textual information of the samples is written in different languages such as; Demotic, Greek, Hieratic, Arabic, Coptic. Each sample is kept between two glass sheets for its preservation. Samples glass cases have various thickness from ~2 - 3 mm. Some of the samples have a paper card background.



Figure 2-7. Some objects from the collection at the Petrie museum that were examined in the research.

2.4 Classical Characterization Methods

2.4.1 Sizing Characterization of Islamic Paper

The presence of starch was investigated using the iodine test (Isenberg, 1967; Baker, 1991). 5 g of I_2 ($\geq 99.8\%$, Sigma Aldrich, Dorset) was added to 10 g of KI (crystals, Sigma Aldrich, Dorset) dissolved in 100 ml of deionized water to prepare the iodine solution. For use, one drop of the prepared solution was then added to $\sim 0.5\text{ cm}^2$ of paper sample after dilution by 1:4. Any change in colour was recorded under low magnification.

Samples that gave negative results for the Iodine test were also tested for the presence of rosin using the Raspail test (Isenberg, 1967; AIC, 1990). The possibility of rosin and starch being present in the same sample was also explored.

After adding one drop of a sucrose solution (35 g sucrose, $\geq 99.5\%$, Sigma Aldrich, Dorset, in 20 ml deionized water) to the paper sample ($\sim 0.5\text{ cm}^2$) and left it for 3 min to ensure penetration, a drop of concentrated H_2SO_4 (95–97 %, Merck, Darmstadt) was then added. Colour change was observed under low magnification.

2.4.2 Surface Characterization of Islamic Paper

Polishing was assessed visually and the ref-collection was divided into 'Polished', 'Unpolished' and 'Uncertain' categories. Visual assessment of a polished surface of a paper could be considered as a challenge either by appearance (looking for sheen marks) or by touch due to the manufacturing technique which resulted into different levels of quality and shine (Loveday, 2001; Karabacek, 2001; Déroche, 2005). Based on the relation between surface roughness and its light reflection (Bhushan, 2001), other measurements were collected to find an instrumental method to reduce the subjectivity of visual assessment such as measuring roughness and gloss characteristics of the surface in addition to its reflectance. Scanning electron microscope was also used to capture the surface topography of the samples which gave the best results among the tested instruments.

Roughness

TRACEiT profilometer (Innowep, Würzburg) was used to measure roughness as an indication of surface texture and irregularities (Leising, 2010). The topographic roughness parameter R_a (Bhushan, 2001) was determined in both directions (X and Y) with the resolution of 1536 lines per 5 mm. The arithmetic average was calculated.

Gloss

Gloss was measured at 20° using Novo-Gloss Lite 45° glossmeter (Rhopoint Instruments, St Leonards) with a resolution of 0.1 gloss units (GU). The average gloss value was calculated from ~10 random measurements, on both sides of each sheet.

Specular/diffuse reflectance ratio

The ratio of intensity of reflected light at 457 nm was determined using a Lab-Spec-5000 spectrometer (ASD, Boulder) at two different angles relative to the incident beam (0°, 45°). This wavelength was selected as it is used to measure paper brightness (Tappi-452-om, 1998; BS-ISO-2470-1, 2009). Using the ratio rather than absolute values also corrected for any influence of potential chromophores.

Scanning electron microscopy (SEM) imaging

Surface topography images of a 5 x 5 sample were obtained using TM3030 tabletop scanning electron microscope (Hitachi, Tokyo) in charge-up reduction mode without any sample preparation. Images were collected using low accelerating voltage (5 kV) and magnification of 100x.

2.4.3 Acidity

pH measurement is commonly used to represent the acidity or alkalinity of a material by measuring the hydrogen ions (H^+) concentration in the solution (Tse, 2007; Mettler-Toledo, 2013). The pH of the samples from canvases and Islamic paper samples collections was

measured using a modified standard cold extraction procedure (ASTM-D778-97, 2002; Strlič et al., 2004). Mettler Toledo (Leicester) SevenGo pH/Ion Meter with a micro-combined glass electrode (3 mm diameter, InLab® Micro, 51343160) was used for measuring pH after calibration with Mettler Toledo pH 4.01±0.02 and pH 9.21±0.02 buffers in the room temperature.

Around 1.14 mg of a sample is soaked into ~ 0.1 ml MilliQ deionized water and left overnight to achieve equilibrium (Strlič et al., 2004; Figure 2-8). Samples were taken out of the extraction liquid during measurement. All values were rounded to the nearest 0.1 pH unit (ASTM-D778-97, 2002; Strlič et al., 2004). The uncertainty of the used method was evaluated which equals ±0.3 pH units.

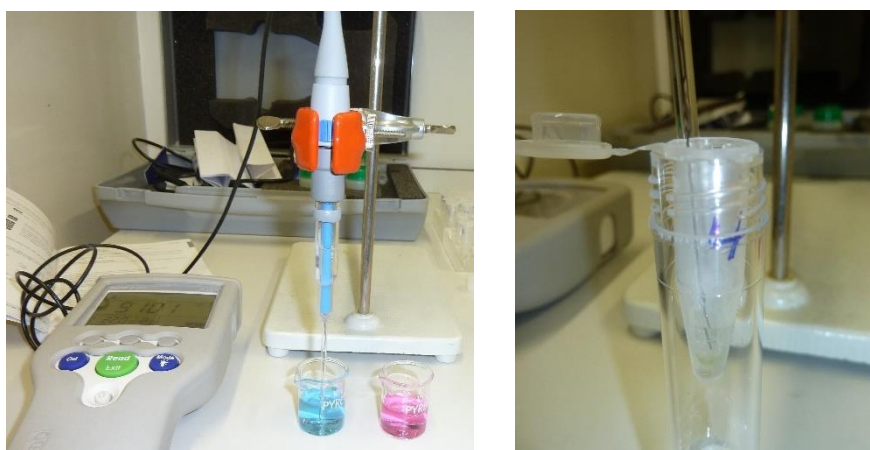


Figure 2-8. pH meter during calibration and measurement processes.

2.4.4 Degree of Polymerization

DP of cellulose in cellulosic based objects is very useful indicator of the condition of the cellulosic chains reflecting object condition. Also, its correlation to the mechanical properties and remaining lifetime of objects was proven (Zou et al., 1996; Strlič & Kolar, 2005; Trafela et al., 2007; BS-ISO-5351, 2010). The standard viscometric method (Evans & Wallis, 1987; BS-ISO-5351, 2010) was used to measure the DP of cellulose in paper and canvas samples. For each sample, an average of 3–5 repeats of the effluent time were used to calculate the DP using Mark–Houwink–Sakurada equation (Evans & Wallis, 1987; Strlič & Kolar, 2005; BS-ISO-5351, 2010). Around 20-30 mg from each sample is required.

Since the determination of water and non-cellulosic additives of each sample was not conducted due to the limited historic samples, 5% of an average content of non-cellulosic compounds (including water) was assumed in the calculations similar to previous publications (Strlič & Kolar, 2005; Trafela et al., 2007; Strlič et al., 2007). It was taken into consideration that an error of 1% in this estimation (i.e. 5% ± 1%) would lead to ΔDP of 1% which is negligible in relation to the observed differences in DP across the collections. The uncertainty of DP determination of a Whatman No. 1 filter paper (Maidstone) sample was <1% ($n = 3$). All measurements were conducted inside a fumehood cupboard

(Safehood120, BIOAIR EuroClone Division) due to the toxicity and corrosiveness of the standard solvent (cupriethylenediamine – CED, Merck KGaA, Copper (II) ethylenediamine solution). Lignin-content samples were not measured using this technique as lignin cannot be dissolved in the standard solvent (Trafela et al., 2007; Zervos, 2007).

A preparation step was needed for the canvases samples before DP analysis due to its heavy sizing with glue and paint remains. Samples were soaked in distilled water (temperature of the water is 90-100 °C) and left overnight. Then, samples were double boiled at 100° C for 10 min. After cooling down, samples were air dried for two days (placed over Whatman No. 1 filter paper sheets, Figure 2-9). After that, DP of the samples were measured using the described method.



Figure 2-9. DP measurement experiment of canvas samples, showing the special preparation process needed for the samples due to the heavy glue and paints.

2.5 Degradation Processes in Cellulosic Materials

The degradation of organic collections is an inevitable process. Like all materials, cellulose-based ones will eventually decompose, however variations in the rates may be significant. Thus, it is important to understand the properties of each material e.g. its nature and production techniques to be able to get knowledge about degradation processes and factors that affect its lifetime which then will allow for the development of effective and efficient preservation methodologies.

A variety of degradation processes affect cellulosic based collections in similar ways. The degradation of cellulose is well explained in literature (Strlič & Kolar, 2005). Briefly, cellulose can undergo chemical or physical changes or both during degradation

processes. Rearrangement of the molecules of a material without changing the chemical structure of its individual molecules can be considered as a physical change such as polymer recrystallization or denaturation of protein structures. On the other hand, chemical changes involve creation of new molecular structures resulted from changes in the bonds between atoms in molecules (Moncrieff & Weaver, 1992). This usually leads to the creation of new substances with new physical properties (Rizzo & Burnstock, 2003). In general, one can say that chemical and physical degradation are correlated (CCI, 2002).

Degradation and its rate can be affected by different environmental parameters; heat, moisture, light, pollutants and microorganisms (Erhardt & Mecklenburg, 1995; Boersma et al., 2007; CCI, 2008; Menart et al., 2011). The type and quality of the raw material introduced in the production process as well as the techniques of production can also affect degradation. Higher temperature and relative humidity (RH) accelerate the degradation rate of cellulose (Zou et al., 1996) while low RH introduces brittleness to materials due to reduced flexibility which may lead to physical damage during handling (Garside & Wyeth, 2006; Menart et al., 2011). In addition, fungal growth accelerates with higher moisture and temperature (Garside & Wyeth, 2006; CCI, 2008). Although there is a disagreement between research opinions about the effect of fluctuations in RH and temperature on the degradation of cellulose-based materials, the recent proved conclusion was that no significant effect on degradation rate due to fluctuation more than it would be expected and what is important is the time spent at each condition per cycle (Menart et al., 2011). Light, especially ultraviolet radiation, also accelerates oxidation of cellulose leading to yellowing and embrittlement (Tímár-Balázs & Eastop, 1998).

Hydrolysis and oxidation are considered as the main degradation processes of cellulosic materials, causing polymer's chain scission and embrittlement of the material. Hydrolysis process is the chemical breakdown of a compound during reaction with water (Pearsall, 1998) and it can occur under acidic (acid-catalysed hydrolysis) or alkaline (alkaline hydrolysis) conditions. Both reactions break the cellulose chains making it shorter that lead to depolymerization thus less mechanical strength and consequently embrittlement of the material (Garside & Wyeth, 2006). Oxidation process mainly happens when a molecule chemically combines with Oxygen (Pearsall, 1998). Cellulose is stable to atmospheric oxidation (autoxidation) (Strlič & Kolar, 2005) at ordinary temperatures although this will still happen progressively especially in the existence of light (Mills & White, 1987) (photo-oxidation (Pearsall, 1998)).

Acid catalysed hydrolysis is considered the main chemical degradation pathway in cellulosic materials where acid is playing the role of a catalyst that speeds up the reaction rate without being consumed, so the more acidity (low pH), the more bond scission happening and thus the higher the degradation rate is. The rate of the degradation depends on the acid strength, concentration as well as on the temperature and duration of the reaction (Dupont, 2003). The full mechanism of acid-catalysed hydrolysis is

explained in literature (Strlič & Kolar, 2005; Oriola, 2011). On the other hand, if the cellulose was suffering from pre-existing damage such as hydrolysis or photo-oxidation, then it will degrade more rapidly under alkaline conditions (Garside & Wyeth, 2006).

In contrast to acid-catalysed hydrolysis, Oxidation is the predominant degradation reaction in neutral to moderately alkaline conditions which depends on the amount of the oxygen in the surrounding atmosphere (Strlič & Kolar, 2005) where the hydroxyl groups in cellulose are converted into carbonyl and carboxyl group (Dupont, 2003). Oxidation could result in both cross-linking (i.e. increase of molar mass leading to loss of flexibility) and chain scission leading to embrittlement of the material and discolouration (Garside & Wyeth, 2006; Oriola, 2011).

As cellulosic materials are very sensitive to acidity increasing the rate of acid-catalysed hydrolysis (Strlič & Kolar, 2005) which in turn results in the breakage of polymer chains (lowering DP) and weakening the fibres (less mechanical strength). Therefore, knowing the DP of cellulose and the acidity (pH) of an object, gives information about its current material state, where DP of the cellulose chains informs about the mechanical strength of an object so its suitability for handling and display while presence of high pH values indicates the high rate of degradation process. However, both of these analyses are destructive and require sampling. Many studies have been successfully conducted to develop non-destructive methods to measure or determine these material properties mostly based on spectroscopy (Trafela et al., 2007; Strlič et al., 2007; SurveNIR; Richardson & Garside, 2009; Možir et al., 2011; Oriola, 2011). This is considered an active field of research.

Many studies have been extensively conducted over the past few decades to investigate cellulose degradation mechanisms and its kinetics analysis especially for western paper (Strlič & Kolar, 2005; Zervos, 2010; Menart et al., 2011). Much of this work is based on the earlier research into the kinetics of cellulose degradation by Zou, Uesaka and Gumagul (Zou et al., 1996-I) in which a general kinetic model of the rate of degradation of paper was established to describe the depolymerisation of cellulose using artificially degraded bleached softwood bisulphite and Kraft pulps. It was based on the first order law, the Ekenstam equation (Ekenstam, 1936) and the Arrhenius relationship (Arrhenius, 1889; Strlič & Kolar, 2005). The model described the dependence of the rate of degradation on moisture content, hydrogen ion concentration and their interaction. Since the goal of the kinetic analysis is to predict the natural degradation behaviour of paper, the authors were able to estimate the effects of storage conditions on the life expectancy of paper, i.e. the time needed for the DP to decrease to some value, regarded as the lower limit of usability (typically 250-300 DP units).

The same authors also provided the first quantitative comparison of accelerated degradation with natural degradation (Zou et al., 1996-II) where a good correlation

between both methods was proved with a statistical confidence in the prediction of paper permanence using accelerated degradation.

Another modelling attempt recently was carried out by Strlič et al. (2015-III) to describe the degradation rate of paper. Their model also was developed based on the Ekenstam equation (Ekenstam, 1936), the Arrhenius relationship (Arrhenius, 1889; Strlič & Kolar, 2005), the linear correlation between the rate of degradation in DP and the moisture content, as well as hydrogen ion concentration. The model is using available observations of paper degradation in literature (Zou et al., 1996-I;1996-II; Kolar & Strlič, 2007; strlič & Kolar, 2005; Baranski et al., 2005) which are all collected from accelerated degradation experiments or model samples. The authors developed a dose-response function linking loss of DP with time and parameters that critically affect the rate of degradation of paper at dark storage such as temperature (T), concentration of acids (pH) in cellulose and water content (RH). That enabled them to predict degradation behaviour of paper leading to the development of a new damage function dedicated for historic European paper which opening the possibility to build scenarios of management of the storage environment as well as level of access for different types of library and archival paper.

According to the general developed kinetic model, the degradation rate constant can be determined from the following simplified Ekenstam equation (Ekenstam, 1936; Zou et al., 1996).

$$\frac{1}{DP} - \frac{1}{DP_0} = k \cdot t$$

where DP and DP₀ are the degree of polymerization of cellulose at time t and zero, respectively, and k is the degradation rate constant (day⁻¹).

The temperature dependence of degradation rate constants is described by the Arrhenius equation under certain conditions (Zou et al., 1996):

$$k = A_a * \exp \left(-\frac{E_a}{RT} \right)$$

where A_a and E_a are the apparent frequency factor and activation energy, respectively. R is the gas constant and T is the absolute temperature. The activation energy represents a measure of sensitivity of the degradation rate to temperature changes, while the constant A represents all other experimental parameters, such as humidity, acidity, exposure to pollutants and light, and physical structure of paper (Calvini & Gorassini, 2006).

The two developed models from the kinetic analysis studies (Zou et al., 1996; Strlič et al., 2015-III) showing the dependence of the frequency factor A_a on the moisture contents [H₂O, %] and hydrogen ion concentration [H⁺] of cellulose sheets as following:

$$k(\text{prediction}) = (A_{a0} + A_{a2} \cdot [H_2O] + A_{a5} \cdot [H^+] \cdot [H_2O]) * \exp \left(-\frac{E_a}{RT} \right) \quad (\text{Zou et al., 1996-I})$$

Where $k(\text{prediction})$ is the predicted degradation rate (day^{-1}), $E_a = 109 \text{ kJ}\cdot\text{mol}^{-1}$, $R = 8.314 \text{ J}\cdot\text{mol}^{-1}$ and $A_{a0} = 4.54 \times 10^{-9} \text{ day}^{-1}$, $A_{a2} = 2.83 \times 10^{12} \text{ day}^{-1}$ and $A_{a5} = 9.85 \times 10^{16} \text{ mol}^{-1}\text{day}^{-1}$ and T is temperature in Kelvin.

$$\ln(k(\text{prediction})) = a_0 + a_1 \cdot [\text{H}_2\text{O}] + a_2 \cdot [\text{H}^+] - \frac{a_3}{T} \quad (\text{Strlič et al., 2015-III})$$

Where $a_0 = 36.918 \text{ year}^{-1}$, $a_1 = 36.720 \text{ year}^{-1}$, $a_2 = 0.244 \text{ year}^{-1}$, $a_3 = 14300 \text{ year}^{-1}$ and K_p is degradation rate in year^{-1} .

$[\text{H}^+]$ was calculated by $[\text{H}^+] = 10^{-\text{pH}}$ where pH is the acidity of the samples measured using the cold extraction method while $[\text{H}_2\text{O}]$ was calculated based on the developed function for 'fine paper' (Paltakari & Karlsson, 1996) as;

$$[\text{H}_2\text{O}] = \left(\frac{\ln(1-\text{RH})}{1.67 \cdot T - 285.655} \right)^{\frac{1}{2.491 - 0.012 \cdot T}}$$

where $[\text{H}_2\text{O}]$ is the moisture content of the samples, RH is the relative humidity of the environment in ratio and T is temperature of the environment.

Thus, in order to further understand the behaviour of the materials under investigation, exploring their degradation rate and study their stability, several accelerated degradation experiments were planned and conducted at different temperature (T) and relative humidity (RH) conditions using Islamic paper and canvas samples (10-12 samples each) (Figure 2-10). Islamic paper samples were selected to represent the various types in the reference collection (samples either starch-sized or polished or both, samples neither polished nor starch sized). Canvases samples were only selected from UCL-ISH collection. Table 2-3 shows the different combinations of T and RH selected and the location of each experiment with information about the chamber type, duration of experiments and sampling rates. pH and DP were determined similarly to the reference samples following the degradation experiment. Then, the data and results (discussed in Chapter 4 - Section 4.5 for Islamic paper and in Chapter 5 – Section 5.3 for painting canvas) obtained from these experiments were used to build models and damage functions to study the different scenarios of storage environment for Islamic paper and canvases which provides an evidence-based management of historic collections.

Table 2-3. The different conditions of the accelerated degradation experiments applied to Islamic paper and canvases samples. The table showing combinations of temperature and relative humidity conditions, the total experiment duration for each material and sampling rate. In addition to experiments' locations and chamber types information.

Conditions (T °C, %RH)	70° / 30%	60° / 70%	90° / 70%	50° / 50%	80° / 50%
Islamic Paper	12 weeks	8 weeks	4 weeks	8 months	8 weeks
Painting Canvases	8 weeks	6 weeks	2 weeks	4 months	4 weeks
Location	University of Ljubljana by Irena Kralj-Cigic			Library of Congress (LoC) by Fenella France	ZFB GmbH by Manfred Andres
Chamber Type	Vötsch (VC0018, Balingen-Frommern, Germany)			-	Binder GmbH (MKF 720, Germany)
Sampling rate	AP: every 3 weeks x 4 times C: every 2 weeks x 4 times	AP: every 2 weeks x 4 times C: every 2 weeks x 3 times	AP: every week x 4 times C: every 5 days x 3 times	AP: every 2 months x 4 times C: every 1 month x 4 times	AP: every 2 weeks x 4 times C: every 10 days x 3 times

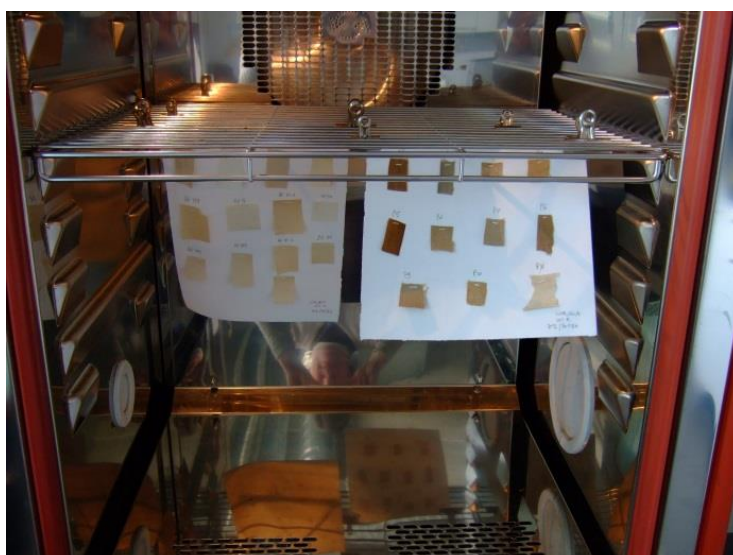


Figure 2-10. Some of the Islamic paper and canvases samples during one of the accelerated degradation experiments.

3. HYPERSPETRAL IMAGING: Characterization and Robustness

Heritage objects are well known for their compositional inhomogeneity due to the use of diverse raw materials and techniques in the production process (Trafela et al., 2007; Oriola et al., 2014). This caused the degradation processes to progress in heterogeneous manner with possibly significant local differences. Therefore, it is of importance to develop tools to collect spatially resolved quantitative chemical information from the heritage materials to represent such inhomogeneity and map the distribution of the chemical composition of a whole object (Strlič & Kolar, 2005; Kubik, 2007; Wang & Paliwal, 2007; Elmasry & Sun 2010; Oriola et al., 2014).

This chapter describes the Hyperspectral imaging technique starting with a background (Section 3.1) about the spectral imaging technique in general with a focus on the hyperspectral imaging system, its instrumentation, data acquisition parameters, important metrics, data analysis methods and usage in the field of heritage conservation.

Section 3.2 includes all the specifications of the current HSI system used in this research with a description of the data acquisition process and the required calibration process.

Section 3.3 focuses on the specifications of the NIR spectroscopic technique (as a spot analysis technique) used through the research for comparison with the HSI system in terms of performance, calibration and data analysis.

Section 3.4 describes the different data analysis techniques used in the analysis of the spectral data collected through the research using the HSI system and the NIR spectroscopy to build different calibration models. The section includes details about two types of calibration models; classification and regression models with the information about the used multivariate data analysis methods for pre-processing the spectral data, building the models and validating its accuracy.

Section 3.5 provides an overview about the HSI system through a series of evaluation test and experiments in terms of function, performance and potential limitations. This helps to understand the robustness of the system especially under different acquisition conditions.

Section 3.6 discusses the performance of the system and the significance of its influence on the cultural heritage applications.

3.1 Background

Spectral imaging technology including hyperspectral imaging (HSI) and multispectral imaging (MSI), has proven itself as a successful and useful technique in the field of heritage conservation by expanding spectroscopy (spot analysis technique) to the examination of an entire surface of an object as it records spectral and spatial information simultaneously. There is a debate about the definitions of MSI and HSI, so for the scope of this research focussing on HSI, MSI will be defined as the collection of spectral data cube of tens to hundreds spectral bands and more than hundreds bands for HSI (bandwidth < 10 nm) (Piccolo, 2014; Cucci et al., 2019). The technique is not new as it has

been used in other fields extensively since 1980s: remote sensing, medicine, forensics and food engineering. Over the last decade, spectral imaging systems have advanced with the evolution of the sensor technology which encouraged researchers to introduce it to the conservation field where it quickly resonated (Lu & Chen, 1999; Fischer & Kakoulli, 2006; Chang, 2007; Kubik, 2007; Elmasry & Sun, 2010; Liang, 2012).

The use of the technique has significantly advanced characterisation and mapping of original and added materials, investigation and monitoring of object condition (through detecting any material changes e.g. colour or deterioration signs), evaluation of conservation treatments, enhancements of obscured texts and accurate colour reproduction (Lu & Chen, 1999; Fischer & Kakoulli, 2006; Chang, 2007; Wang & Paliwal, 2007; Cséfalvayová et al., 2011; Liang, 2012; Dooley et al., 2013).

Since the use of HSI has increased in the field of cultural heritage, it is important to better understand the technique in terms of the instrumentation, the data acquisition parameters and the data resulted from the use of different instruments and methodologies to assure its accuracy and reliability in addition to its suitability to the purpose of the research.

Primarily, the technique is based on the interaction of light with matter similar to any spectroscopic technique, which can happen using any band in the electromagnetic spectrum. This nomenclature is usually used to represent groups of the wavelengths used: visible (VIS): 400–700 nm; near-infrared (NIR): 700–1000 nm; or visible and near infrared (VNIR): 400 – 1000 nm; short-wave infrared (SWIR): 1000–2500 nm; and mid-infrared (MWIR): 2500–15000 nm (Fischer & Kakoulli, 2006). In this research, the focus will be on the use of hyperspectral imaging in the SWIR region. The three-dimensional dataset (hypercube) resulting from HSI in the SWIR region contains two spatial dimensions and one spectral dimension, which can be used to study physical characteristics as well as chemical composition, i.e. the state of an object (Lawrence et al., 2003; Elmasry & Sun, 2010; Yao & Lewis, 2010). It has the ability to identify a large number of inorganic and organic materials which do not show discriminative features in the VNIR region, which facilitates the analysis of pigments and inks as an example (Fischer & Kakoulli, 2006; Chang, 2007).

Generally, HSI system consists of five main parts; lens, wavelength filtering or dispersion device (spectrograph) attached to a camera/2D detector interfaced with dedicated software that controls the acquisition process in addition to the illumination source (Chang, 2007; Elmasry & Sun, 2010).

The most important part is the imaging spectrograph as it is responsible for the collection of spectral and spatial signals through an entrance slit onto a detector (Elmasry & Sun, 2010). There are different ways to separate or filter wavelengths and each presenting advantages and disadvantages. The most common used ones are either based on filters; optical or tunable that are operated electronically such as liquid crystal tunable filter (LCTF), or based on prism-grating-prisms (PGP) (Fischer & Kakoulli, 2006; Chang, 2007).

For hyperspectral imaging, PGP dispersing devices are a better option due to their high diffraction efficiency and its ability to collect spectral information in one spatial dimension at a time while sampling (collecting data through time based on movement of either instrument parts or the object itself) the other spatial dimension (Aikio, 2001; Fischer & Kakouli, 2006). On the other hand, the other dispersing devices based on filtration are collecting the two spatial dimensions at once and sample the spectral dimension (collecting spectral data through time based on filtering) (Fischer & Kakouli, 2006; Chang, 2007).

Detectors have evolved over the last decade allowing for the collection of signals from different parts of the electromagnetic spectrum then convert them into electrical signals using different materials e.g. silicon (Si), aluminum gallium nitride (AlGaN) and indium gallium arsenide (InGaAs) for VIS, UV, IR ranges respectively (Norton, 2003; Rogalski, 2004; Fischer & Kakouli, 2006). For the Infrared range, a variety of materials such as platinum silicide (PtSi), indium antimonide (InSb), indium gallium arsenide (InGaAs) and mercury cadmium telluride (MCT/HgCdTe) are used for the development of the detectors with different characteristics for each in terms of quantum efficiency, spectral sensitivity, operating temperature and cost (Fischer & Kakouli, 2006; Chang, 2007). InGaAs and MCT detectors are the most widely used detectors for the SWIR region (Sizov, 2000; Rogalski & Chrzanowski, 2002; Fischer & Kakouli, 2006). MCT cameras have the ability to cover the whole infrared spectral range while InGaAs ones cover from 850 – 1700 nm. However, MCT cameras are only available with a 320 x 256 pixel array and considered very expensive (Fischer & Kakouli, 2006; Chang, 2007; Elmasry & Sun, 2010). The detector selection process depends on the needs of the research where the system is going to be used. It is a trade-off between the cost and the required performance. Detector performance influences the quality of the collected images and there are many parameters to be taken into account in the selection of a detector such as sensor size, pixel size, dynamic range, spectral response, dark and readout noise (Qin, 2010). Extensive development in the technology of detectors is ongoing leading to improvements and new capabilities becoming available in the market.

There are three common ways to collect a HSI hypercube: area, point, and line scanning (Chang, 2007; Elmasry & Sun, 2010). Area scanning (wavelength scanning) needs no motion as it is collecting images one wavelength after another with a fixed field of view. Point scanning (whiskbroom) measures the spectrum of one pixel at a time then the scanner or the sample moves to the next position to construct the hypercube data for the whole sample. Line scanning (pushbroom) is similar to the whiskbroom but it acquires the spectral information from a line (one row of pixels) of the sample at one time, rather than a single pixel then moves line by line using a moving stage or mirrors to collect the other spatial dimension (Lu & Chen, 1999; Elmasry & Sun, 2010; Wang et al., 2012; Nouri et al., 2013). Pushbroom scanners have many advantages over the other types as they have

higher scanning speed and lower overall exposure to light and heat as one line of the sample needs to be illuminated resulting in a better signal to noise ratio (due to the distribution of light on the scanned line and the higher light collected thus higher input signal) (Cucci, 2014). Also, they reduce non-uniformity of sampling due to the fixed spacing between sensors in the array collecting line pixels (Chang, 2007). However, they are expensive, work with a limited field of view and need processing and calibration to compensate for detector non-uniformity (Chang, 2007).

Recently, a new way to collect a hypercube has been developed, i.e. framing cameras or snapshot scanning. These acquire a whole cube at once including spectral and spatial data. No motion is needed, which increases platform stability in addition to high geometric fidelity. However, they are expensive and need more processing to correct for non-uniformity than the other detector arrays (Chang, 2007).

One of the main metrics in a HSI system is the resolution, both spatial and spectral resolution. The spatial resolution (optical resolution) can be defined as the ability to record the spatial detail required in an image and it can be represented by the total number of pixels (pixel resolution) (Cucci, 2014). It depends on the scanning distance, lens, aperture, wavelength and electronics (detector) (Polder & Van der Heijden, 2001; Chang, 2007; Qin, 2010; Macdonald, 2010; Cucci, 2014).

Spectral resolution is the power of a HSI system to resolve spectral details (Elmasry & Sun, 2010). This is determined by the size of the slit (entrance aperture in front of the spectrograph), the dispersing device and the detector (Elmasry & Sun, 2010) e.g. a small slit gives higher spectral resolution but less light to enter to spectrograph (Polder & Van der Heijden, 2001; Elmasry & Sun, 2010).

All detectors/sensors suffer from random errors and many noise sources such as readout noise (electronic noise in the detector generated while reading the charges and digitizing the signals in the CCD readout), shot (photon) noise (statistical variation in the number of photons incident on the detector) and dark current noise (statistical changes in the number of electrons thermally generated in a dark state by electron movements depending on sensor temperature) (Photometrics, 2010; B&W TEK, 2019). The total noise of a detector is the root square sum of all the noise sources (B&W TEK, 2019).

HSI systems also may suffer from pattern noise causing artefacts in the images e.g. the striping noise in pushbroom systems due to the non-uniformity corrections and sensitivity variations of the detector (Chang, 2007; Rasti et al., 2018)

In addition to instrumental noises, detectors also can be affected by atmospheric parameters such as temperature and bias voltage variations (Chang, 2007; Rasti et al., 2018)

Signal to noise ratio (SNR or S/N) is the ratio between the measured signal to the background noise in the system. The higher the ratio is, the less prominent the background noise is (Elmasry & Sun, 2010). It is the main metric for all random errors of the detector.

SNR is wavelength-dependent because of overall decreasing radiance towards longer wavelengths so should be defined per spectral channel (Chang, 2007; Elmasry & Sun, 2010). Pixel binning can be a way of raising the SNR through combining charge from neighbouring pixels of a CCD array during readout into a single superpixel but it lowers the spatial resolution (Photometrics, 2010).

Moreover, detectors usually have pixels (“bad pixels”) that are either giving a zero or full response (dark or white) in the collected data. These are commonly called dead/hot pixels which can be easily identified and replaced by an average response of their neighbour pixels (Arngren, 2011). Most manufacturers compensate for such pixels in the camera software itself during the calibration process.

Since a HSI system represents a combination of different optical, mechanical and electronic components, each with their own characteristics, calibration is a vital step before reliable data analysis can be attempted or even before acquiring the images to adjust the overall system performance (Yao & Lewis, 2010; Elmasry & Sun, 2010; Nouri et al., 2013). The main goals of the calibration process include wavelength alignment and assignment using a standard emission lamp as the light source, such as a mercury lamp (wavelength calibration). It also includes the conversion of the collected radiance to percentage/relative reflectance based on an image from a high reflectance standard (white, ~100% reflectance) and a dark current image (dark, ~0% reflectance). This is called radiometric reflectance calibration, which compensates for any drifts in the illumination or any background noise (Lawrence et al., 2003; Elmasry & Sun, 2010; Yao & Lewis, 2010). Other tests can be conducted for spatial and spectral calibration of the system, to assess the spectral and spatial resolution, evaluate system stability and reproducibility of the collected data especially under different acquisition conditions (Elmasry & Sun, 2010; Wang et al., 2012).

Hyperspectral imaging provides a large amount of data which requires the involvement of multivariate data analysis methods to view, interpret and analyse the complex hyper-cubes (Fischer & Kakouli, 2006; Cucci et al., 2011). Data processing methods include pre-processing methods in addition to quantitative and qualitative analysis methods. Pre-processing methods are used to remove backgrounds, reduce noise and dimensionality of the data. It includes spectral and spatial operations such as spectral and spatial filters, differentiation and smoothing. Normalization using methods such as mean centring and auto-scaling is also important after pre-processing the spectra to make sure all variables have comparable ranges and distributions. Then, quantitative and qualitative analysis methods are needed to help to extract meaningful information from the collected data especially in the SWIR region where the spectra contain thousands of C-H, O-H and N-H molecular bonds representing the chemical and physical features of the object under investigation (Elmasry & Sun, 2010). The quantitative analysis identifies the different components in the object and their spatial distribution via using correlation and

classification techniques while the qualitative analysis methods are used to build calibration models where spectral data are related to the actual quantitative measurements e.g. regression and classification methods (Elmasry & Sun, 2010). Once generating the calibration models, it can be used for the prediction of chemical properties for unknown samples which can be used to generate chemical maps to visualize how these predicted properties are distributed across a whole surface of a sample. However, applying the multivariate data analysis (MVA) methods should be done with care as if wrong method/parameter was selected, it may discard the useful information of the spectra e.g. selection of wrong window size when using Savitzky-Golay (SG) derivation filter may increase noise (if small) or eliminate important peaks (if big) (Vidal & Amigo, 2012).

All the developed models need to be validated to assess their quality and to assure better prediction. Cross-validation is the most selected method especially using leave-one-out method when dealing with small dataset to make better use of the data and to estimate the accuracy of a predictive model in an actual practice (Westerhuis et al., 2008; Lee et al., 2018). However, if possible and when larger datasets are available, it is more common for validation to use independent dataset (by splitting the dataset into calibration and validation sets) that have not been used for the calibration models. Leave-one-out cross-validation (LOOCV) is performed by constructing a validation set from the calibration set by leaving out each observation in turn.

Different metrics are available to assess the performance of the models such as the proportion/percentage of correctly identified samples (%correctness or success rate or classification accuracy) for the discrimination/classification methods and the root-mean-square error of cross-validation (RMSECV) and of prediction (RMSEP) for the regression models (Næs et al., 2002). RMSECV value is the cross validation error exists in the predicted values of the calibration so the lower it is, the smaller the error of the calibration is, which is the better. RMSEP is the expected uncertainty when predicting new unknown samples so also the lower its value, the better (Beebe et al., 1998).

Two linear regression plots with an R value (correlation coefficient) can be obtained when we plot the values of the calibration set estimated using the calibration model against the real measurements or plot the predictions of the independent validation set against their real measured values. R is a metric for the quality of the model showing how well prediction and reality match. It describes how distant from the regression line the scores are. In a perfect match all the scores would fall on the line and R would be 1, so the closer the R is to 1, the better the model is (and the closer the scores will be to the regression line).

Although the applications of spectral imaging in the field of cultural heritage have evolved and there is a significant increased need for the use of the technique with many historic materials, most of these applications/studies have focussed on qualitative examination due to different reasons, mainly the complexity of the materials and the need for standard reference materials for calibration. In 2011, the first 2D quantitative chemical map was

generated to visualize the degradation and material properties of iron gall ink on paper (Cséfalvayová et al., 2011). One of the main conclusions/recommendations of the study was to emphasize the need to study the influence of different measurement conditions and calibration parameters e.g. spectral distribution and intensity of the illuminant, or surface morphology on the quality of the collected data. Another issue raised was the calibration stability of the system. There is a clear need to focus on the metrology of quantitative chemical mapping generated using hyperspectral imaging. This is considered an active area of research that needs further studies (Fischer & Kakoulli, 2006; Dooley et al., 2013).

3.2 Hyperspectral Imaging (HSI) System: Current System

In this research, an HSI system consisting of a pushbroom (line) scanner from GILDEN Photonics Ltd was used to collect hyper-cubes in the short wavelength infrared (SWIR) range from 1000-2500 nm with a spectral resolution of 6.3 nm using a mirror scanning setup (Figure 3-1). The scanner consists of five main components: MCT camera with a cooled 2D detector array, spectrograph (PGP type), translational stage, illumination system based on halogen lighting and a computer (Figure 3-1). Each component has its own characteristics influencing the total accuracy of the system. It is based on a line-spectrograph (Specim (Finland), ImSpector N25E) with a 30- μm slit connected to a Mercury-Cadmium-Telluride (MCT) camera and an infrared imaging lens (either 30 or 56 mm). The spatial resolution is ~ 0.8 px/mm using 30 mm lens and ~ 2 px/mm using the 56 mm lens. The maximum frame rate of the camera is 100 fps with a fixed aperture F/2.0. The system has a 2D detector array which simultaneously acquires one spatial dimension (X-direction: 320 px) and one spectral dimension (256 wavelength channels) along the direction of the scanning stage (Y-direction). A linear translation stage controlled by electric motors designed by the manufacturer moves the view slot of the camera, allowing it to acquire the hyperspectral image and collect the second spatial dimension. It is able to accommodate objects with a maximum of A3 size ($\sim 30 \times 40$ cm). Based on the current setup where the camera and the scanning stage have fixed positions, the distance to object (Scan Distance) is fixed and equals 110 cm. The object is illuminated uniformly along the scan line by a line of tungsten halogen lamps (with an option to change light intensity between 250 and 500 W) at approx. 30° angle and at ~ 18 cm distance. The light source and part of the mirror system are controlled by electric motors to move back and forth along the Y-direction to spectrally scan the sample.

In all measurements, a spectral flattening filter was used in front of the lens. No binning of pixels was used and the gain of the camera was equal to 1 in the whole acquisition process. The room lights were off and windows were covered with black curtains during all scans to eliminate the background light impact. Two standard diffuse reflection bars (Spectralon) are fixed on the scanning stage in both directions to serve as a calibration standard during the experiments to calculate the reflectance and compensate for any variances (Figure 3-1).

Proprietary software (SpectraSENS) provided by the manufacturer was used to control the whole process of acquisition and some of the calibration processes. Some automated processing steps for image acquisition such as light compensation and radiometric reflectance calibration are available through the software, which can be avoided anytime to have maximum control of the entire imaging process. On the other hand, a series of Matlab code was developed to compensate for any missing process in the manufacturer software e.g. hot/dead pixel removal.

The HSI system allows for some acquisition parameters such as scan speed, exposure time and camera gain to be adjusted to tune the camera for optimal performance depending on the sample, light intensity, lens, etc. Table 3-1 and Table 3-2 depict the specifications of the system and the different acquisition parameter combinations used during the measurements in the research.

Table 3-1. Main specifications of the used HSI system provided by the manufacturer.

Camera	Specim SWIR – MCT Camera
Spectrograph	Specim ImSpector N25E
Spectral range	932.2 – 2530.5 nm
Spatial pixels/pixel dimension	320 px
Spectral channels	256
Spectral sampling	6.3 nm
Spatial resolution (FWHM)	rms spot radius < 15 μ m
Bit resolution	14 bit
Slit width	30 μ m
Effective slit length	9.6 mm
Frame rate	100 fps (maximum full frame)
Working/scan distance	1100 mm
Pixel size	30 x 30 μ m

Table 3-2. Hyperspectral imaging system acquisition parameters used in the research.

Lens (focal length)	30 mm	30 mm	56 mm
Exposure	5.8 ms	9.4 ms	7 ms
Scan speed	51.13 mm/s	51 mm/s	26.8 mm/s
Illumination Intensity	500 W	250 W	500 W
Aperture	F/2.0	F/2.0	F/4.0
FOV	18°		10°
Binning	None (1X1)		
Gain	1		
Spectral Range	1000-2500 nm		
Filter	Spectral Flattening Filter		
Saturation	10% - 90%		

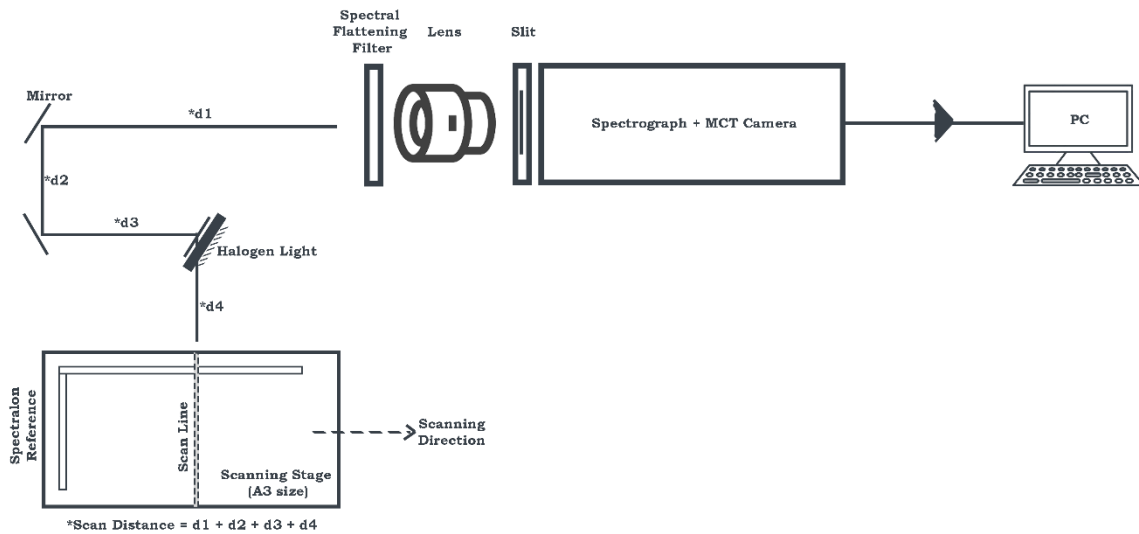
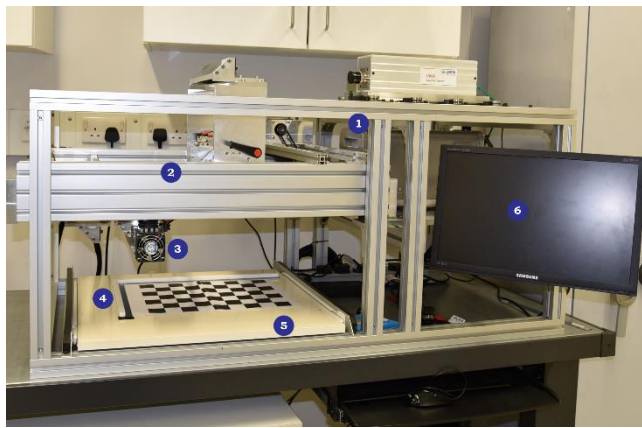


Figure 3-1. Gilden Photonics hyperspectral imaging system (Translational setup); Top: HSI system in situ and its components; 1: SWIR Camera, 2: Mirror system, 3: Halogen Light source, 4: Spectralon 99% calibration standard, 5: Scanning stage, 6: PC. Bottom: Diagram of the HSI system showing the scanning pipeline and system components.

The data acquisition process is described briefly as follows. The object is placed on the stage and lit by a line of halogen lamps as the light source. Lights were warmed-up for ~1 h (determined after several tests using calibration standards) before data acquisition to allow them to stabilize avoiding any variations (fake reflections and undesired artefacts) in the spectra collected. Scanning stage and camera are fixed and only the lights together with part of the mirror system move to acquire the required area.

The light signal reflected from the scanned line of the object travel to the lens through the mirrors system, and the light is collected and focused on the slit on the front end of the spectrograph. After dispersion, and mapping different wavelengths to their physical locations, image is formed on the 2D array detector with the spatial information of the scanned line recorded on the X direction and the spectral information on the Y direction orthogonal to the direction of the entrance slit. The collected data is transmitted to the computer for processing, display and storage. Then, the scanner moves to the next line and the process is repeated until the whole required area is scanned.

The scan speed needed for scanning the required area is calculated based on the selected system and acquisition parameters, e.g. slit width, lens focal length, detector size and scanning distance (Figure 3-1, Figure 3-2), following the equations below;

$$\text{Scan Speed (mm/s)} = \text{Frame Rate (fps)} * \text{Distance per Pixel/Spatial Resolution (mm/px)}$$

$$\text{Spatial Resolution} = (\text{Scanning Distance} * \text{Binning} * \text{Detector Width}) / \text{Lens Focal Length}$$

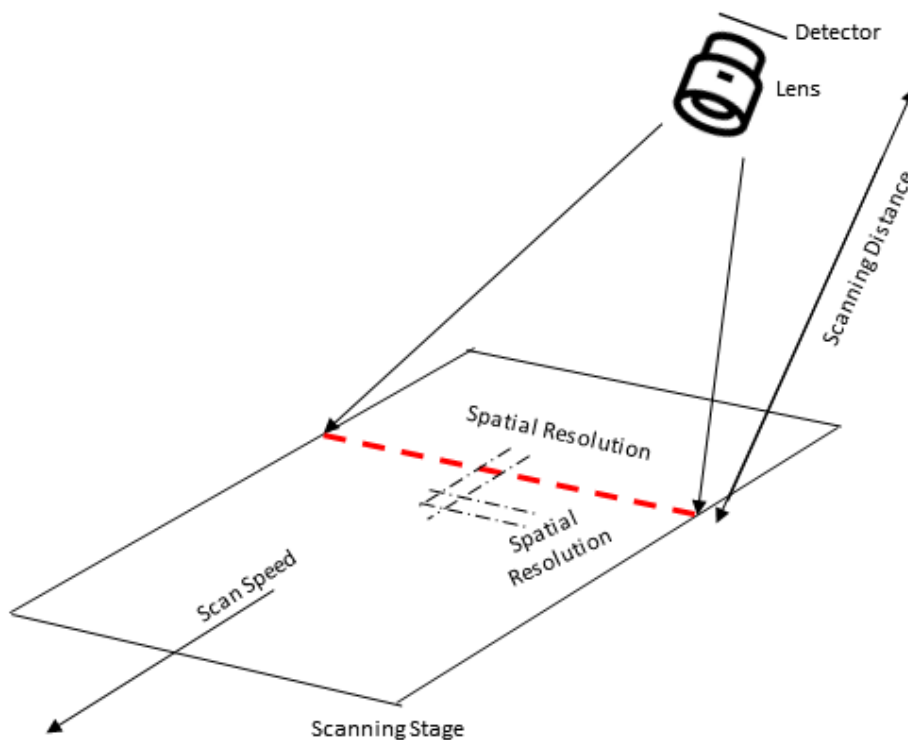


Figure 3-2. Diagram shows the different acquisition parameters required to calculate the scanning speed of the HSI system.

As an example, using the above equations and parameters described in Table 3-1 and Table 3-2, the scan speed required to scan 200 mm to ensure collecting of square pixels would be ~55 mm/s using the 30 mm lens. As the scanning distance, slit width and binning are constant for the current setup, the scan speed mainly depends on the focal length of the used lens.

As part of the scanning process, calibration is a critical step for hyperspectral imaging systems. It helps to diagnose instrumental errors and ensure measurement accuracy and reproducibility under different acquisition parameters (Lu & Chen, 1999; Burger & Geladi, 2005; ElMasry & Sun, 2010; Wang et al., 2012).

Spectral calibration was performed by the manufacturer (GILDEN Photonics Ltd) by acquiring a calibration lamp, i.e. Mercury then using SpectraSENS software the spectral peaks at different wavelengths and their pixel positions on the X-direction were identified and adjusted.

The image calibration (Normalization/flat-field correction) can be performed using the same software during the scanning process. SpectraSENS has an option to acquire the calibration tiles needed (99% diffuse reflectance standard (W) and camera dark current (D)) for the reflectance correction/calibration of the scanned hyper-cubes converting the raw data in A/D counts (I) into relative reflectance (R) (Akbari et al., 2011; ElMasry & Sun, 2010; Kubik, 2007; Lu & Chen, 1999; Qin, 2010).

The accuracy of the spectra can play an important role in the analysis of the hyperspectral imaging data and building calibration models so pre-processing steps are needed for the preparation of the data (Burger & Geladi, 2005; 2006). One of the main preparation steps is to remove hot/dead pixels from the spectra resulted from the sensor detector. Also, dust particles on any part of the optical system might be considered as dead pixels. Since SpectraSENS does not include this option (in the used version) to compensate for these pixels automatically, a Matlab code was developed to do an iterative pixel removal process for each hyperspectral image. The hot/dead pixel positions are detected, then replaced with an average response of its surrounding neighbours.

Before using the corrected data to build the calibration models either for classification or regression, different spectral pre-treatment methods can be applied to optimize the quality of calibration models. The methods help to remove unwanted variability in the spectra from scatter effects or from the instrumentation without affecting the chemical information e.g. derivatives, standardised normal variates (SNV) and multiplicative scatter correction (MSC) (Fearn, 2001). In addition to that, principal component analysis (PCA) can be used for data reduction or compression.

3.3 Near-Infrared Spectroscopy

For comparison purposes, a portable Labspec 5000 UV/VIS/NIR spectrometer (Analytical Spectral Devices, USA) in the spectral range 350-2500 nm (average of 200 scans) and operated in a diffuse reflection mode was used. Since the spectrometer includes three detectors to cover the whole spectral range, the spectral resolution is variant based on the used region. From 350 – 1000 nm, the resolution is 3 nm while the resolution is 10 nm from 1000 – 2500 nm. Measurements were carried out using a fibre optics probe with a spot diameter ~2 mm connected to a custom-made attachment to fix the measurement angle on 45°. 99% diffuse reflectance Spectralon standard (Labsphere, North Sutton, USA) and Whatman filter paper No. 1 sheets (Maidstone) were used as the background for measurements in areas that contained no inks or visible soiling and away from the margins for Islamic Paper samples and in areas that contained no dirt or stains for canvases samples. An average of three measurements was collected from each sample. Data then were pre-treated and analysed using multivariate data analysis methods to build calibration models for different chemical properties of the samples. A special software

(Indico Pro) developed by the manufacturer was used to acquire the measurements and Matlab was used for the analysis.

3.4 Data Analysis Techniques

Multivariate data analysis (MVA) methods were used to analyse the NIR spectra collected from the HSI system and the NIR spectrometer due to its complexity.

As mentioned above, spectral data were acquired in raw format then calibrated and converted into reflectance using Spectralon reference standard and dark current as calibration references in preparation for further data analysis.

Matlab (R2015b) with the aid of PLS toolbox library (EIGENVECTOR, 2019) was used to process spectra, develop calibration models and build chemical maps.

Different spectral pre-processing methods (Manley, 2014) were used to optimise the quality of calibration and compensate for any variations; Standard normal variate (SNV), Multiplicative scatter correction (MSC) and Savitzky-Golay (SG) filtering methods. This was followed by either a classification/discriminant method using linear discriminant analysis (LDA; Stuart, 2007; Blanco & Villarroya, 2002; Brereton, 2009; Miller & Miller, 2010; Brereton & Lloyd, 2014) or a regression method using partial least squares (PLS) regression method. Principal component analysis (PCA) was also used in some cases to reduce variances/noise and do some data compression without losing a significant amount of information especially before classification models (Blanco & Villarroya, 2002; Næs et al., 2002; Stuart, 2007; Miller & Miller, 2010).

3.4.1 Classification Models

For classification, linear discriminant analysis (LDA) was used for several historic materials with good results (Stuart, 2007; Blanco & Villarroya, 2002; Brereton, 2009; Miller & Miller, 2010; Brereton & Lloyd, 2014), therefore this method was used to estimate the presence of starch-sizing and surface polishing of Islamic paper based on spectral data from spectrometer and HSI system for comparison. Calibration and validation datasets were selected randomly.

Prior to the use of LDA technique to build the HSI models, either PCA or PLS technique was used on the spectra to reduce variability in the data then LDA was applied on the selected PC scores/factors. PCDA (PCA followed by LDA) can be considered as a semi-supervised classification method where PCA is an unsupervised method and LDA is a supervised one while PLSDA (PLS followed by LDA) is a supervised classification method (Blanco & Villarroya, 2002; Næs et al., 2002; Stuart, 2007; Miller & Miller, 2010; Barker, & Rayens, 2003; Westerhuis et al., 2008; Ruiz-Perez & Narasimhan, 2017; Lee et al., 2018). The classification method was used with the spectral data of all the samples in the Islamic paper calibration target.

The proportion of correctly identified samples (% Correctness / success rate/ classification accuracy) which is the number of the samples that were correctly classified into a group based on the model was used to validate the accuracy of the discrimination models. Details of the developed models are written in the following chapters to be in context.

3.4.2 Regression Models

PLS regression method (Næs et al., 2002; Brereton, 2009; Miller & Miller, 2010; Brereton & Lloyd, 2014) was used extensively to develop quantitative models to study different materials properties, e.g. European paper (Trafela et al., 2007; Strlič et al., 2007; SurveNIR), textiles (Richardson, 2009; Garside et al., 2011), parchment (Možir et al., 2011) and easel paintings (Oriola et al., 2014). Thus, the method was used to build calibration models for the determination of pH and cellulose DP for unknown samples using Islamic paper and canvas reference collections based on the spectral data collected from the calibration targets (described in Chapter 2; Section 2.1 and 2.2) and the actual measurements of the samples. Models were also built for the data collected from the spectrometer for comparison.

To check how good a developed model is, validation is an important step. Leave-one-out cross-validation (LOOCV) method was used to validate the results of the calibration models using the values of Root mean square error of the cross-validation (RMSECV) and the correlation coefficient (R_{cv}) (Næs et al., 2002) calculated based on the following equations;

$$RMSECV = \sqrt{\frac{\sum(y_i - y_i^{cv})^2}{n}}, \quad R_{cv} = \frac{\sum(y_i - y_m)(y_i^{cv} - y_m^{cv})}{\sqrt{\sum(y_i - y_m)^2 \sum(y_i^{cv} - y_m^{cv})^2}}$$

Where y_i contains the known values of DP/pH for each sample, y_i^{cv} contains the DP/pH values that are estimated by cross-validation and n is the total number of the samples used in the model. y_m and y_m^{cv} are the mean of the known and estimated DP/pH values respectively.

To be in context, the details of all the developed models are written in the following two chapters; 4 and 5 in relation to the materials under study; Islamic paper and painting canvas.

3.5 System Performance and Calibration: HSI Robustness

Recently, the use of HSI for the documentation and investigation of cultural heritage objects has increased, and there is a need for a better understanding of the instrumentation and the elements of data acquisition as this will help to understand the limitations and advantages of the system which consequently means better understanding of the accuracy and precision of the acquired data (MacDonald et al., 2017; Cucci et al., 2019).

Similar to all analytical and imaging systems, and since HSI is a comprehensive process that includes the selection of optical, electronic and mechanical elements, calibration steps are vital to characterize the overall system performance (Yao & Lewis, 2010; Elmasry & Sun, 2010; Nouri et al., 2013). Each component in the system has its own properties that affect the total accuracy of the system and the obtained results. Thus, it is important to optimize the various metrics to assess the quality of the acquired hypercube (Chang, 2007; Elmasry & Sun, 2010).

In this section, a series of evaluation tests and assessment methods are introduced to get a better understanding of the HSI system performance and its limitations taking into consideration the quality (in terms of accuracy and precision) of the collected spectral information. The focus will be on the main system properties that could affect the performance and require inspection or monitoring before or during the acquisition process.

This is to evaluate the system stability, accuracy and reproducibility of data, especially under different acquisition conditions (Lu & Chen, 1999; Burger & Geladi, 2005; Elmasry & Sun, 2010; Wang et al., 2012).

The following properties will be investigated: spectral/wavelength calibration (relationship between wavelength and pixel position), radiometric reflectance correction (relative reflectance), detector dead pixels, illumination and the spectral and spatial performance of the system, in addition to the stability of the instrument.

3.5.1 Detector Dead Pixels

It is common for all sensors/detectors to have some malfunctioning pixels (~1 %) that either have no response (dead/dark) or saturated response (hot/white). Although it is not possible to fix these hot/dead pixels, they can easily be identified by capturing a white reference or a dark current image and then replaced with the average response of its surrounding neighbours (Arngren, 2011). This percentage of pixels' loss is considered insignificant for image quality taking in consideration the manufacturer's recommended replacement point of the detector (3-5 %-pixel loss) and the study by Padgett and Kotre (2004) about assessment of image quality based on semi-quantitative and quantitative methods which proved that little difference is perceived up to 20 %-pixel loss.

It should be noted that dust particles might also be identified as bad pixels in the system by error, therefore the optical system need to be cleaned beforehand.

A Matlab function was developed to detect hot/dead pixels and compensate for its response since the proprietary software (SpectraSENS) does not have a built-in option for automatic compensation (in the version as used).

For the Specim SWIR camera sensor, around 40 dead pixels are identified (Figure 3-3). Figure 3-4 shows an example of a spectrum that have a spike representing one of the dead pixels at ~ 2077 nm.

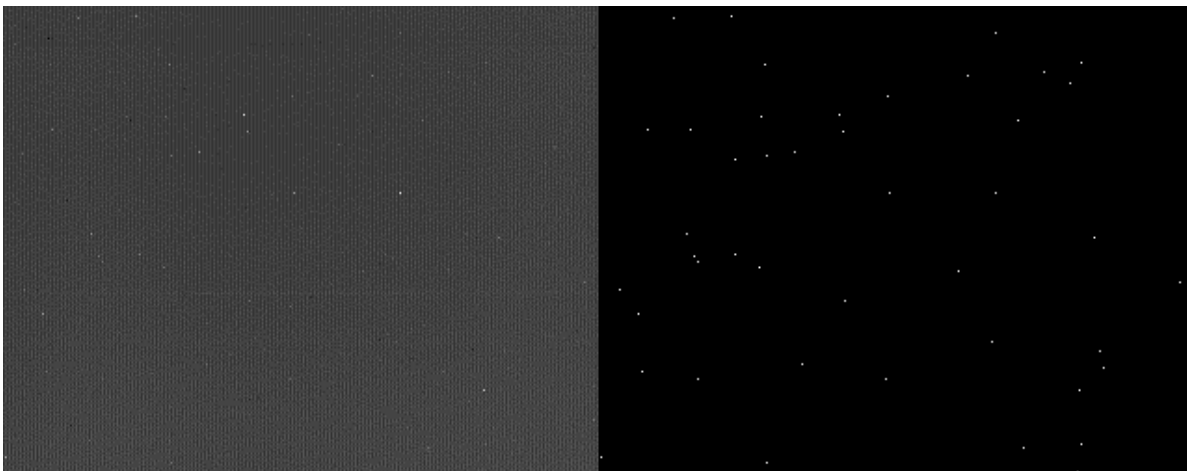


Figure 3-3. Sensor frame image (left) and same image after applying a threshold (right) identify some dead pixels. The image size is 320 (scan line) x 256 (bands).

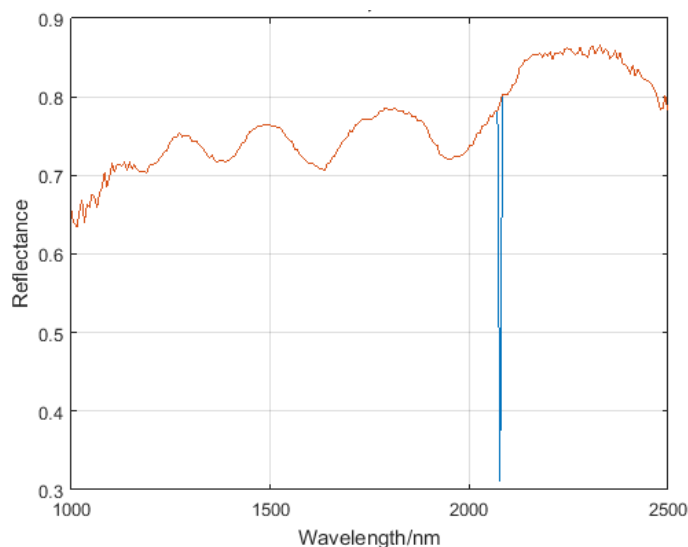


Figure 3-4. Reflectance spectra collected in the column 303 out of 320 of the scanning line demonstrating the effect of the dead pixel on spectra. The spike at around 2077 nm (band number 183) represents the position of the detected dead pixel. The figure shows the spectra before (blue) and after (red) removal of the dead pixel response by replacing it with the average response from its surrounding neighbours.

3.5.2 Radiometric Reflectance Calibration

It is a pixel-by-pixel process using the following formula to calculate the relative reflectance from the collected radiance based on reference images; white (~100% reflectance) and dark (0% reflectance) collected using the same spectral and spatial parameters used to collect the raw spectral image:

$$R = \frac{(I-D)}{(W-D)},$$

Where R is the relative reflectance image, I is the RAW image, D is the dark reference image and W is the white reference one (Lu & Chen, 1999; Kubik, 2007; Qin, 2010; Elmasry & Sun, 2010; Akbari et al., 2011).

The white reference image is collected from a 99% diffuse reflectance Spectralon standard tile fixed on the scanning stage while the dark current image is measured by keeping the camera shutter closed. The conversion can be done either using the spectraSENS software or Matlab to assure the full control over the acquisition process.

3.5.3 Spatial Performance

Spatial resolution (Optical resolution) can be expressed as the ability of the system to identify the desired spatial details of an object, e.g. the size of the smallest object that can be seen on the surface of the specimen by the sensor as a distinct object separate from its surroundings (Elmasry & Sun, 2010). Acquiring high spatial resolution data depends on the scanning distance (object to camera distance) and components of optical systems including lens, aperture... etc. (Polder & Van der Heijden, 2001; Chang, 2007; Qin, 2010; Macdonald, 2010; Cucci, 2014; Cucci et al., 2019).

The HSI system has limited control of spatial resolution as it has a fixed working distance due to the used setup, so only the interchangeable lenses (30 and 56 mm) can increase/decrease the resolution.

There are various methods that can be used to assess the spatial resolution of a system such as Modulation Transfer Function (MTF) method (MacDonald, 2010) and the calculation of observed line pairs per millimeter (lp/mm) (Nouri et al., 2013). However, in this study, for simplicity and unavailability of standard resolution targets in the time of research, I used three methods for the assessment: visual assessment of image details, plot of vertical profiles and calculating sample density. The first method is very direct by looking at the quality of the images in resolving details of an object, e.g. how clearly the lines can be seen and separated (Figure 3-5, Figure 3-6, Figure 3-7). The second one is similar to the MTF calculations with spatial frequencies by plotting the vertical profiles for an area with lines from a target that has line pairs to determine the contrast between lines and spaces. The higher the resolution is, the higher is the distance between peaks and valleys in the vertical profile plot, which means better ability to differentiate between lines and spaces (Figure 3-8). Due to availability, the line patterns from a test panel painted with a medieval Tuscan technique created in an earlier study (Vitorino, 2014) as a built-in resolution target was used to assess the resolution using the described methods (Figure 3-5). Although the target is not a standard, it was made by conservators to be part of a round robin test (RRT) with more than 10 institutions and laboratories collaborating in the COST-Action TD 1201 Colour and Space in Cultural Heritage (COSCH) to highlight the performances of the different imaging devices and better understand the instrumentation, elements of data acquisition, and their effects on the accuracy and reliability of the data. The target was scanned using the HSI system using the two lenses and the measurements were assessed relative to the provided measurements from the RRT. As seen in the Figures, spatial resolution positively correlates with the lens focal length.

The third method is a quantitative way to assess the resolution by calculating the sampling density (the number of pixels per unit distance when converting from an analog signal to digital). It can be calculated by dividing the number of pixels in a known distance by that distance and is expressed as pixels (px) /mm, so increasing the pixel size resulting in smaller sampling density. It is limited by the number of pixels in the recorded image, so zooming or magnification would allow to scan smaller physical distance, reducing the pixel size, which means higher spatial resolution taking into consideration the diffraction on the used lenses and avoiding over- or under- sampling which would lead to either losing information from the image or adding aliasing artifacts (SVI, n.d.).

HSI system has a sampling density of 0.83 and 1.85 px/mm when using the 30 and 56 mm lenses respectively. Although both lenses have the ability to resolve the 13 lines (2 mm-drawn on the gypsum background in the first part of the panel), the resolution is considered not high enough using the 30 mm lens with a slight improvement using the 56 mm lens. This is considered the smallest detail that the system with the used setup can resolve as the smallest detail of interest cannot be smaller than the pixel size (Kumar, 2005) taking into consideration that the working distance cannot be changed. Although higher spatial resolution for the system is preferable (~ 5-10 px/mm) as the system would not be able to detect fine spatial details but still with this spatial resolution accompanied with a reasonable spectral resolution would be enough for material characterization and mapping applications which is the purpose of the research.

Made by Elena Prandi & Marina Ginanni
(Restoration Laboratories of the Polo Museale Toscana)

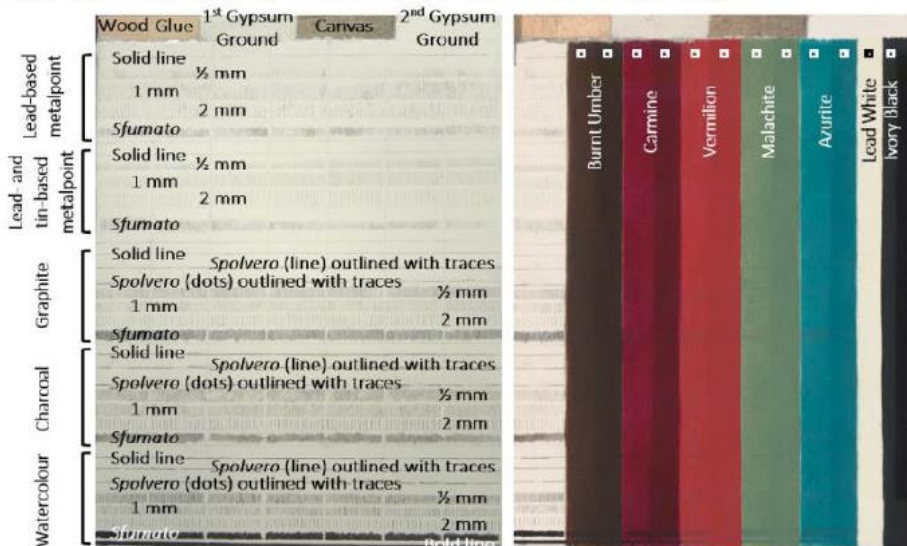


Figure 3-5. The painted test panel target from Vitorino’s work (2014) showing the line patterns used as resolution target.

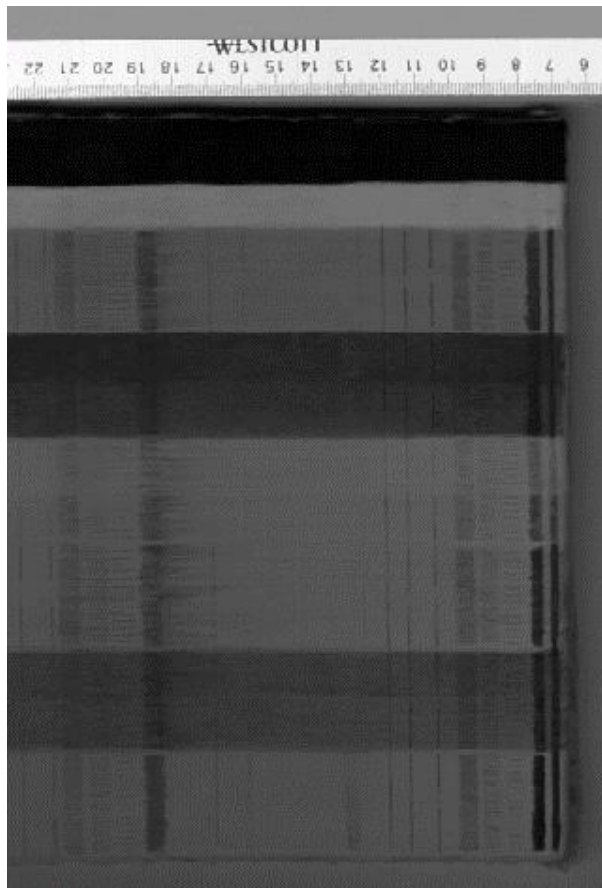


Figure 3-6. A grey image at 1486 nm for part of the test panel (resolution target from Vitorino's work (2014)) scanned with the HSI system using the 56 mm lens.

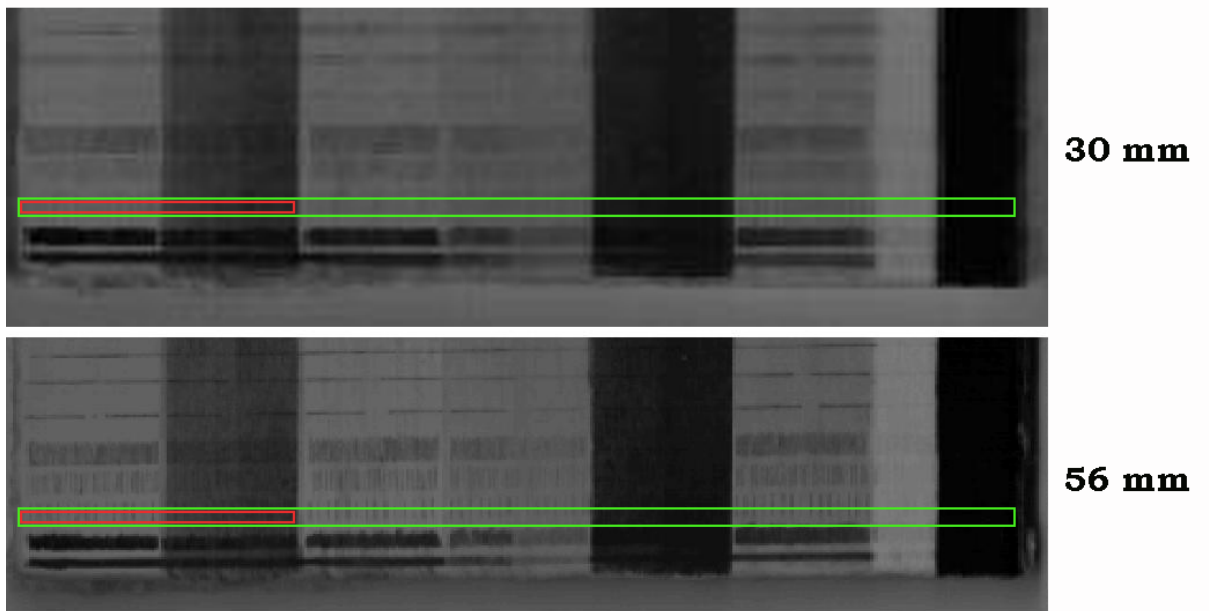
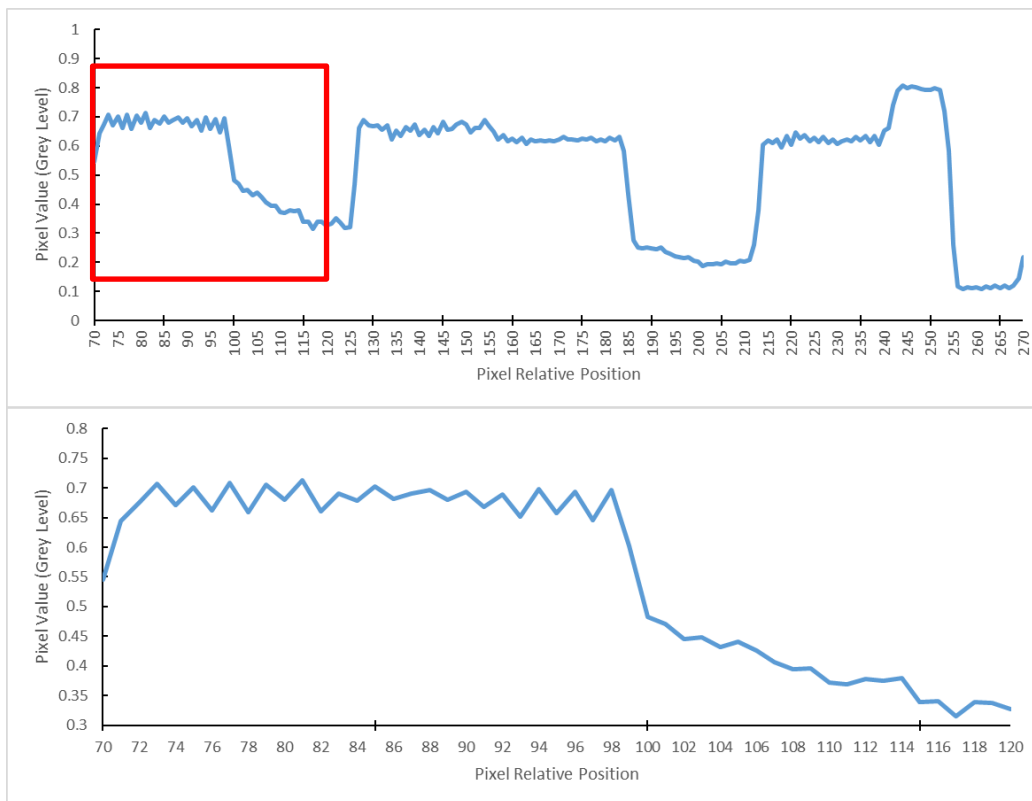
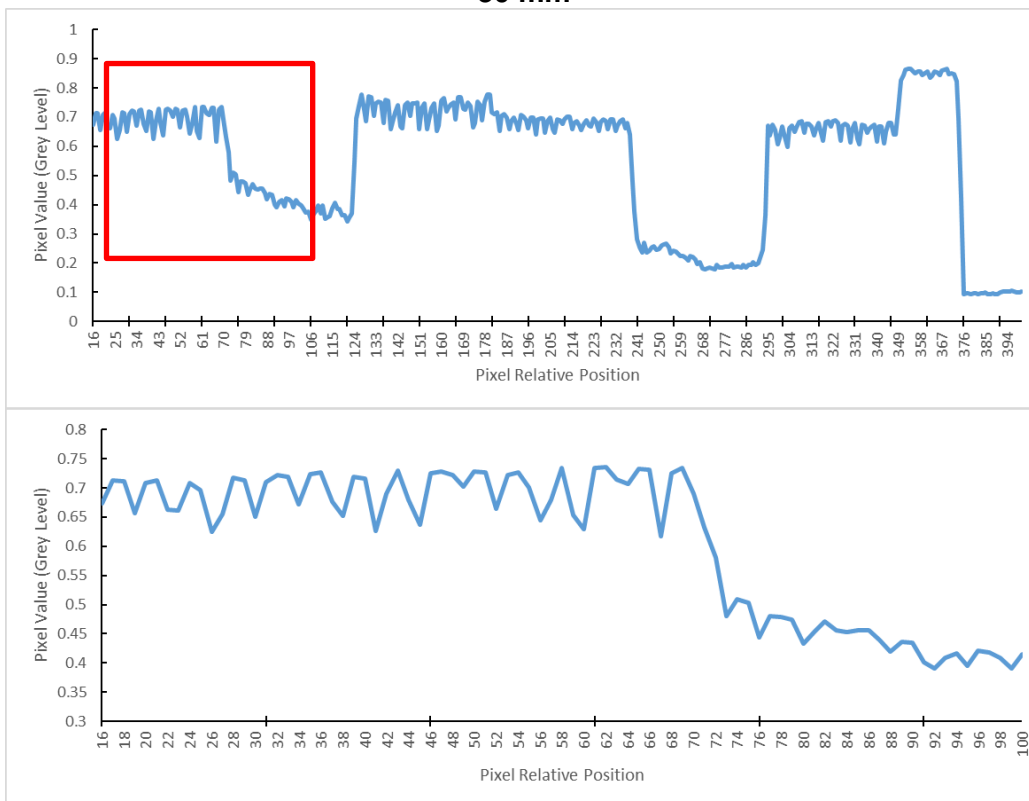


Figure 3-7. Visual assessment of how well the details of the line patterns of the resolution target (Vitorino's test panel (2014)) can be resolved to assess the spatial resolution of the HSI system. The figure shows two grey images at 1240 nm scanned using the HSI system by 30 mm lens (top) and 56 mm lens (bottom). The green and red rectangles represent selected areas of a scale of 2 mm of the watercolour line patterns.



30 mm



56 mm

Figure 3-8. Plots of vertical profiles of watercolor lines (2 mm) from the resolution target (Vitorino’s test panel (2014) – red and green rectangles in Figure 3-7) to assess the spatial resolution of the HSI system using two lenses 30 mm (top) and 56 mm (bottom).

3.5.4 Spectral Performance

The spectral performance of the HSI system depends on the calibration of many parameters such as spectral resolution, wavelength accuracy, stability and signal to noise

ratio (SNR), among others (Xie et al., 2016). Although most of these parameters are already calibrated and tested by the manufacturer, integrating all into one system would change the overall performance in addition to the effect of temperature and vibration during the use of the system that could lead to variations and shifts in the performance (Xie et al., 2016). Thus, it is important to assess most of these parameters before putting the system into use.

Spectral Resolution

Spectral resolution has an important influence on the characterization and mapping of materials (Picollo, 2014). It indicates how well the HSI system can resolve the spectral details (Elmasry & Sun, 2010) e.g. discriminate two adjacent peaks. Based on how narrow or wide the spectral features of a material are, an HSI system with a specific spectral resolution can be assessed if it is suitable to investigate such material or not e.g. the spectral resolution should be high enough to resolve the spectral bands associated with the material to be measured (Xie et al., 2016).

Some factors affect the spectral resolution such as the detector, the slit and the diffraction grating (B&W TEK, 2016). There is a linear correlation between the slit size and the spectral resolution where small slit gives higher resolution, taking into account that the amount of light onto the spectrograph is negatively correlated with the slit size (Polder & Van der Heijden, 2001; Elmasry & Sun, 2010). On the other hand, the detector decides on the maximum size and how many discrete points the spectrum can be digitized to while the grating is related to the total wavelength range of the spectrophotometer (B&W TEK, 2016).

Thus, I attempted to calculate the spectral resolution of the system (as used). The resolution is determined by the full width at half maximum bandwidth (FWHM) of the peak of interest (width of the spectral response function at one-half of its peak height (Min et al., 2008)). Thus, the calculated spectral resolution of the system is around 15 nm using a 30 μm slit and 320 pixel detector in the wavelength range from 932.2 – 2530.5 nm. Alternatively, a light source with a well-known spectral features can be measured, then the FWHM (spectral resolution) can be calculated for its spectra (Xie et al., 2016). Despite the importance of the spectral resolution as one of the main characteristics of HSI system, some studies were conducted about its effect on the quantitative calibration accuracy which revealed its less importance compared to other parameters such as SNR (Xie et al., 2016; Armstrong et al., 2006; Kolomiets & Siesler, 2004; Wang et al., 2015).

Wavelength accuracy and precision (repeatability and reproducibility)

One of the main calibration steps of any HSI system is the wavelength calibration where images of spectrally well-known light sources such as Mercury Argon (HgAr) lamp, positioned in front of the spectrograph lens, are acquired, then the pixel positions are correlated with the signature peaks at specific wavelengths using linear regression

(Specim, 2008; ElMasry & Sun, 2010). This step is usually performed by the manufacturer, as is the case of the HSI system by Gilden Photonics Ltd. to improve the wavelength accuracy of the system.

Wavelength accuracy is the deviation from known peak positions of a standard target. It measures the ability of the system to reproduce spectral peaks at the true measured wavelengths. It can be assessed by the difference between the wavelengths of characteristic peaks of a wavelength standard target measured by the system and the manufacturer's equivalent values (Xie et al., 2016; Workman et al., 2014).

Wavelength precision is related to wavelength accuracy where it measures the stability of the wavelength measurement and the ability of the system to return to the same wavelength in every measurement. It can be determined by calculating the standard deviation of each characteristic peak position of a replicate spectra collected from the same wavelength standard target (Workman et al., 2014).

For the assessment of these two parameters for the HSI system, two wavelength standards; Spectralon Multi-Component wavelength target (Spectralon) and SphereOptics Zenith Polymer Wavelength calibration standard (Zenith) were selected due to their standard spectral characteristics. The main peaks of each target (Table 3-3) were extracted from the average spectra of the collected data using the HSI system (Figure 3-9) then compared to the manufacturer data (Figure 3-10). The HSI spectrum includes most of the peaks given by the manufacturer, but with small variation in their position (wavelength accuracy is $\pm 1-2$ nm for Spectralon target and up to ± 5 nm for Zenith target) while in some cases the spectral features could not be resolved e.g. the characteristic peak in the Spectralon target at 1476 – 1478 nm that could not be seen in the HSI spectra. This may be due to the difference in the spectral sampling between instruments. The manufacturer's data with the high spectral sampling, allowing to resolve very fine details (spectral features) which seems not the case for the HSI system with spectral sampling of 6.3 nm.

In Figure 3-11, the comparison between the spectral data of the Zenith standard scanned by the HSI system and the manufacturer's data demonstrates the difference in the reflectance intensity between both but resolves most of the characteristic peaks in more or less same positions. Unfortunately, I did not have the manufacturer's full spectrum of the Spectralon target to be able to compare it with the spectra of the HSI system to confirm the obtained results. However, I measured the spectralon target with the NIR Labspec-5000 spectrometer and used the measured spectra, as a reference for comparison of the main characteristic peaks (Table 3-4). The two instruments are performing in a similar way, having almost the same accuracy (± 2 nm for spectrometer spectrum) and same missing

peak at 1476-1478 nm compared to the manufacturer data (Figure 3-12). It also can be noticed the difference in the reflectance intensity between the two instruments.

Variations/errors in the wavelength that are not on the spectrum edges and keeping the main structure of the spectrum with no changes would not have a significant influence on the performance of the calibration models but high accuracy is very important if models will be transferred between instruments (Fearn, 2001; Xie et al., 2016).

Table 3-3. Main characteristic peaks in two wavelength standard targets (Spectralon and Zenith) provided by the manufacturer. The peaks are shown in nm.

Spectralon Multi-Component Wavelength (Spectralon)	SphereOptics Zenith Polymer Wavelength (Zenith)
1009.5 – 1013.5	1119.3
1134.1 – 1138.1	1299.9
1198.6 – 1202.6	1471.6
1230.5 – 1234.5	1535.1
1299.3 – 1303.3	1684.3
1470 – 1474	1919
1476 – 1478	
1682 – 1686	
1932.5 – 1936.5	

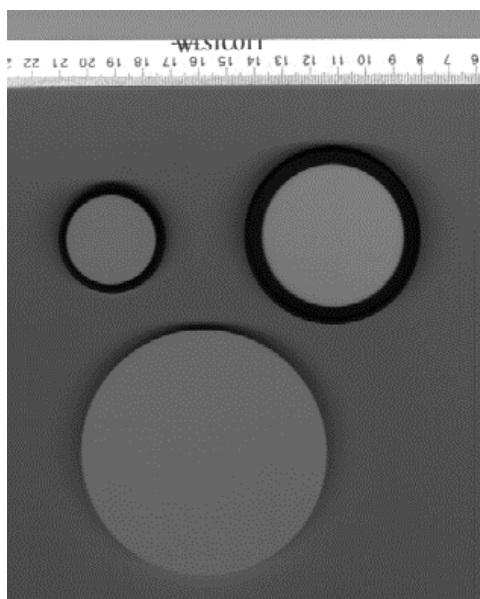


Figure 3-9. A grey image (1404 nm) for the wavelength standard targets (Spectralon (top left) and Zenith (bottom)) scanned with the HSI system using the 56-mm lens. The 99% diffuse reflectance Fluorilon standard from Avian Technologies LLC (top right) was scanned as well.

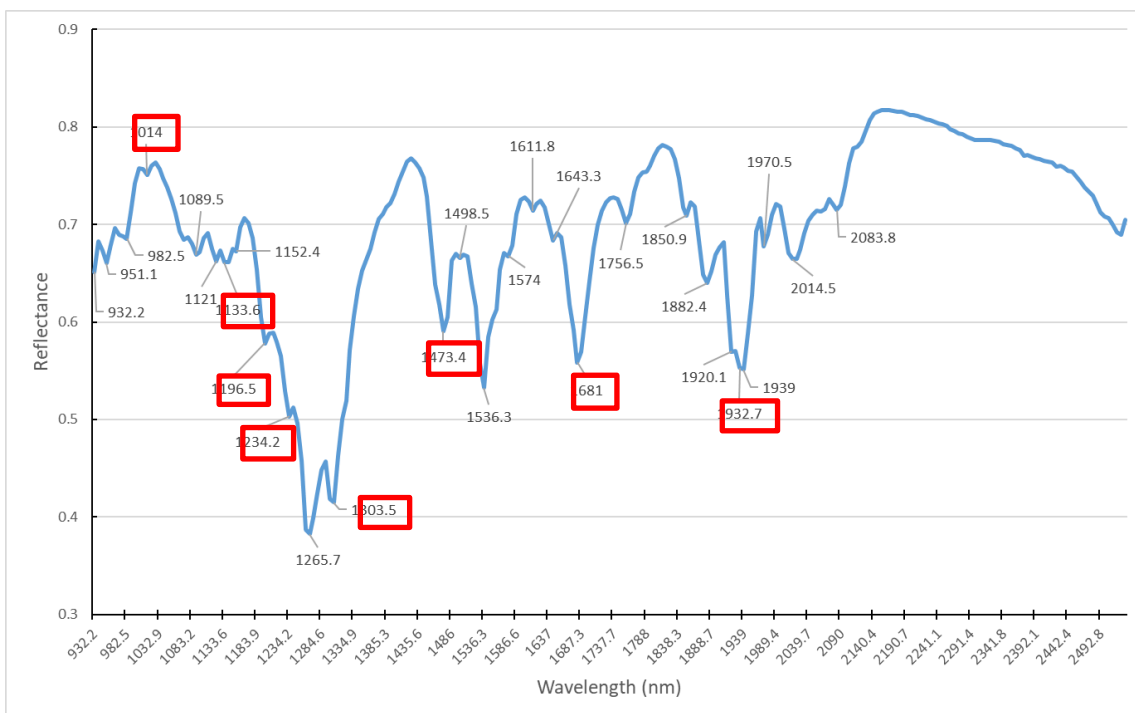
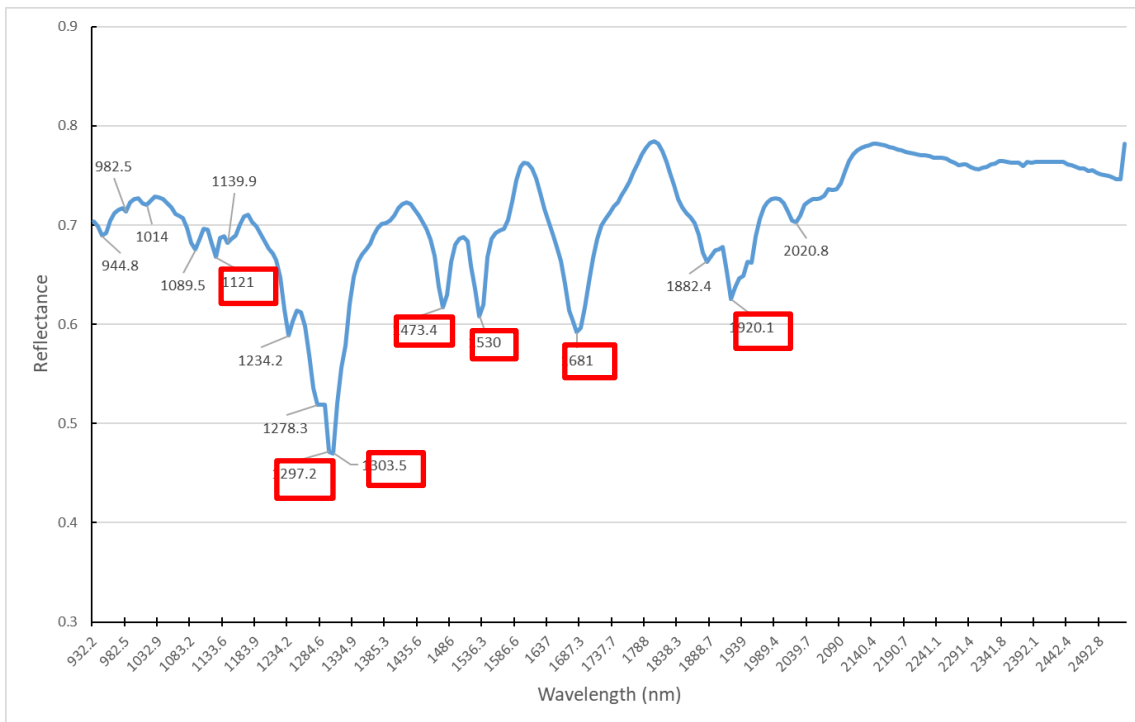


Figure 3-10. The average spectra of the two wavelength standard targets; Zenith (top) and Spectralon (bottom) scanned with the HSI system demonstrating the main characteristic peaks in both spectra. The red boxes show the characteristic relative to the provided manufacturer peaks shown in **Table 3-3**.

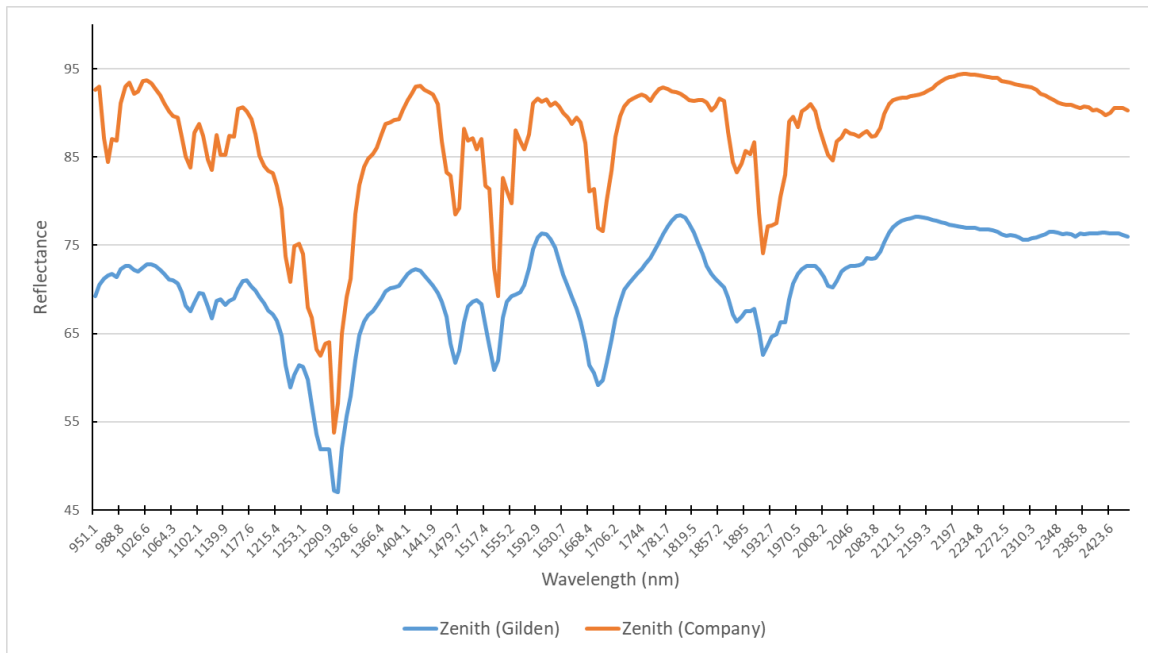


Figure 3-11. Comparison between an average reflectance spectrum of Zenith standard scanned with the HSI system (Gilden in blue) and the provided spectra from the manufacturer (in orange).

Table 3-4. The main peaks from the average spectra of the Spectralon standard collected using the HSI system and NIR LabSpec-5000 spectrometer corresponding to the provided data from the manufacturer.

Manufacturer	1009.5 – 1013.5	1134.1 – 1138.1	1198.6 – 1202.6	1230.5 – 1234.5	1299.3 – 1303.3	1470 – 1474	1682 – 1686	1932.5 – 1936.5
HSI	1014	1133.6	1196.5	1234.2	1303.5	1473.4	1681	1932.7
Labspec	1012	1135	1196	1236	1301	1475	1684	1936

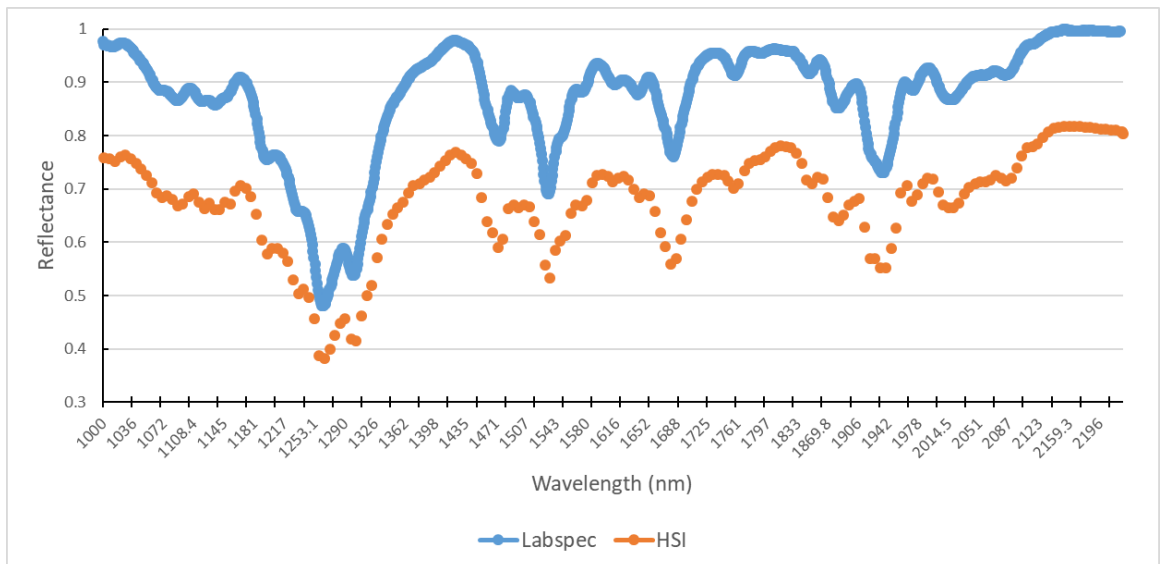


Figure 3-12. Comparison between average reflectance spectra of Spectralon target collected by the NIR LabSpec-5000 spectrometer and the HSI system.

Moreover, wavelength repeatability/precision was calculated for the HSI system using the Spectralon target by scanning the target in the same position at the same acquisition parameters for 3 times, then calculate the coefficient of variation (CoV) of three average

spectra of the target. Similarly, the CoV was calculated for three average spectra of the target collected using the Labspec-5000 spectrometer for comparison.

The wavelength precision of both instruments gave almost the same CoV (=0.2%) indicating the good repeatability of the HSI system.

Stability (Instrumental Uncertainty)

Many external factors such as temperature, time and the environment in general can affect the acquisition process stability and HSI system components, e.g. light source, optical components, electronics... etc., so monitoring of such effects is important in addition to the correction process using the white reference and dark current to compensate for any drift. Moreover, the whole system needs to be warmed up for some time to stabilize all of its components ahead to any acquisition session. Stability of the system (same performance over time) correlates to its repeatability and reproducibility (Min et al., 2008; Xie et al., 2016).

Thus, based on this correlation, I tried to assess the stability of the HSI system by calculating the CoV of repeated average spectra obtained from the Islamic paper calibration target after being scanned for several times using same acquisition conditions. After the system was warmed up for ~ 1 h, the IP calibration target was scanned three times in the same location with a 5 min gap between each scan (Figure 3-13). The mean and variance of each wavelength in the spectrum of the whole target from each scan are calculated then the CoV is estimated using the average variance and mean which gave 0.49%. There are no variations between the measurements except for some random noise on the edges indicating the good repeatability and stability of the system, especially if we put the results in context with the wavelength precision.

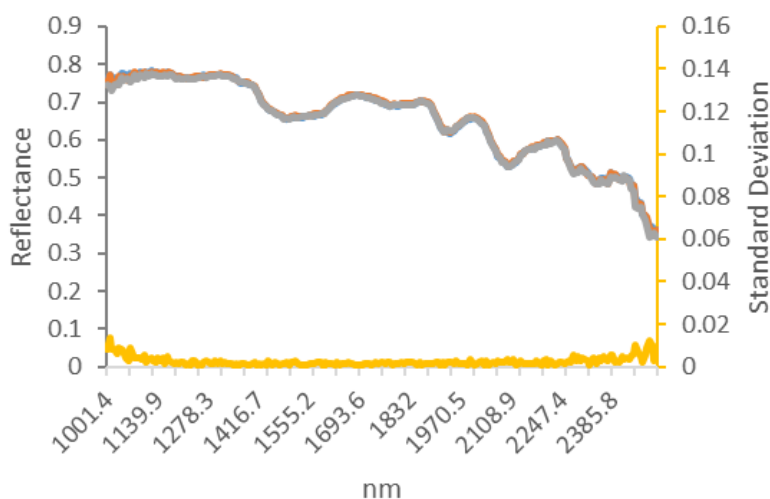


Figure 3-13. Three mean reflectance spectra of data collected from the IP calibration target using the HSI system in addition to their standard deviation to visualize any variability in the measurements.

3.5.5 Illumination

Illumination in any imaging system has a great influence on its performance and on the reliability of the collected data (Fischer & Kakoulli, 2006; Qin, 2010).

There is always a trade-off between the intensity of illumination and the exposure/integration time needed to achieve the optimal conditions for a measurement, which additionally depends on the sensitivity of the object under investigation, e.g. scanning a light/heat sensitive material such as parchment would require either being exposed to the minimum light intensity or scanned at a very fast exposure time or both in some cases. Therefore, both modes of illumination (250 and 500 W) were tested to evaluate their effect on the collected spectra.

After warming up the system for ~1 h, spectral measurements of the Islamic paper calibration target (IP target) were collected under both intensities. For the acquisition parameters for each intensity, see Set 1 and Set 2 in Table 3-5.

The difference of the average spectra of the whole target from both scans is showing no variation except for random noise at the edges (Figure 3-14). A slight peak in the range 1900 - 1950 nm was observed, which could be the effect of changes in the relative humidity from one scan to another (moisture/water peak). I also attempted to calculate the CoV of the average spectra from both scans with and without the noisy edges to check how significant these variations are which gave 1% and 0.6% respectively. The results show reasonable improvement due to excluding the noisy edges which would be a factor to take into account while doing further analysis or modelling.

Table 3-5. Acquisition parameters of HSI system used in the experiments of this section.

	Set 1	Set 2	Set 3
Lens (Focal Length)	30 mm	30 mm	56 mm
Exposure	6 ms	9.4 ms	7 ms
Scan speed	54.9 mm/s	51 mm/s	29 mm/s
Illumination intensity	500 W	250 W	500 W
Aperture	F/2.0	F/2.0	F/4.0
Binning	None (1x1)		
Gain	1		
Spectral Range	1000-2500 nm		

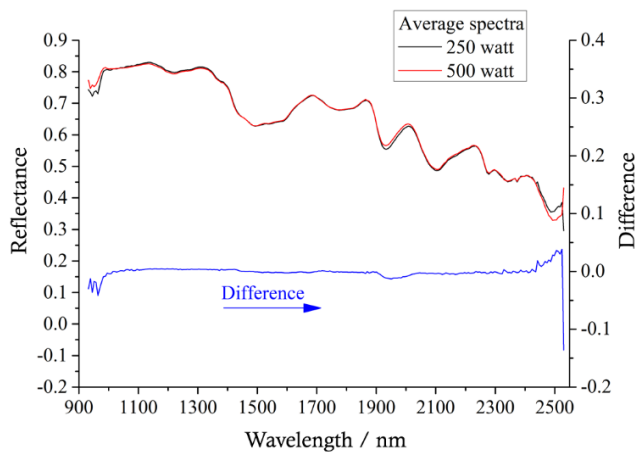


Figure 3-14. Average reflectance spectra and its difference, collected from the Islamic paper target using HSI scanner using different acquisition parameters; two illumination intensities: 250 and 500 W to spot any differences.

It is vital that the illumination is stable during image acquisition and across the scanning stage. If it is unstable or drifts over a short time, then this will induce fake reflections and undesired artefacts in the collected spectral data. Many parameters can affect the stability of the illumination such as background light from surrounding lights (e.g. room lightings) or reflections from surrounding objects in the room, any defects in the associated power supply and the lamps themselves. In this research, all experiments were done in a dark room to avoid any influence from the surrounding environment on the quality of the spectra. Moreover, the lights were left for 1 h before any acquisition session to warm up and stabilize. Also, spectral measurements of the reference standards were checked and collected in each scan for the correction process.

I conducted an experiment to test the variability in the illumination of the HSI system over the scanning stage. Therefore, I divided the scanning stage into 9 different positions using an A3 paper (Figure 3-15) to be as a guide for the collected measurements. The 3x3 division was selected as 2x2 would not be enough to spot any patterns in case of variations in the measurements and 4x4 or more would be time consuming regarding calculations.

The illumination variations were evaluated based on the lux value measured by the light meter (GL Spectics 1.0 Touch). The measurements were collected as an average of three measurements per position during scanning after warming up the light for 1 h (Figure 3-16). The detection of the position of the meter sensor was verified using the live camera in the SpectraSENS software to assure the accuracy of the measurements (Figure 3-16). Measurements were also collected from the fixed white tile from different points to check the variations over the tile itself, taking into consideration that the meter is higher by 1 cm while taking these measurements. The results (Table 3-6, Table 3-7) show that there are some variations in the illumination over the scanning stage with $11793 \text{ lux} \pm 3.13\%$ (RSD). It seems that the intensity of the illumination tends to be higher along the middle of the

stage and there is a noticeable decreasing trend from top to bottom that needs further investigation to explain its causes.

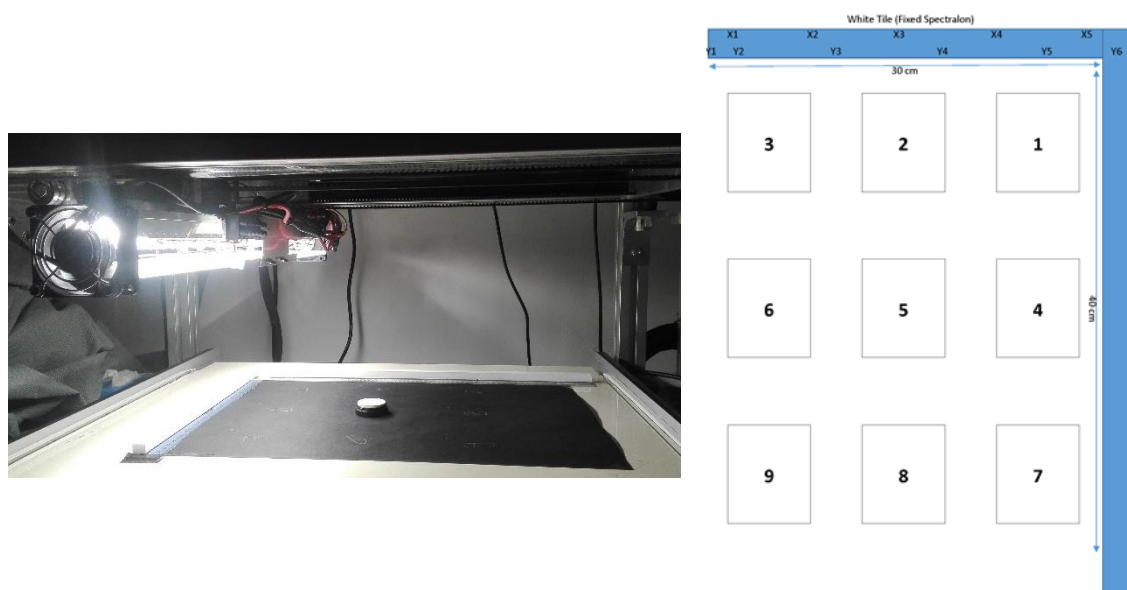


Figure 3-15. Design of the scanning Stage divided into 9 positions using A3 paper (right) and scanning of the Spectralon multi-component wavelength standard in position 5 (left).

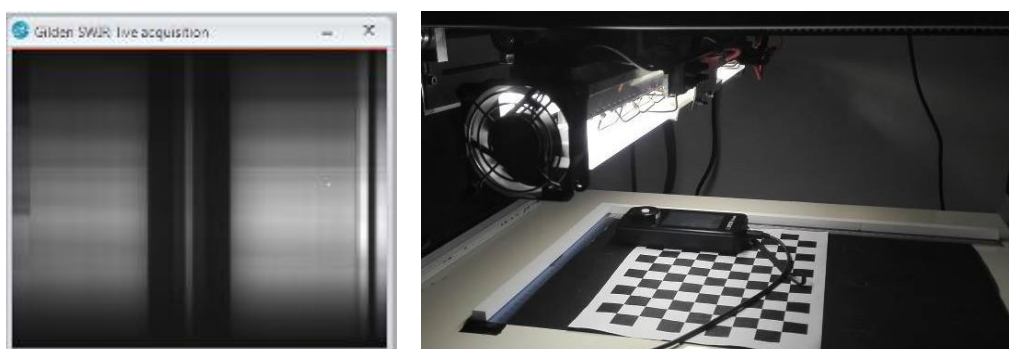


Figure 3-16. Collection of lux measurements using a light meter (GL Spectics 1.0 Touch) over the HSI scanning stage from different positions (right). Live view from the HSI software showing the meter sensor to verify its location on the stage (right).

Table 3-6. Lux measurements collected using GL Spectis 1.0 Touch from 9 positions over the HSI scanning stage. M1, M2 and M3 represent three measurements per position. Average (Avg), standard deviation (SD) and relative standard deviation (RSD) are calculated for each position and overall the stage.

	1	2	3	4	5	6	7	8	9
M1	11800	12326	11156	11996	12258	11444	11841	11939	11431
M2	11796	12319	11141	11991	12256	11436	11836	11923	11426
M3	11792	12313	11138	11986	12251	11435	11829	11917	11422
Avg	11796	12319	11145	11991	12255	11438	11835	11926	11426
SD	3.27	5.31	7.87	4.08	2.94	4.03	4.92	9.29	3.68
RSD	0.03%	0.04%	0.07%	0.03%	0.02%	0.04%	0.04%	0.08%	0.03%

Overall Average (Avg) = 11793

Overall Standard deviation (SD) = 370

Overall Relative standard deviation (RSD) = 3.13% (11793 ± 3.13%)

Table 3-7. Distribution of the average lux values per each position on the HSI scanning stage in addition to the average lux over the white tile (appears in blue).

12437			
11145	12320	11796	
11438	12255	11991	
11426	11926	11836	

Moreover, I attempted to conduct an experiment to investigate the effect of the detected lux variations on the quality of the spectra collected from the different positions on the stage. Using Spectralon multi-component wavelength Target (Height=1.3 cm), spectral measurements of the target were collected after placing it in different 9 positions over the scanning stage (Figure 3-15). The data collected was then processed and an average spectrum for each position was extracted from almost the same area of the target with the same size. The 9 average spectra were compared to each other (Figure 3-17) to show any variations. As seen in the figure, there are some differences between the 9 average spectra which is probably due to the variations noticed in the illumination as the spectral variations have similar trend from the top to the bottom of the scanning stage where the estimated CoV of each position increases from 0.4% to 9.5%. Using the 9 average spectra, CoV was estimated to assess the significance of the observed variations which gave 7.7%. This is relatively significant compared to the previous results, e.g. stability CoV, which highlights the need for further investigation of the causes of these variations and possible methods to correct or reduce it.

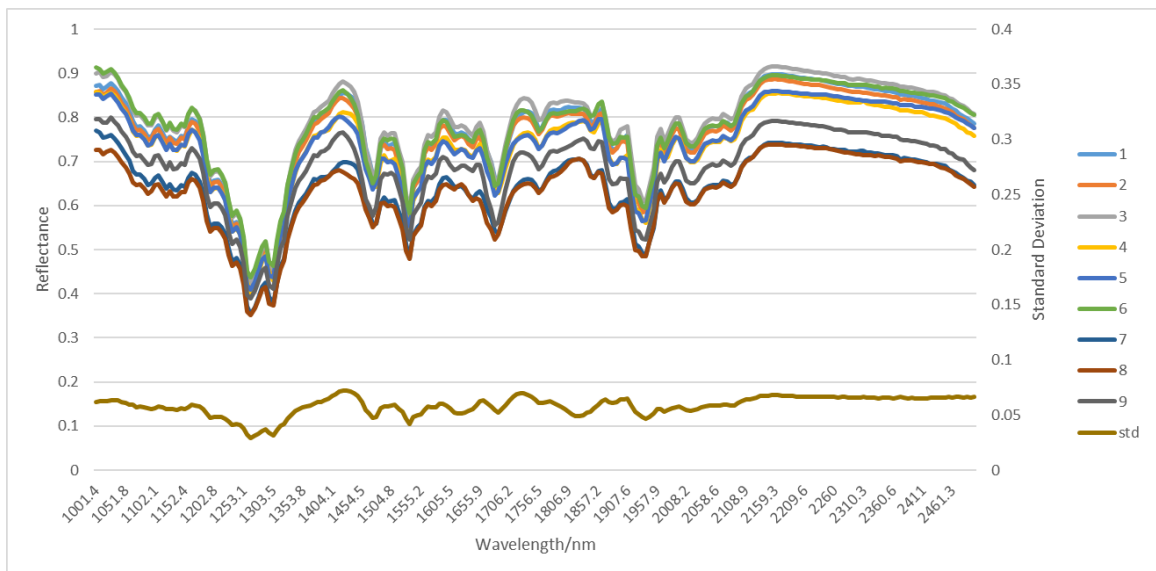


Figure 3-17. Comparison between 9 average reflectance spectra of Spectralon multi-component wavelength target collected using the HSI system after placing it in 9 different positions over the scanning stage. The standard deviation (SD) shows the variations between the spectra from one position to another.

3.6 Discussion

This chapter discussed the evaluation of the performance of the used HSI system in this research, beginning with a background about the technique itself then characterization aspects of the system focusing on the quality, accuracy, stability and precision of the collected data, highlighting the importance of the spatial, radiometric and spectral calibration processes.

The effect of different measurement conditions and acquisition parameters such as illumination distribution and intensity, optics and scanning background on the quantitative calibrations based on the spectral measurements collected by the HSI in the SWIR region were explored, which is an active research area (Fischer & Kakoulli, 2006; Cséfalvayová et al., 2011; Dooley et al., 2013).

Although it is important to understand the system components, acquisition parameters, calibration processes and acquisition workflow to help in increasing the accuracy, reliability and reproducibility of the data, understanding cultural heritage objects being investigated and how the collected HSI data will be used is also very important. This will decide on many aspects regarding the spatial and spectral needs of the system, e.g., high spatial resolution is needed when investigating fine details such as underdrawings while high spectral resolution is needed in material characterization applications (Webb, 2015; Cucci et al., 2019).

As shown, the system at hand has a relatively low spatial resolution with a maximum sampling density of 1.85 px/mm and a reasonable spectral resolution with a 15 nm FWHM and spectral sampling of 6.3 nm using the current setup in comparison to similar HSI systems (Fischer & Kakoulli, 2006; Arngren, 2011; Wang et al., 2012; Cucci, 2014). This

indicates the potential of using the system in materials characterization and mapping applications.

It was explored that the system has similar performance compared to the NIR LabSpec-5000 spectrometer in detecting spectral features with a ± 2 nm wavelength accuracy and 0.2% CoV representing the wavelength precision.

Illumination intensity can be lowered from 500 to 250 W whenever needed based on the sensitivity of the investigated materials with no effect on the quality of the spectra especially if noisy edges were excluded. However, the distribution of the illumination over the scanning stage is considered an issue that needs further investigation. Although the variations based on the lux measurements are acceptable with an RSD=3.13% and the fact that the spectral measurements are stable collected from the same position and on different scanning time (CoV = 0.49 % for stability), it was noticed that the spectra are affected by some variations from one position to another with an estimated CoV of 7.7% which could lead to significant variations in the quantitative predictions based on these spectral data. This will need to be investigated in future work looking for the causes and potential methods to reduce these variations. One possible correction method is to use the spectralon white tile fixed vertically along the scanning stage to compensate for any changes in the illumination.

Using different lenses to increase the spatial resolution have some spectral differences with a CoV of 2.7% which is a bit higher compared to instrumental uncertainty (CoV = 0.49%), but this did not affect the performance of calibrations. Moreover, changing some of the measurement conditions such as scanning background and the ROI size used to obtain the average spectra in addition to the pre-treatments applied to the spectra during analysis were found to have no significant effect on the obtained calibrations as well.

More acquisition parameters and measurement conditions should be assessed to better understand the system performance and to assure the robustness of the obtained data and calibrations such as the wavelength linearity, spatial distortions, the effect of the used illumination on the materials under investigation, concentrations of the imaged component and the effect of the surface morphology of the scanned objects. However, overall this study provides a foundation of new evaluation methodology not only based on the system performance but also taking into account its performance when it is applied to artworks.

4. HISTORIC ISLAMIC PAPER

Paper is one of the most important information carriers of knowledge enabling its transfer between generations and cultures (Hunter, 1947; Bloom, 2001). Its material characteristics changed as the knowledge of paper production travelled from China through Islamic countries (in this period) until it reached the West. Along this route, a fascinating variety of raw materials and techniques have been used (Hunter, 1947; Pedersen, 1984; Bloom, 2001; Loveday, 2001) imparting unique properties to papers from distinctly different cultural environments.

Apart from its value in historical and technological studies, understanding of paper as a material is also important from the conservation point of view, in order to develop sustainable preservation methodologies (Strlič & Kolar, 2005). European paper is reasonably well known and studied through different projects such as Papyrus, 2001-2004; PaperTreat, 2005-2008 and SurveNIR, 2005-2008 (Kolar et al., 2004). In contrast, little to no scientific effort went into understanding of Islamic paper despite its cultural value, which resulted in a severe lack of preservation plans for Islamic collections and an increased risk of loss of such collections.

It is known that Islamic papermaking utilized unique techniques and processes such as starch sizing and surface polishing. These make Islamic paper distinct from other types of paper, such as Indic, Sino-Asian or European (Baker, 1989; Baker, 1991; Bloom, 2001, Karabacek, 2001; Loveday, 2001; Déroche, 2005). However, less is known about how the distinct papermaking techniques affect material stability, and what proportion of Islamic paper forms manuscripts in Islamic library collections, especially since intensive trade led to significant imports of European paper into Islamic countries from the 17th century on (Baker, 1991; Bloom, 2001; Loveday, 2001; Déroche, 2005). From the preservation, as well as from the cultural and historical point of views, it is essential that we start building this knowledge.

This chapter focusses on studying Islamic paper. It begins by exploring the material properties of Islamic paper through applying a systematic scientific survey on a collection of Islamic paper in Section 4.1. Section 4.2 explores if any of the characteristics of Islamic properties (starch-sizing and polishing) has a significant effect on the stability of the paper with the aid of accelerated degradation.

Section 4.3 is divided into 2 sub-sections; the first sub-section describes a new non-destructive methodology which was developed to identify properties of Islamic paper based on the spectral data collected from the collection using hand-held spectroscopy and multivariate data analysis methods. The methodology was then used in surveying the real Islamic collection at Wellcome Collection to evaluate the use of such methodology to fulfil the scientific gap in the knowledge about the material properties of Islamic paper and their effect on the stability of paper.

The second sub-section investigates quantitative NIR imaging using the HSI system in the 1000 – 2500 nm range for mapping the chemical properties of Islamic paper. New prediction models based on the spectral data collected by the HSI system were developed to determine Islamic paper properties, following which chemical maps were generated for each pixel in a scanned object.

Section 4.4 describes a new evaluation methodology to study the metrology of quantitative calibrations using the spectral measurements collected by the HSI system in the SWIR region. The following section (4.5) focuses on a degradation study of Islamic paper samples in controlled environmental conditions to determine the degradation rates and explore if the Ekenstam equation (Ekenstam, 1936) and recently modelled dose-response function for European paper (Strlič et al., 2015) can be applied to Islamic paper. The last section (4.6) summarizes all the main conclusions that were achieved through the chapter.

4.1 Islamic Paper Survey

This section describes a systematic survey of an Islamic paper collection with the aim to understand and identify the material properties of Islamic paper deducing what might be considered as its most significant characteristics and to assess the current material state of the collection. The work described is an extension of the MRes research that I carried out prior to the start of this PhD research (2014) where the survey of the Islamic paper was conducted and a non-destructive characterization methodology to estimate some properties of Islamic paper using handheld spectrometer was developed (Mahgoub et al., 2016). The description of the survey and the obtained results are briefed with some new interpretation of the results in the following sub-sections (Section 4.1.1 and 4.1.2). The details from the developed methodology are also briefed later in the sub-section 4.3.1 due to its importance for the context of the rest of the Chapter.

4.1.1 Characterization of the Reference Collection

For the purpose of the survey, a set of 228 samples (ref-collection), part of the UCL Institute for Sustainable Heritage (UCL-ISH) historic reference material collection was selected. The full description of the samples can be found in Chapter 2 (Section 2.1). Briefly, samples were collected from different sources in central Asia, Near East and North Africa and mainly represent the period of 18th - 19th century.

The samples were documented and investigated by recording all obtained measurements and information in a reference database using a unique ID for each sample e.g. AP 4. Several chemical analytical methods were conducted (Table 4-1, Mahgoub et al., 2016) to investigate paper sizing, surface characteristics, e.g. gloss and roughness and fibre furnish in addition to determination of pH and cellulose DP in paper as an indicator of the average material state of the samples. The description of the analytical methods and the instruments can be found in Chapter 2 (Section 2.4).

Table 4-1. Summary of the characterization techniques used in the Islamic paper survey, with the corresponding number of samples. The numbers differ for each technique for different reasons; no enough samples for DP determination analysis (as it requires big amount of samples ~ 20-30 mg) or available data is enough for calibration to support a hypothesis as in the case of pH analysis. All of the available samples were analysed for the presence of starch and polishing.

Technique		No. of samples analysed
Sizing	Iodine test	228
	Raspail test	146
Surface Polishing	Visual assessment for polishing	228
	Surface roughness	100
	Surface gloss	228
	Specular/Diffuse reflectance ratio	22
	SEM imaging (scanning electron microscopy)	20
	FTIR	37
	Fibre Furnish	15
pH determination	70	
DP determination	60	

4.1.1.1 Morphology

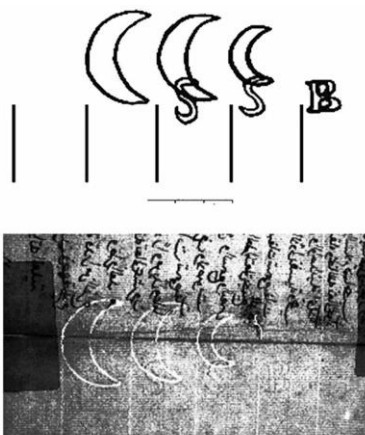
Based on the visual examination of the ref-collection and using digital micrometer, the thickness of the samples ranges from 87 to 240 μm . Table 4-2 lists the different sheet-forming techniques for papers found in the ref-collection and whether the paper is hand- or machine-made. It was noticed that no special patterns of the papers with chain lines were detected as reported in previous studies (Baker, 1989; Loveday, 2001) for some Islamic papers. On the other hand, a zig-zag indentation (Figure 4-1) in diagonal lines from the sheet's head to tail (Loveday, 2001) was observed in three hand-made laid samples (AP 36, AP 37 and AP 38). The technique known as *Waṣṣālī* was noticed in two of the samples (AP 44 and AP 97; Figure 4-2) where the paper was made by gluing together two sheets, and polished only on the outer sides resulting in thicker polished paper (Karabacek, 2001; Al-Sāmarrā'ī, 2001). Although watermarks are not a typical Islamic paper property (Loveday, 2001; Déroche, 2005), 61 samples from the ref-collection contain watermarks, some of which were used in European factories for paper exported to Islamic countries such as the 'three crescents' or the 'tre lune' (Wiesmüller, 2008-2012; Figure 4-3).



Figure 4-1. Example of Zig-zag indentation (AP 37) in diagonal lines from the sheet's head to tail. Visible image (left), back-lighting image (middle) with the indentation illustration, selected area (right).



Figure 4-2. Example of the strengthening technique observed in two samples (AP 44, AP 97) from the ref-collection involving two sheets being glued together on their unpolished sides (known as Waṣṣālī method).



AP 116

Figure 4-3. Example of the triple-crescent watermark found in the samples, that was used for papers exported from European paper mills to Islamic countries.

Table 4-2. The frequency of sheet-forming techniques for paper samples in the ref-collection.

	Laid and chain lines	Laid with no chain lines	Wove	Wire-mesh*	Total
Machine-made	16	4	28	28	76
Hand-made	96	50	2	4	152
Total	112	54	30	32	228

*Type of paper mold with narrow-meshed lengthwise (laid lines) and transversal wires (chain lines).

4.1.1.2 *Sizing*

Starch sizing could be seen as one of the defining characteristics of Islamic paper (Ibn Bādīs, 1025; Baker, 1989; Loveday, 2001; Al-Hassan, 2001). Using the iodine test (Isenberg, 1967; Baker, 1991), almost half of the samples (110) were shown to contain starch. Variations in the reactions to iodine were observed, which could be related to the differences in starch source and quantity (Bloom, 2001).

The presence of rosin was explored using the Raspail test (Isenberg, 1967; AIC, 1990) for samples that tested negatively for starch as it was assumed that only one sizing material should be present in the same sample. The assumption was verified by examining some samples that are tested positively to starch using the Raspail test. The whole reference collection was not tested for rosin due to time constraint and the lack of evidence in the literature that rosin was used in the Islamic papermaking. Starch was selected as the typical sizing material used in Islamic paper making as reported in the literature (Loveday, 2001) while rosin was selected for being the common used sizing material in this period (19th century) (Garlick, 1986). Only 4 samples out of 146 reacted positively to the test with one starch sized sample (AP 125-2) reacting positively to rosin as well.

Since the test gives false positives for casein, ATR-FTIR was used to ensure the absence of peptide bonds. Two samples were found to contain protein (AP 125-2, AP 129-2). Thus, only three samples (AP 98, AP 105, AP 128) are undoubtedly sized with rosin. The three samples are written in Arabic, with no watermark and all are mechanically produced (2 wove and 1 wire-mesh).

4.1.1.3 *Surface Characterization: Polishing*

Based on visual observation, more than 50 % of the samples were classified as polished. Since the decision is subjective due to the way the visual assessment is conducted either by appearance, e.g. checking sheen marks or by touch in addition to the variations of the polishing quality in terms of the shine and smoothness of the surface based on the manufacturing technique (Loveday, 2001; Karabacek, 2001; Déroche, 2005), thus other instrumental tests were explored based on the relation between surface roughness and its light reflection (Bhushan, 2001).

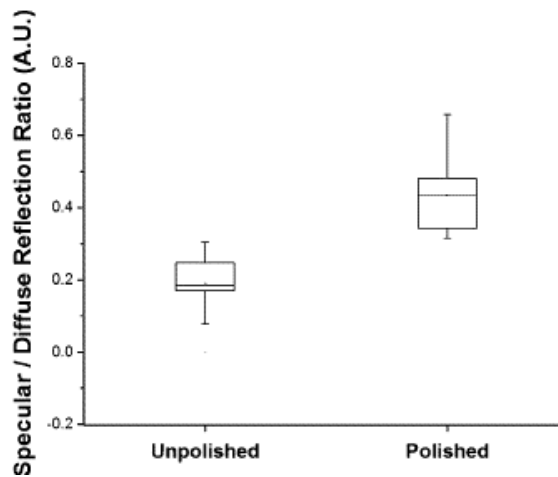


Figure 4-4. Box plot of 20 values of the specular vs. diffuse reflectance ratio at 457 nm calculated from the spectral measurements collected from Islamic paper samples using LabSpec-5000 spectrometer. The “Polished” and “Unpolished” categories were determined visually. Each box shows the distribution of the measurements based on the median, 1st and 3rd quartile. The whiskers represent minimum and maximum values.

Roughness measurements using a profilometer and gloss measurements using a glossmeter were collected in addition to the ratio between specular and diffusely reflected light collected using a spectrometer at 0° and 45° from the 457 nm (band to measure paper brightness, (APPI-452-om, 1998; BS-ISO-2470-1, 2009)). Scanning electron microscopy (SEM) imaging was also used to test its potential to differentiate between polished and unpolished surfaces.

Only the ratio of specular/diffuse reflectance can assess the polishing level and differentiate between polished and unpolished surfaces (categorized based on the visual assessment) (Figure 4-4) compared to the roughness and gloss measurements.

On the other hand, the high resolution images of SEM can visualize the differences between the various levels of roughness (Figure 4-5) in paper samples. However, SEM is a destructive technique which cannot be applied to papers of historic significance.

It is important to understand that the assessment based on the tested instrumental methods is still subject to error as the results depend on the sampled area and many papers are not uniformly polished in addition to being compared to the visual assessment categories.

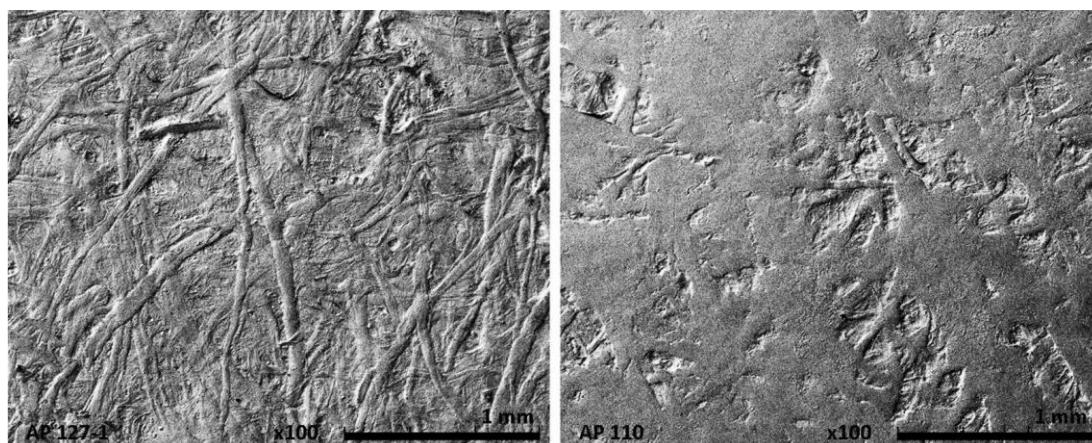


Figure 4-5. SEM images ($\times 100$) of an unpolished sample (left, AP 127-1) and a polished sample (right, AP 110).

I also tried to use ATR-FTIR spectroscopy to identify the coating material that may be used for polishing. Therefore, laboratory-made reference samples made of pure cellulose (Whatman No.1 paper) were prepared and coated with either egg-white (from fresh egg) or gum tragacanth (Cornelissen & Son, London) as an example of the typical polishing coatings used in Islamic papermaking (Ibn Bādīs, 1025; Levey, 1962; Loveday, 2001; Karabacek, 2001; Al-Sāmarrāī, 2001). The spectra of the coated reference samples were collected and compared with an available online spectral database (IRUG, 2000; Mahgoub et al., 2016). The spectra of 37 samples (selected randomly from the polished samples) from the ref-collection were peak normalized around 1026 cm^{-1} to be able to identify the coatings. There is an indication of proteins based on the peaks at $\sim 1533\text{ cm}^{-1}$ and $\sim 1639\text{ cm}^{-1}$ (amide group bands) (Baker, 1989; Stuart, 2007; Gorassini et al., 2008). Almost half of the samples contained well-identifiable proteinaceous peaks. In some cases, the peak at $\sim 1630\text{ cm}^{-1}$ (cellulose) minimized the possibility to distinguish gelatine, casein or egg-white (Baker, 1989; Stuart, 2007). There was no indication in the literature (Garlick, 1986; Baker, 1991) that gelatine was used in Islamic countries due to the 'high temperature' so this could empower the hypothesis that starch-sized samples could have been polished using egg-white or casein as a coating material.

It is also very difficult to distinguish between gums based on FTIR spectra only (Baker, 1989), despite the peak at $\sim 1720\text{-}1740\text{ cm}^{-1}$ that identifies the gum-tragacanth (Mahgoub et al. 2016). Although 10 samples showed peaks in this region that could indicate the presence of gums, none of them were as strong enough as the reference sample. It is also worth mentioning that the presence of this peak could also indicate the presence of oxidised degradation products (Zervos, 2007) which makes gums more difficult to be identified than proteins. Two polished samples (AP 48, AP 131) showed no protein or gum tragacanth peaks.

4.1.1.4 Fibre Furnish

Up till now, there is no historical information on the use of special fibres in Islamic papermaking different than the common bast and cotton that were also used for European papermaking (Loveday, 2001; Karabacek, 2001; Al-Sāmarrā'ī, 2001; Déroche, 2005, Al-Hassan, 2001). It is very important to identify paper fibres as it can be of decisive importance for identification of paper provenance, as was shown in the case of Tibetan paper (Helman-Ważny & Van-Schaik, 2012). To achieve that, a systematic fibre analysis study should be conducted on a representative reference samples of Islamic papers with known provenance and date, this could reveal information about the presence of less usual fibres such as papyrus, rice and silk.

As a showcase and due to the time constraint of the research, 15 samples from the ref-collection were selected randomly to explore Islamic papers' fibres (Table 4-3) and investigate the fibre composition of the samples using the standard procedure (BS-7463, 1991) with the aid of Herzberg reagent. The samples were examined with and without staining under transmitted light using optical microscopy (Brunel Microscopes Ltd, Wiltshire) attached to a DSLR camera (Canon EOS 1100D). Based on the fibres' morphological characteristics (Ilvessalo-Pfäffli, 1995; Stuart, 2007), only bast (hemp and flax), cotton and wood-based (hardwood and softwood) fibres were found. However, it is noticed that most of the samples made from wood-pulp are not sized with starch, which may indicate that these papers were imported.

Table 4-3. List of 15 samples from the ref-collection and their properties (starch-sized, polished surface, written text and type of paper (identified visually based on mould features and alignment of the fibres (Cornell University Library 2005)) that were selected randomly for the fibre furnish analysis.

Samples	Starch-sizing	Polished surface	Text	Type
AP 3	Y	Y	Arabic	Laid with no chain lines) / hand-made
AP 5	Y	Y	Arabic	Laid + chain lines / hand-made
AP 6	Y	Y	Arabic	Laid + chain lines / hand-made
AP 7-1	N	Y	Arabic	Laid + chain lines / hand-made
AP 7-2	N	Y	Arabic	Laid + chain lines / hand-made
AP 11-1	Y	N	Arabic	Wove / machine-made
AP 28-2	Y	N	Persian	Laid with no chain lines) / hand-made
AP 31	Y	N	Persian	Wove / machine-made
AP 56-3	Y	Y	Arabic	Wove / machine-made
AP 71-1	N	Y	Persian + Arabic	Laid + chain lines / hand-made
AP 75-Type1	N	Y	Arabic	Laid + chain lines / hand-made
AP 84	Y	Y	Coptic	Wove / machine-made
AP 128	N	N	Arabic	Wire-mesh / machine-made
AP 131	Y	Y	Persian	Laid with no chain lines) / hand-made
AP149	N	Y (one side)	Persian	Laid with no chain lines) / hand-made

4.1.1.5 Acidity and Degree of Polymerization

Acidity (pH values) in paper has a negative effect on the permanence of paper (Zou et al., 1996) while cellulose DP in paper is a good indicator of the condition of the cellulosic chains reflecting object condition and it correlates with the mechanical properties and

remaining lifetime of objects (Zou et al., 1996; Strlič & Kolar, 2005; Trafela et al., 2007; BS-ISO-5351, 2010). Knowing both properties can give very useful information about the current material state of the paper. As the two techniques are time consuming, the pH and cellulose DP of only 70 samples from the ref-collection were measured (excluding 10 samples contain lignin from the viscometric measurements) using a modified standard cold extraction procedure (ASTM-D778-97, 2002; Strlič et al., 2004) and the standard viscometric method (BS-ISO-5351, 2010) with Mark–Houwink–Sakurada equation (Evans & Wallis, 1987) respectively.

The distribution of pH across the ref-collection (Figure 4-6) shows a potentially bi-modal distribution similar to what is usually observed in European paper. Rosin-sizing was acknowledged as the main cause of European paper acidity, however, this was not the case for Islamic paper since only 3 samples were found to be rosin-sized compared to ~36 % of Islamic paper samples with pH < 6. There are only 4 samples with a pH < 5, 2 of them contain lignin while the other is sized with rosin.

I attempted to test the distribution bi-modality using the chi square test (χ^2 - goodness of fit) for normality (Miller & Miller, 2010). The test is a quick way to check whether or not a model follows an approximately normal distribution. Putting the null hypothesis that distribution is normal and then apply this equation;

$$\chi^2 = \sum \frac{(\text{Observed} - \text{Expected})^2}{(\text{Expected})}$$

Comparing the value obtained to the critical chi-square value from a chi-square table, given a specific degrees of freedom. If chi-square statistic is larger than the table value, then the distribution is not normal.

The test confirmed the non-normality of the distribution ($\chi^2 = 11.02$ with a degree of freedom of 2). Despite the test results and in the absence of rosin-sized papers that are strongly acidic, it could be suggested that the bi-modality distribution is a result of acidification of some samples during degradation.

On the other hand, the distribution of the DP values is biased towards low values around the interval 500-750 DP units. This is of some concern if encountered in real collections, as the risk of paper accumulating mechanical degradation due to handling increases substantially for DP <300 based on a study on Western papers (Strlič et al., 2015).

As it is unknown yet if the ref-collection represents the average Islamic paper collections in libraries and archives, there is a strong need to know whether such low DP values are typical of Islamic paper collections and to verify if same DP threshold at 300 is also applied to Islamic paper increasing the risk of its mechanical degradation with handling which can be achieved through surveys. As a hypothesis, the low observed average DP could be the result of high temperature during storage in the past but this needs to be further explored. Although the environmental history of the ref-collection samples is not known, it is still interesting to study the relation between pH and DP values with the presence of starch

and polishing to get an idea about the effect of these characteristics on Islamic paper stability. Based on the results shown in Figure 4-7, polished samples are mostly associated with high DP and pH values indicating its good state while starched samples are less acidic than neither polished nor starched ones which is typically of European papermaking.

Knowing such information is important, but it cannot be taken as a general conclusion about the positivity or negativity of the effect of Islamic paper characteristics (polishing and starch sizing) on the stability of Islamic paper. Thus, to verify the obtained information and to get a deeper understanding of such effect, a degradation study in a controlled environmental conditions was conducted which will be discussed later in the chapter (Section 4.5).

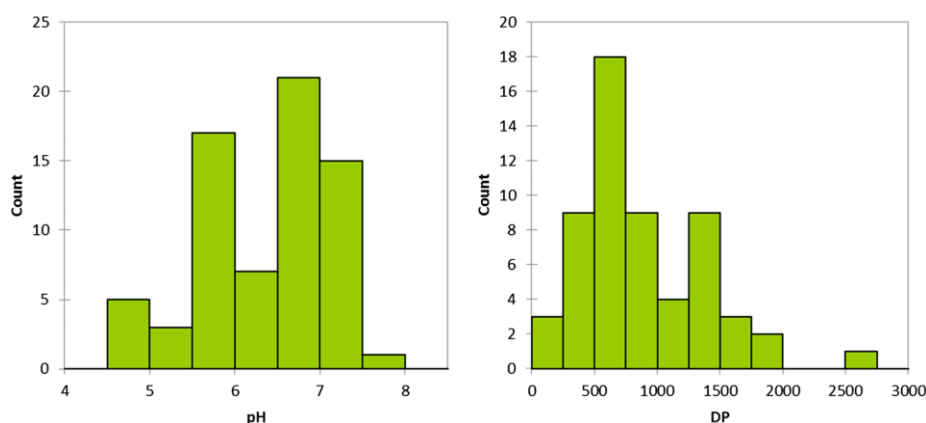


Figure 4-6. Frequency plots for pH ($n = 70$) and DP ($n = 60$) of Islamic paper samples in the ref-collection.

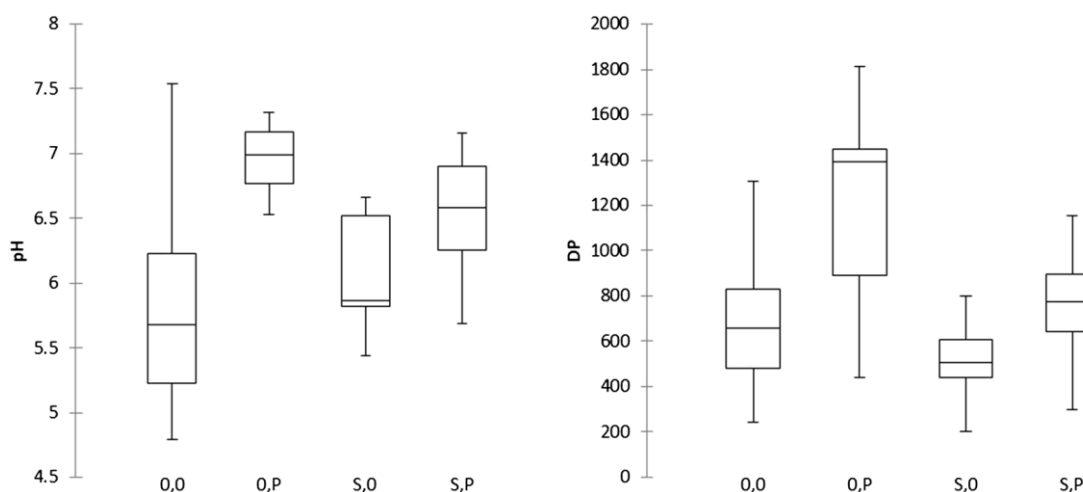


Figure 4-7. Boxplots for pH ($n = 70$) and DP ($n = 60$) showing the 1st and 3rd quartile, the median and minimum and maximum values (whiskers) for categories with identified polishing (P), starch (S) or not (0).

4.1.2 Discussion and Conclusions of the Survey

For the first time, the survey systematically reviewed the evidence of specific papermaking practices associated with paper used in the Islamic cultural realm, adding a scientific layer to codicological, historical and palaeographical research.

Four properties of Islamic paper were investigated using a reference historic materials database of 228 Islamic paper samples from north Africa, the near East and central Asia, mostly from the 18th and 19th century.

Although there is no certain information about the age or the provenance of most of the ref-collection samples, I tried to explore whether it is possible to identify the typical material properties of Islamic paper given that the samples represent a random cross-section of paper production that can be found in the Islamic cultural realm.

A number of analytical characterization techniques to explore paper sizing, polishing, fibre furnish, acidity and degree of polymerization were conducted.

Many conclusions were established as following:

- 48 % of the ref-collection contains starch and 64 % are polished with 57 samples being both polished and starched. ~ 12% of the samples are neither polished nor contain starch.
- Most of the unpolished and not starch sized samples are written in Arabic ($n = 23$), of these, a small proportion (~2 %) are rosin-sized and mechanically produced. It can be concluded that rosin sizing and the absence of starch or polishing are not typical of Islamic papermaking practices.
- Polishing was assessed visually and with the aid of different instruments to minimize the time consumed in assessment and its subjectivity. Islamic papers were found to have different qualities of shine resulting from the uneven application of the polishing technique. Among the explored instrumental methods, specular/diffuse reflectance ratio at 457 nm gave results that were most consistent with the visual observation. SEM also was found to be a reliable technique, albeit destructive.
- With ATR-FTIR to investigate materials used for polishing, the presence of proteinaceous coatings (casein, egg white) can easily be detected, while the presence of gums is difficult to establish due to the absence of specific absorption bands.
- No specific fibres were found in fibre furnish analysis of 15 samples from the ref-collection. Only bast, cotton and wood-derived fibres found which are also typically found in European papermaking as well.
- Regarding acidity, the collection shows a bi-modal distribution, with two peaks in the intervals of 6.5–7.0 and 5.5–6. Only 4 samples are very acidic ($\text{pH} < 5$), 2 of which contain lignin, and 1 is rosin-sized. No explanation yet was derived about the cause of the non-normality of the distribution, as sizing materials cannot be the cause as is the case with rosin and gelatine in European collections.

- 69 % of the ref-collection have DP < 1000. Given that the typical fibres are bast and cotton with high initial DP, these results are likely a reflection of high temperatures during past storage.
- Polished samples were found to be associated with higher DP and pH in the studied collection, which could be a reflection of ageing or past storage. Further research is needed to study the effect of polishing and presence of starch on paper stability which will be discussed later in the chapter.

There is no unequivocal evidence for what should or should not be considered as Islamic paper. Neither the textual evidence (could be written on an imported paper) nor the presence of starch or polished surface (both could be applied to imported paper, prior to writing) is enough as a proof of provenance of the writing support (paper). Also, fibres of Islamic paper are typically the same as the ones used in European papermaking and the paper itself has no watermarks or any special identifiable features. The literature reports specific cases of sieve patterning, the use of rice or papyrus fibres, but there is no evidence of this in the studied collection (ref-collection). However, since ~88 % of the ref-collection are starch-sized and/or polished, these two practices could be considered typical of Islamic paper of the 18th and 19th century.

It is of great importance to start to have a clearer view of how widespread specific papermaking practices were through time and geographically which can be achieved through surveying Islamic paper collections with high historic value, well-dated and provenanced in libraries and archives and establishing its material properties since the reference collection was lacking these features (provenance and date). Such survey can only be carried out using a non-destructive methodology to access the valuable collections which I developed to determine some of the Islamic paper characteristics (described in Section 4.3.1). Additionally, we would gain a better insight into the state of conservation of such collections, as well as develop collection specific preservation advice, as we will discuss later in the chapter.

4.2 Effect of Starch Sizing

To explore if any of the characteristic Islamic properties (starch-sizing and polishing) has a significant effect on the paper rate of degradation, PCA analysis was applied to the measurements collected from 40 Islamic paper samples from the ref-collection (Chapter 2 – Section 2.1) using Origin Pro 9.0 software to explore any correlation between the different characteristics in the current state (Figure 4-8 - right).

Moreover, to study if there is any influence from any of these properties on the stability of the paper, the DP was measured for the same 40 sample after being degraded at 80 °C and 65% RH for two weeks then the percentage of DP loss (Initial DP - DP after degradation / Initial DP) for each sample was calculated and analysed with the other properties (Figure 4-8 - left).

The PCA biplots (Gower & Hand, 1996) plots simultaneously information on the observations (as dots) and the variables (calibrated axes) in a multidimensional dataset allowing you to project the observations onto the axes to make an approximation of the original values of the variables.

The results verify the same conclusion about the polished samples being associated with high pH and DP values (as seen earlier in Figure 4-7) based on the positive correlation between the three properties as seen in Figure 4-8 (right). Although no conclusions can be derived from the same figure (right) about the starch-sizing property based on the initial measurements, the left figure emphasizes the positive effect of starch on stability of paper through the negative correlation with the %DP loss (represented by the lines of starch and %DP loss being almost 180 degrees to each other). Therefore, I decided to investigate this further.

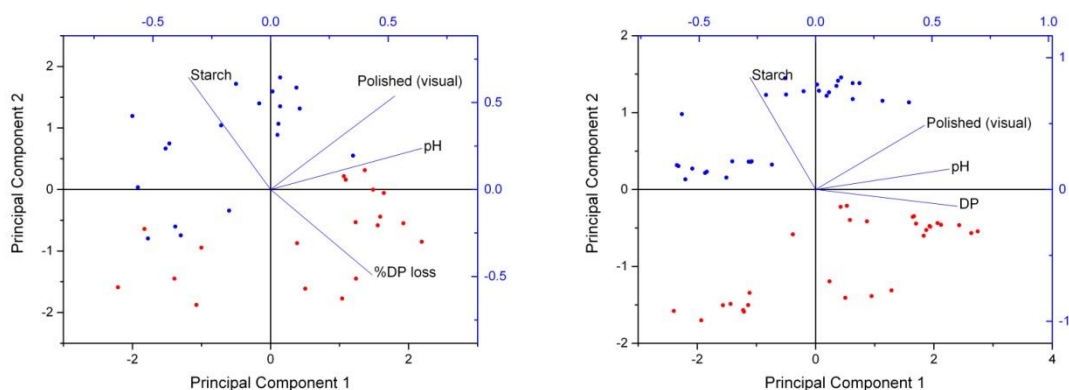


Figure 4-8. Two biplots from the correlation analysis using PCA of four paper characteristics for 40 samples from the Islamic paper ref-collection to study the effect of the different techniques on paper stability. The left and bottom axes are of the PCA plot showing the scores of the samples (dots) while the top and right axes belong to the loadings plot which shows how strongly each characteristic (vectors) affect the principle components. On the right, the biplot shows the analysis of the initial values of DP and pH with the starch-presence and polishing characteristics. On the left, the biplot shows the correlation between pH, polished surfaces, starch-presence and % DP loss characteristics. % DP Loss is calculated from the initial DP values and the DP measured after ageing the samples (at 80 °C and 65% RH for two weeks). The two figures show the PCA scores of PC1 vs PC2 categorized according to starch-sizing property (Starched samples in blue and unstarched samples in red).

An experiment was conducted to explore the effect of starch by applying starch suspension with different quantity (%m/m starch) on Whatman No.1 filter paper samples (5x5 cm) then with the aid of artificial accelerated degradation and standard viscometric method, the changes in DP in relation to starch content was monitored.

25 g of potato starch was mixed in 250 ml deionized water (cold) then the suspension was put in the ultrasound bath for 30 min and with continuous stirring in 80 °C. The suspension then was heated on the hotplate till it reached 130° C with continuous stirring until the starch was cooked.

A 500 ml of de-ionized water was mixed with 5 teaspoons of the starch suspension then was stirred on the hotplate until its temperature was ~60 °C.

18 pieces of Whatman paper with 5X5 cm were cut and weighed individually. Each piece was immersed in the starch suspension and the immersion process repeated for several times to get pieces with gradually more and more starch. The excess was blotted between two Whatman papers. The samples were numbered from 1 to 18 representing the number of times a sample was immersed. The pieces were dried in the oven at 80 °C for 5-10 minutes between repeated treatments in order to dry fast and all the pieces were left to dry overnight at the end of the experiment. All the pieces were weighed again after the immersion and being dried. A reference sample of Whatman paper was washed in deionized water then dried. All the samples were divided into 3 strips: one for the initial measurement and the other two to be degraded for 21 and 60 days at 80 °C and 65% RH. DP measurements were measured for all the samples using the standard viscometric method before and after degradation, described in Chapter 2.

As seen in Figure 4-9 representing the DP measurements of starch-containing samples, the effect of starch content on sample mass and DP is evident from the data of non-aged samples "0 days-uncorrected". Approximately 1% increase of mass of paper due to the addition of starch leads to ~ 1-1.5% difference in the calculated DP due to the decrease of the actual cellulose content in the weighed sample which needs to be taken in consideration in DP calculations.

A correction factor was calculated and applied to the mass of samples to compensate for the amount of starch introduced as can be seen in "0 days-corrected" data where all DP values are almost similar since they are the same for the non-aged Whatman samples. The data are not showing any patterns for the aged starch samples. If we compared between the reference sample with no starch and the sample with the least amount of starch (1 immersion), we can reach the conclusion that starch has no effect on cellulose degradation as both samples degrade in the same rate (Figure 4-10).

This is a good conclusion, however, further work needs to be done to try to figure out if starch itself has a DP value that can be measured with the viscometry method then try to establish the knowledge about the typical % of starch in Islamic paper. Also, determining if other non-pure types of starch have an effect on cellulose degradation is worth further investigation.

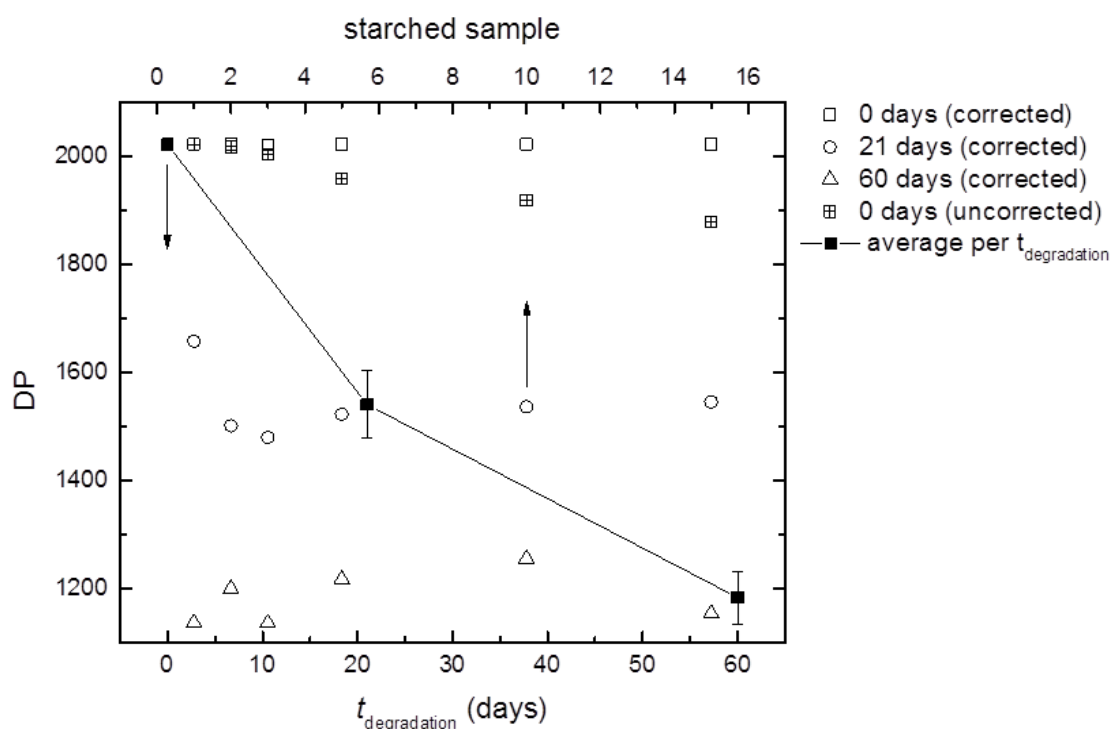


Figure 4-9. Scatter plot representing the DP measurements of Whatman samples (1st X-axis on top) before (0 days) and after degradation at 80 °C and 65% RH for 3 weeks (21 days) and 2 months (60 days). A correction factor for the sample mass due to the addition of starch was used. The full square points show the standard deviation per degradation period (2nd X-axis on bottom), taking the average value of DP for all the samples (after correction) degraded for 21 and 60 days.

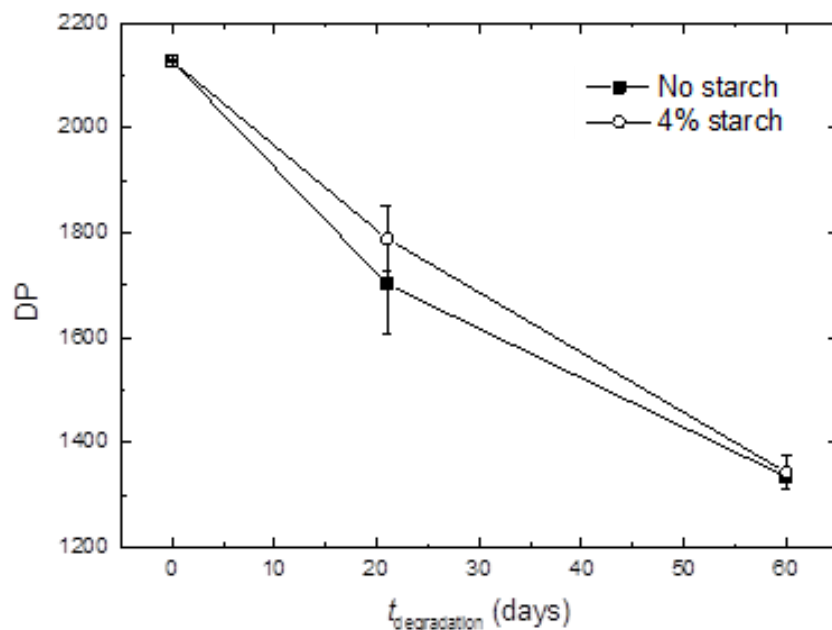


Figure 4-10. Degradation rates of the reference sample with no starch and sample no. 1 with the least amount of starch (1 immersion). The error bars represent standard deviations for duplicate DP determinations.

4.3 Non-Destructive Characterization Methodology

Non-destructive techniques requiring neither sampling nor sample preparation have become prominent for the investigation of historic objects (Derrick et al., 1999; Stuart, 2007; Trafela et al., 2007). Infrared spectroscopy is a non-destructive technique that has

been successfully used in studies of different heritage materials (Trafela et al., 2007; Strlič et al., 2007). It became an important analytical tool to characterize physical and chemical properties of various materials in non-heritage applications (Antti et al., 1996; Blanco & Villarroya, 2002) due to its ability to reflect combination and overtone vibrations associated with C-H, O-H and N-H chemical bonds (Blanco & Villarroya, 2002; Stuart, 2007). Spectral data then can be used to classify or estimate properties of unknown samples when correlated with measured physical properties obtained from reference analytical methods applied to well defined and representative samples (Blanco & Villarroya, 2002; Small, 2006; Strlič et al., 2007; Trafela et al., 2007). Multivariate data analysis techniques are used to build such correlations.

Although NIR spectroscopy has received considerable attention, such investigations have so far focused on point analyses whilst processes of degradation advance in a heterogeneous way with possibly significant local variations due to the utilization of various materials and added substances, such the sizing and finishing layers in the papermaking process (Trafela et al., 2007; Oriola et al., 2014).

Therefore, it is of importance to develop tools to collect spatially resolved quantitative chemical information from the heritage materials to represent such inhomogeneity and map the distribution of the chemical composition of a whole object (Strlič & Kolar, 2005; Kubik, 2007; Wang & Paliwal, 2007; Elmasry & Sun 2010; Oriola et al., 2014).

Hyperspectral imaging (HSI) has proven itself as a successful and useful technique in the field of heritage conservation by expanding spectroscopy (spot analysis technique) to the examination of an entire surface of an object as it records spectral and spatial information simultaneously. It has expanded imaging and material characterization possibilities (Fischer & Kakoulli, 2006) through building chemical images or maps, which has the potential to improve knowledge of distribution of material properties while investigating an entire object (Lu & Chen, 1999; Wang & Paliwal, 2007; Liang, 2012; Dooley et al., 2013). This section is divided into two sub-sections; The first section (4.3.1) focusses on developing a non-destructive characterization methodology of Islamic paper using NIR spectroscopy accompanied by multivariate data analysis methods. The methodology could be applied to Islamic collections in libraries and archives to expand the reference collection database of Islamic paper with information about material properties of papers of known age and provenance and thus better understand geographic and temporal distributions of papermaking practices in Islamic. In addition to that, the methodology was validated by surveying part of the Islamic Collection of the Wellcome Collection and the results are described in the sub-section (4.3.1.3).

Section 4.3.2 explores the potential for mapping some characteristics of Islamic paper using HSI in the SWIR range due to its ability to resolve information spatially and spectrally for the whole surface of an object. Quantitative calibration models were developed to

determine these properties for unknown samples based on the spectral information collected by the HSI system of Islamic paper reference collection in the range 1000-2500 nm. The calibration models and the analysis of the results in addition to the development of quantitative chemical maps for Islamic paper samples are also described in the section.

4.3.1 Handheld Portable VIS-NIR Spectroscopy Analysis

Sampling historically valuable collections is rarely permitted, and most of the used traditional characterization methods are destructive or semi-destructive and or time consuming. Therefore, it is of great importance to develop non-destructive characterization methodologies as a replacement tool that can be used in-situ in libraries and archives. NIR spectroscopy is a very powerful tool, proved the success of its applications, especially for material characterization (Blanco & Villarroya, 2002; Flinn, 2005; Oriola et al., 2014; SurveNIR). Using PHAZIR NIR analyzer (Polychromix, now Thermo Fisher, Hemel Hempstead), spectral data of the ref-collection samples were collected in the interval 1600 – 2400 nm (average of 10 scans, resolution 8 nm). The measurements were carried out using single sheets with a Spectralon 99% diffuse reflectance target as the measurement background, in areas that contained no inks or visible soiling and away from the margins. Different models were developed, two classification methods using linear discriminant analysis (LDA) method (Blanco & Villarroya, 2002; Stuart, 2007; Brereton, 2009; Miller & Miller, 2010; Brereton & Lloyd, 2014) to identify the presence of starch and polishing, and two regression methods using partial least squares (PLS) method (Brereton, 2009; Miller & Miller, 2010; Brereton & Lloyd, 2014) to estimate the degree of polymerization and the content of acidity. XLSTAT 2013 v.5.01 software was used for the development of the classification models, while Polychromix method generator v.3.101R2-64 software was used for the regression models.

4.3.1.1 Presence of Starch and Polishing

To build the classification model for starch presence, the spectra of all the ref-collection samples (228) were analysed using LDA method where it was divided randomly into two datasets; Calibration (138) and validation (90). The number of starched and non-starched samples was almost equal. On the other hand, only 104 samples were used to build the model for the identification of polished surfaces. 74 samples were selected randomly for calibration and 30 samples were used for independent validation. For both models, the spectral interval of 1600 – 2400 nm was used without any spectral pre-treatments applied to the spectra. Table 4-4 shows that the results of the two models are highly satisfactory, with 90 % and 87.6 % of successfully identified samples for starch and polished surface respectively.

Both models are very useful for collection surveys. However, it is worth emphasizing that the model for polishing is built based on the visual assessment of the presence of polishing so it still suffers from subjectivity in addition to the dependency on the local spot from where the spectral data were collected from each sample. The predictive value and

subjectivity of the model can be improved by using other scientific assessment techniques to confirm the presence of polished surfaces such as SEM and FTIR as described earlier. But the model as it is, is still beneficial in terms of time taken to predict the results compared to the visual assessment which is a very time consuming procedure.

Table 4-4. Validation matrices for LDA models for identification of starch and polishing. 138 and 74 samples were used for calibration, respectively.

From/To	No starch	Starch	Total	%correct
No starch	39	3	42	92.9
Starch	6	42	48	87.5
Total	45	45	90	90.0
From/To	Unpolished	Polished	Total	%correct
Unpolished	14	1	15	93.3
Polished	3	12	15	80.0
Total	17	13	30	86.7

4.3.1.2 Determination of pH and DP

For the PLS regression models, a calibration dataset of 70 spectra of samples with pH values measured using the cold extraction method, and another of 60 spectra of samples with DP determined using the standard viscometry method were used. Fewer samples were used for the DP model as samples with lignin could not be measured using the traditional method so they were excluded. Spectral pre-treatments were applied to the datasets in order to optimize the quality of calibration for the regression models. Standard normal variate method (SNV) and Savitzky-Golay filter (2nd derivative, 3rd polynomial order, 9-point window) in the spectral interval 1600 – 2400 nm were used for the pH model while only Savitzky-Golay filter (2nd derivative, 3rd polynomial order, 7-point window) was used for the DP model using the same spectral interval. Regression statistics for both methods are given in Table 4-5. Using independent validation datasets and based on the root mean square error of prediction (RMSEP), it was found that pH model does not perform well (RMSEP = 0.7 pH units), because the error is more than twice the uncertainty of the experimental method (= 0.3 pH units). The quality of prediction might be improved by using more samples with better distribution, but the model as it is can be used for a broad classification of samples. On the other hand, DP model errors are satisfactory (RMSEP = 177 DP units) and comparable to the models previously developed for European paper (Trafela et al., 2007). The developed models can thus be used as part of a non-destructive methodology for collection surveys.

Table 4-5. Specifications (calibration and validation parameters) of PLS regression models for pH and DP using NIR spectra obtained with the PHAZIR hand-held spectrometer; *n*-number of samples.

PLS model	Calibration					Validation		
	<i>n</i>	RMSE C	RMSEC V	R²	Factors	<i>n</i>	RMSE P	R²
pH	52	0.37	0.45	0.70	4	18	0.72	0.47
DP	45	263	298	0.60	3	15	177	0.78

It was of interest to explore the applicability of the PLS regression models developed for European paper to Islamic papers (SurveNIR). To achieve this, the same Islamic paper samples were measured using the SurveNIR instrument (Lichtblau, Dresden) in the interval 1100 – 2200 nm (average of 8 spectra/sheet with 300 scans each, 2 nm resolution). Then, the SurveNIR software, models and database for European papers were used to analyse the collected spectra and determine pH and DP values.

As seen in Figure 4-11, comparing the actual values of pH and DP (measured using invasive methods) to the predicted values obtained using SurveNIR method and the model developed especially for Islamic paper, SurveNIR regressions perform less well for both pH and DP by looking into the regression lines and correlation coefficients (R^2). The nearer the points to the regression line, the higher the correlation between the actual and predicted values and the higher the applicability of the model. This means that such regressions (Figure 4-11, below) are not applicable to Islamic papers and special models need to be developed for it. This is particularly the case for DP.

I also attempted to explore whether starch contributes to the results obtained from the application of SurveNIR models (Mahgoub et al., 2016), so starched samples were plotted with a different symbol (hollow squares) to visualize possible patterns as shown in Figure 4-11. Based on the predictions, it is evident that starch strongly affects the SurveNIR DP model where samples with starch and without starch tends to separate in two groups forming a pattern.

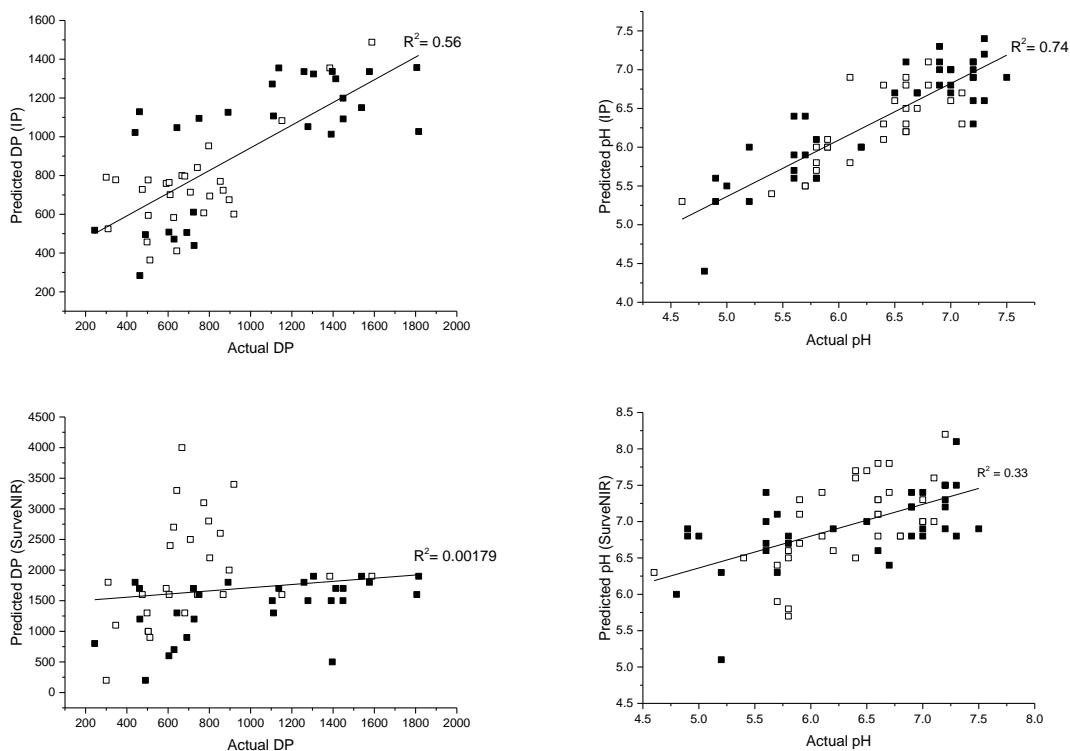


Figure 4-11. Comparisons of predicted and actual pH and DP values obtained with models developed specifically for Islamic paper (IP, above) and with models developed for European paper (SurveNIR, below). Hollow squares samples with starch, black squares no starch. R^2 was calculated for each set of data.

4.3.1.3 *Wellcome Collection Survey*

This sub-section describes a survey of a part of the Islamic Collection of the Wellcome Collection that was conducted using the developed non-destructive scientific characterization methodology for Islamic paper described above. This survey can be considered as a validation for the applicability of the developed methodology to real collections in situ. Using the non-destructive characterization methodology, it is possible to estimate paper characteristics of an unknown sample using only an NIR spectrum, based on the correlations of reference samples and spectral information obtained by multivariate data analysis (Trafela et al., 2007; SurveNIR). The survey aimed at identification of the most significant characteristics of Islamic paper: presence of starch and polishing, and also at determination of two chemical properties: acidity and degree of polymerization of cellulose in paper. The latter were of interest in order to assess the current material state (condition) of the collection and its stability. Moreover, in the sub-section we will explore the possibility of developing a dating model for Islamic paper using the NIR technique based on the spectral data collected from the same Islamic collection.

4.3.1.3.1. *Wellcome Collection Objects*

Historic objects (43 in total) were selected randomly from the Wellcome Library Islamic collection based on the digitally available catalogue (<http://wamcp.bibalex.org/home>). These objects represent different types of paper found in Islamic libraries and archives. The ID and date details of the selected objects are listed in Table 4-6. The objects were dated from 1652 and 1880 AD based on the date provided by the library 'Librarian date' and were all are written in Arabic. The sample set includes 305 randomly selected single sheets, where always 5 individual sheets were chosen to represent each type of paper, which means 61 different paper types in the 43 objects.

4.3.1.3.2. *Spectral Data*

Spectroscopic data were collected using the PHAZIR handheld NIR instrument (Polychromix) in the interval of 1600-2400 nm as an average of 10 scans per sample with a resolution of 8 nm (Figure 4-12) similar to the collection method used in the development of the non-destructive methodology. The measurements were carried out using single sheets with a Spectralon 99% diffuse reflectance target as the background, in areas that contained no inks or visible soiling and away from the margins. The handheld device was calibrated using the instrument built-in Spectralon reference. The location of each measurement was recorded photographically.

The repeatability of the instrument and reproducibility of the measurements (Williams, 2013; Bazar et al., 2016) were evaluated through the calculation of standard deviation (SD) of a series of spectral measurements in addition to the calculation of the coefficient of variance (CoV%) which represents the ratio of SD over the average of the spectral data.

For repeatability, a series of five spectral measurements were collected from same spot of same sample which gave SD = 0.002 and CoV = ~ 1%. Another series of 5 measurements from different spots on the same sample were collected for the evaluation of the reproducibility giving SD=0.01 and CoV = ~ 6%.



Figure 4-12. Collection of spectral data using PHAZIR handheld NIR instrument (Polychromix) in the interval 1600 – 2400 nm from the Wellcome Library Islamic collection.

4.3.1.3.3. *Survey Results*

Starch

The presence of starch was surveyed in the Wellcome collection as starch sizing was widely used in Islamic papermaking (Ibn Badis, 1025; Garlick, 1986; Baker, 1991; Loveday, 2001). However, it should be taken into consideration that starch was also used in the production of paper in China and in the early western paper as well (Garlick, 1986; Déroche, 2005). However, no such papers were surveyed as only Islamic collection from the 17th – 19th century were used in the survey.

The decision on the presence of starch was made by calculating the average probability for the presence of starch (%starch) in the 5 measured samples of the same paper type. For this, I used the multivariate classification method (linear discriminant analysis) developed using the ref-collection resulting from the ISH-survey (starch presence model) with 90% of correctness for the validation set. If %starch is higher than 50%, then the paper type was identified as a starch-containing one (Table 4-6).

Focusing on starch property, the survey results have shown that out of 61 different types of paper, only 27 show >50% probability of starch presence. These results indicate that about 44% of paper in the Wellcome Library Islamic collection contains starch and is therefore potentially of Islamic origin.

Polishing

The polishing process was distinct to Islamic papermaking, and reduced roughness of the paper surface. Good quality paper had to be polished, almost translucent, with or without

a material such as gum tragacanth or egg white (Baker, 1991; Loveday, 2001; Déroche, 2005). The calibration model from the Islamic paper survey based on the LDA discrimination method was applied in the Wellcome Collection survey to identify polished papers, and to compare instrumental assessment with the visual examination of the samples.

The results have shown that 85% of the surveyed samples were polished (probability >50%), confirming the spread of this technique in Islamic collections (Table 4-6). About 70% of the samples were visually identified as polished as well, which shows that instrumental identification of polishing is not as accurate as visual identification. However, this difference in estimation is consistent with the prediction model error rate (~13%).

Acidity (pH)

It is common practice in surveys of paper collections to assess pH as a good indication of paper stability combined with the information about the cellulose DP (Strlič & Kolar, 2005; Tse, 2007). Unfortunately, most traditional techniques used to measure pH are either destructive or micro-destructive, which is not suitable for collection surveys.

Using the calibration regression model (pH model), pH of Wellcome samples was determined based on their collected spectral data. The average and standard deviation of pH values for the 5 individual sheets of each paper type are shown in Table 4-6. Most of the estimated pH values were greater than or equal to 7 which means that the samples are neutral to mildly alkaline and thus their rate of deterioration is low.

The error of prediction is 0.7 pH units which is sufficiently good for identification of very acidic samples (pH < 5), as finer classification is barely needed, besides, the uncertainty of the traditional method of pH determination is ± 0.3 pH units, which is comparable. For very acidic samples, de-acidification is often considered as a suitable conservation intervention (Strlič & Kolar, 2005; Hubbe et al., 2017). These results can therefore provide a quick assessment of the stability of the collection and in combination with DP, they could be used to make preservation as well as intervention decisions.

Degree of Polymerization (DP)

Determination of DP is a destructive process and traditionally requires sampling, which is impossible for historic documents. However, in this survey the calibration method developed based on the PLS regression method (DP model) was used to determine the DP of Wellcome Collection samples. The range of DP values (average and standard deviation out of the 5 individual samples per paper type) is listed in Table 4-6.

The results show significant variation. For reference, paper with DP 300 is considered at high risk of mechanical damage during handling due to brittleness. Most European rag paper has DP of ~1500 or higher, and bleached pulp paper (contemporary paper) has DP of ~2500 (SurveNIR). Most of the surveyed papers have a DP value over 800 which is

safe for handling; however, it is evident that the paper is more degraded than European rag paper of comparable age, which must reflect its past storage environments, which may have been comparatively warmer than European storage environments. The lowest DP value was measured for WMS.AR.735, which is at significant risk of accumulating mechanical degradation. The prediction error of the method is 177 DP units, which is considered good for surveys as it is comparable to the error of the reference laboratory method.

Table 4-6. Estimated properties of the surveyed papers from the Wellcome Islamic collection: probability of the presence of starch (%starch), probability of the presence of polished surfaces (%polishing), predicted average degree of polymerization (DP) and predicted average pH with the standard deviation (\pm). Colour shading indicates a positive ID for starch and polishing. If both are present, the paper has been classified as Islamic paper.

Sample	Year (AD)	%starch	%polishing	DP	pH
WMS:AR.471	1652	61	76	1380 \pm 90	7.6 \pm 0.1
WMS:AR.820	1696	93	97	1170 \pm 20	7.5 \pm 0.1
WMS:AR.592-Type1	1700	23	98	1390 \pm 70	7.6 \pm 0.1
WMS:AR.592-Type2	1700	0	93	1420 \pm 50	7.7 \pm 0.1
WMS:AR.592-Type3	1700	48	100	1280 \pm 70	7.4 \pm 0.2
WMS:AR.592-Type4	1700	22	100	1500 \pm 70	7.6 \pm 0.1
WMS:AR.592-Type5	1700	1	100	1330 \pm 40	7.5 \pm 0.2
WMS:AR.592-Type6	1700	0	100	1220 \pm 70	7.7 \pm 0.1
WMS:AR.609	1703	0	100	1310 \pm 130	7.5 \pm 0.1
WMS:AR.734	1705	30	79	1050 \pm 70	7.3 \pm 0.2
WMS:AR.278	1717	10	100	1240 \pm 60	7.1
WMS:AR.22	1719	24	98	1440 \pm 60	7.6 \pm 0.1
WMS:AR.519	1724	2	57	1480 \pm 80	7.4 \pm 0.1
WMS:AR.454	1734	19	100	1300 \pm 60	7.4 \pm 0.1
WMS:AR.521	1738	42	56	1230 \pm 40	7
WMS:AR.583	1750	100	100	880 \pm 70	8
WMS:AR.791	1758	32	100	1160 \pm 90	7.1 \pm 0.2
WMS:AR.26	1761	9	100	1220 \pm 170	7.1 \pm 0.1
WMS:AR.292-Type1	1764	100	100	560 \pm 90	7.6 \pm 0.3
WMS:AR.292-Type2	1764	87	1	680 \pm 50	7.7 \pm 0.2
WMS:AR.385	1771	100	100	700 \pm 70	7.2 \pm 0.1
WMS:AR.621-Type1	1773	89	99	1000 \pm 40	7.2 \pm 0.1
WMS:AR.621-Type2	1773	1	0	1320 \pm 130	7.6 \pm 0.1
WMS:AR.621-Type3	1773	82	98	930 \pm 10	7.4 \pm 0.1
WMS:AR.621-Type4	1773	69	100	1280 \pm 70	7.3 \pm 0.1
WMS:AR.621-Type5	1773	61	82	1260 \pm 60	7.4 \pm 0.1
WMS:AR.621-Type6	1773	42	93	1210 \pm 70	7.3 \pm 0.1
WMS:AR.456	1782	58	100	1380 \pm 120	7.3 \pm 0.1
WMS:AR.821-Type1	1786	27	90	1420 \pm 30	7.5 \pm 0.1
WMS:AR.821-Type2	1786	57	97	1410 \pm 100	7.3 \pm 0.2
WMS:AR.573	1788	1	100	1560 \pm 50	7.6 \pm 0.1
WMS:AR.201	1797	100	100	520 \pm 90	7.3 \pm 0.2
WMS:AR.267-Type1	1800	1	0	1190 \pm 80	8.6 \pm 0.2

WMS:AR.267-Type2	1800	1	20	1110±70	8.5±0.6
WMS:AR.624-Type1	1810	25	1	1090±80	7.7±0.1
WMS:AR.624-Type2	1810	15	0	1150±30	7.7±0.1
WMS:AR.624-Type3	1810	57	3	980±60	7.6±0.1
WMS:AR.397	1811	5	100	1240±70	7.6±0.1
WMS:AR.445-Type1	1812	100	100	750±50	7.1±0.2
WMS:AR.445-Type2	1812	85	100	1130±250	7.2±0.1
WMS:AR.445-Type3	1812	100	100	1080±100	7.2±0.1
WMS:AR.726	1819	100	100	630±80	7.7±0.1
WMS:AR.286	1825	100	100	770±60	7.6±0.1
WMS:AR.382	1829	36	95	1180±110	6.9±0.1
WMS:AR.116	1830	79	97	1400±80	7.5±0.1
WMS:AR.459	1835	45	100	1280±170	7.8±0.2
WMS:AR.18	1838	100	100	690±30	7.2±0.1
WMS:AR.594-Type1	1844	1	100	1400±70	8
WMS:AR.594-Type2	1844	23	100	1240±40	8.1±0.1
WMS:AR.444	1845	2	100	1150±70	7.6±0.1
WMS:AR.34	1846	16	100	1080±140	7.3±0.2
WMS:AR.606	1847	11	77	1200±110	7.3±0.1
WMS:AR.746	1850	55	100	1490±40	7.4±0.2
WMS:AR.588	1851	30	94	1370±30	7.3±0.1
WMS:AR.291	1857	100	100	710±80	8
WMS:AR.460	1858	99	99	850±80	7
WMS:AR.664	1867	45	12	1200±80	6.8
WMS:AR.831	1876	68	24	820±30	8.1±0.3
WMS:AR.254	1880	100	100	800±90	7.1±0.1
WMS:AR.735	1883	100	100	330±40	6.1±0.2
WMS:AR.593	1887	11	100	810±30	7.2±0.1

Moreover, I attempted to assess the distribution of the predicted pH and DP of the tested Wellcome collection samples in relation to paper categories (presence of starch and polishing, either one or none or both) to explore if there is any patterns or trends indicating their influence on the condition of the objects. No particular trend can be identified as evident from Figure 4-13. However, samples with either starch or polishing or both (potentially classified as Islamic paper) have slightly higher DP values than the other samples.

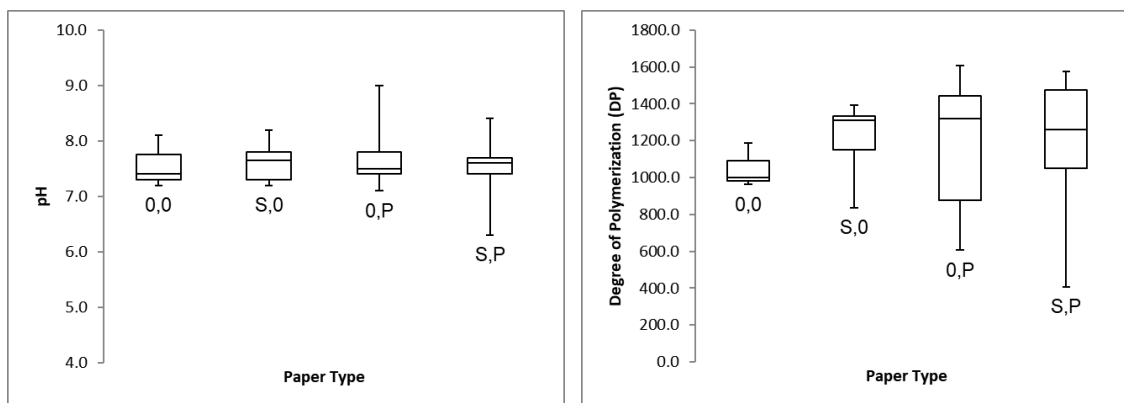


Figure 4-13. Boxplots of the distribution of the pH (left) and DP (right) values predicted for samples (43 objects) of the Wellcome Islamic collection as a measure of stability using a non-destructive characterization methodology based on NIR spectroscopy. Values are grouped according to the two main characteristics of Islamic papermaking; starch-sizing and surface polishing which have been also estimated using same methodology. (0) means samples with no starch/unpolished, (S) means samples are starch-sized and (P) means samples are polished. Each box shows the distribution of the measurements based on the median, 1st and 3rd quartile. The whiskers represent minimum and maximum values.

Dating

Dating of historical objects is of significant importance to scholars. There are numerous dating techniques for historic materials: empirical techniques require excellent experience and instrumental techniques require sampling (May & Jones, 2006). Lately, NIR spectroscopy has been used to date historic objects non-destructively (Trafela et al., 2007; Možir et al., 2011).

The age of a paper sample is reflected in the chemical changes taking place during its lifetime, represented by lower DP, lower pH, higher crystallinity etc. (Trafela et al., 2007). However, different composition (fibre type, sizing, polishing) also reflected historic development in papermaking and could therefore be used for dating. All of these properties are represented in the IR spectra allowing for dating objects using a proper calibration model as is the case described in the literature (Trafela et al., 2007; Brown et al., 2017) where the authors in the first study were able to build calibrations to date historical European paper based on spectral data of a considerable number of samples taking into account the change in paper production occurred at approximately 1850 with a standard error of ~ 9 years while in the second study authors were able to date Chinese paper (19th and 20th C.) with a satisfactory uncertainty (~13 years).

Similarly, during the Wellcome survey, it was possible to develop a dating model for Islamic papers based on the NIR spectral data collected from the 43 historical books (the surveyed papers from the Wellcome Islamic collection described in Section 4.3.1.3.1) with the aid of multivariate data analysis methods. As the books were dated between 1652 and 1880 AD (Table 4-6), the developed dating model can be used to date Islamic paper sample of unknown date in this approximate range.

The Polychromix method generator v.3.101 R2-64 software and partial least squares (PLS) method (Garthwaite, 1994; Miller & Miller, 2010) were used to develop the model using the collected NIR spectra of the surveyed Wellcome paper samples and their corresponding librarian date. Different spectral pre-processing has been used in the interval 1600-2400 nm to optimize the quality of the calibration such as standard normal variate (SNV) and Savitzky-Golay algorithms. The model was cross-validated using the leave-one-out method. Root mean square errors for calibration (RMSEC) and validation (RMSECV) were calculated to evaluate the model.

Dating model was developed using all the samples as a calibration set ($n=298$), which gave a validation error (RMSECV) of 44 years and correlation coefficient (R^2_{cv}) of ~ 0.5 . To check whether starch presence influences the uncertainty of the model, the calibration set was divided into two subsets: samples with and without starch according to the estimated results in Table 4-6 and different dating models were developed for each set. The surveyed samples with $> 50\%$ probability of starch presence (Table 4-6) were considered as a separate sample set. A dataset of 170 samples with no starch, and another one of 128 samples with starch were used. Table 4-7 lists the specifications of all the developed dating models.

Looking into Figure 4-414, for the starched samples, the calibration error (RMSEC) is 21 years and the validation error (RMSECV) is 33 years, and for the samples without starch, it is 32, 45 years, respectively. Results are a bit better, especially for the model of samples with starch. The uncertainty of the developed dating models is acceptable and comparable with other studies (Trafela et al., 2007; Možir et al., 2011; Fenech et al., 2012; Martins et al., 2012; Brown et al., 2017) taking into consideration the different number of samples, materials and the spectroscopic techniques used in addition to the accuracy of the historic data (librarian date) which show their applicability to date unknown samples of these paper types. However, this should be explored further for better results using wider range of well-characterized Islamic samples.

Table 4-7. Specifications of the PLS models for dating; n – number of samples, RMSEC – calibration error, RMSECV – validation error, and R^2 – correlation coefficient.

Model	n	RMSEC	RMSECV	R^2
Dating (All samples)	298	39 (years)	44 (years)	0.49
Dating (starch samples)	128	21 (years)	33 (years)	0.78
Dating (no starch samples)	170	32 (years)	45 (years)	0.71

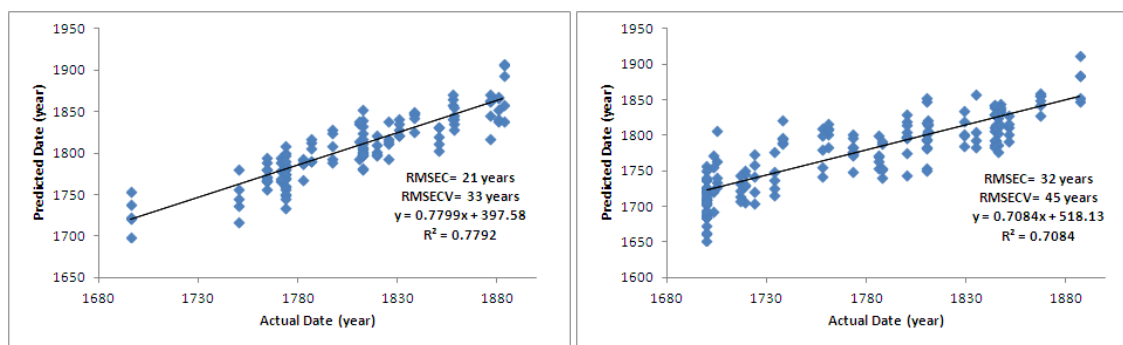


Figure 4-414. Validation of two dating models developed based on spectral data collected from Wellcome Collection samples using NIR spectroscopy (**Table 4-6**). The blue dots in both plots represent paper samples with (right) and without starch (left). The figure shows the correlation coefficient between the actual and predicted date for both models.

4.3.1.3.4. Conclusions of the Survey

This sub-section validates a new non-destructive spectroscopic method for characterization and surveying of Islamic paper based on NIR spectroscopy. 43 books from the Islamic collection of the Wellcome Collection were surveyed using the portable and non-destructive method from the Islamic paper survey, in order to identify four paper properties: presence of starch and polishing, pH and degree of polymerization (DP). The first two could be used for identification of Islamic paper (those with starch and polishing have most probably been produced in Islamic countries), while pH and DP can reflect the current condition of paper.

The survey results have shown that ~90% of the Wellcome Library Islamic collection are of Islamic origin in respect to the two main characteristics of Islamic paper; the presence of starch and polishing. Moreover, the results show that most of the collection is in a good condition (DP > 800 and pH >= 7) and can be handled safely with the exception of a few papers based on the estimated pH and DP values.

In addition, a dating model was developed using NIR spectral data based on multivariate data analysis, which can now be used to date historic Islamic paper from the 17th-19th century (1652 -1880) AD.

Such successful results demonstrate the applicability of NIR spectroscopy in the study and surveys of Islamic paper collections. This is considered as the first such study, if applied across Islamic paper collections, it could be used to systematically develop evidence-based preservation policies in Islamic libraries and archives.

4.3.2 HSI Spectral Analysis

This sub-section explores the potential for mapping the chemical composition of Islamic paper, specifically starch-sizing, polishing, pH and cellulose degree of polymerization (DP) using NIR HSI due to its ability to resolve information spatially and spectrally for the whole surface of an object. From the Islamic paper survey (Section 4), starch and polished surfaces are potentially considered as the main characteristics of Islamic paper while the pH and cellulose DP provide essential information about an object's conservation

condition. Being able to visualize the spatial distribution of these chemical properties over the whole surface of an object would add a new layer of information about the homogeneity of the object working as a guidance for conservators and researchers for better conservation decisions.

To achieve this, quantitative calibration models need to be developed to determine these properties for unknown samples based on spectral information collected by the HSI system of a representative reference samples of Islamic paper in the range 1000-2500 nm.

Therefore, I developed a special calibration target using the well-characterized reference collection of Islamic paper (ref-collection of Islamic paper survey, Section 4). The target includes only 105 out of 228 samples selected from the ref-collection due to availability of samples and information about their properties (e.g. both pH and DP). A description of the target is shown in Chapter 2 (Section 2.1) and the full list of the samples with their properties can be found in appendix I. The target was scanned using the acquisition parameters in Table 4-8 and the spectral information was extracted and analysed to build the models and quantitative chemical maps of the different characteristics of Islamic paper.

Table 4-8. Acquisition parameters of HSI system used in the experiments of this section.

Lens (Focal Length)	30 mm
Exposure	6 ms
Scan speed	54.9 mm/s
Illumination intensity	500 W
Aperture	F/2.0
Binning	None (1x1)
Gain	1
Spectral Range	1000-2500 nm
Scanning Background	Whatman No.1 paper (4 layers)

Out of 105 samples, there are 45 starch-containing samples and 43 samples have been categorized to have polished surfaces. pH is available for ~70 samples ranging from 4.5-7.5 pH, while DP values are available only for 57 samples as the rest have high lignin content. The average DP of all the 105 samples is 848 while the average pH is 6.4. The distribution of the DP and pH values for the calibration target is shown in Figure 4-15.

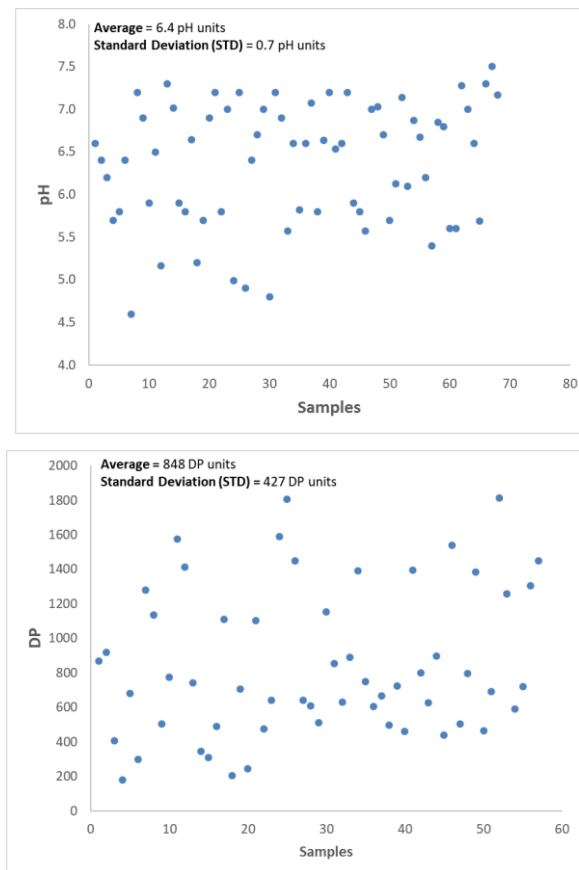


Figure 4-15. Distributions of pH (left) and DP (right) of the Islamic paper target samples.

Multivariate data analysis methods were selected for building and validating the calibration models in addition to the optimization of the spectral data. Methods are commonly chosen based on the type of the calibration model; classification or regression and the collected spectra where the widely used methods in the literature were adapted here as explained in Chapter 3 (Section 3.4).

Two different methods were used to build the classification models for determination of starch presence and polished surfaces in the samples; by applying either principal component analysis (PCA) or partial least squares regression analysis (PLS) for data reduction (Næs et al., 2002; Brereton, 2009; Miller & Miller, 2010; Brereton & Lloyd, 2014) before discrimination, then follow that using linear discriminant analysis (LDA) method (Blanco & Villarroya, 2002; Stuart, 2007; Brereton, 2009; Miller & Miller, 2010; Brereton & Lloyd, 2014) on selected PC scores or factors; the two methods are known as PCDA (Blanco & Villarroya, 2002; Næs et al., 2002; Stuart, 2007; Miller & Miller, 2010) and PLSDA (Barker, & Rayens, 2003; Westerhuis et al., 2008; Ruiz-Perez & Narasimhan, 2017; Lee et al., 2018).

For the determination of pH and cellulose DP in Islamic paper, PLS regression (Næs et al., 2002; Brereton, 2009; Miller & Miller, 2010; Brereton & Lloyd, 2014) was used to build the calibration models for both chemical properties.

To optimize the collected spectra and compensate for any variations or noise before building the models, different spectral pre-processing methods (Fearn, 2001; Manley,

2014) were applied such as standard normal variate (SNV) and Savitzky-Golay (SG) derivation filter (Savitzky & Golay, 1964).

Validation of most of the models was conducted using leave-one-out cross validation (LOOCV) while assessment of the performance of the models was done differently depending on the method. Mainly, the proportion of correctly identified samples (%correctness or success rate) was used for the discrimination methods and the root-mean-square error of cross-validation (RMSECV) with the correlation coefficient R_{cv} were calculated to evaluate the regression models (Næs et al., 2002).

Models then were used as the basis for the development of quantitative chemical maps of some examples of Islamic paper from the ref-collection to provide visual cues as to the current conservation condition of the document.

Matlab with using the PLS toolbox library (EIGENVECTOR, 2019) was used to process the datacubes, develop models and build chemical maps.

4.3.2.1 Sample Selection

As a preparation step, and after scanning the Islamic paper calibration target with the HSI system, then applying the relative reflectance calibration method using the Spectralon 99% diffuse reflectance white target and dark current images, a representative spectrum for each sample in the target was extracted and associated with the corresponding sample ID to prepare the datasets for the development of the quantitative calibration models. To identify the sample pixels in the calibration target, an average image was calculated from the datacube. Then, based on the values, a threshold was selected to differentiate between sample and the surrounding holder pixels (Figure 4-16). Each sample square is $\sim 7 \times 7$ pixels ($\sim 1 \text{ cm}^2$). The representative spectra were collected from the middle of each sample from a ROI – region of interest – of 3×3 pixels (Figure 4-17). Note that the effect of using spectra of different ROI sizes on the calibrations/results was explored in and demonstrated in Chapter 4. All the selection process was conducted using Matlab code, which I developed.

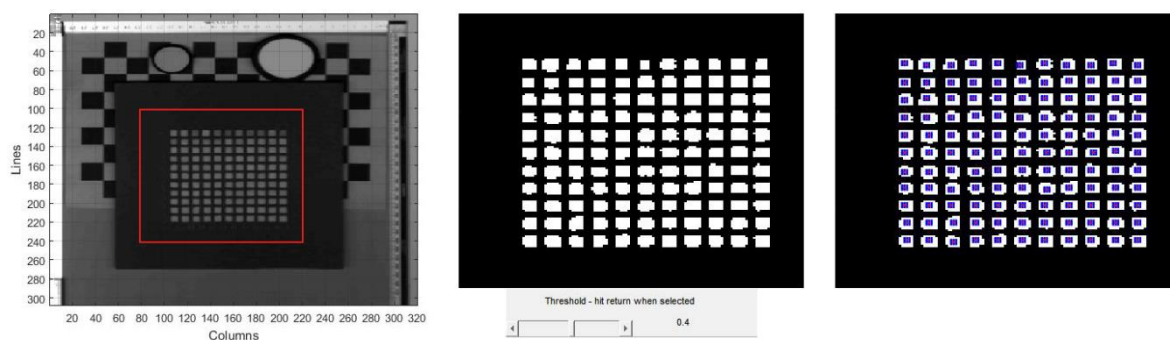


Figure 4-16. Pixel selection process: left: the area from where samples are extracted; middle: average image of the calibration target calculated over the spectral dimension for each pixel, following which a threshold was applied (default 0.4); right: minimum average value (black) assigned to the holder pixels, maximum values (white) representing the sample pixels, and the position of selected ROI (3×3 pixels) of each sample (blue).

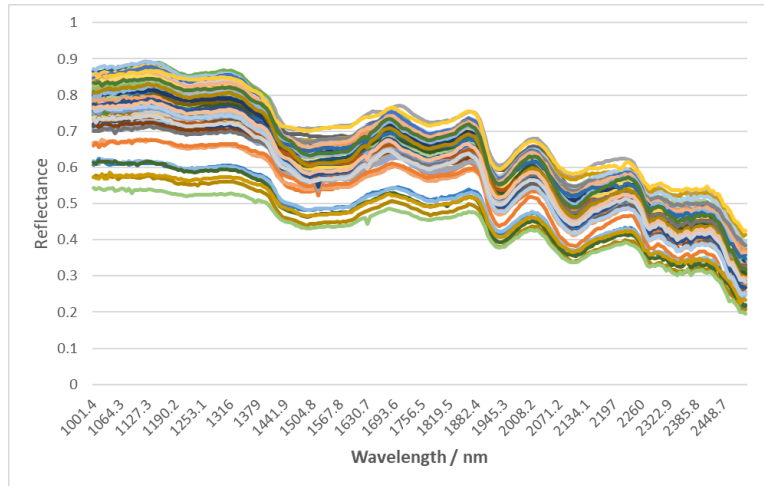


Figure 4-17. Reflectance spectra of 105 samples collected by the HSI system in the spectral range 1000 – 2500 nm from the calibration target. These samples were for subsequent calibration.

4.3.2.2 Data Analysis: Calibration Models

4.3.2.2.1 Discrimination Models

Starch

Based on the spectral information collected from all the samples (105) of the Islamic paper calibration target (Figure 4-17), a calibration model was developed to discriminate between samples with starch (=1) and without starch (=0). PCDA (PCA followed by LDA) method was used with the aim to get the lowest error rate on cross-validation results. The success of the validation of the model was expressed as the percentage of correctly identified samples.

The spectral region 1450-2350 nm was used and the average spectra of the samples were pre-treated using SNV method. Firstly, PCA was applied, followed by the LDA method to each PC from 1-25 PCs generated from the PCA where the PC number that gave the highest % correctness (success rate) on cross-validation was selected.

The optimal results were given at 9 PCs, with approx. 84% successfully identified samples out of the 105 used in the calibration (Table 4-9). This proves the good ability of the HSI technique for discrimination, especially when compared to its peer LDA model (described earlier in Islamic paper survey, Section 4) developed using the PHAZIR hand-held spectrometer in the spectral range 1600 – 2400 nm. The latter was a bit better with 90% correctness using 138 samples for calibration. Many differences should be taken into consideration while comparing the two models such as the spectral resolution of the two instruments and the calibration dataset size in addition to many acquisition parameters, e.g. illumination, backgrounds, selected spectral range for the models etc. However, these differences should have been accounted for in the process of calibration.

To explore which wavelengths in the selected spectral range are used for the development of the model contributed most to it, I calculated the weights for each wavelength in the

discriminant function by combining the coefficients of the LDA model with the loadings from the PCA (Figure 4-18). The spectral range of 1600–1950 nm appears to have the most pronounced influence. The use of this range might improve the calibration model results if applied, but this was not explored further due to research time constraint and that the obtained results are sufficient as a proof of the concept about the potential of HSI technique to be used for discrimination.

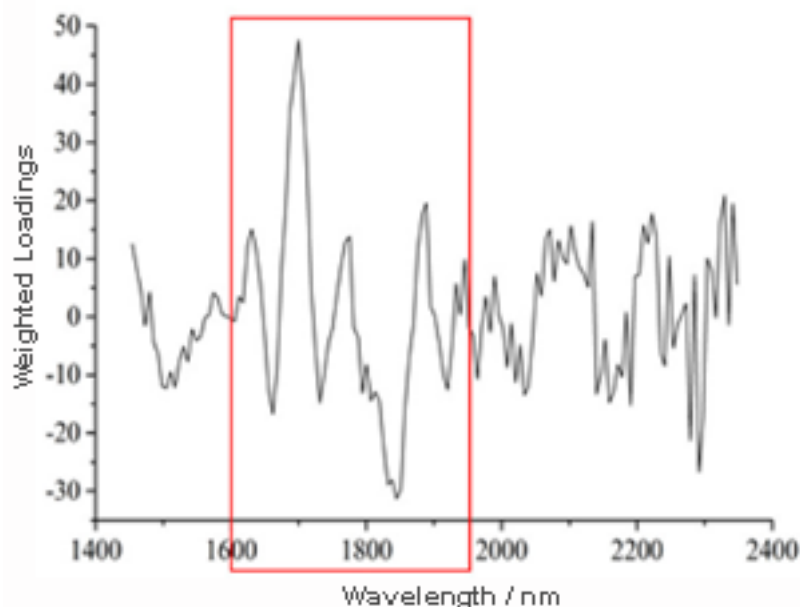


Figure 4-18. Weighted PCA loading vectors based on LDA coefficients, indicating the wavelengths with the highest contribution (1600–1950 nm) to the starch discrimination model developed for Islamic paper using HSI system.

Polishing

To develop the discrimination model for the identification of polished surfaces (marked as =1), PLSDA method (Barker & Rayens, 2003) was applied to the HSI spectral data of the whole samples of the Islamic paper calibration target (105 samples (divided into 43 polished and 62 unpolished samples), Figure 4-17). Another common classification method was explored, PLSDA combines dimensionality reduction through applying PLS method and discriminant analysis using the LDA method on the scores into one algorithm. Applying a dimension reduction as a first step, gives the potential to reduce the computational cost and time in addition of over-fitting risks (Lee et al., 2018). PLSDA is considered as a supervised version of the PCDA method as it reduces dimensionality with a prior knowledge of the classes needs to be separated (Ruiz-Perez & Narasimhan, 2017). While PCA works on the total variability of the sample (covariance matrix) as the base for the reduction, PLS emphasises the among-groups variability (between groups sums of squares and cross products matrix) (Barker & Rayens, 2003; Ruiz-Perez & Narasimhan, 2017). However, the method is prone to overfitting problem (Ruiz-Perez & Narasimhan, 2017), so cross validation is often used as an important step for validation of the model, especially Leave-one-out method (LOOCV) when the size of the dataset available is small

so it makes better use of the data (Westerhuis et al., 2008; Lee et al., 2018). There are many quality measures to assess the performance of the PLSDA model (Lee et al., 2018) such as the root mean squared error (RMSE), classification error rate, specificity (number of samples predicted as not in the class divided by actual number not in the class), sensitivity (number of samples predicted as in the class divided by number actually in the class) of the model and the area under the receiver operating characteristics curve (ROC curve) (Lee et al., 2018) but similar to the PCDA starch model, % correctness (success rate) will be reported here as the main parameter to assess the polished model.

Spectral data were treated using Savitzky-Golay filter (1st derivative, 2nd polynomial order, 15 pt window) in the spectral range 1000-2450 nm. Based on the results shown in Table 4-9 and compared to the results of the model developed using the spectrometric data from the Islamic paper survey section 4 (correctness ~87%), the PLSDA model of polished surfaces performs in a very good way with an approx. 86% successfully identified samples and ~ 0.14 cross-validated error rate.

Table 4-9. Validation matrices for PCDA and PLSDA models for identification of starch and polishing using leave-one-out cross validation (LOOCV) method. Cross validated (CV) success rate for the different classes and the total are shown.

		Predicted			
	From/To	No starch	Starch	Total	CV Success rate (%)
Actual	No starch	50	10	60	83.3
	Starch	7	38	45	84.4
	Total	57	48	105	83.8
		Unpolished	Polished	Total	CV Success rate (%)
Actual	Unpolished	35	8	43	81.4
	Polished	7	55	62	88.7
	Total	42	63	105	85.7

4.3.2.2.2. Regression Models

Acidity (pH)

For the PLS regression model to determine pH of Islamic paper samples, 68 spectra of samples from the IP calibration target with pH ranges from 4.5 – 7.5 pH units measured by the cold extraction method and collected using the HSI system using the acquisition parameters at Table 4-8 were used as a calibration dataset. Spectral data were treated by mean-centring to make sure all variables have comparable ranges and distributions. Savitzky-Golay filter (1st derivative, 2nd polynomial order, 11-point window) in the spectral interval 1400 – 2200 nm were also used in the pH model and then it was validated using LOOCV method. The optimal validation results (Figure 4-19) gave an RMSECV=0.5 pH units and correlation coefficient (R_{cv})=0.69 using 4 factors.

The performance of the model is consistent with the pH model based on the spectral data collected by PHAZIR hand-held spectrometer from the Islamic paper survey (Section 4.1)

(RMSECV=0.45, R_{cv} =0.70, 4 factors, n =52). Therefore, similarly, it is only expected to be used for general classification of Islamic paper samples regarding their acidity.

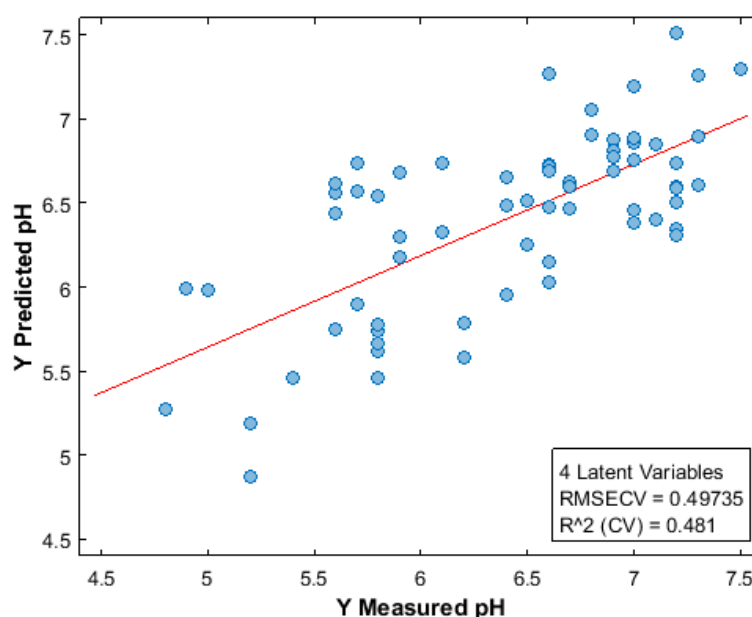


Figure 4-19. The results of the developed PLS regression model for the determination of pH using spectral measurements of 68 samples scanned by the HSI system.

Degree of polymerization (DP)

A regression model was developed for the prediction of DP values for unknown samples based on the samples from the IP calibration target that were measured using the viscometric method. Only the samples without lignin (57 samples) so with known DP values were used to build the model. Although it is considered as a small dataset, its size still conformed to the relevant ASTM E1655 standard (ASTM, 2000).

Similar to the other models, spectral data were collected using the HSI system with the acquisition parameters described in Table 4-8. The spectra were pre-treated with Savitzky-Golay (SG) filter (1st derivative) using different polynomials (2, 3 and 4) and filtering window sizes from 5-55 points then the optimal parameters for the model were selected. To select the best validation results, the model was calculated for each PLS factor from 1-25 and the factor that gave the smallest root mean square error of the cross validation (RMSECV) and high correlation coefficient (R_{cv}) was selected.

The optimal model results gave an RMSECV=285 DP units and R_{cv} =0.77 using 13 factors, 3rd polynomial order and 7-points window size, in the spectral interval 1450 – 2300 nm in addition to the mean-center treatment (Figure 4-20). The model has a potential to be used in collection surveys, performing in a similar manner as the model reported in the Islamic paper survey for Islamic paper (n =45, RMSECV=298, R_{cv} =0.88) and the model previously developed for European paper (n =86, SEE=161, R =0.99; Trafela et al., 2007). However, it should be taken into account the differences in spectral resolution of the used instruments and the different sizes of datasets, in addition to the different pre-processing

and calibration methods used. It is possible that better results could be obtained with a bigger dataset in the future.

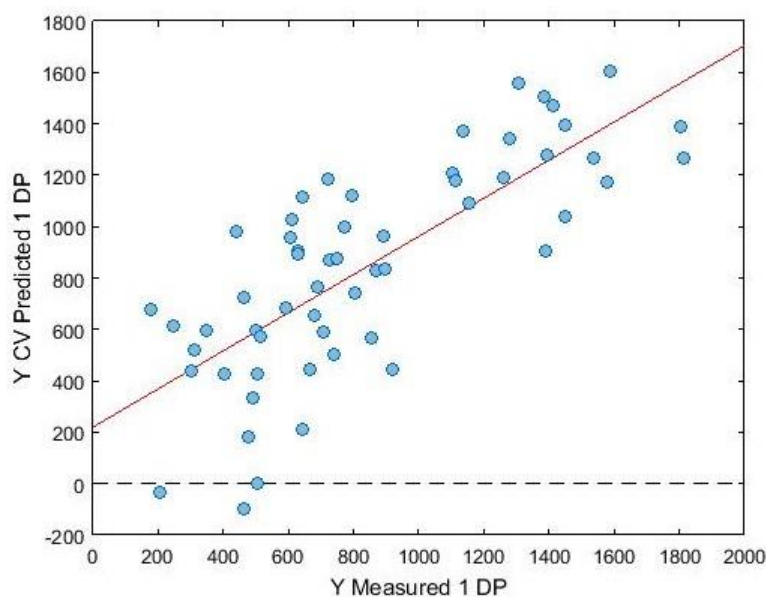


Figure 4-20. The results of the developed PLS regression model for the determination of DP of cellulose in paper using 57 Islamic paper samples with an RMSECV= 285 DP units and correlation coefficient $R_{cv}=0.77$ using 13 factors. The plot correlates predicted with actual DP measurements.

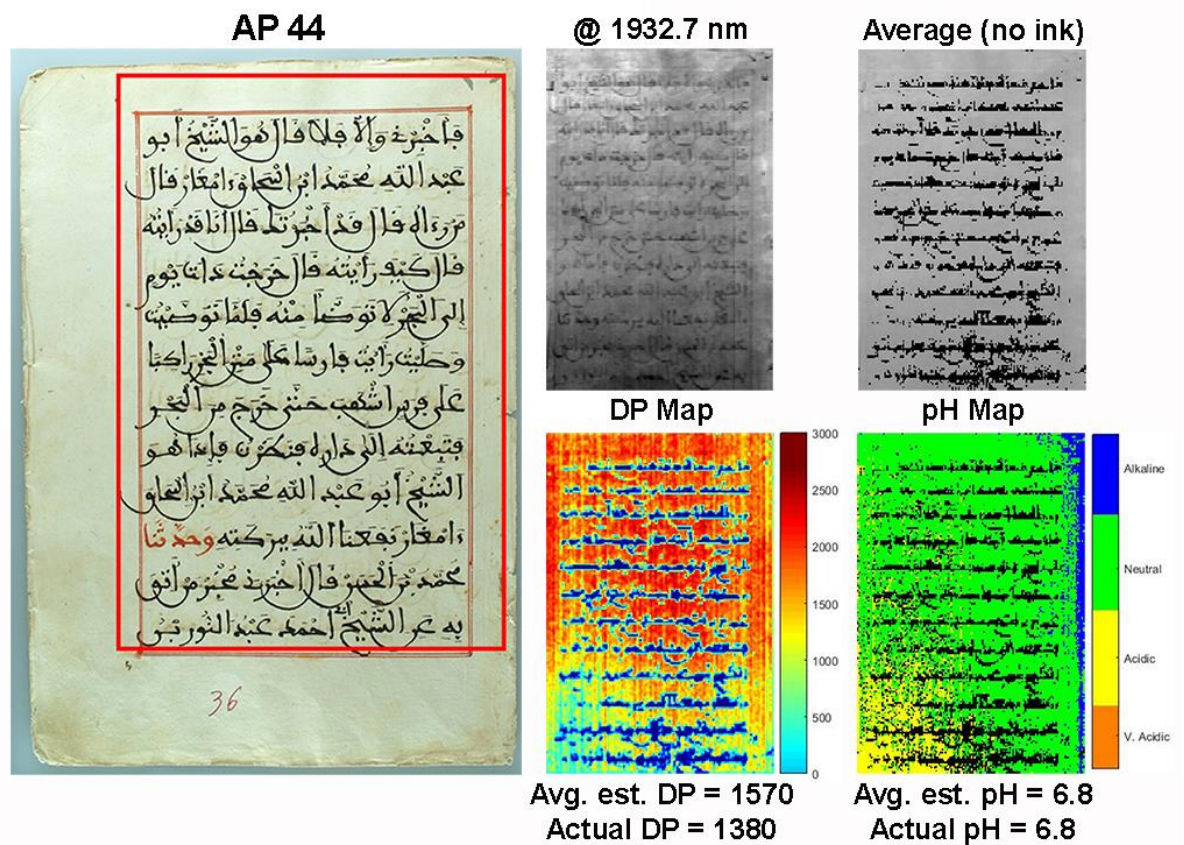
4.3.2.3 Quantitative Near-Infrared Chemical Mapping

Although the calibration models developed based on the HSI spectral data are performing in a similar way to the models using spectroscopic (Phazir) data (described in the Islamic paper survey, Section 4), the HSI technique is more advantageous due to its ability to produce chemical images, and consequently allows the visualization of the spatial distribution of chemical composition in non-homogeneous samples (Manley, 2014).

Using the developed PLS regression models to determine the pH and DP of cellulose in Islamic paper, quantitative pH and DP maps were generated for some selected documents (AP 44, AP 35, AP 127-1, AP 57) from the ref-collection (Chapter 2, Section 2.1) (Figure 4-21). The figure shows the predicted pH and DP values for each pixel in the image. The pixels with ink were excluded as a different regression models should be used for these. The actual measured pH and DP of the documents together with the average predicted values are also shown.

Although most of the selected documents are visually fairly homogeneous objects, they demonstrate the importance of visualizing the distribution of the material properties across the whole surface of an object. pH and DP maps are consistent with each other for most of the examples, where areas with low pH values are with low DP values as well. As seen for AP 44, AP 35 and AP 127-1 (left side), the composition of the document changes from the spine towards the margins (cf. acidity map) while for AP 57, the composition changes from top to bottom. It is also worth considering the effect of the morphological changes on the surface of the documents while interpreting the results of the chemical maps generated

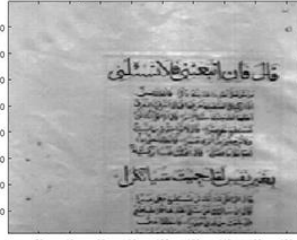
from the papermaking techniques such as polishing and sizing variations when applied manually (which means unevenly) or any other deterioration effects from dirt, water, soil etc. Some noise-like features can be observed in the maps, which needs further research to evaluate their causes in details. It is unclear if this originates from spectral noise or from the variations in paper surface morphology which could lead to minor differences in the spectra and the modelled values. Despite this, the maps still can show the potential of using quantitative imaging in visualizing deterioration across an object's surface which could be of great use to conservators and researchers providing them with a tool that help them to take evidence-based conservation decisions for their collections, e.g. identification of areas that require preferential treatment such as the areas with lower pH values that can be locally deacidified. Also, researchers can use maps to study the effect of some factors on the object in terms of handling or display such as exposure to a localized light source or how readers as an example handle a document in a library through investigating the deterioration locations on the object's surface.



AP 35



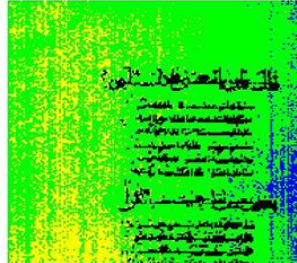
@ 1932.7 nm



Average (no ink)

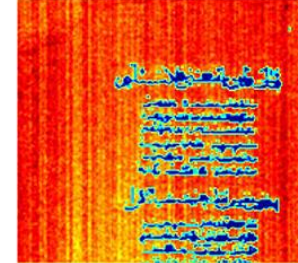


pH Map



Avg. est. pH = 6.8
Actual pH = 7.2

DP Map



Avg. est. DP = 1383
Actual DP = 1806

AP57

Front



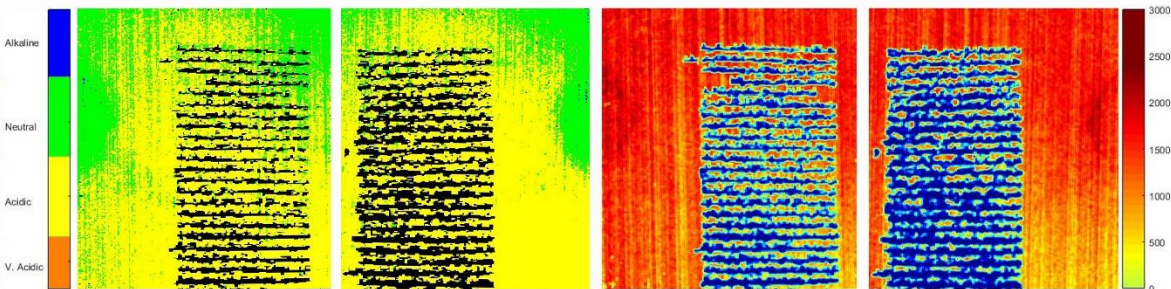
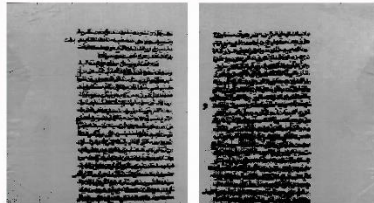
@ 1932.7 nm



Back



Average (no ink)



pH map
Avg. est. pH = 6.0
Actual pH = N/A

DP map
Avg. est. DP = 1260
Actual DP = N/A

AP127-1

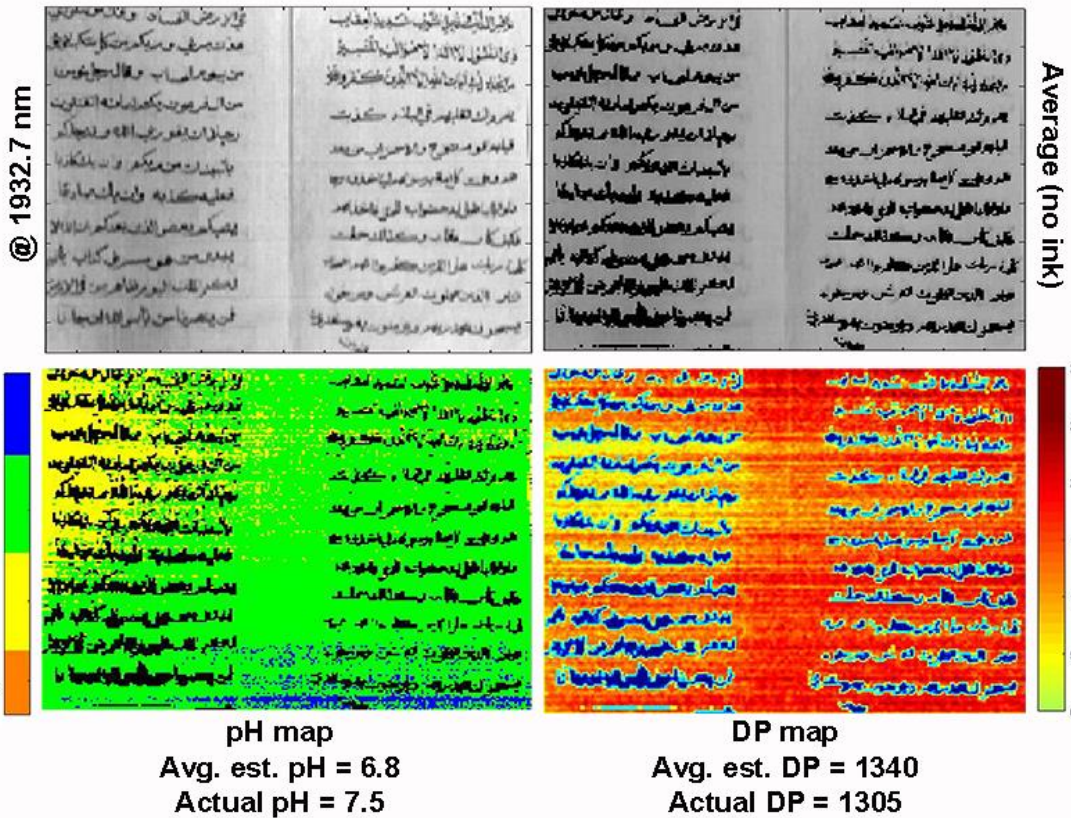
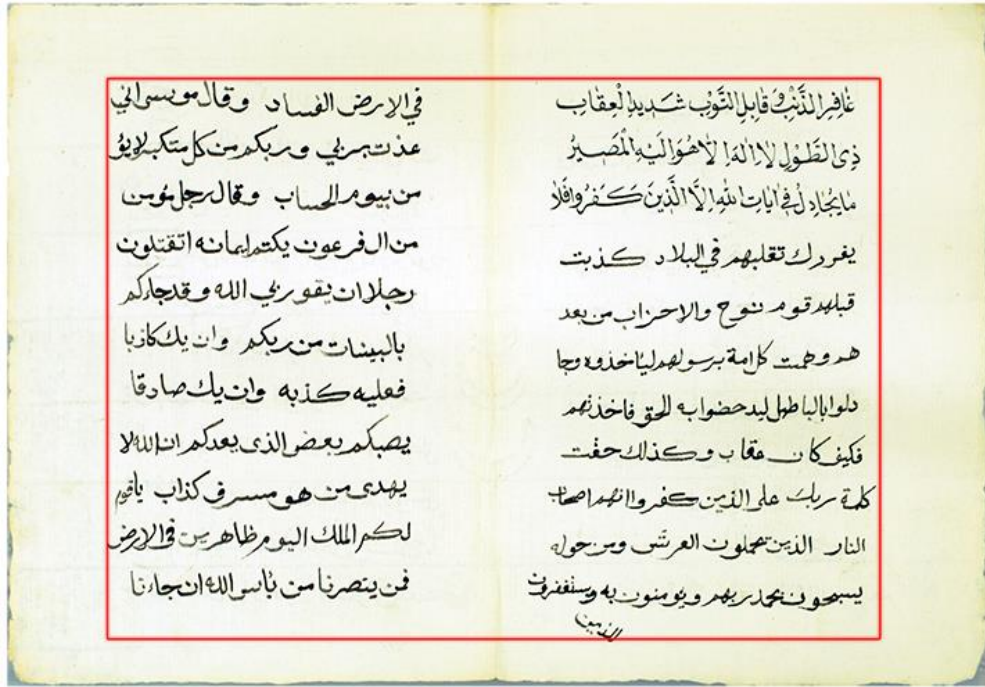


Figure 4-21. Chemical maps of the distribution of DP and pH values of selected area of some examples of Islamic paper samples from the ref-collection (Islamic paper survey) (AP 44, AP 35, AP 57, AP 127-1), estimated based on the developed calibration models of HSI system. The figure shows the visible image with the selected area (red rectangle) and that area at 1932.7 nm. In addition to the average image with ink pixels excluded and the actual and average estimated DP and pH values for each sample.

4.4 Evaluation Methodology: Effect of Acquisition Parameters on Calibration

Different measurement conditions and acquisition parameters may have an effect on the accuracy of the collected spectra such as the spectral power distribution of illumination and its intensity, optics and scanning backgrounds. Even post-processing methods used in the data analysis step could affect the quantitative results.

In view of this, I tried to study the metrology of quantitative calibrations based on the spectral measurements of Islamic paper calibration target samples collected by the HSI in the SWIR region. The results from the developed regression (PLS) and discrimination (PCDA) models for determination of DP and starch presence of Islamic paper respectively, were used as an evaluation methodology to study the effect of the different measurement conditions, acquisition parameters and processing methods such as scanning backgrounds, illumination intensity, lens, ROI size for the average spectra and pre-treatment methods on the accuracy of the models. The details of the developed models and the used methods are described in Section 4.3.2.

Spectralon 99% diffuse reflectance standard is considered as one of the common reference standards used in most of the spectroscopic applications and calibrations due to its flatness and constant reflectivity over the range 250-2500 nm (Kubik, 2007; Yao & Lewis, 2010). However, it was not available due to cost and time to get such standard in the same size of the scanner stage (A3 size) to act as a background for the scanning while collecting the measurements, thus Whatman filter paper No. 1 (Maidstone) was seen as an alternative as a pure cellulose material similar to the objects under investigation.

Islamic paper calibration target (IP target) was scanned using the two different backgrounds (covering samples area only) and without any background (put directly on the plastic stage) then using multivariate data analysis methods, the PLS regression models to determine cellulose DP in Islamic paper were calculated for each scan to evaluate the effect of changing backgrounds on the accuracy of calibrations.

On the other hand, spectral pre-treatment methods are also important in the development of calibration models due to their ability to remove unwanted variability in the spectra due to scatter or due to instrumentation without affecting the chemical information (Fearn, 2001), however, their selection depends on extensive testing and experience (Wang & Paliwal, 2007; Yao & Lewis, 2010). Thus, a selection of different commonly used methods was evaluated to show their effect on the results. Three different methods were selected as the most common used pre-treatment methods in spectroscopy (Næs et al., 2002; Miller & Miller, 2010; Manley, 2014) multiplicative scatter correction (MSC), standard normal variate (SNV) and Savitzky–Golay filter (1st and 2nd derivatives) (SG) to process the spectral data of the IP target collected (with the different backgrounds) using the HSI

system in the range 1450 – 2350 nm then the PLS regression models were calculated for each.

The results of the PLS models (Table 4-10) show that the calibration errors (RMSECV) exhibit no significant variation taking into consideration the error of the standard viscometric method to determine the DP of the reference samples (see Chapter 3, Section 3.2.2.4). In addition to that, it is noticed that in all the models, SG method gives better results.

Table 4-10. PLS regression model results for determination of DP using spectral measurements of the IP target collected by the HSI system with two different backgrounds (99% diffuse reflectance Spectralon and Whatman paper) and without any backgrounds (plastic stage). The calculations were done using different pre-treatment methods for the collected spectra in the range 1450 – 2350 nm to avoid noisy edges.

Background	Pre-treatment	PLS factor	RMSECV	Rcv	Mean ± SD
Spectralon	No pre-treatment	7	330	0.66	305 ± 17
	MSC	9	310	0.71	
	SNV	7	314	0.70	
	(SG) 1 st derivative	10	286	0.75	
	(SG) 2 nd derivative	10	286	0.75	
Whatman	No pre-treatment	10	332	0.68	326 ± 10
	MSC	8	337	0.66	
	SNV	8	329	0.70	
	(SG) 1 st derivative	14	308	0.73	
	(SG) 2 nd derivative	3	322	0.65	
Without (Plastic)	No pre-treatment	21	292	0.75	302 ± 9
	MSC	15	308	0.72	
	SNV	15	316	0.71	
	(SG) 1 st derivative	5	300	0.71	
	(SG) 2 nd derivative	9	296	0.75	

Moreover, the discrimination model using PCDA method (Næs et al., 2002; Stuart, 2007; Miller & Miller, 2010) to determine starch presence in Islamic paper was also re-calculated based on the spectral measurements of the IP target samples with the different backgrounds explained above to confirm results. The model results which are validated based on the percentage of correctly identified samples, show that Spectralon background model has the best results as expected with 93.3% accuracy compared to 88.6% using Whatman background (4 layers) and 79% using no background.

A scanning test using the IP target with Whatman paper as background was conducted using two lenses (30 and 56 mm) to evaluate the influence on the collected data as it is the only parameter that can be changed in the current setup to increase/decrease spatial resolution (Qin, 2010; Macdonald, 2010) as most of the other parameters are fixed. Table 3-5 (Set1 and Set3) lists the acquisition parameters used for the test. The average spectra of the IP target samples from the two scans were compared to each other. As seen in

Figure 4-22, there is a noticeable uncommon difference between both scans which may be due to a coating layer over the lenses, but this would require more investigation to verify in addition to an assessment of its effect on the calibrations performance. I also estimated the CoV of the two average spectra which gave 2.7% to evaluate its significance in comparison to the previous results e.g. CoV of instrument stability.

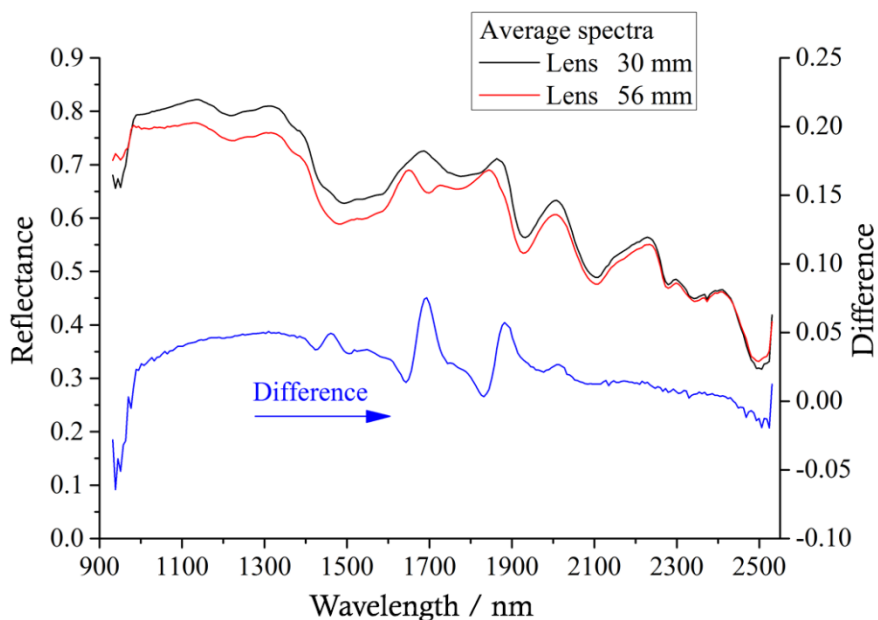


Figure 4-22. Average reflectance spectra and its difference, collected from the IP target by the HSI scanner using different lenses: 30 and 56 mm to visualize the variability in the measurements.

Since a difference in the spectra was observed using the different lenses, the PCDA discrimination model was calculated using these data to check if this variation in the spectra affects the calibration results as well.

ROI size from where the average spectra was calculated could also be another parameter that may affect the results/calibrations, so this was also investigated using the same spectral data of the two different lenses. Some could argue that the more pixels we get for each sample square (7x7 pixels) in the IP target, the more representative the sample will be. Therefore, two different ROI sizes; 3x3 and 5x5 pixels from the IP target scans for each sample were tested and used to calculate the PCDA models. The model was calculated for the spectral range 1450 – 2350 nm using Whatman paper as background and pre-treated using SNV method. The results in Table 4-11 show that both parameters; different lenses and ROI size have a slight change in the results indicating its low effect on the calibrations accuracy.

Table 4-11. PCDA model results for identification of starch presence using HSI data of IP target collected by two different lenses (30 and 56 mm). The calculations were done based on an average spectrum of two different ROI sizes (3x3 and 5x5 pixels) from each sample in the target. Measurements were collected in the range 1450 – 2350 nm with Whatman paper as background and pre-treated using SNV method.

Lens	ROI	PCs Number	% Correct
30 mm	3x3	9	83.8%
56 mm	3x3	17	84.8%
30 mm	5x5	21	86.7%
56 mm	5x5	15	84.8%

4.5 Degradation Study

Studying the properties of materials makes it possible to understand the degradation processes and factors affecting them which consequently helps to develop effective preservation plans to decrease the rate of degradation and prolong material lifetime. Environmental parameters such as heat, moisture or light are considered as the main factors that influence the degradation of objects (PAS 198, 2012) in addition to the raw materials and techniques used in the production process.

From the study conducted on Islamic paper collection (Section 4), it was found that more than a half of the samples of the ref-collection have DP < 1000 despite the use of bast and cotton fibres with high initial DP (Lewin, 2007). This could be related to exposure to high temperatures or RH during past storage.

Moreover, the survey applied to the Wellcome Library Islamic collection, revealed that most of the surveyed samples tend to be neutral to mildly alkaline and DP over 800 indicating a low deterioration rate. Although samples are considered safe for handling it is noticed that they are more degraded than European papers of similar age (SurveNIR, Strlič et al., 2015).

Since the environmental history of the samples is not known and to verify the hypothesis about the effect of higher temperatures, a degradation study in controlled environmental conditions is required.

Therefore, I conducted different accelerated degradation experiments (5 experiments) using ~10 Islamic paper samples per experiment, from the ref-collection under various combinations of relative humidity (from 30 – 70% RH) and temperature (from 50 – 90 °C) to determine its degradation rate. The samples were selected to represent the different categories in the collection; starch-sized and/or polished, or neither. Table 4 in Chapter 3 shows the details of the degradation experiments while Table 4-12 lists the different combinations of T and RH selected and the associated Islamic paper samples used in each experiment and its properties.

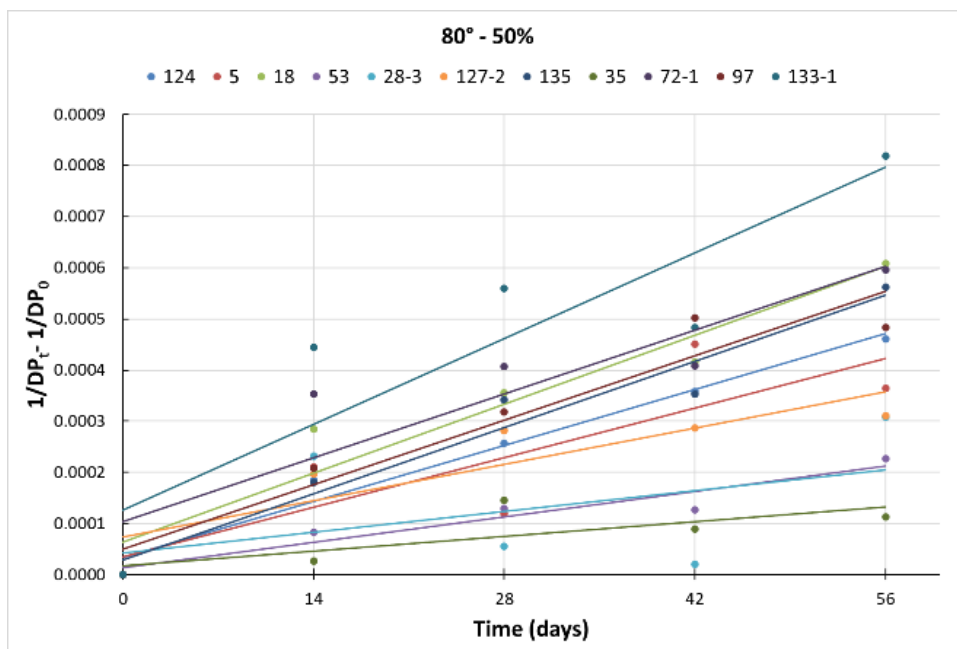
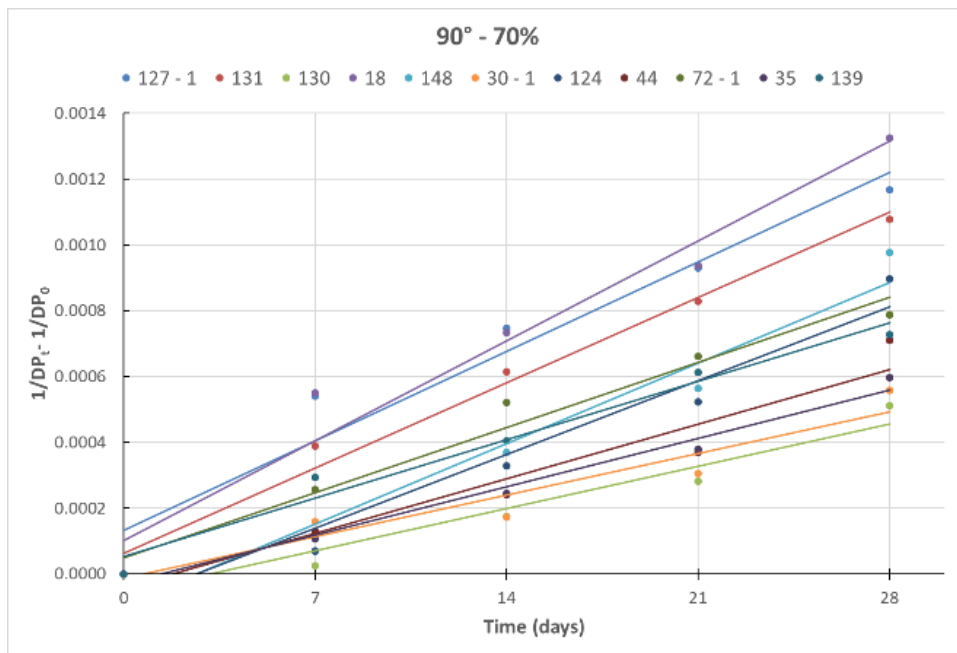
Table 4-12. Different conditions of the accelerated degradation experiments conducted using Islamic paper samples to assess its degradation behaviour. The table shows the selected samples for each experiment with its properties (pH, DP) and whether the sample is starched or polished.

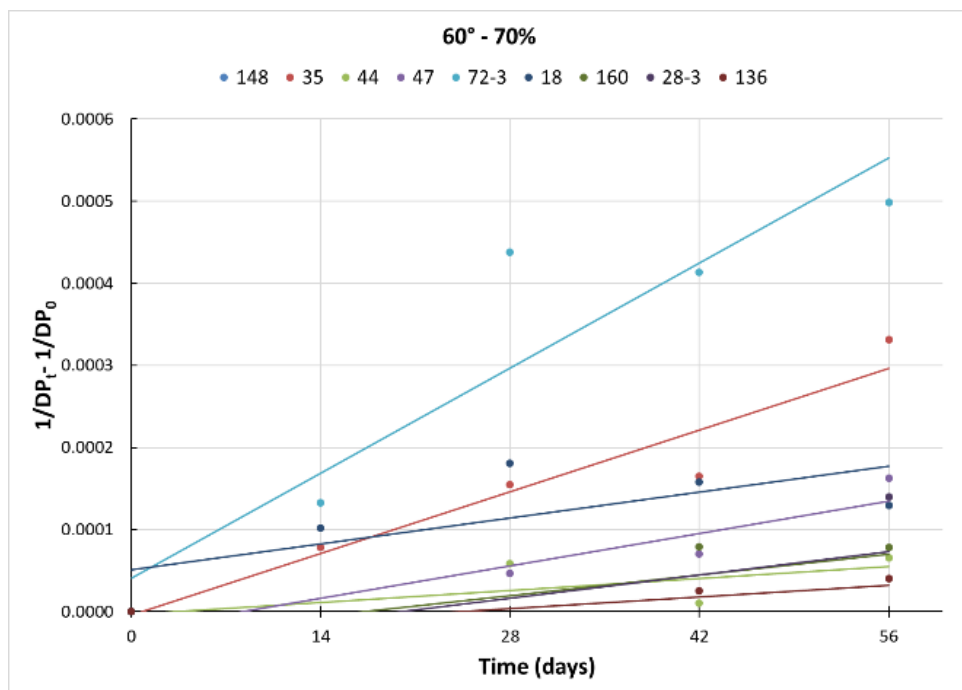
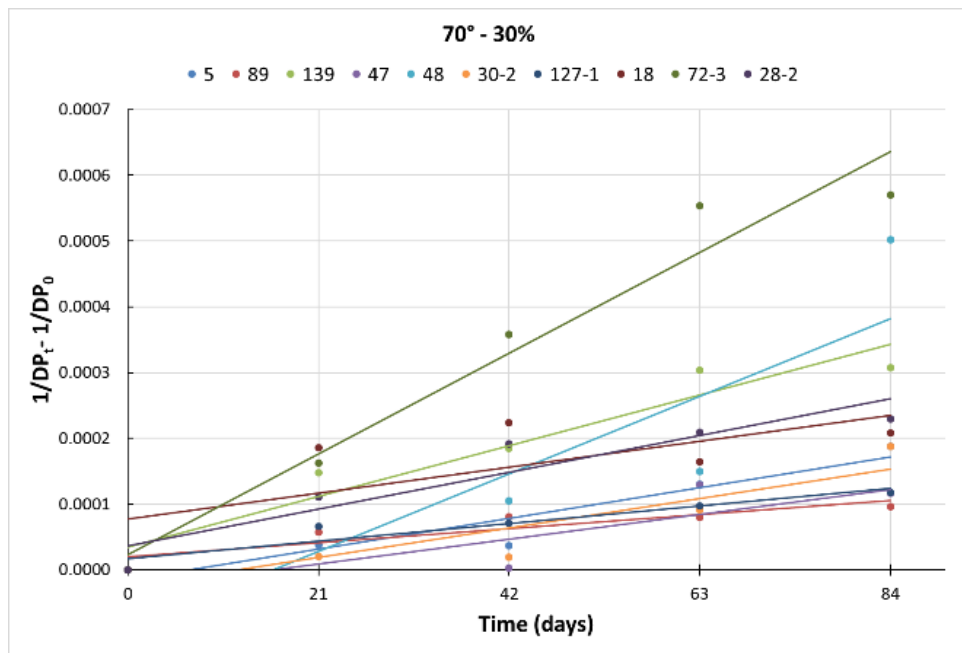
Sample	Starch-sizing	Polishing	pH	Initial DP	Degradation conditions	Degradation duration
AP 5	Y	Y	7.7	642	80 °C - 50% 70 °C - 30%	8 weeks 12 weeks
AP 18	N	N	7.4	1292	90 °C - 70% 80 °C - 50% 70 °C - 30% 60 °C - 70% 50 °C - 50%	4 weeks 8 weeks 12 weeks 8 weeks 8 months
AP 28-2	Y	N	7.3	569	70 °C - 30%	12 weeks
AP 28-3	Y	N	7.4	516	80 °C - 50% 60 °C - 70% 50 °C - 50%	8 weeks 8 weeks 8 months
AP 30-1	Y	N	7.1	592	90 °C - 70%	4 weeks
AP 30-2	Y	N	7.2	549	70 °C - 30%	12 weeks
AP 30-3	Y	N	7.2	584	50 °C - 50%	8 months
AP 35	N	Y	7.8	1409	90 °C - 70% 80 °C - 50% 60 °C - 70% 50 °C - 50%	4 weeks 8 weeks 8 weeks 8 months
AP 44	Y	Y	7.9	1207	90 °C - 70% 60 °C - 70% 50 °C - 50%	4 weeks 8 weeks 8 months
AP 47	N	Y	7.6	1458	70 °C - 30% 60 °C - 70%	12 weeks 8 weeks
AP 48	N	Y	8.3	1391	70 °C - 30% 50 °C - 50%	12 weeks 8 months
AP 53	N	Y	7.2	1157	80° - 50%	8 weeks
AP 72-1	Y	N	6.1	506	90 °C - 70% 80 °C - 50%	4 weeks 8 weeks
AP 72-3	Y	N	5.9	512	70 °C - 30% 60 °C - 70% 50 °C - 50%	12 weeks 8 weeks 8 months
AP 89	N	Y	7.9	1413	70 °C - 30% 50 °C - 50%	12 weeks 8 months
AP 97	Y	Y	8.4	1441	80 °C - 50%	8 weeks
AP 124	N	Y	6.7	1335	90 °C - 70% 80 °C - 50% 50 °C - 50%	4 weeks 8 weeks 8 months
AP 125-1	Y	Y	4.6	322	50 °C - 50%	8 months
AP 127-1	N	N	8	1280	90 °C - 70% 70 °C - 30%	4 weeks 12 weeks
AP 127-2	N	N	8	1204	80 °C - 50% 50 °C - 50%	8 weeks 8 months
AP 130	N	Y	7.9	1103	90 °C - 70% 60 °C - 70%	4 weeks 8 weeks
AP 131	Y	Y	6.2	1091	90 °C - 70%	4 weeks
AP 133-1	N	N	5.8	681	80 °C - 50%	8 weeks
AP 135	Y	Y	7.2	795	80 °C - 50%	8 weeks
AP 136	Y	Y	7.3	935	60 °C - 70% 50 °C - 50%	8 weeks 8 months
AP 139	Y	Y	7	813	90 °C - 70% 70 °C - 30%	4 weeks 12 weeks
AP 148	N	N	5.7	900	90 °C - 70% 60 °C - 70%	4 weeks 8 weeks
AP 160	Y	N	7.3	872	60 °C - 70%	8 weeks

Following the degradation experiments, DP was measured using the standard viscometric method (Chapter 2 – Section 2.4.4). Then, data were analysed to calculate the degradation rate of Islamic paper and to explore its fit to the modelled dose-response function for European paper (Strlič et al., 2015), to open the opportunity for studying the effect of the different storage scenarios for Islamic paper (Strlič et al., 2013).

Since DP is a property representing the material state of cellulose-based materials, the degradation rate was calculated using Ekenstam equation (Ekenstam, 1936), describing DP as a function of time (using Islamic paper samples DP before and after degradation). The calculated degradation rate constants were also compared to the rate constants of historic western paper from a recent study of Strlič et al. (2015). The applicability of the modelled dose-response function for Western paper from the same study (Strlič et al., 2015) on Islamic paper was explored where the degradation rate constant is quantitatively related to environmental factors (T and RH%) and material properties (pH and DP) to predict its degradation behaviour (Strlič et al., 2013; 2015).

Based on the established Ekenstam linearity of change $1/DP$ over time, it was found that the data for the samples show linear correlations (first-order kinetics) consistent with the results from the previous studies (Zou et al., 1996; Strlič et al., 2015) (Figure 4-23). Table 4-13 depicts the calculated degradation rate constants (k) for each degradation experiment. It is noticed that k of samples degraded at higher ageing temperatures is higher which is consistent with the results from other similar experiments. However, data scattering started to increase with decreasing temperature as can be seen at 50 °C - 50% experiment.





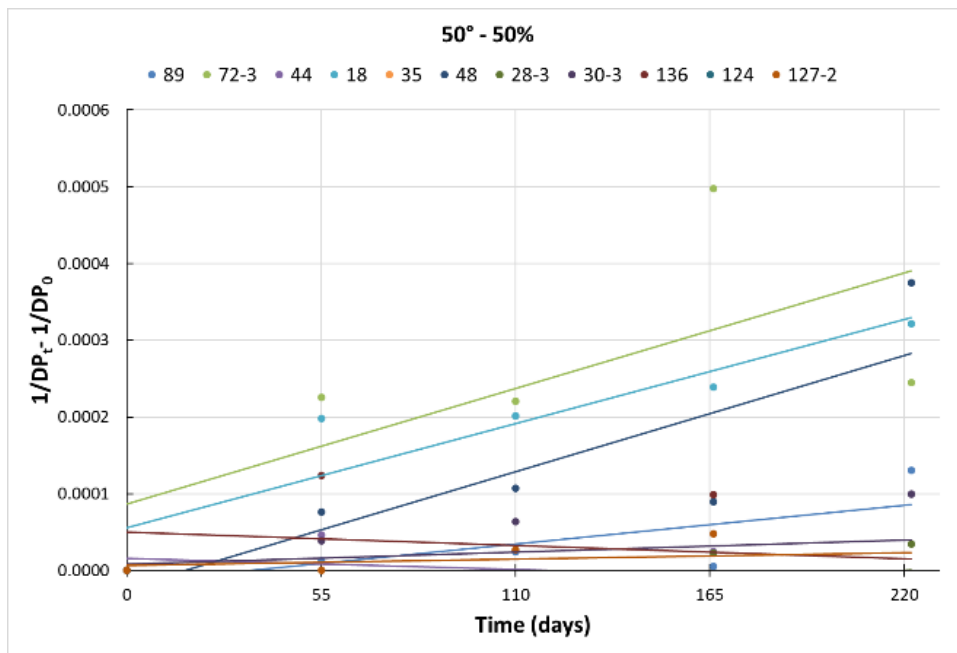


Figure 4-23. Linear fits as per the Ekenstam equation, for Islamic paper samples degraded at different conditions as follows (90 °C - 70% RH, 80 °C - 50% RH, 70 °C - 30% RH, 60 °C - 70% RH and 50 °C - 50% RH for 4, 8, 12, 8 weeks and 8 months respectively). DP_0 is the initial degree of polymerization of cellulose and DP_t is at time t.

Table 4-13. Rate constants ($k - \text{day}^{-1}$) for the degraded samples and the corresponding correlation coefficients (R^2) of linear fit for the paper samples used in the study. The samples are categorized by colour representing: starched and polished (orange), neither starched nor polished (red), starched but not polished (green) and not starched but polished (blue).

	Sample	$k [\text{day}^{-1}] * 10^{-5}$	R^2		Sample	$k [\text{day}^{-1}] * 10^{-5}$	R^2
90° - 70%	127-1	4	0.94	80° - 50%	124	0.8	0.98
	131	4	0.99		5	0.7	0.71
	130	2	0.94		18	1	0.93
	18	4	0.96		53	0.4	0.91
	148	3	0.95		28-3	0.3	0.21
	30-1	2	0.92		127-2	0.5	0.77
	124	3	0.95		135	0.9	0.95
	44	2	0.93		35	0.2	0.57
	72-1	3	0.97		72-1	0.9	0.82
	35	2	0.98		97	0.9	0.92
70° - 30%	139	3	0.97	133-1	1	0.8	
	5	0.2	0.91	148	-0.2	0.18	
	89	0.1	0.81	35	0.5	0.93	
	139	0.4	0.92	44	0.1	0.47	
	47	0.2	0.73	47	0.3	0.87	
	48	0.6	0.78	72-3	0.9	0.86	
	30-2	0.2	0.83	18	0.2	0.50	
	127-1	0.1	0.90	136	0.1	0.55	
	18	0.2	0.48	160	0.2	0.51	
	72-3	0.7	0.96	28-3	0.2	0.41	
50° - 50%	28-2	0.3	0.87				
	89	0.05	0.55				
	72-3	0.1	0.46				
	44	-0.01	0.11				
	18	0.1	0.83				
	35	-0.02	0.23				
	48	0.1	0.71				
	127-2	0.008	0.09				
	28-3	0.03	0.10				
	30-3	0.01	0.03				
136	-0.02	0.04					
124	-0.009	0.50					

Modelling the predicted and measured rate constants (k) of Islamic paper samples using the scatterplot reported in the study by Strlič (2015) reveals its good fit to the modelled function confirming its applicability to Islamic paper (Figure 4-24 - Top). The coloured points added to the plot are located within the previously reported data (empty symbols) (Zou et al., 1996; Strlič & Kolar, 2005; Strlič et al., 2015). Most of the data from 70 °C - 30% RH, 60 °C - 70% RH and 50 °C - 50% RH are placed below the line which indicates that the measured rate constants of Islamic paper samples are higher than the corresponding measured ones. I also explored if the characteristic Islamic paper properties (starch-sizing and polishing) have any influence on the results (Figure 4-24 - Bottom) by

categorizing the symbols in colour according to the different properties. However, no meaningful conclusion can be derived from this as no clear patterns emerge.

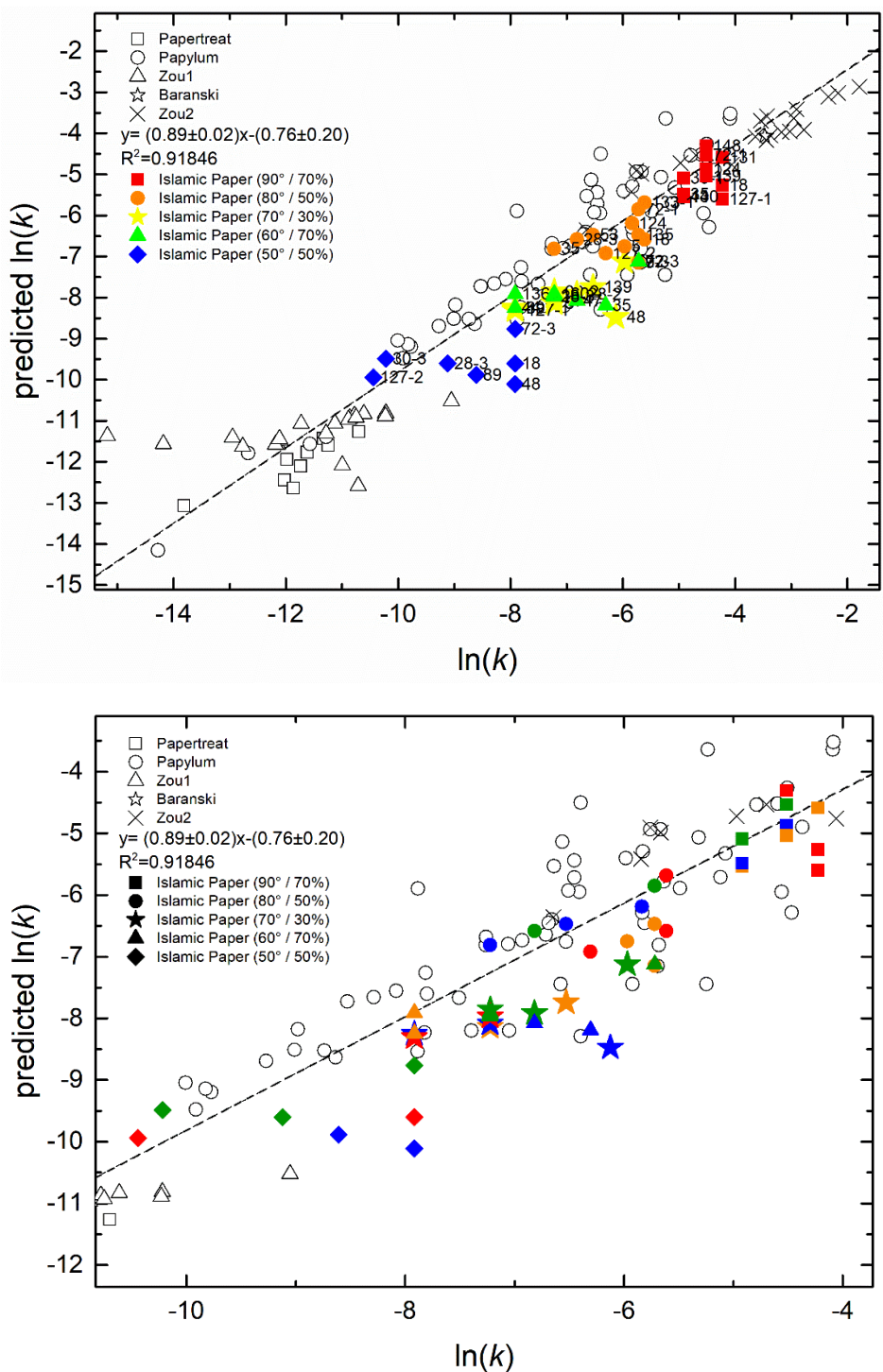


Figure 4-24. Comparison of degradation rates as measured and as predicted for Islamic paper samples and paper samples as reported by Strlič et al. (2015), represented by empty symbols. $\ln(k)$ is the natural logarithm of the degradation rate. In the bottom figure, the solid symbols are coloured according to Islamic paper properties (starch-sizing and polishing); starched and polished (orange), neither starched nor polished (red), starched but not polished (green) and not starched but polished (blue).

It is evident that both Ekenstam equation and the modelled dose-response function are suitable for predicting Islamic paper degradation rate and for studies of its degradation

behaviour. Such information is very useful for the development of evidence-based plans for storage conditions for Islamic paper and the potential risks based on that. Moreover, it is important to consider the effect of other parameters that could affect the degradation either in storage environment such as pollutants (Menart et al., 2014; Strlič et al., 2015) or in the samples themselves, such as starch, which needs further investigation.

On the basis of that and using the survey data (Section 4.2), I tried to calculate the lifetime for each object in the collection before it becomes unfit for handling (DP=300) using the estimated pH and DP data. Then, I developed demographic plots (Strlič et al., 2015) for the collection objects to explore the costs and effects of different storage conditions and conservation plans on the degradation of the collection in comparison to the expected rate of degradation under the current standard environmental conditions (18 °C, 50% RH). This can inform how storage at a lower temperature or applying deacidification treatment would affect the degradation of an object. Since most of the objects in the collection have pH \geq 7 so deacidification scenario would not be useful here.

At these standard conditions, the average lifetime of the collection is ~2000 years with one object only expected to be unfit for use (requires treatment) in about 100 years. As seen in

Figure 4-25, almost the whole collection (~95%) would survive 500 years (this is selected according to a recent assessment of a suitable long-term planning horizon for collections of objects of no ascribed exceptional value (Dillon et al., 2013)) before reaching the unfit state. However, by changing the conditions to simulate the average environmental conditions at different place e.g. Cairo, Egypt, with an average temperature of 35 °C and average RH% of 56%, none of the collection would survive till the 500 years in this case and most of the collection would become unfit for use in ~300 years. Thus, it is now clear for this collection that, cooled storage condition (meanwhile humidity controlled) would increase the period of time until intervention is needed.

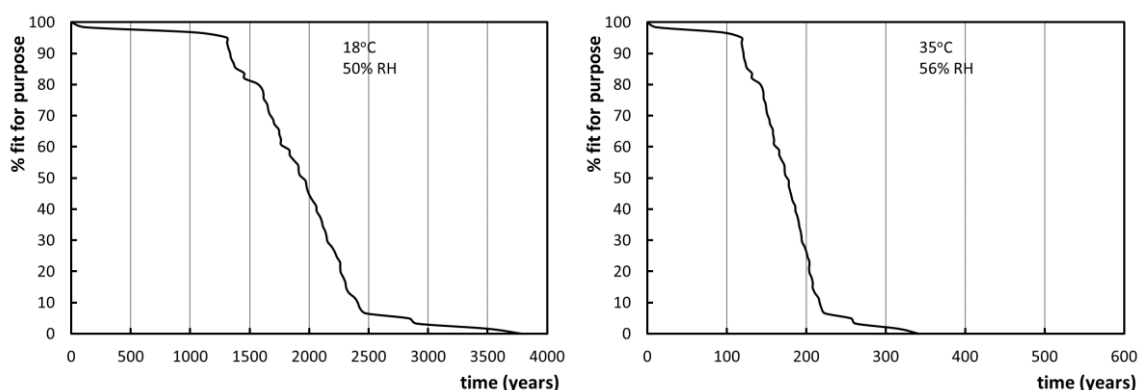


Figure 4-25. Demographic plots for the surveyed Wellcome collection objects at the standard environmental conditions (18 °C, 56% RH) (left) as well as another hypothetical scenario at 35 °C, 56% RH (right).

4.6 Summary

This chapter described a systematic survey of an Islamic paper collection consists of 228 samples (around ~40% of the samples are from the 18th – 19th century) to characterize the material properties of Islamic paper deducing its significant characteristics and assess the collection's current material state. Four properties were investigated: paper sizing, polishing, acidity and degree of polymerization.

Almost half of the collection samples are sized with starch and around 64% were polished. A non-normal distribution of pH was detected, although it is unclear why, as the causes for such a distribution are not a reflection of rosin sizing, as is usual in European paper collections. Most of the collection samples have DP < 1000, which reflects the fact that bast and cotton fibres (with high initial DP) are typically used in Islamic paper. This may indicate the unsuitable environmental conditions during past storage.

The effect of starch on paper stability was also explored through a preliminary experiment where it was found that starch has no effect on cellulose degradation as samples with and without starch have same degradation rate despite the relationship detected using PCA analysis between starch presence and inaccuracy results obtained from the DP model developed for European paper (SurveNIR) when applied to Islamic paper.

A non-destructive methodologies using NIR spectroscopy was developed for the characterization of Islamic paper instead of the destructive and time-consuming classical ones. Discrimination models were developed for the identification of starch presence and polished surfaces, while regression models were built to determine pH and cellulose DP of Islamic paper. The models are satisfactory for collection surveys based on the validation and prediction errors. Thus, the methodology could be applied to Islamic collections in libraries and archives for better understanding of the properties and to fulfil the gap in the knowledge of what Islamic paper is and about what proportion of Islamic paper constitutes manuscripts in the libraries collections.

For the validation of the non-destructive scientific characterization methodology developed using NIR spectroscopy, another survey of Islamic collection was conducted at the Wellcome Collection where the same four properties were estimated for 43 historic objects based on their collected spectral data. The survey results showed that around 90% of the collection has the potential to be of Islamic origin relating to starch presence and polishing. Also, most of the collection is in a good condition and can be handled safely except few samples based on the estimated pH and DP values. Moreover, a dating model for Islamic paper was developed using the same NIR spectral data collected from the surveyed samples with the aid of multivariate data analysis methods. The model allows for dating Islamic paper sample with unknown date (only from 1652 to 1880 AD).

Due to the heterogeneity nature of the cellulosic materials, the potential of using the HSI technique in the SWIR region to map the chemical properties of Islamic paper on the whole surface of an investigated object was also discussed and explored. Using multivariate data

analysis methods, firstly, discrimination and regression models were developed based on the HSI spectral data collected from a special calibration target devised from 105 well-characterized Islamic paper samples from the Islamic paper survey. Then, chemical maps were constructed for some examples of Islamic paper samples using their collected HSI spectral data and the estimated pH and DP values per pixel based on the developed models. The results prove that the quantitative imaging method can act as a tool to visualize degradation which allows for the identification of areas that would require special intervention and treatment. The study could have a significant impact on our understanding of heritage surfaces as spatially resolved quantitative data could improve the interpretation and conservation of historic cellulose-based materials. The chapter also opens new areas of further research into quantitative imaging, including the effect of the different measurements conditions and acquisition parameters on the predictions which was demonstrated. A degradation study using accelerated degradation with a combination of controlled environmental conditions (temperature and relative humidity) was conducted on some of the Islamic paper samples from the Islamic paper survey to explore their degradation rate and performance with the aid of both Ekenstam equation and the recently modelled dose-response function developed for European paper which proved their applicability to Islamic paper. Such information is very useful for the development of evidence-based plans for storage conditions for Islamic paper and the potential risks based on that which was also explored.

5. PAINTING CANVAS

In this chapter, another example of a heterogeneous material, painting canvas, is explored using the near-infrared (NIR) hyperspectral imaging (HSI) system (Figure 5-1) as a condition assessment tool. This could be beneficial to conservators as it makes it possible to map the chemical state of a canvas and therefore its current state of preservation (condition), which may differ substantially across a large painting.

An earlier study on 2011 (Oriola, 2011) was conducted using NIR spectroscopy technique and multivariate data analysis to develop a method to assess some characteristics of painting canvas: cellulose DP, pH and fibre type. Despite the success of the developed method and the important information provided regarding the material state of canvases, it so far focused on point analysis whilst the distribution of these characteristics across a canvas can be very heterogeneous causing possible local differences during degradation which is very important to be known for conservators.

Thus, I developed new analytical methods to non-destructively determine pH and degree of polymerization (DP) of cellulose in painting canvases as good indicators of its material state/condition (Oriola, 2011) based on NIR imaging and with the aid of multivariate data analysis methods. A special well-characterized reference collection was gathered and analysed to develop quantitative calibration models. A portable LabSpec-5000 spectrometer (ASD, Boulder) operating in the same spectral region was used to collect the spectral data of the same collection for the purpose of performance comparison. Regression models were developed using partial least squares (PLS) method (Næs et al., 2002; Miller & Miller, 2010) using the collected spectral data from both instruments and the results are compared. Calibration and prediction errors were used as an evaluation metrics to assess the performance of the models.

The developed assessment methodology was validated using real paintings from the historic reference material collection of UCL Institute for Sustainable Heritage (UCL-ISH). Quantitative chemical maps were also generated to enable easy visualization and study of the distribution of material properties.

Moreover, different accelerated degradation experiments were conducted under various combinations of relative humidity (RH) and temperature (T) using the historic real samples (UCL-ISH collection) to assess the degradation performance of painting canvases, exploring its degradation rate and study its stability which is the first time to be investigated. DP measurements were collected and analysed to explore the applicability of the dose-response function model of European paper (Strlič et al., 2015) on canvases as a similar cellulosic based material. The dose-response function has the ability to connect the degradation rate with material properties and environmental factors to be able to study the

different scenarios of storage environment conditions and build evidence based preservation plans.

Four sections are included in this chapter:

- Section 5.1 describes the reference collection of painting canvases used for the development of the assessment methodology.
- Section 5.2 describes the details of the analysis of the collected spectral data and details of for the development of the assessment methodology. It is divided into three sub-sections where the first sub-section is about the analysis of the spectral data collected using the NIR spectroscopy and building the regression models to predict pH and cellulose DP of a canvas in addition to the validation of the models on real paintings. The second sub-section describes the details of the development of the calibration models from the spectral data collected using the HSI and its validation. The last sub-section is about building NIR chemical maps using the pH and DP predictions from the developed models.
- Section 5.3 describes the details for the degradation study conducted on canvases to assess their degradation performance and stability.
- Section 5.4 summarizes the chapter and lists all the findings of the study.



Figure 5-1. Hyperspectral Imaging Scanner

5.1 Reference Collection

As described earlier in chapter 2 (Section 2.2), the reference collection used in the study of painting canvas is based on a well-characterized collection of a prior study (Oriola et al., 2011; Oriola, 2011) consisting of around 150 historic canvas samples. 72 samples with known pH and DP measurements were selected from the canvas collection to be used as calibration target. The target is used for the development of the condition assessment tool using HSI system and quantitative regression models. The number of samples used for the HSI canvas calibration target was limited by the size of the scanning stage (~ A3 size) to be able to fit all samples in one scan to avoid any possible variations in the collected data. Appendix II lists the selected samples for the calibration target showing their properties; DP, pH, fibre type, sample source and date. Most of the selected samples are made from linen or cotton with a pH ranges from 4.7 to 7.4 and DP from 415 to 2333. Spectral measurements were collected using the LabSpec-5000 spectrometer and HSI

system with different acquisition parameters. As a cellulose-based background similar to canvases, Whatman No. 1 filter paper (Maidstone) was used as background for the measurements for both instruments. It replaced the commonly used background; 99% diffuse reflectance Spectralon standard (Labsphere, North Sutton, USA) as it was not possible to afford the standard one in the same size as the calibration target due to its cost. The use of different backgrounds while using the LabSpec-5000 spectrometer was investigated in literature (Oriola et al., 2014) where the authors concluded that it has no statistically significant effect on the results. For HSI system, the number of Whatman sheets needed was determined based on an experiment to investigate penetration level (Appendix III) where approximately 2-3 Whatman sheets was concluded to be enough. Moreover, the effect of the use of different backgrounds on the quality of the predictions from HSI calibration models was explored and the results were demonstrated in Chapter 4. Data were analysed with the aid of multivariate data analysis methods to build regression models for the determination of cellulose DP and pH of the samples.

Another 10 historical oil paintings from UCL-ISH Reference Collection were used for validation of the developed models and for a degradation study for canvases. The real measurements of the paintings properties (pH, DP and fibres) are listed in chapter 3 and the full description of the paintings is in Appendix IV. UCL-ISH Paintings characteristics are similar to the reference collection samples where most of them are made of linen fibres with only two cotton samples. Also, most of the paintings were dated back to the 19th/20th AD centuries. pH ranges from 4.5 to 6.4 while cellulose DP ranges from 880 to 3800.

5.2 Spectral Analysis: Condition Assessment Tool

Regression calibration models were developed using PLS regression method (Næs et al., 2002; Brereton, 2009; Miller & Miller, 2010; Brereton & Lloyd, 2014) for the determination of pH and DP of cellulose in canvases based on the reference samples for each instrument. All modelling and data analysis were performed using Matlab with the aid of PLS toolbox library (EIGENVECTOR, 2019).

5.2.1 Spot Analysis: NIR Regression Models

5.2.1.1 Acidity (pH)

Spectral measurements of 142 samples measured by LabSpec-5000 spectrometer (Figure 5-2) were used to develop the regression model to determine the pH of canvas. The samples were divided into two sets randomly; calibration (102 samples) and validation (40 samples). Data were pre-processed to optimize the quality of calibration using Savitzky-Golay filters (1st derivative, 2nd polynomial, with a window of 21 points), standard normal variate (SNV) methods and mean-centring (Savitzky & Golay, 1964; Manley, 2014) in the spectral interval 1402 – 1805 nm and 1864 – 2395 nm to avoid the effect on spectra from the exchange between the two detectors at 1830 nm. Validation was performed using

leave-one-out cross validation (LOOCV) method based on the root-mean-square error of cross validation (RMSECV) and the correlation coefficient (R_{CV} ; the nearer to 1 the better) (Næs et al. 2002).

The optimal calibration model (Figure 5-3) gives $RMSECV=0.54$ pH unit and $R^2_{CV}=0.44$ using 6 factors. The root-mean-square-error of prediction using the independent validation set gives $RMSEP=0.55$ pH unit with 0.4 correlation (R^2_P).

The results of the model are less satisfactory compared to the model developed in the earlier study especially in terms of the prediction error (Oriola et al., 2014, $n=127$, $RMSECV=0.58$, $R^2_{CV}=0.58$, 9 factors, $n_P=43$, $RMSEP=0.43$, $R^2_P=0.75$, 1000-2250 nm) taking the differences in spectral resolution, different sizes of datasets, and pre-processing methods used into account, in addition to any chemical changes that may have happened to the reference collection samples during storage since the prior study from 2011 (Oriola et al., 2011; Oriola, 2011). However, comparing $RMSEP$ to the uncertainty of the standard method used for the actual measurements of pH (which is ± 0.3 pH unit), the developed model could still be used for classification of samples or a general overview of the acidity level of the sample.

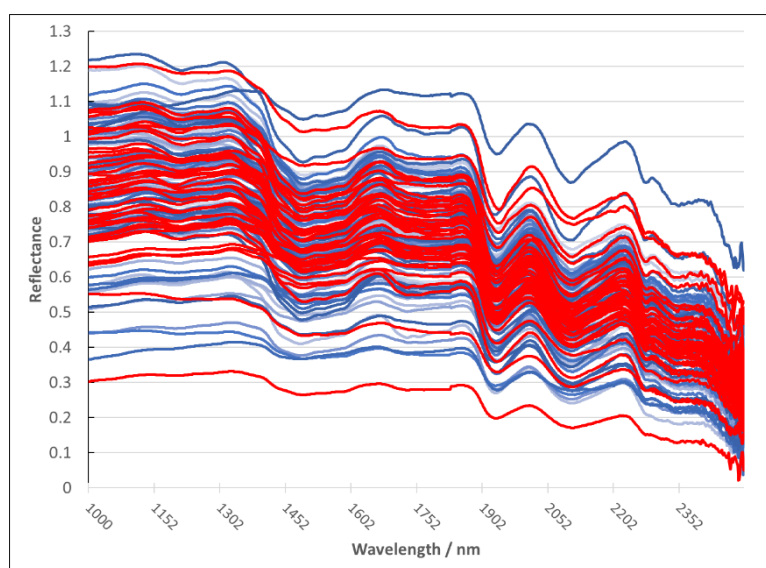


Figure 5-2. Reflectance spectra of 142 historic canvas samples collected by LabSpec-5000 Spectrometer in the spectral range 1000 – 2500 nm. Samples were used to develop PLS regression model to determine pH of unknown canvases. Blue shades lines show the spectra of calibration dataset while red lines represent validation dataset.

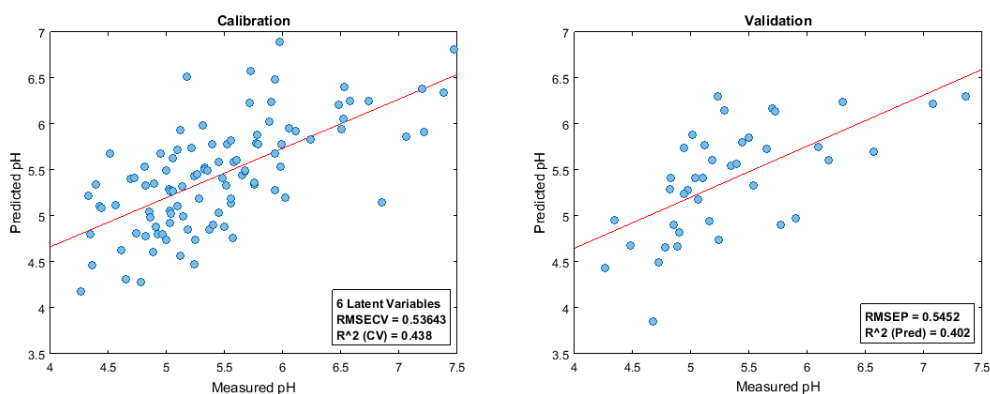


Figure 5-3. The results of the developed PLS regression model; calibration (Left) and validation (Right) for the determination of pH in painting canvas using spectral measurements of 142 historic samples collected by LabSpec-5000 spectrometer. The plot correlates predicted with actual pH measurements.

5.2.1.2 Degree of Polymerization (DP)

On the other hand, the developed DP model (Figure 5-4) is performing very well based on the calculated root-mean-square error of cross-validation (RMSECV= 269 DP unit, 12 factors) and the correlation coefficient $R^2_{cv}=0.72$ in comparison to the performance of other similar developed DP models (Oriola et al., 2014, $n=70$, RMSECV=270, $R^2_{cv}=0.72$, 14 factors, $n_p=32$, RMSEP=275, $R^2_p=0.77$, 1200 – 1870 nm and 2000 – 2250 nm). Using independent validation dataset, the prediction error is RMSEP=297 DP unit with 0.75 correlation (R^2_p) which indicates the suitability of the model to be used in collection surveys of similar materials.

The regression model was developed based on the spectral measurements of ~90 samples (60 for calibration set and 29 for validation set) from the canvas reference collection measured by the spectrometer. All spectra were converted from reflectance to absorbance (Figure 5-5) then Savitzky-Golay filter (1st derivative, 2nd polynomial, with a window of 11 points), SNV and mean center methods (Savitzky & Golay, 1964; Manley, 2014) were used to prepare the sets in the spectral interval 1198 – 2252 nm and leave-one-out method was used for cross validation.

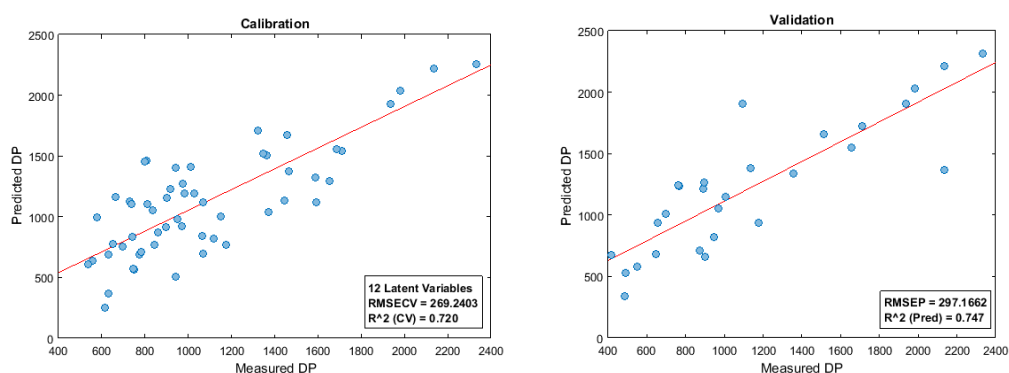


Figure 5-4. The results of the developed PLS regression model; calibration (Left) and validation (Right) for the determination of DP of cellulose in painting canvas using ~90 historic samples based on their spectral measurements from the Spectrometer. The plot correlates predicted with actual DP measurements.

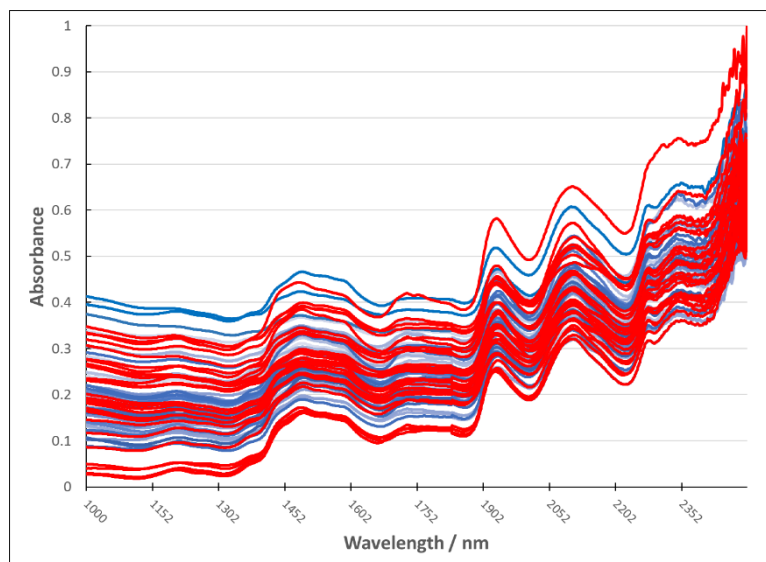


Figure 5-5. Absorbance spectra of 89 historic canvas samples collected by LabSpec-5000 Spectrometer in the spectral range 1000 – 2500 nm. Samples were used to develop PLS regression model to determine DP of cellulose in canvases. Blue shades lines show the spectra of calibration dataset while red lines represent validation dataset.

5.2.1.3 Predictions for Real Paintings

The two developed regression models were applied to the spectral measurements collected from real paintings (Figure 5-6) from the collection of UCL-HSL to validate the models and mimic the real scenario of surveying real collections. Since the models are based on spot analysis, eight positions were selected to determine its pH and DP values representing the whole canvas which would give an overview about its current condition/material state. No background was used while collecting the spectral measurements from the painting due to sensitivity of the paint layer. The effect of not using background on spectra was explored and no noticeable difference was detected as seen in Figure 5-7. All the positions were successfully predicted with an average predicted DP = 1253 ± 463 and 1284 ± 337 and an average predicted pH = 5.7 ± 0.4 and 5.7 ± 0.2 for the two presented painting canvases p8 and p9 respectively (= average of measurements \pm standard deviation). The real measurements for the two paintings are DP = 899 and pH = 4.9 for P8 and DP = 3826 and pH = 5.8 for P9. The accuracy of the measurements of pH and DP should be evaluated taking into consideration the standard error (uncertainty) of the used measurement method and the prediction error of the developed model. DP variability within each painting was found to be quite high while pH predictions are acceptable within the expected uncertainty. It is worth mentioning that the DP value of P9 is out of the range of DP values of the calibration dataset so it is expected that the prediction of such value would not be accurate.

The noticeable differences (based on the calculated standard deviation value between measurements within the same painting) especially in the DP values between positions (Figure 5-6) might be due to the actual variations in the condition across the canvas or differences in the spectra collected from the dirt or dust or from the paint layers.



Figure 5-6. The results of the pH and DP predictions for two painting canvases; P8 (left, bottom) and P9 (right, bottom) from the UCL-ISH collection based on the developed regression calibration models. Yellow dots representing the different selected positions for the spectral measurements. The top row shows the front side of the two paintings; P8 (left, top) and P9 (right, top).

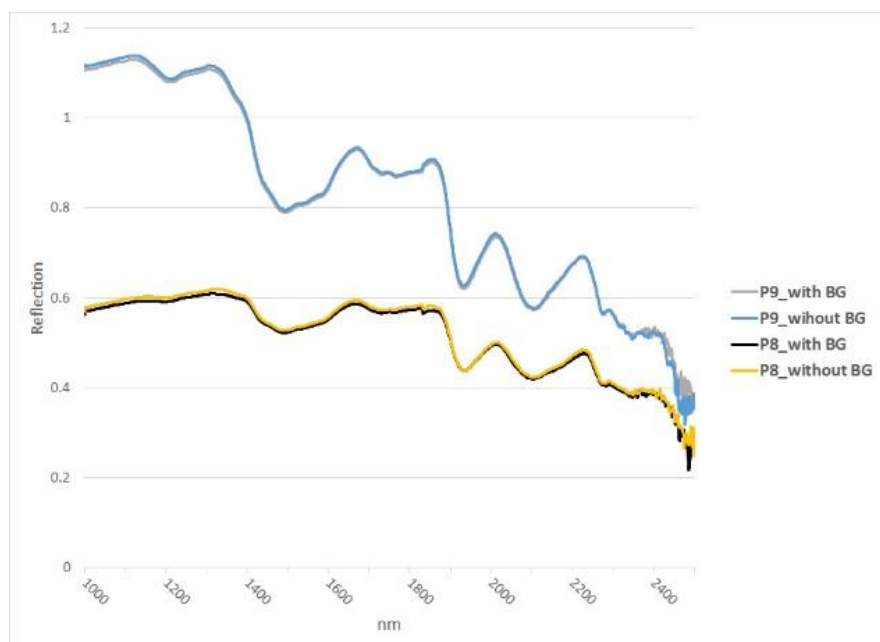


Figure 5-7. Reflectance spectra measurements of two paintings (P8 and P9) with and without background (BG) collected by LabSpec-5000 spectrometer to investigate its effect on the spectra.

5.2.2 HSI Analysis: NIR Regression Models

5.2.2.1 Sample Selection

In order to build the calibration spectral database to develop the quantitative calibration models to predict pH and DP of cellulose in painting canvas using HSI system, the canvas

calibration target (~70 samples) was scanned with Whatman sheets as background then the collected HSI hypercubes/images were corrected and hot/dead pixels were removed as a preparation step. A representative average spectrum was selected manually from each sample (ROI – region of interest – of 3 × 3 pixels) and was given an ID (Figure 5-8).

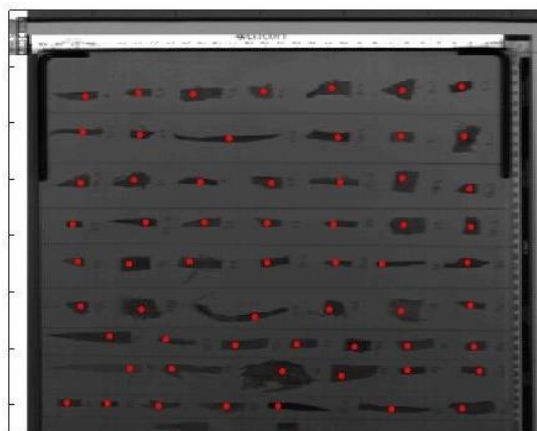


Figure 5-8. An image at 1932 nm resulting from a scan of the canvas calibration target using the HSI system. The red points are showing the manually selected position from each sample to collect average representative spectra (3x3 ROI) from the historic samples to build the quantitative calibration models to determine pH and DP of cellulose in canvas.

5.2.2.2 Calibration models: pH and DP

Two regression models were developed for the prediction of DP of cellulose and pH values for unknown samples based on spectral measurements of ~ 70 samples from the canvas calibration target (Figure 5-9) to give an overview of the current material state in terms of preservation condition.

The specifications of the two models are shown in Table 5-1 where the reference samples were divided into calibration and validation sets randomly then pre-processed using Savitzky-Golay filter and SNV methods and then mean-centred (Savitzky & Golay, 1964; Manley, 2014).

The optimal DP calibration model (Figure 5-10) gave an RMSECV=340 DP units and $R_{cv}=0.61$ using 4 factors in the spectral range 1200 – 2300 nm. The model has a potential to be used in collection surveys similar to the models previously developed using the spectroscopic technique with a prediction error of 400 DP units with a 0.62 correlation (R_p).

Based on these results and by using the proposed calibration model, the DP predictions will have an error of ± 400 DP units, which in the context of paintings conservation is good, especially if we take into account the differences between the techniques such as spectral resolution, datasets size, processing methods and heterogeneity of canvas samples in addition to the uncertainty of the standard method (=8%, a triplicate DP measurements of a real painting sample from UCL-ISH collection). However, the prediction error is still higher than the uncertainty found for paintings in earlier study (Oriola, 2011; ± 275 DP

units) and for historic paper which is in this case more homogeneous material (Trafela et al., 2007; ± 175 DP units).

Regarding the PLS model of pH determination, the best results (Figure 5-10) were obtained using the full spectral range (1000 – 2500 nm) with 8 factors where RMSECV=0.46 pH unit and $R_{CV}=0.57$. The prediction error RMSEP=0.38 pH unit is consistent with the measurement uncertainty of the standard method ($=\pm 0.3$ pH units) and the other prediction errors developed for paintings (Oriola, 2011; ± 0.43 pH units) and paper (Trafela et al., 2007; ± 0.3 pH units) in earlier studies which reflects the potential to use the model for the prediction of unknown samples.

There are reasonable correlations between predicted and measured values for the developed PLS methods.

Table 5-1. Specifications of PLS regression models for determination of pH and DP of cellulose in canvases based on spectral measurements of ~ 70 historic samples using HSI system.

	DP Model	pH Model
Num. Samples	54 (C) and 18 (V)	54 (C) and 18 (V)
Spectral range	1200 – 2300 nm	1000 – 2500 nm
Pre-treatment	Savitzky-Golay (1 st Derivative, 2 nd polynomial, 15-points window), SNV, Mean-Center	Savitzky-Golay (1 st Derivative, 2 nd polynomial, 21-points window), Mean-Center
RMSECV (Leave-one-out)	340, $R_{CV}=0.61$ (4 factors)	0.46, $R_{CV}=0.57$ (8 factors)
RMSEP	400, $R_P=0.62$	0.38, $R_P=0.64$

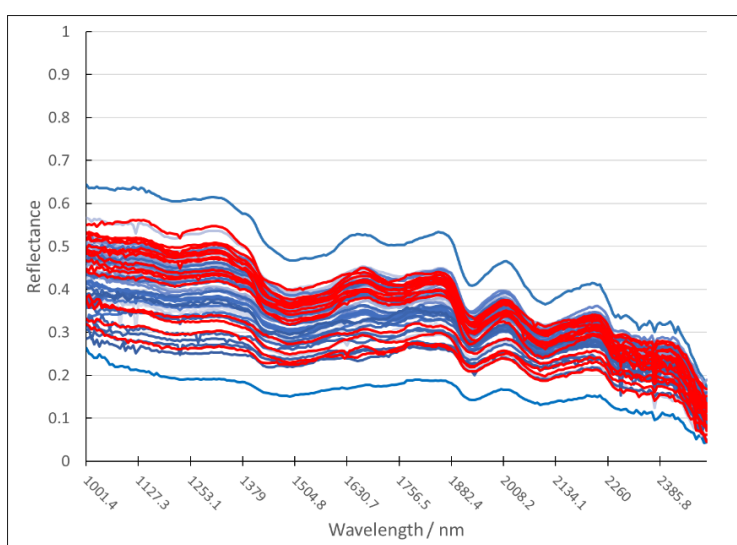


Figure 5-9. Reflectance spectra of 72 historic canvas samples collected by HSI system in the spectral range 1000 – 2500 nm. Samples were used to develop PLS regression models to determine cellulose DP and pH of unknown canvases. Blue shades lines show the spectra of calibration dataset while red lines represent validation dataset.

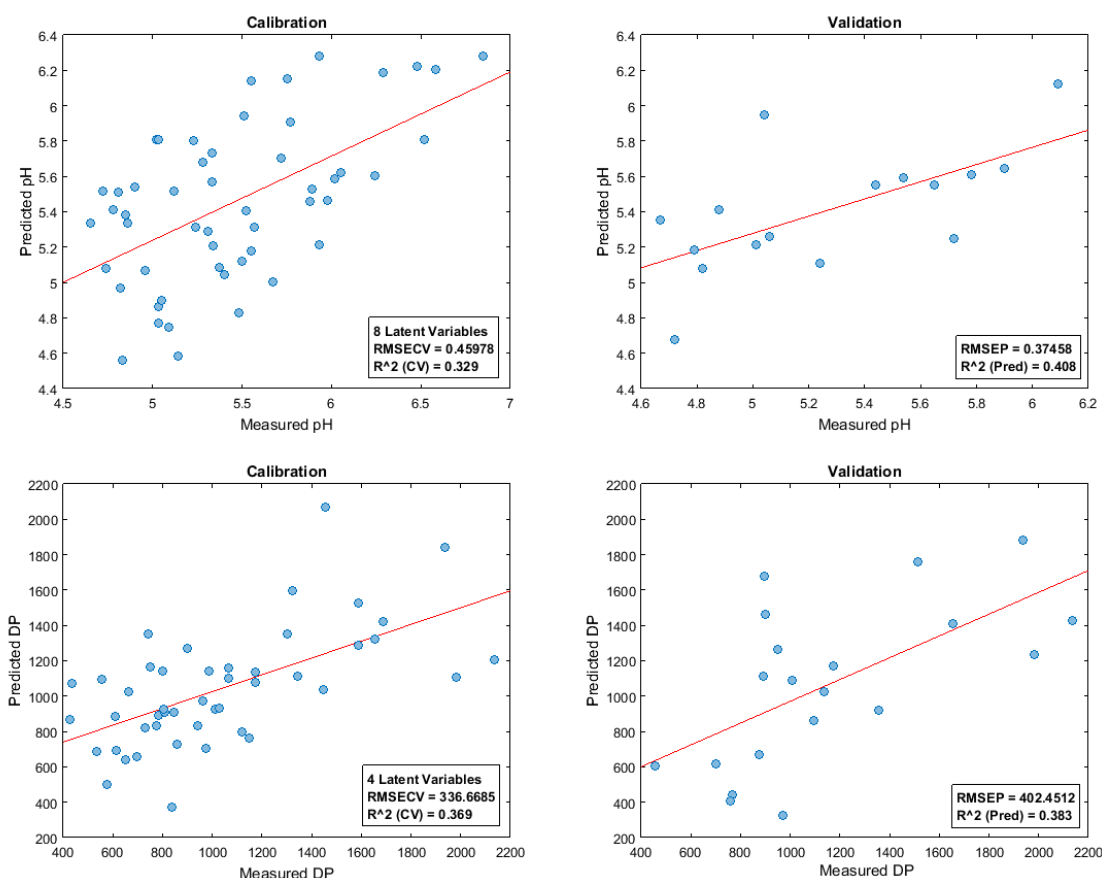


Figure 5-10. The results of the developed PLS regression models for the determination of DP of cellulose (bottom) and pH (top) using spectral measurements of ~ 70 canvas samples scanned by the HSI system. The plot correlates predicted with actual values.

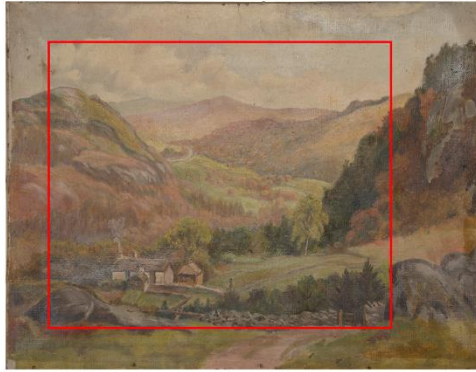
5.2.3 Near-Infrared Chemical Mapping

Since the HSI calibration models developed perform in an acceptable way and similar to the previously published spectroscopic models, and taking advantage of the chemical maps that can be generated using the HSI system with the ability to show the distribution of chemical properties over an entire surface, the developed PLS regression models were used to build quantitative DP and pH maps for a selection of real paintings (canvases) from the UCL-ISH collection (Figure 5-11).

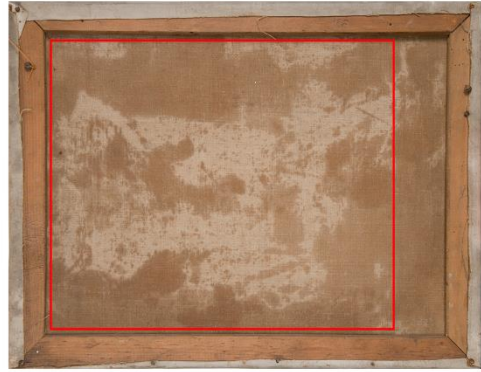
As shown in the figure, the average estimated pH and DP values are within the prediction error of each model and the standard measurement error. This is a good indication of the performance of the developed models in surveying real collections. The maps can demonstrate the variations in the estimated values across the painting surface which reflects the heterogeneous nature of the canvas. Usually DP and pH values are correlated as observed in the literature (Oriola, 2011), from the generated maps this is not clearly observed except for some areas in the two paintings, e.g. right side of the pH and DP maps in painting 6 where neutral acidity condition (green) associated with the high DP values (green-yellow) from the painting perspective. This is actually consistent with the scatter plots showing the correlation between the estimated pH and DP values for each pixel in the image (Figure 5-12) where almost for both paintings, there is no correlation

between the values with a correlation coefficient (R^2) =0.01. It is also noticed that the chemical maps are not presenting the visual pattern that can be seen in the canvases e.g. the mottled image on the back of painting 7. Although DP map of painting 7 shows a kind of similar pattern (presented in cyan colour), surprisingly associating low DP values to the light areas, pH map is not performing similarly. Painting 6 maps are not showing any noticed patterns. This is interesting and needs further investigation. However, it should be taken into consideration that the developed PLS models are only useful for analysis of samples with similar characteristics to those of the reference collection used for calibration and building the correlation, such as fibre type and date to ensure the robustness and reliability of predictions (Fearn, 2005). Also, other parameters could affect the quality of the predictions such as the painting layers, dust or dirt, and environmental conditions while collecting the spectral information.

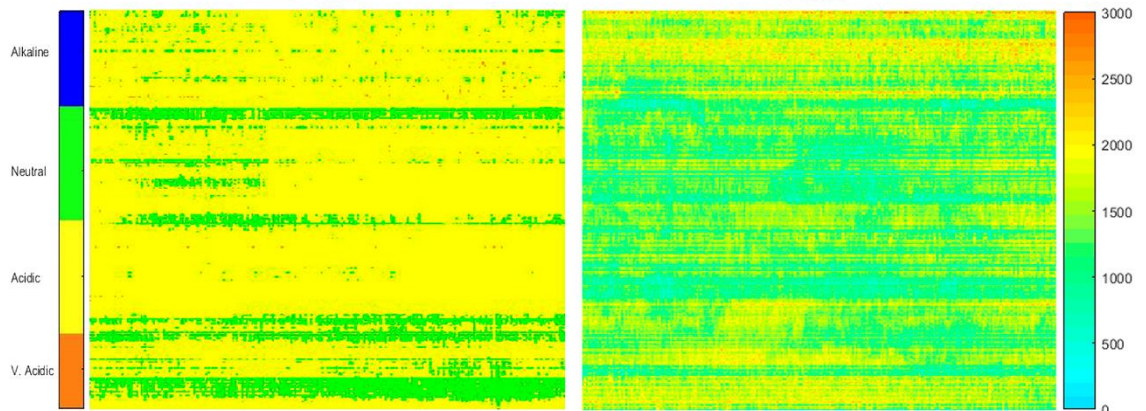
Painting 7



Front



Back



pH Map
Avg. est. pH = 5.3
Actual pH = 5.4

DP Map
Avg. est DP = 1395
Actual DP = 1397

Painting 6

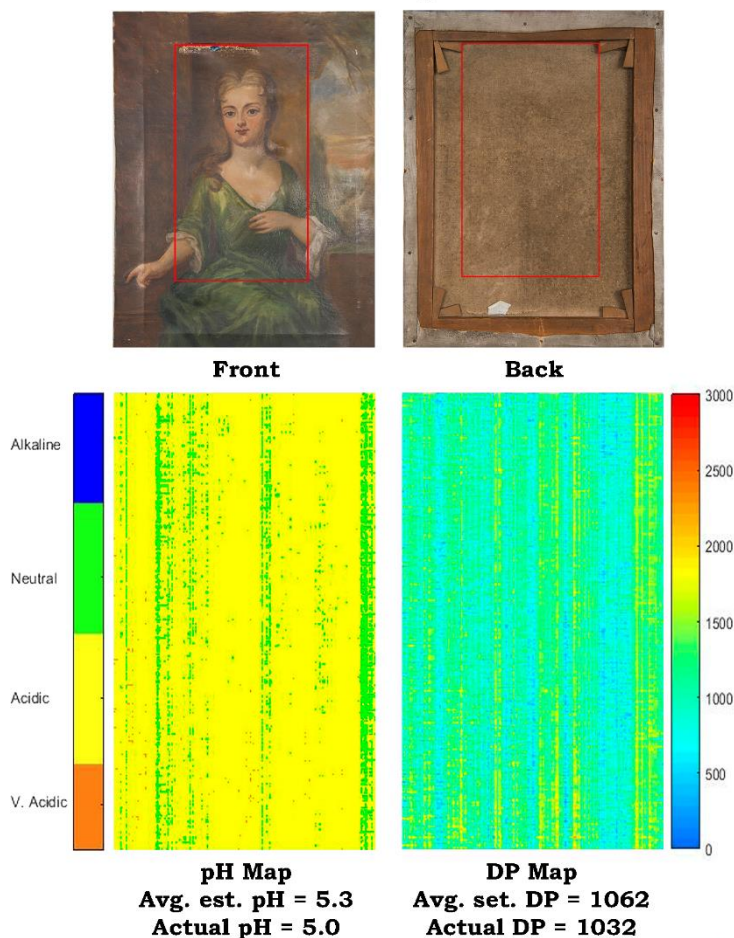


Figure 5-11. Chemical maps of the distribution of DP and pH values of selected areas of some examples of historic canvas paintings from the UCL-ISH collection (P6, P7), estimated based on the developed calibration models of HSI system. The figure shows the front and back sides of each painting with the selected area (red rectangle) and the actual and average estimated DP and pH values for each painting.

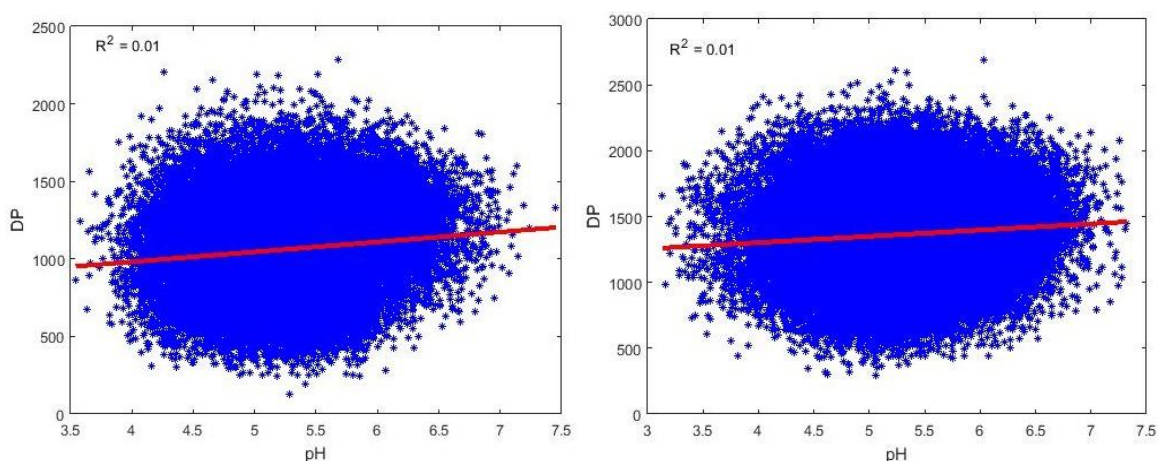


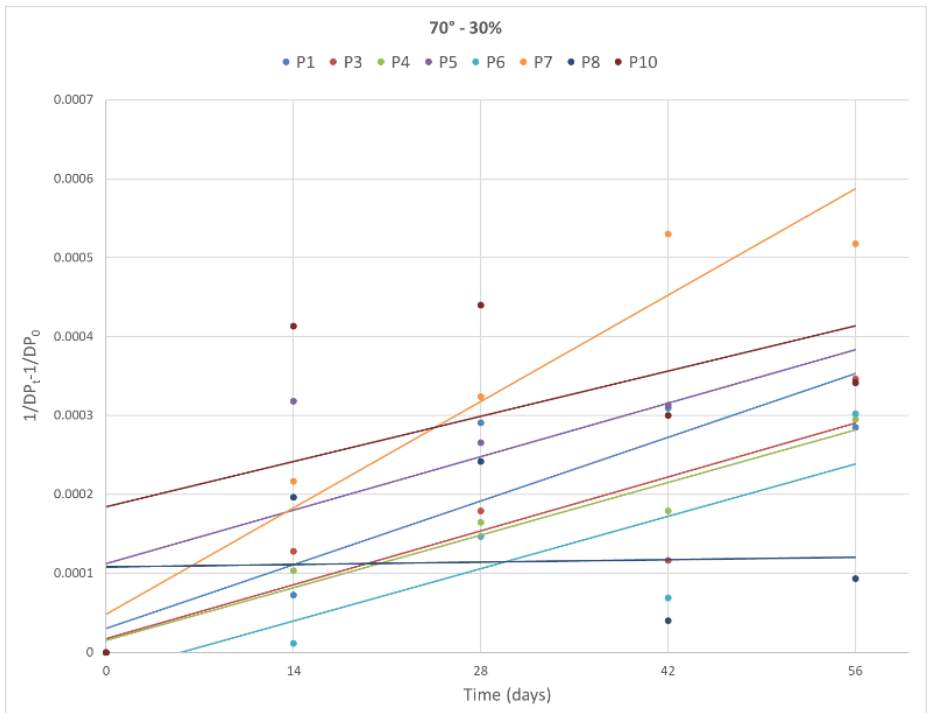
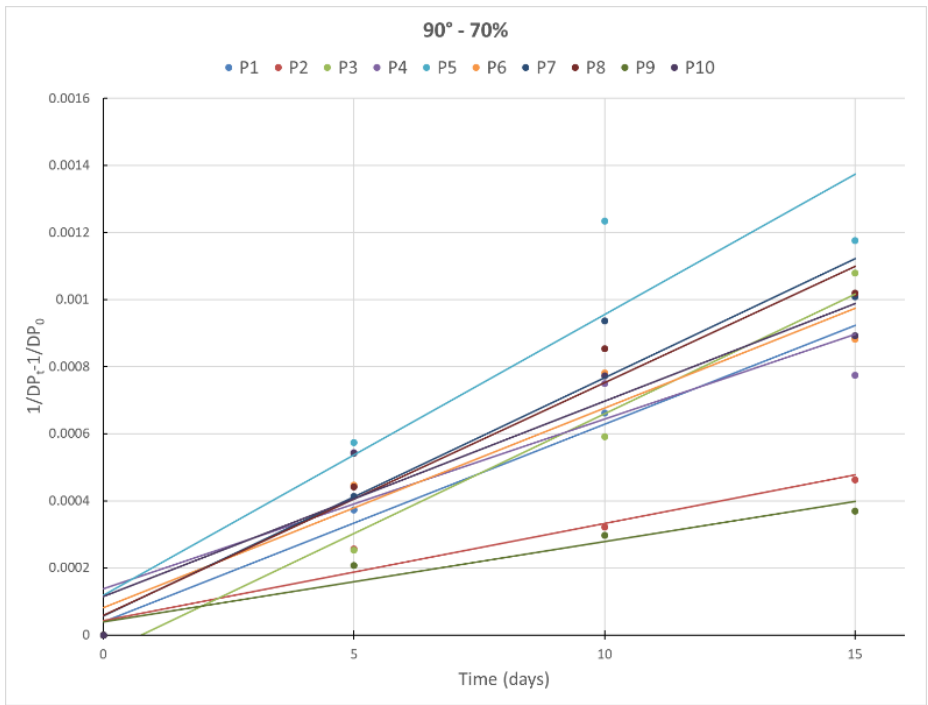
Figure 5-12. Scatterplots of the correlation between estimated DP and pH values for the two paintings (P6 – left and P7 – right). The figure also shows the correlation coefficient (R^2) for each painting.

5.3 Canvas Degradation Study

Different accelerated degradation experiments were conducted at various combinations of relative humidity (from 30 – 70% RH) and temperature (from 50 – 90 °C T) for the real historic canvas samples from the UCL-ISH collection (10 paintings, labelled as P1, P2, ... P10) to explore the degradation behaviour of canvases which consequently helps to gain more understanding about its life expectancy. Humidity and temperature are considered very important agents of deterioration for cellulose-based materials (Strlič & Kolar, 2005). Table 2-3 in chapter 2 lists all the details of the degradation experiments, including the total duration and sampling rate for each experiment. Samples then were analysed using viscometric measurements to determine DP as a function of time to evaluate the degradation extent. DP is one of the most important material properties which is a good indicator of the material state of cellulosic materials and correlates with the rate of degradation through the Ekenstam equation (Ekenstam, 1936).

Based on the Ekenstam linearity of change $1/DP$ over time that was established for paper, the applicability of this linear relationship on canvases was investigated as well as the recently modelled dose-response function from the study of Strlič et al. (2015). The degradation rate constants of canvases are calculated and compared to the rate constants of historic western paper from the study. Dose-response function has the ability to represent the dependency relationship between material change (degradation rate constant) and environmental factors and material properties in a quantitative way (Strlič et al., 2013) that can be used to predict the degradation behaviour of materials as recently modelled for Western paper based on T, RH% and pH (Strlič et al., 2015).

Due to time constraint, the DP measurements were collected and analysed from only three degradation experiments (90 °C - 70%, 70 °C - 30% and 50 °C - 50% for 2, 8 and 16 weeks respectively) including 10 canvases samples in each experiment (labelled as P1, P2, ... P10). The Ekenstam linear relationship was tested on the available samples from each experiment as shown in Figure 5-13.



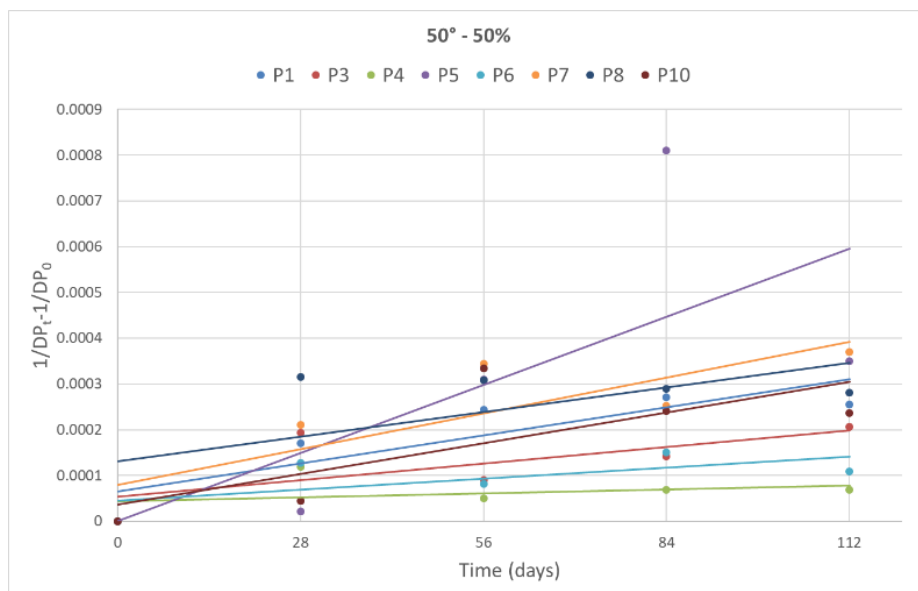


Figure 5-13. Linear fit of the Ekenstam equation (change of $1/DP$ as a function of time) on canvases samples (from 10 historic paintings labelled as P1, P2, ...etc.) degraded at three different conditions (90 °C - 70% (top), 70 °C - 30% (middle) and 50 °C - 50% (bottom) for 2, 8 and 16 weeks respectively). DP_0 is the initial degree of polymerization of cellulose and DP_t is the one at time t .

Most of the samples show reasonable linear correlation data indicating first-order kinetics with an order of magnitude (10^{-6} day^{-1}) which is in line with the previous studies (Zou et al., 1996; Strlič et al., 2015) taking into account pH, T and RH effects. Table 5-2 lists the calculated degradation rate constants (k) of the three experiments. As shown and expected, k of samples degraded at higher ageing temperatures is higher.

Table 5-2. Calculated Rate constant ($k - \text{day}^{-1}$) of the accelerated degraded samples (90 °C - 70% RH, 70 °C - 30% RH and 50 °C - 50% RH) and the corresponding correlation coefficients (R^2) values of linear fit of the Ekenstam equation on 10 historic painting canvases from UCL-ISH collection.

Samples	90 °C, 70% RH		70 °C, 30% RH		50 °C, 50% RH	
	$k (\text{day}^{-1}) \times 10^{-6}$	R^2	$k (\text{day}^{-1}) \times 10^{-6}$	R^2	$k (\text{day}^{-1}) \times 10^{-6}$	R^2
P1	60	0.99	6	0.87	2	0.75
P2	30	0.94	-	-	-	-
P3	70	0.98	5	0.73	1	0.46
P4	50	0.82	5	0.95	0.3	0.1
P5	80	0.87	5	0.58	5	0.51
P6	60	0.93	5	0.71	1	0.43
P7	70	0.93	10	0.93	3	0.71
P8	70	0.97	0.2	0.002	2	0.4
P9	20	0.93	-	-	-	-
P10	60	0.9	4	0.26	2	0.55

For validation of the applicability of the modelled dose-response function, the predicted and measured rate constants (k) of canvases are modelled and then compared with the previous data using the reported scatterplot by Strlič et al. (2015) as demonstrated in Figure 5-14. The measured rate constants are fitting well the modelled function for historic paper proving its suitability for canvases. All the new points (coloured solid circles) are

around the previously reported data except some of them, 50-50% experiment samples in particular, are placed below the line, indicating that their measured degradation rate constants of canvases are higher than the corresponding predicted values. Also, at lower temperatures, data tends to be scattered due to the long experimental time leading to higher uncertainties (Strlič et al., 2015-III).

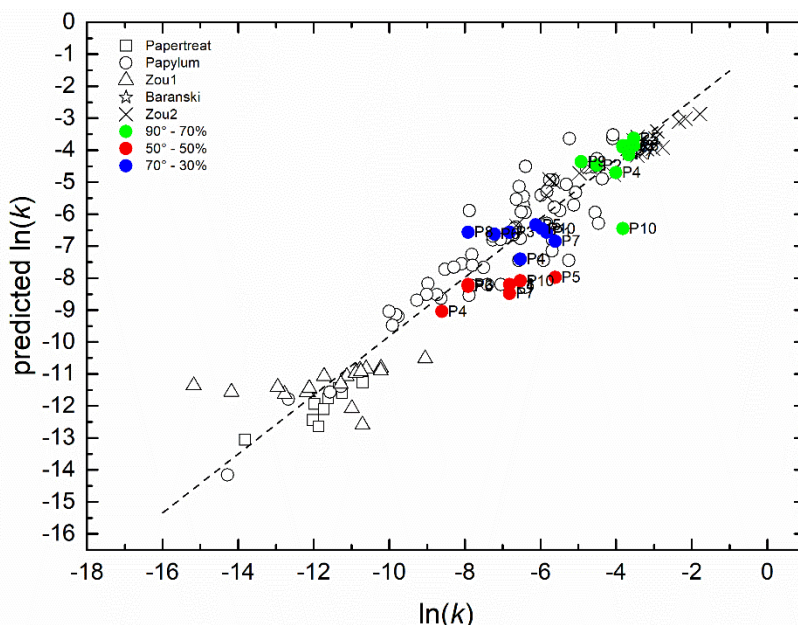


Figure 5-14. Comparison of rates of degradation as measured and as predicted of 10 real painting canvases samples from UCL-ISH collection and paper samples using the dose-response function as reported in Strlič et al. (2015). Solid circles represent the rate constants at different degradation conditions; 90 °C - 70% (green), 70 °C - 30% (blue) and 50 °C - 50% (red). Empty symbols represent rate constants of paper samples from earlier studies (Zou et al., 1996; Strlič & Kolar 2005; Strlič et al., 2015).

From the obtained results and due to the similarities between the two cellulose-based materials; paper and canvas in terms degradation mechanisms, Ekenstam equation and the modelled dose-response function were able to some extent to represent the degradation behaviour of canvases allowing for the prediction of its degradation rate. As both are based on a general kinetic model to describe the depolymerisation of cellulose. That will increase our understanding about the collection, resulting in better preservation plans by having the ability to forecast the expected lifetime of canvases until it becomes not fit for use and potential risks based on different storage environmental conditions/scenarios.

In this regard, and based on the validity of the kinetic analysis, an attempt to determine the expected remaining time of a canvas with a certain DP and pH that might have until it becomes unfit (Strlič et al., 2015-I) (lifetime) was conducted. Although real lifetime of an object depends on the strategy/plan of its use, predicting its lifetime allows for simulating the effect of different storage conditions on its degradation under natural ageing conditions. To achieve that, the developed functions for the prediction of lifetime of paper

from the work done by Zou et al. (1996) and Strlič et al. (2015-III) were applied on two painting canvases from the UCL-ISH collection (Figure 5-15). The functions depend on the degradation rate constant (k) and the expected storage conditions; temperature (T) and relative humidity (RH). In addition to the condition of the object in terms of acidity (pH) and cellulose DP. A threshold in regards of DP needs also to be assumed in order to represent when the canvas is no more fit for use. Following the study conducted in 2011 (Oriola et al., 2011; Oriola, 2011), DP value of 600 was set as the threshold/limit for canvases before it loses all mechanical strength and becomes no more suitable for general access.

Using data from pH and DP maps generated (Figure 5-11) based on the developed calibration models for the two paintings (P6 and P7) to substitute in the below equations (Zou et al., 1996; Strlič et al., 2015) together with the canvas threshold DP, lifetime maps were also generated relative to 'standard' values of storage environment where T = 20 °C and RH = 50% (Sebera, 1994).

$$lifetime = \frac{1}{A_a} \left(\frac{1}{Threshold\ DP} - \frac{1}{DP} \right) \exp \left(\frac{E_a}{RT} \right)$$

$$lifetime = \left(\frac{1}{Threshold\ DP} - \frac{1}{DP} \right) \frac{1}{\exp(\ln(k))}$$

$$\ln(k) = a_0 + a_1 \cdot [H_2O] + a_2 \cdot \ln(10^{-pH}) - \frac{a_3}{T}$$

$$[H_2O] = \left(\frac{\ln(1 - RH)}{1.67 \cdot T - 285.655} \right)^{\frac{1}{2.491 - 0.012 \cdot T}}$$

Where A_a is frequency factor, E_a is activation energy, R is the gas constant and H_2O is the water content in paper/canvas. The parameters values a_0 , a_1 , a_2 and a_3 are substituted using the values generated in Strlič study (2015-III) where $a_0=36.9812$, $a_1=36.72$, $a_2=0.2443$, and $a_3=14299.8$.

Lifetime maps (Figure 5-11) show the distribution of rough estimation of the usable life (expected lifetime) of a canvas on its whole surface reflecting the effect of the current state of the canvas on its lifetime in respect to pH and DP maps under specific storage conditions. As an example, as shown in painting 7, the bottom side of the painting has high pH values and relatively high DP values thus it is expected to live longer. Similar to chemical maps, lifetime maps are useful to visualize the different spots / positions where intervention is required, such as the application of lining or consolidation/de-acidification treatments. Areas in the canvas associated with low expected lifetime are in need for more care and conservation. It is also noticed that lifetime maps in the figure are following mostly the pattern of acidity maps reflecting the effect of the property on the calculations. This correlates with the results from the plots in Figure 5-16 where the calculated lifetime (in

years) for each pixel in the image is compared to the estimated pH and DP values for each painting. Correlation coefficients show that there is somehow a correlation between the chemical properties and the lifetime, but no conclusion can be derived about which property has the highest influence. It can be seen that there is an increment pattern in the correlation between pH and lifetime values in the two paintings indicating that increasing the acidity (pH values) of the object gives it more lifetime while that is not noticed in the correlation between estimated DP values and expected lifetime values. Recalling the note about the patterns shown on the pH and DP maps, lifetime maps are also not reflecting the visual pattern of the painting canvases which is not expected from the conservators' perspective.

There is a general striping phenomena (linear pattern) appears in the developed maps which needs further investigation. For first glance, the stripes can be associated with the weaving pattern in the canvases which would be very interesting if confirmed. However, the resolution of the used scanner is not that high, so it cannot support the hypothesis.

Another assumption, is that the images are affected with a well-known noise problem seen in remote sensing field (stripe noise) for pushbroom HSI systems (Tsai & Chen, 2008; Rogass et al., 2014; Sun et al., 2019) caused by calibration errors and sensitivity variations of the detector, e.g. dropped lines while scanning, unequal gains and offsets or variations in the calibrations across the sensor (Rasti et al., 2018). It is usually when detected, corrected by replacing the stripe with the average of the values of neighbouring pixels. Many destriping algorithms (Tsai & Chen, 2008) were and still being developed such as histogram-based and statistics-based methods. This assumption is probably the cause of the linear pattern especially after noticing similar patterns in the chemical maps of Islamic paper (in DP maps in particular). Unfortunately, due to research time constraint this could not be investigated more as it would need further detailed evaluation, thorough examination and more computation. It would be interesting to verify if the pattern is due to spectral noise or variations in object surface morphology in future work.

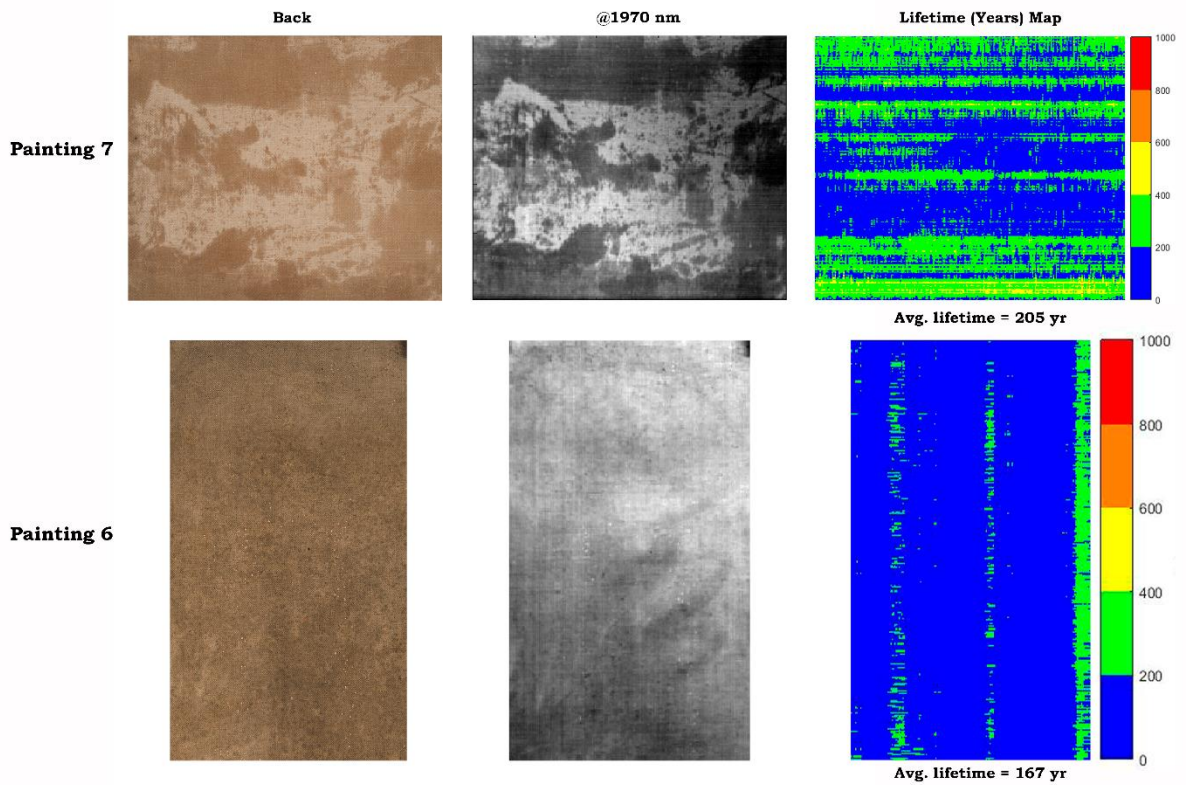
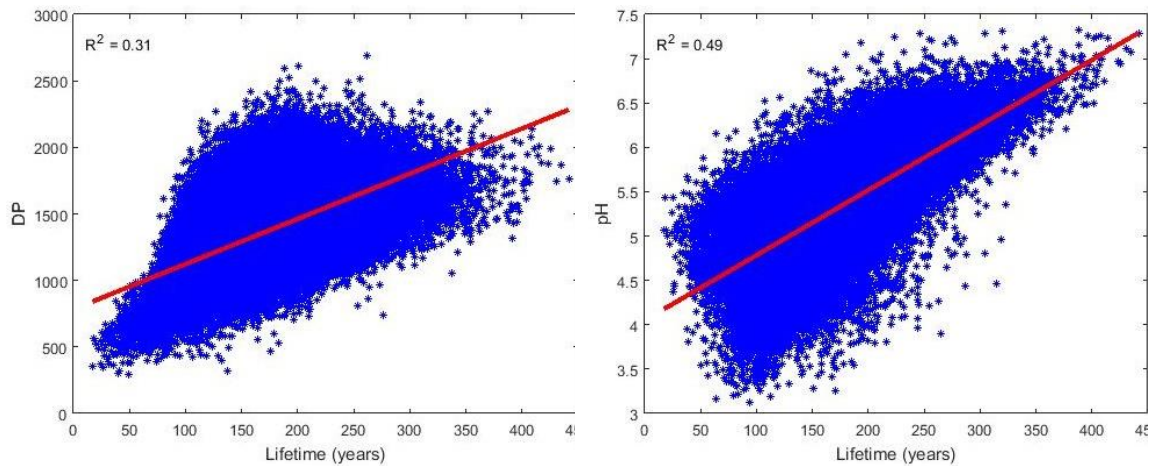


Figure 5-15. Lifetime maps of selected area of two examples of historic canvas paintings from UCL-ISH collection (P6, P7), estimated using the pH and DP maps generated based on the developed calibration models of HSI system and relative to 'standard' values of storage environment where $T = 20\text{ }^{\circ}\text{C}$ and $\text{RH} = 50\%$ and Canvas DP threshold=600 DP units. The figure shows the back side of the selected area from each painting and that area at 1970 nm. In addition to the maps of calculated lifetime (expected remaining time of a canvas until it is not fit for use) for each painting with the average in years.



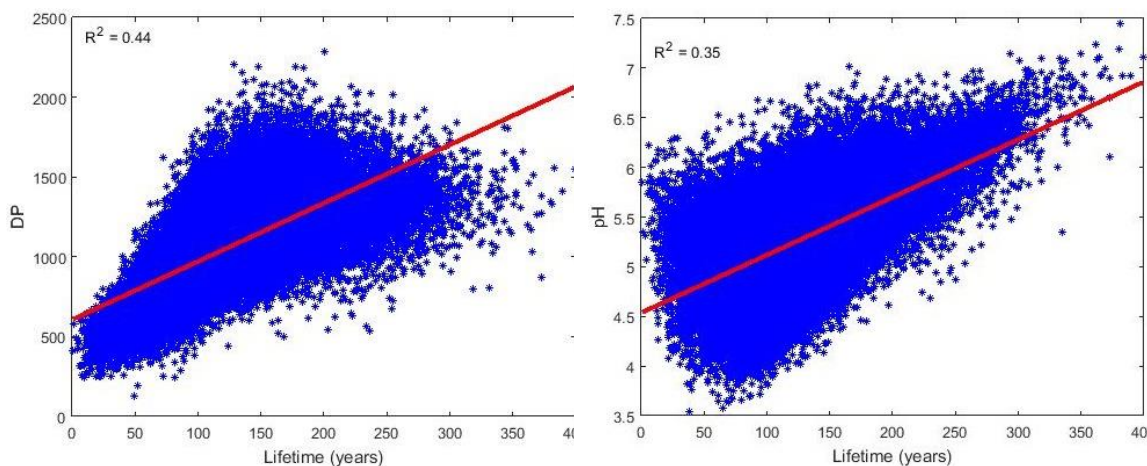


Figure 5-16. Scatterplots of correlation between estimated pH and DP and calculated lifetime maps of selected area of two canvas paintings (P7 - top, P6 - bottom). The figure shows the correlation coefficient (R^2) for each painting.

In practice, this gives a good guideline for conservators and heritage managers to develop evidence-based plans for preservation and storage conditions for historic canvases and its costs, especially with such new derived knowledge about the influence of pH slightly more than the DP on the lifetime of canvases and the inapplicability of visual assessment of the canvases for the determination of its material state.

5.4 Summary of Results

This chapter discussed the possibilities of using HSI system in the spectral interval 1000 – 2500 nm to develop non-destructive analytical method for the prediction of two main properties of painting canvases; pH and cellulose DP. Using a well-characterized reference sample set of historic canvases, quantitative calibration models were developed with the aid of multivariate data analysis methods.

Two regression models were developed and proved its potential to be used for the prediction of pH and DP for unknown canvas samples in comparison with other developed models for similar materials. The prediction errors for both models are consistent with the uncertainty of the standard measurement methods indicating its suitability for collections survey. Quantitative NIR chemical maps of pH and cellulose DP for a selection of real painting canvases were successfully generated based on the developed models spotting areas with different conditions and mapping vulnerable areas that require intervention. The maps are able to visualize the heterogeneous nature of the canvas, but no correlation between pH and DP was detected despite what can visually be seen in the maps where some of areas with high DP values are associated with high pH values.

The performance of HSI models was compared to models based on spectral data collected using the LabSpec-5000 spectrometer for the same reference canvas collection. Models are performing similarly, where both can be used for surveying canvas collections. However, a limitation to explain the variability of the results within a canvas while validating

the spectroscopic models on real canvases, especially in DP values was noticed which can be overcome by using the advantage of HSI chemical maps.

Moreover, the degradation behaviour of canvases was investigated with the aid of accelerated degradation where Ekenstam equation and modelled dose-response function recently developed for western paper were successfully suitable for canvases allowing for the prediction of its degradation rate. Based on the results of the kinetic analysis of canvases and paper lifetime equation from earlier studies, lifetime maps were generated for few real paintings as an example of its ability to simulate the effect of different storage conditions on the canvas degradation at natural ageing conditions. Correlation was detected between pH and DP and lifetime, but no evidence which one has the highest effect on the calculations of the lifetime. However, the lifetime maps visually show a similar pattern as the acidity maps supported with incremental pattern detected in the correlation between pH values and the calculated lifetime. The developed chemical maps and the lifetime maps are not showing any strong relation with the visual pattern of the canvases' backs. A linear pattern was detected in all the maps which would need further investigation to identify the real causes of it either from spectral noise or real variations in the surface morphology of the objects.

This is the first time to apply these equations and generate chemical and lifetime maps for canvases where the availability of such information would enable better preservation plans. Future work will investigate this new condition assessment tool and degradation behaviour of canvases in more depth, including larger and more representable canvas data set.

6. POPYRI

This chapter focuses on the application of near infrared (NIR) hyperspectral imaging (HSI) on ancient papyri, exploring the potential of imaging through glass and its effect on the spatial and spectral accuracy of the collected information. This will give conservators the opportunity to survey, understand and visualise papyri, particularly considering that most papyri collections are kept in glass frames.

Despite papyri being the oldest writing materials (Grasselli, 1983), little is known scientifically about papyrus with respect to its material properties, as well as about the writing materials such as inks and pigments (Frösén, 2012). One possible explanation for the rarity of research is the inaccessibility of collections and/or unavailability of information (Grasselli, 1983; Bülow-Jacobsen, 2012). I attempted to use the advantage of scanning through glass using HSI system in the SWIR region (1000 – 2500 nm) to obtain chemical information focusing on characterization of materials such as the papyrus support itself and ink as the writing material. This would enrich our knowledge about the development of material use through time, especially the ones used for writing and could reveal some information about the manufacturing process if applied to collections with known dates.

The chapter is divided into four sections where the first section (6.1) focuses on the evaluation of the potential of scanning objects through glass using the HSI system then the second one (Section 6.2) presents a survey that was conducted on 60 objects (Papyri collection) with known dates from the Petrie museum at UCL. These were scanned by the HSI system, then the data were processed with the aid of multivariate data analysis methods and the obtained chemical information were investigated. Section 6.3 discusses an attempt to classify papyri samples that have different degradation levels with the aid of accelerated degradation based on their cellulose degree of polymerization (DP) predicted using partial least squares (PLS) regression model developed for the determination of DP for Islamic paper considering that it is a similar cellulose-based material. Such information could have a great impact on the management and preservation plans of papyri collections. A summary of all the chapter and conclusions obtained is described in the last section (6.4).

6.1 Scanning through Glass

The aim of this section is to explore the effect of scanning an object using HSI through a layer of glass in the SWIR region (1000 – 2500 nm) on the quality of the spectra. Samples of glass frames from the Petrie museum were provided, representing typical glass types used for papyrus collections. Different objects such as standard calibration targets and Islamic paper (IP) calibration target were scanned with and without the glass frame for comparison. The main purpose of this experiment was to see whether the spectra obtained

through glass can be used for subsequent analysis and image generation without the need to obtain the characteristics of the used glass frame.

Since glass samples were of various thickness (~2 mm – 3 mm), scans of the objects were collected with all the varieties in thickness using thin and thick glass samples in addition to two of the glass samples together (Two thin samples) to achieve a thicker layer of glass (~ 4 mm).

The duration of the whole scanning process for an object was less than 60 s for 3 repeated scans. The average lux of the illumination used is $11792.46 \pm 3\%$ (relative standard deviation – RSD %) and the range of the temperature reaching scanning stage is between ~ 38 – 40 °C. Table 6-1 shows the acquisition specifications throughout the experiment.

Table 6-1. Acquisition parameters of the scanning experiment.

Exposure	5.5 ms	Lens	30 mm
Gain	1	Scan speed	54.86 fps
Light	500 W	Spectral range	1000-2500 nm

Different scanning options were compared, such as inclusion of the glass layer in the calibration/correction process which is considered similar to the process of taking the absorption spectra of the glass and compensate for it later on. To achieve that, the glass frame was positioned over the white calibration tile (standard diffuse reflection Spectralon bar) fixed on the scanning stage.

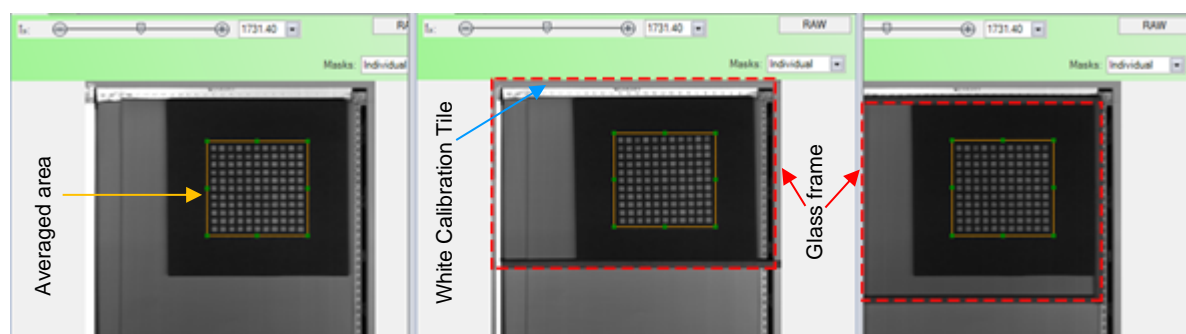


Figure 6-1. Scanning of the Islamic paper target using the HSI system showing the different positions of one of the glass samples; Without a glass frame (left), over the white calibration tile and the IP target (middle) and only over the IP target (right). The red rectangle represents the glass frame. The orange squares represent the area used to calculate the average spectra.

Figure 6-2 shows a comparison between the average spectra obtained in the different scanning experiments with various glass layer thickness (no glass, thin glass, thick glass and two thin glass panes) for the Spectralon multi-component wavelength standard and Islamic paper calibration target. In each case, the glass sample was scanned while positioned over the white tile and named as ‘Calibration’ in the figures. No noticeable differences in the spectra are detected. However, it seems as if the glass layer is acting as a filter where the intensity of the reflection is related to the thickness of the sample. The

thicker the glass sample, the lower is the intensity of the spectra. It is also noticed that when the glass sample is taken into consideration in the calibration process, its effect is eliminated or compensated for and the spectra are then very similar to the spectra of scans without glass which is expected as a correction step.

There is a very good correlation between the results that come from the scans with and without glass which indicates that having a glass layer does not change the collected reflected spectra (Figure 6-3).

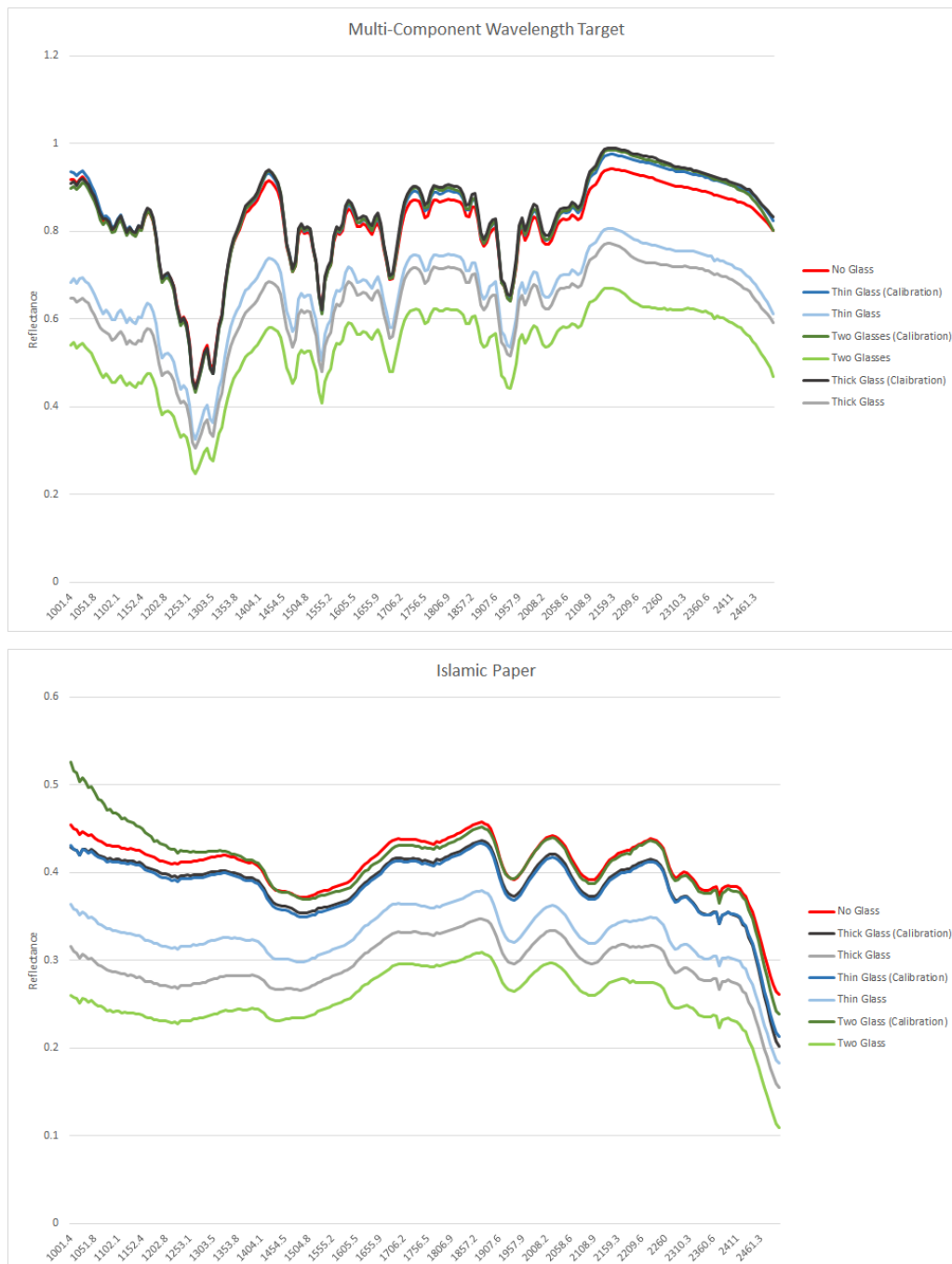


Figure 6-2. Average reflectance spectra of Spectralon multi-component wavelength standard (top) and Islamic paper calibration target (bottom) from different scans using HSI. Scans show the effect of scanning with and without glass using different frames with various thicknesses. Also, the figure shows the effect of including the glass frame in the calibration process.

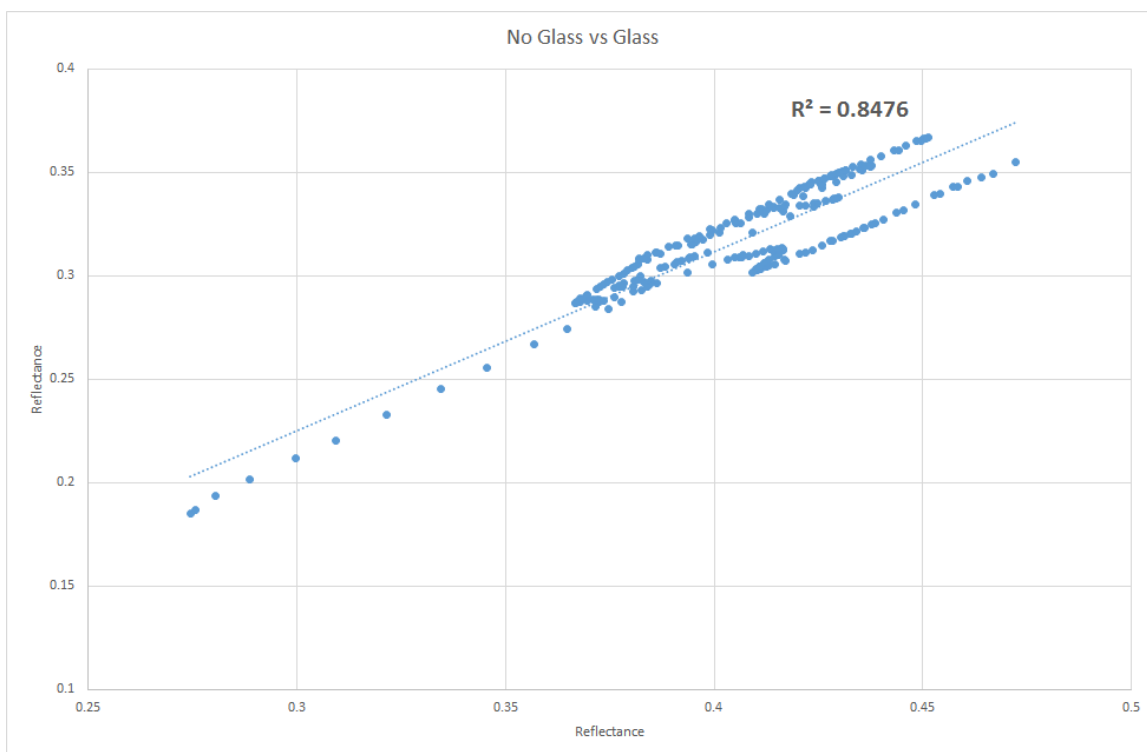
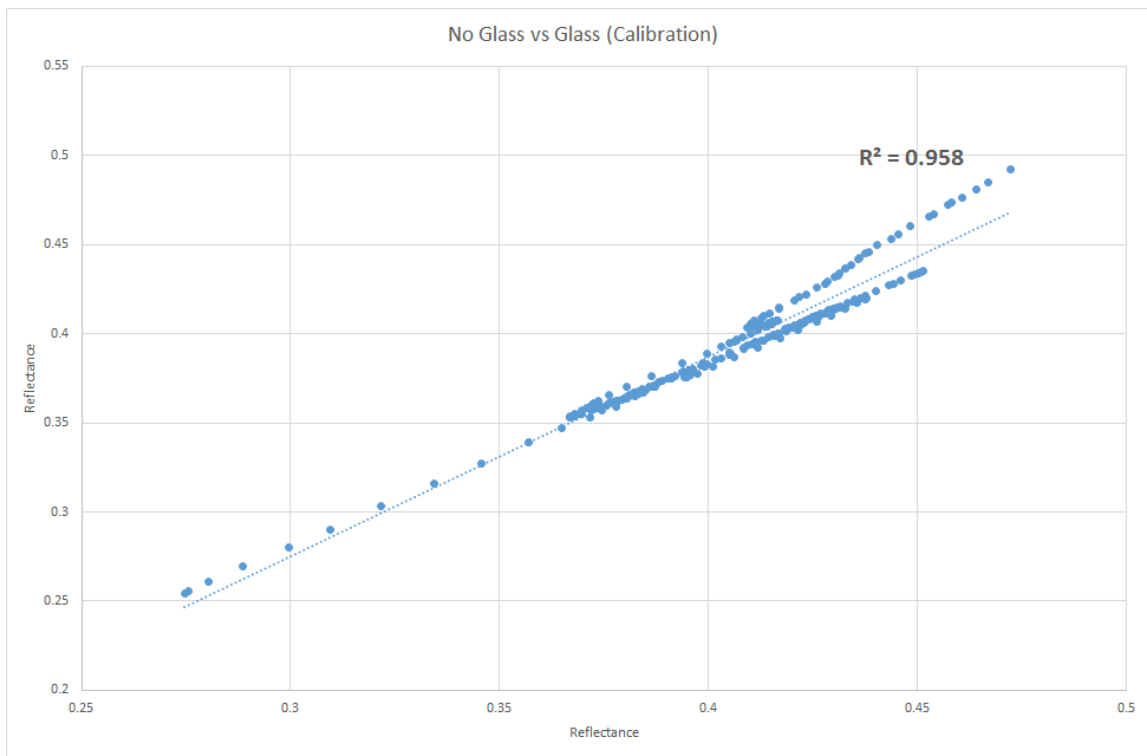


Figure 6-3. Scatter plots show the reflectance correlation between scans of Islamic paper calibration target with and without glass in the two scenarios; when the glass is used in calibration (left) and when it only covers the tested object (right).

Moreover, to evaluate the influence of glass on the quality of the spectra and consequently on the accuracy of the calibrations/predictions, I re-built the developed PLS models for the determination of cellulose DP in paper using the spectral data of the scans of IP calibration target with and without glass in relation to the actual measurements of the IP samples. Also, I explored the effect of glass used in the process of calibration. To evaluate the

results, the root mean square error of cross-validation (RMSECV) from each model was calculated and compared to each other.

Table 6-2 shows the optimal results of each model using different pre-processing methods for the spectra in the spectral interval 1450 – 2350 nm. Reasonable variations in the calibration errors are evident in the RMSECV taking into account the standard error of the viscometric measurement, which indicates that there is no effect from the glass frames on the quality of spectra.

Table 6-2. Root mean square errors of cross-validation (RMSECV) resulting from the developed PLS models for the determination of DP of cellulose in paper. The Leave-one-out cross-validation method was used. The models were developed based on the spectral data of the HSI scans of IP calibration target without and with glass (~ 2 mm thickness) taking into account its involvement in the calibration process while scanning. Different pre-processing methods were used to clean the spectra from any noise. The table also shows the correlation and number of factors selected to generate the optimal results for each model.

1450 – 2350 nm	No Glass			Thin Glass (Calibration)			Thin Glass		
	RMSECV	R _{cv}	Factors	RMSECV	R _{cv}	Factors	RMSECV	R _{cv}	Factors
RAW	347	0.6	5	332	0.64	5	357	0.58	5
SNV	357	0.58	5	355	0.62	5	359	0.58	4
SG 1 st Derivative	341	0.66	11	349	0.58	3	324	0.69	14
SG 2 nd Derivative	332	0.65	6	347	0.65	8	322	0.7	14

On the other hand, since most of the papyri collections are embedded into glass frames so to check the reliability of the predictions of a calibration model and to check if a parameter such as using the spectral data of samples with or without glass while building the calibration model need to be considered, I tried to determine DP for IP target samples using their spectral data scanned with glass using the calibration models developed based on the spectral data of same IP target samples without glass to figure out its applicability. I also determined DP for same samples without glass and with glass (after calibration) for comparison. From the prediction errors (RMSEP) shown in Table 6-3, it seems that in most cases (using thin glass and different pre-processing methods for the spectral data) the prediction error is high (highlighted in yellow colour) despite the good correlation of the predictions indicating its uncertainty and maybe the need to either scan with the glass layer similar to the calibration models or take the glass layer into account in the calibration step.

Table 6-3. Prediction errors and its correlation resulted from validating the developed regression PLS model for determination of cellulose DP in paper. The model is based on the spectral data of IP target samples without glass. Spectral data of same samples but scanned with glass were used as a validation set.

1450 – 2350 nm	Validation Set					
	No Glass		Thin Glass		Thin Glass (Calibration)	
	RMSEP	R _p	RMSEP	R _p	RMSEP	R _p
RAW	282	0.75	482	0.7	312	0.71
SNV	265	0.78	662	0.75	311	0.77
SG 1 st Derivative	202	0.88	290	0.78	555	0.79
SG 2 nd Derivative	243	0.82	547	0.78	295	0.78

6.2 Qualitative Evaluation

In the previous section, it was proven that there is a potential to get useful information from scanning an object through glass using HSI system in the spectral range from 1000 – 2500 nm. Thus, I attempted to qualitatively analyse spectral data gathered from real papyrus collection in a trial to gather new chemical information collected either about the writing materials used or the support itself.

A survey of ~60 objects from the papyri collection of Petrie museum was conducted (Figure 6-4). The description of the objects is described earlier in section 2.3. Table 6-4 shows the full list of the objects with their details. Each object was stored between two glass panes and in some cases two or three objects were combined in the same glass frame. Glass panes have various thickness from ~2-3 mm similar to the investigated glass samples in the previous section (Section 6.1). Papyrus objects are dated from the Middle Kingdom (2024 BC) to the Islamic Period (1000 AD) and are written in different languages such as Demotic, Greek, Hieratic, Arabic and Coptic. The ink used in most of the objects is black except one object with additional red ink. No information about the type of the inks is available which will be investigated through the survey. Some of the objects are mounted onto paper backing.

Table 6-4. Details of 62 objects from the papyrus collection of Petrie museum showing the ID, dimensions, language and date for each object.

Object ID	Dimensions (mm)			Language	Period
	Height	Width	Depth		
27934iii	284	280	8	N/A	New Kingdom: 1550 – 1350 BC
31906	249	179	7	Demotic	Ptolemaic Period: 305 – 30 BC
31915	185	114	7	Greek	Greek School
31916	264	165	7	Greek	Greek School
32069	239	180	5	Greek	Byzantine Period: 395 – 641 AD
32070				Greek	Roman Period: Late 3 rd - Early 4 th C. AD
32071a	186	115	7	Greek	Roman Period: Mid-3 rd C. AD
32071b				Greek	Roman Period: Late 3 rd C. AD
32072a-e				Greek	Roman Period: Late 2 nd - Early 3 rd C. AD

32427ii	250	210	7	Demotic	Middle Ptolemaic Period: 203 – 117 BC
55854	250	200	7	Demotic	Ptolemaic Period: 305 – 30 BC
55856	251	261	7	Demotic	Ptolemaic Period: 305 – 30 BC
55857	284	191	8	Demotic	Ptolemaic Period: 305 – 30 BC
55858	299	200	7	Demotic	Ptolemaic Period: 305 – 30 BC
55859	285	191	8	Demotic	Ptolemaic Period: 305 – 30 BC
55860	279	230	7	Demotic	Ptolemaic Period: 305 – 30 BC
55861	250	201	7	Demotic	Ptolemaic Period: 305 – 30 BC
55866	295	256	7	Greek	Middle Ptolemaic Period: 203 – 117 BC
55892ii	300	210	7	Demotic	Middle Ptolemaic Period: 203 – 117 BC
55898	288	220	7	Demotic	Ptolemaic Period: 305 – 30 BC
55899	214	185	7	Demotic	Ptolemaic Period: 305 – 30 BC
55900	290	230	7	Demotic	Ptolemaic Period: 305 – 30 BC
32781	192	171	7	Hieratic	Ramessid Period: 1295 – 1069 BC
32782	295	205	7	Hieratic	Akhenaten Period: 1352 – 1336 BC
32787	260	152	8	Hieratic	Dynasty 19: 1295 – 1186 BC
32788	305	274	7	Hieratic	Dynasty 19: 1295 – 1186 BC
32791	230	178	7	Hieratic	Dynasty 19: 1295 – 1186 BC
32792	254	203	7	Hieratic	Ramses II: 1279 – 1213 BC
32793	290	152	8	Hieratic	Ramses II: 1279 – 1213 BC
32796	168	159	5	Hieratic	Ramessid Period: 1295 – 1069 BC
32798	305	228	7	Hieratic	Dynasty 20: 1186 – 1069 BC
32799				Hieratic	Dynasty 19: 1295 – 1186 BC
32800	228	153	8	Hieratic	Dynasty 19: 1295 – 1186 BC
32801	221	153	8	Hieratic	Dynasty 21: 1069 – 945 BC
32806 A-D	302	123	7	Hieratic	Ramessid Period: 1295 – 1069 BC
32802	203	222	7	Hieratic	Ramessid Period: 1295 – 1069 BC
32808	300	204	7	Hieratic	Ramessid Period: 1295 – 1069 BC
38177	243	203	8	Hieratic	Amenhotep III: 1390 – 1352 BC
55721	240	120	7	Demotic	Ptolemaic Period: 305 – 30 BC
55840	250	160	7	Greek	Ptolemaic Period: 305 – 30 BC
55869	198	166	7	Demotic	Middle Ptolemaic Period: 203 – 117 BC
55884	250	200	7	Demotic	Middle Ptolemaic Period: 203 - 117BC
37436	230	162	7	Greek	Greco-Roman Period: 332 – 395 BC
59445	172	84	4	Arabic	Islamic Period: 641 – 1510 AD
6570	160	140	7	Greek	Byzantine Period: 395 – 641 AD
55870ii	300	250	7	Demotic	Middle Ptolemaic Period: 203 – 117 BC
55872ii	285	258	7	Demotic	Middle Ptolemaic Period: 203 – 117 BC
55874	300	280	7	Demotic	Middle Ptolemaic Period: 203 – 117 BC
55881	300	225	7	Demotic	Middle Ptolemaic Period: 203 – 117 BC
55883	290	230	8	Demotic	Middle Ptolemaic Period: 203 – 117 BC
55885	230	190	8	Demotic	Middle Ptolemaic Period: 203 – 117 BC
55886	290	249	7	Demotic	Middle Ptolemaic Period: 203 – 117 BC
55889	249	200	7	Demotic	Middle Ptolemaic Period: 203 – 117 BC
71069iv	240	130	8	Greek	Ptolemaic Period: 305 – 30 BC
71073	180	172	7	Coptic	Byzantine Period: 395 – 641 AD
71078	232	200	8	Greek	Roman Period: 30 – 395 AD

32159	240	190	7	Hieratic	Late Middle Kingdom: 1850 – 1700 BC
32161	120	117	7	Hieratic	Late Middle Kingdom: 1850 – 1700 BC
32164	307	180	7	Hieratic	Late Middle Kingdom: 1850 – 1700 BC
38178A	253	248	7	Hieratic	Amenhotep III: 1390 – 1352 BC
38178B				Hieratic	Amenhotep III: 1390 – 1352 BC
32778	202	200	7	Hieratic	Dynasty 13: 1795 – 1650 BC



Figure 6-4. A papyrus sample (ID=32781) from the papyri collection of Petrie museum.

All the papyri objects were scanned using the HSI system (Figure 6-5) with different acquisition parameters (listed in Table 6-5). The collected spectral images were then analysed visually and with the aid of multivariate data analysis methods such as principal component analysis (PCA) and K-means clustering methods (Naes et al., 2002; Miller & Miller, 2010). Processing and data analysis were performed with Matlab R2015b and Hypertools v.1.0 software. One purpose of surveying the collection is to discover the potential of using the scanning method to characterize or differentiate papyrus support. As no reference database is available to help us to achieve that, it is hard to work on the papyri objects on an individual basis. Instead, objects were compared to each other to find any correlation. As seen in Figure 6-6, the two objects (ID = 32069 and 32070) seem to have different supports. Both objects are combined together under the same glass frame mounted onto same paper backing which minimizes the possibilities of errors/variations while collecting the spectral data as both were exposed to similar acquisition conditions in the same scan. The background was separated and the whole image was pre-processed using Savitzky-Golay (SG) derivation filter and standard normal variate (SNV) methods. It is noticed that the two papyri can be characterized using the two wavelengths of 1393 nm and 1879 nm. The results also were confirmed by using PCA and K-means clustering

methods where the first principal component (PC1) shows the separation between both objects in addition to the two clusters using the later method (Figure 6-6). This shows the potential of extracting chemical information from HSI images of glass framed objects which can be used in its characterization.

Table 6-5. Hyperspectral imaging system acquisition parameters used in the survey.

Lens (focal length)	30 mm	56 mm
Exposure	5.5 ms	7.5 ms
Scan speed	54.8 mm/s	26.5 mm/s
Lights	500 W	500 W
Aperture	F/2.0	F/4.0
Binning	1X1	
Gain	1	
Spectral Range	1000-2500 nm	

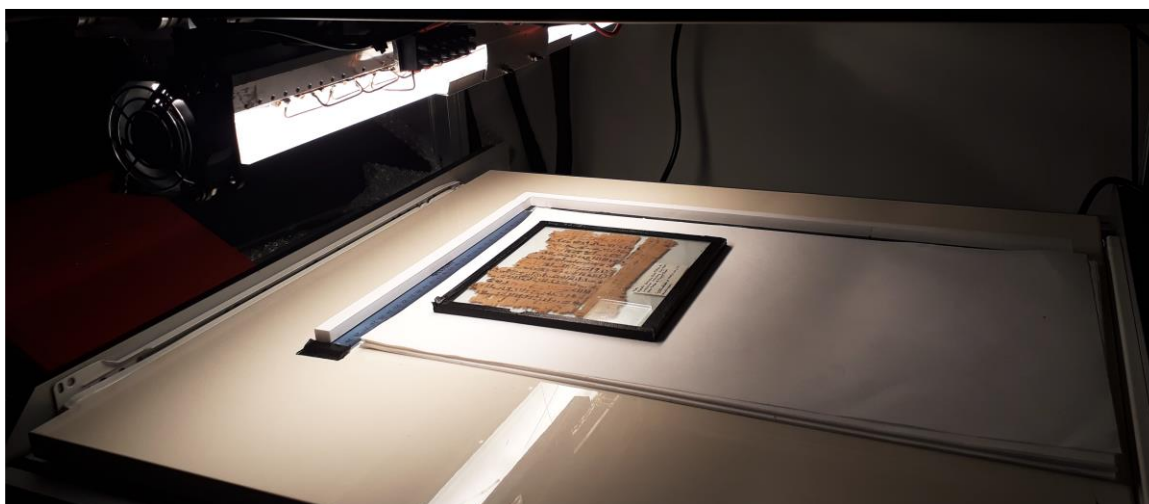
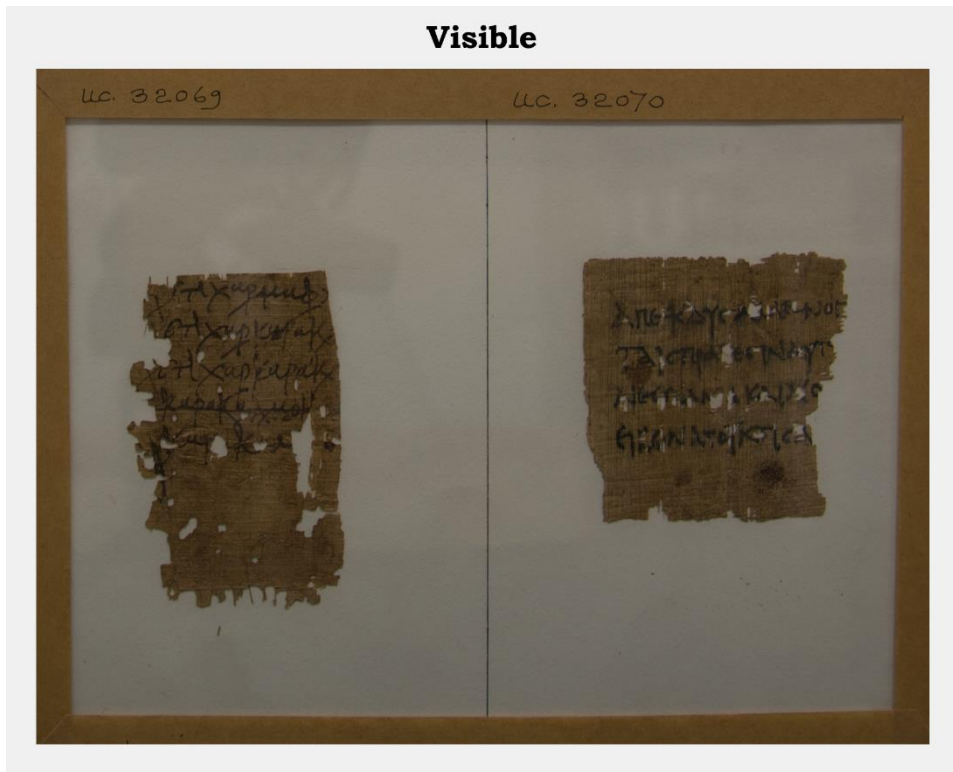
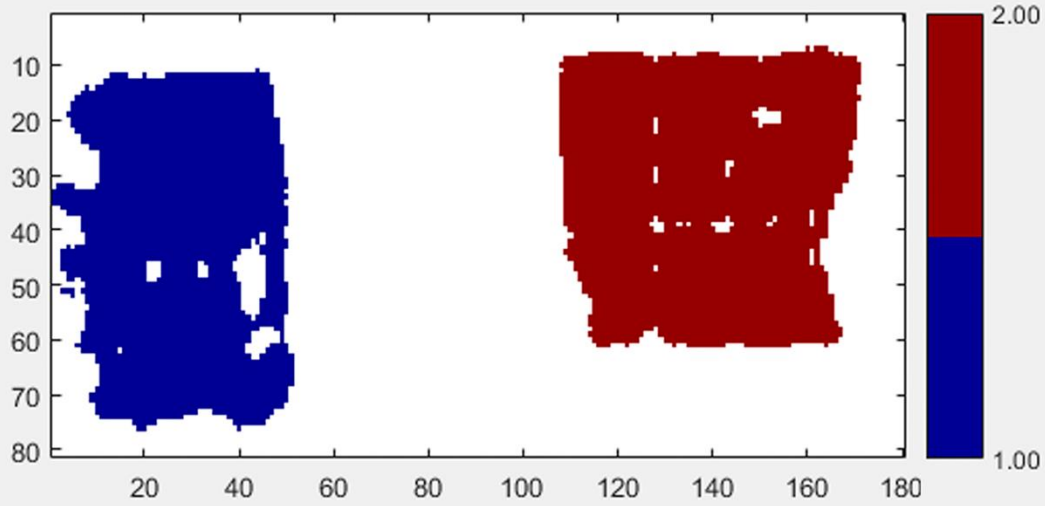


Figure 6-5. Scanning of a papyrus object from the Petrie museum collection using the HSI system.

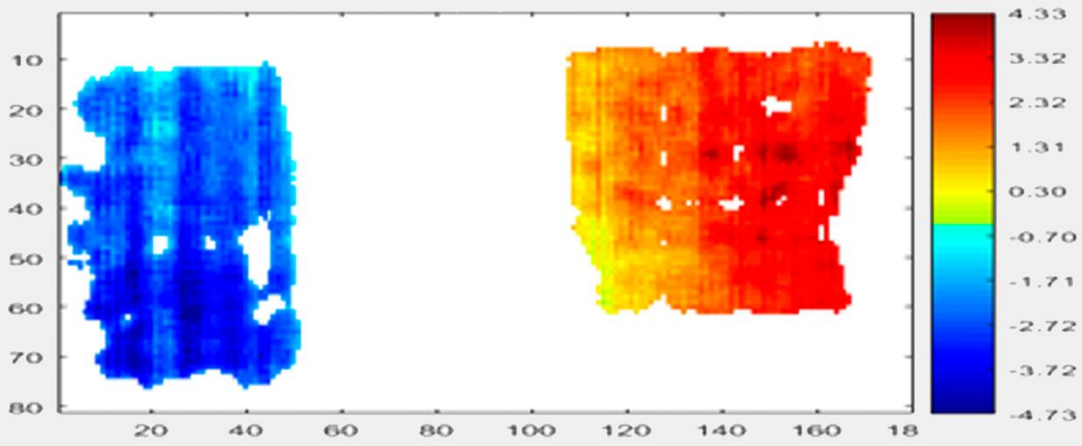
Visible



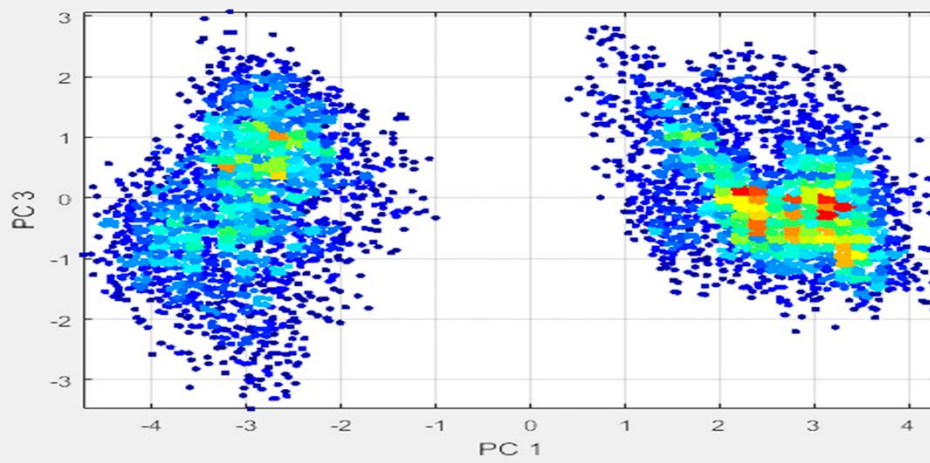
K-means Clusters



PC 1 Var(%) 49.25



Scores



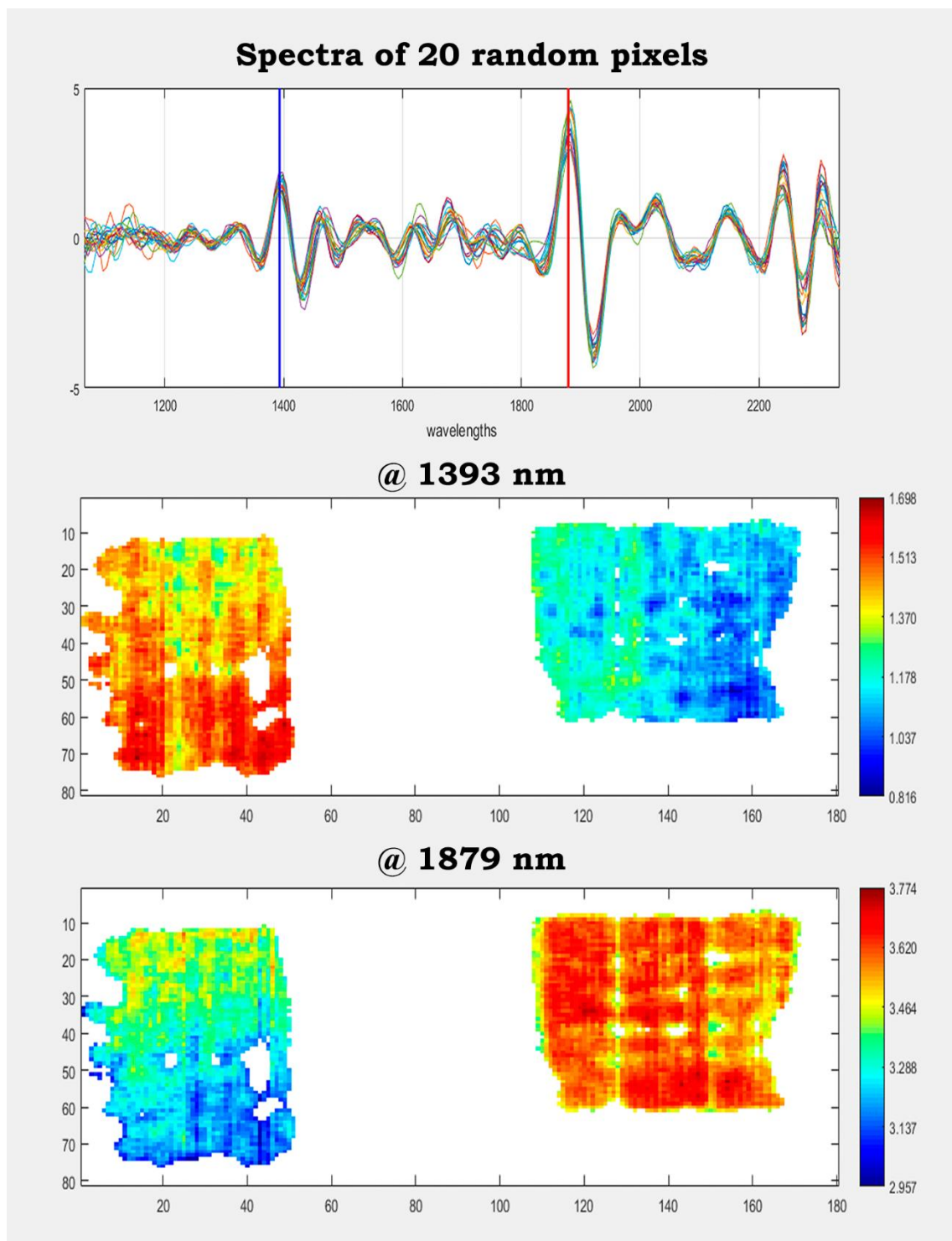


Figure 6-6. Results of the analysis of spectral image of two papyri (ID = 32069 and 32070-blue cells in **Table 6-4**) from the Petrie museum collection acquired by the HSI system in the spectral range 1000-2500 nm. In the first row, the figure shows a visible image of the two papyri. Then, the results of PCA and K-means clustering are shown where the distribution of the values of the spectral image based on the K-means clusters on the top and the score image of the first principal component (PC1) with the scatter plot of PCA scores for the first and third PCs are in the bottom part. On the last row, the spectra of 20 pixels (top) selected randomly by the software from the spectral image after pre-processing by Savitzky-Golay (SG) derivation filter and SNV methods, in addition to color maps of the spectral image at two bands (@1393 nm, @1879 nm) that can be used to characterize the two papyri.

Another attempt was conducted using the spectral data of the papyri objects to explore the used inks as a writing material. It is known from the literature that ink made of soot is the oldest and most common ink material used in Egypt since the 1st dynasty BC (Lucas & Harris, 1962) while metallic ink (Iron-gall ink) was also reported to be used from the 2nd – 3rd century AD onward (Lucas, 1922; Mitchell & Hepworth, 1937; Lucas & Harris, 1962; Bülow-Jacobsen, 2012). However, few evidences referred to the possibility of the use of iron-gall ink at 3rd century BC (Lucas, 1922; Bülow-Jacobsen, 2012).

Spectral imaging proved its success in the field of material identification, especially for pigments and inks (Neevel, 2006; Strlič et al., 2010; Gál et al., 2013; Cosentino, 2014). It has the ability to differentiate the different types of inks, carbon and iron based inks in particular. Several studies (Havermans et al., 2003) have shown that iron-gall inks can be detected in the NIR region due to their characteristic transparency while the carbon ink is a strong absorber of NIR radiation so it appears completely black.

Based on that, I tried to investigate if any iron gall ink can be detected among the surveyed Petrie collection objects since it can demonstrate the development of ink through the different periods. The collected spectral data were processed and analyzed using PCA. Most of the used ink in the collection is carbon-based except only one Papyrus (ID = 71073) from the 4th/5th century AD that was written using iron gall ink (Figure 6-7). As seen in the figure, the text of the papyrus has faded at 1750 nm in comparison to a carbon ink used in another papyrus (ID = 32778) from the dynasty 13th BC where the text appears black. This is a good evidence of the use of iron-gall ink in this period, which is consistent with the literature (Lucas, 1922; Bülow-Jacobsen, 2012). PCA also gave good analytical results for papyri where it can be used to separate between the support and the ink as seen in Figure 6-7 for papyrus with carbon-based ink.

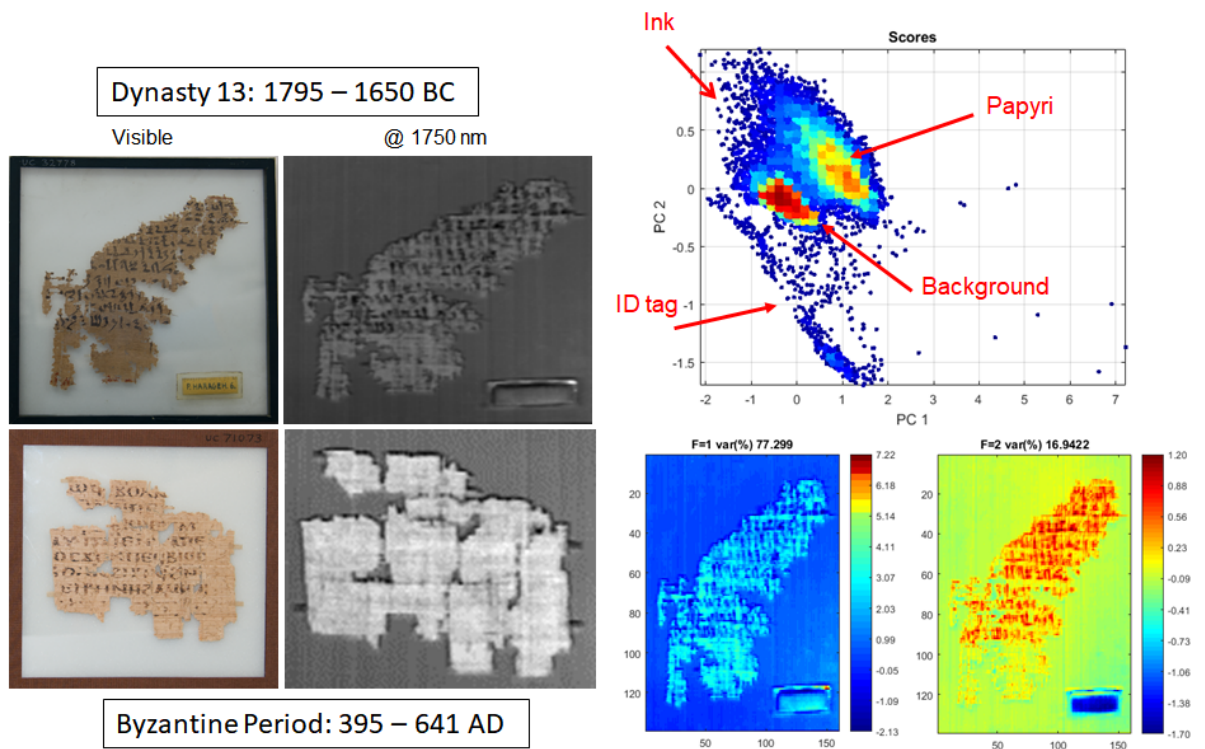


Figure 6-7. The results of the analysis of spectral images of two papyri (blue cells in **Table 6-4**) collected using the HSI system to investigate the type of used ink. On the left side, visible images and grey images at 1750 nm are shown where object 32778 with carbon-based ink is shown at the top and object 71073 with iron-based ink is at the bottom. The right side shows the scatter plot of PCA scores (top) for the first two PCs where the different types of materials of the spectral image separated from each other as indicated. The score images of PC1 and PC2 are shown in the lower part where the first emphasizes the papyrus support and the other separates the ink.

6.3 Quantitative Aspect (A Trial Study)

In this section, an experiment was conducted to try to develop a method to classify papyri samples based on their material from less to more degraded state. To achieve that, four historic papyri samples (P3, P7, P8, P9) in addition to one recently purchased new papyrus (Pnew) were prepared (Figure 6-8). The samples have low historic value with no information about their provenance or date. All the samples were aged at 80 °C and 65% RH for 2 weeks to have them in different degradation states (naturally aged (historic), naturally/artificially aged, new and new/artificially aged). Spectral measurements were collected using HSI system in the SWIR region (1000 – 2500 nm) from the samples before and after ageing then the data were analysed using multivariate data analysis methods.

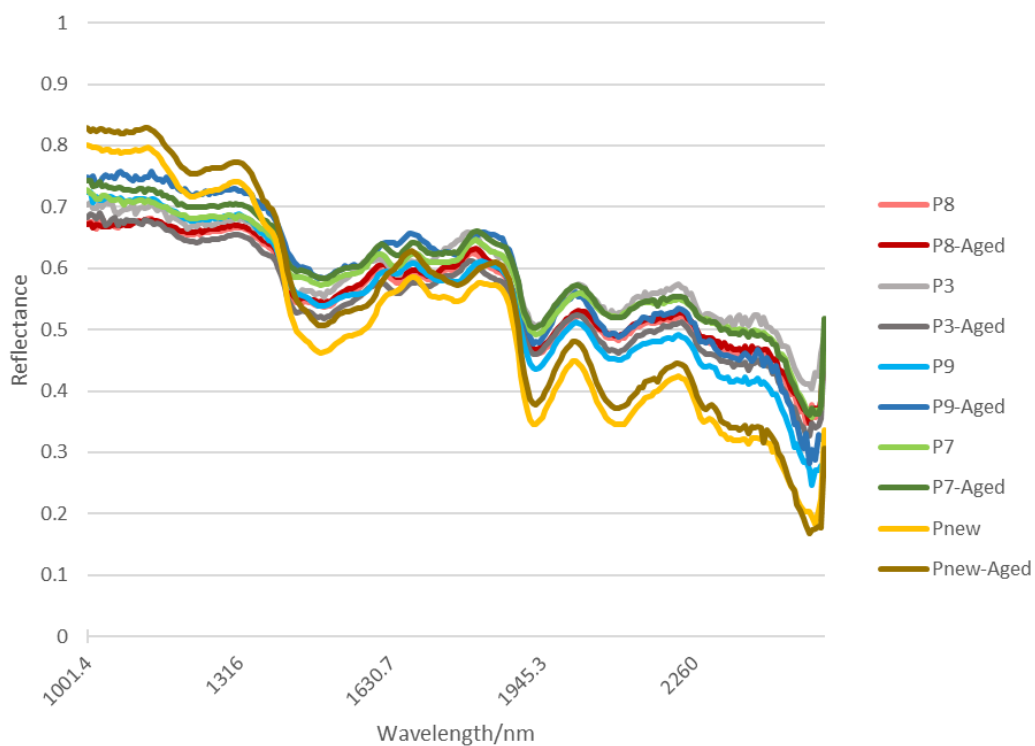
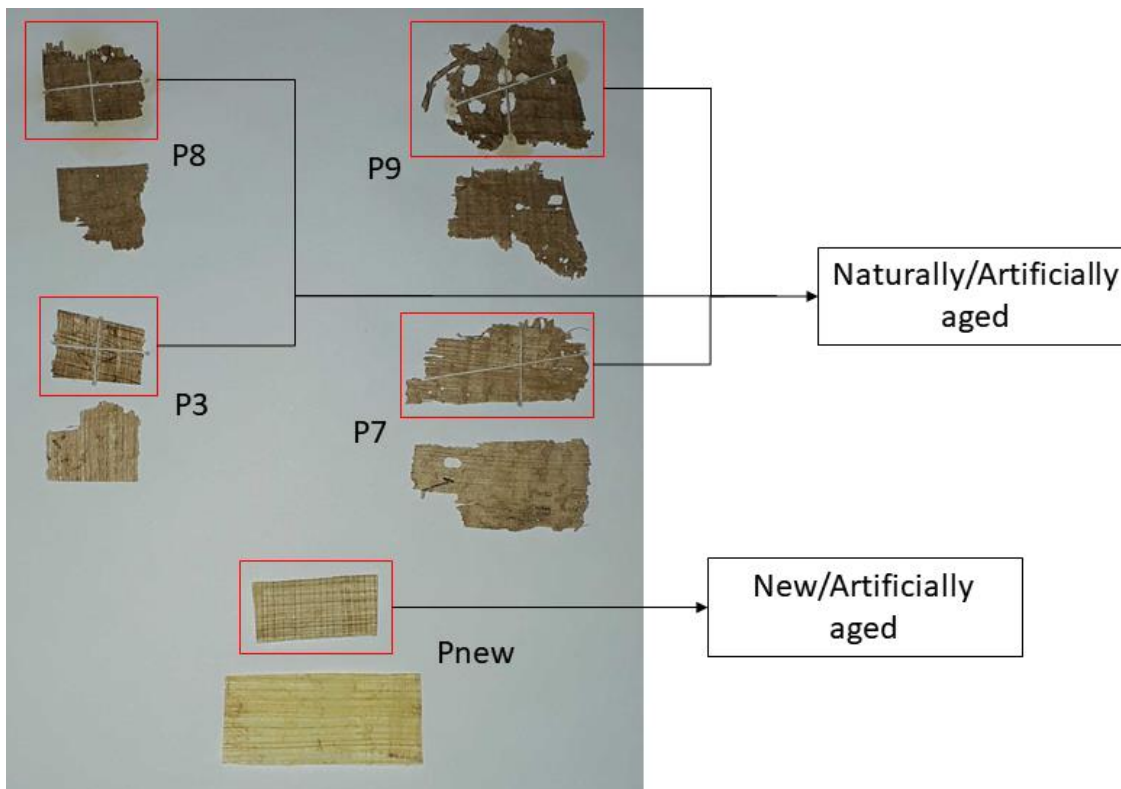


Figure 6-8. Papyri samples (4 historic (naturally aged) and 1 new) (top) with its corresponding spectra collected by HSI system in spectral interval 1000 – 2500 nm (bottom). Red rectangles highlight the samples after ageing at 80° C and 65% RH for 2 weeks.

Firstly, when using PCA to analyse the spectral image of the papyri, it only separated historic/old (naturally and naturally/artificially aged) and new (new and new/artificially aged) samples based on their spectral characteristics without taking into account their degradation state as seen in Figure 6-9.

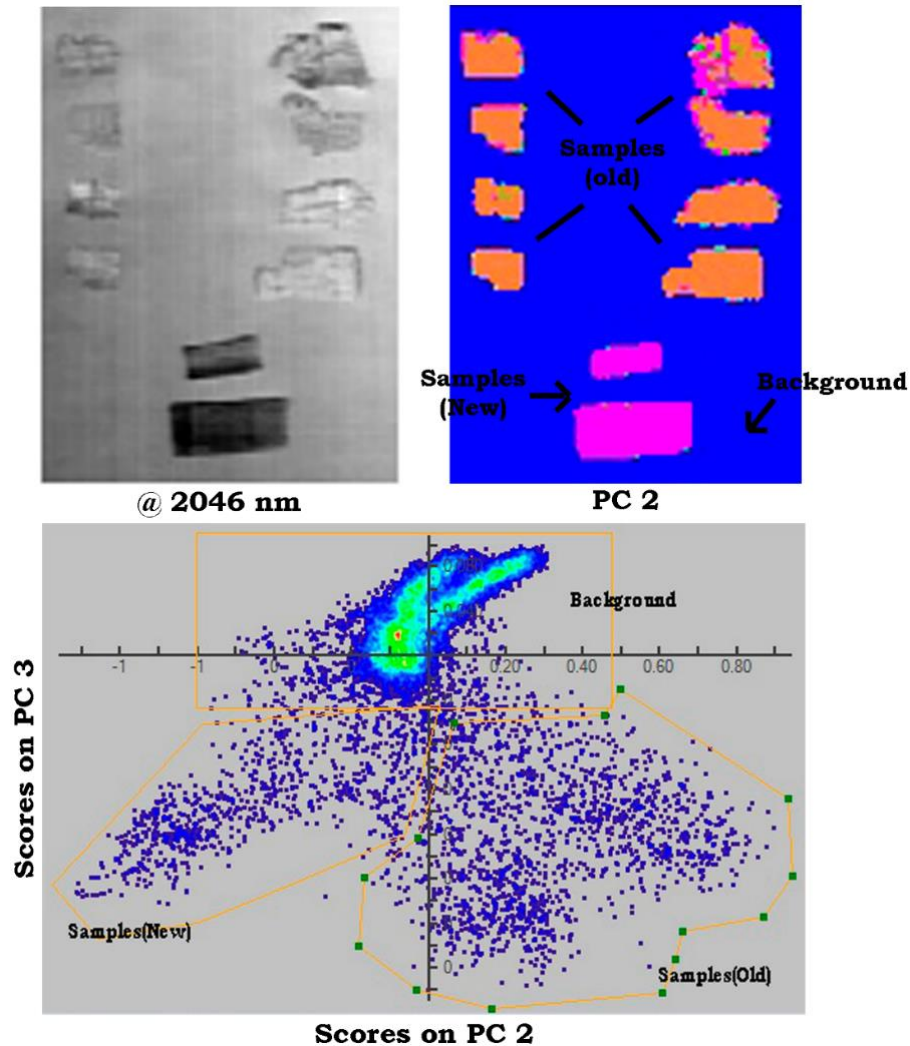


Figure 6-9. Results of PCA analysis of spectral image of 5 papyri samples (4 historic (naturally aged-old) and 1 new) before and after artificial ageing. Grey image at band 2046 nm (top left), score image of PC 2 (top right) masked with colors in relation to the scatter plot (bottom) for PC 2 and PC 3 for the papyri samples which highlights spatial locations with similar spectral signatures.

Thus, in order to classify the samples based on their state/condition, cellulose DP of the papyri samples was predicted as a classification metric using a PLS regression model developed for Islamic paper based on the spectral data of Islamic paper calibration target samples. The model was used without taking into account the real predicted values of DP as it would not make any sense in this case. Since there are no available reference samples of papyri to build calibration models dedicated to it and as both materials papyri and Islamic paper are cellulose based so I tried to use the Islamic paper model to check its suitability for the classification purpose.

The specification of the model is listed in Table 6-6 (Model 1). Figure 6-10 represents the bar plot of the predicted DP values focusing on the classification pattern which clearly demonstrates the potential of separating the new papyri sample from the historic samples. All the samples are also correctly classified into more and less degraded state as required.

This experiment and such results are setting an example and would encourage conservators and researchers to start gathering a representative reference database of papyri to build similar calibration models for better preservation of papyri collections.

Table 6-6. Specifications of two PLS regression models developed for the determination of cellulose DP in Islamic paper based on the spectral data of the Islamic paper calibration target samples collected by HSI system.

	Model 1 (old)	Model 2 (new)
No. samples	57	57
RMSECV	293	315
R²_{CV}	0.5	0.46
Factors	7	8
Spectral range	1450 – 2350 nm	1900 – 2400 nm
Pre-processing	SG (2 nd Derivative, 3 rd polynomial order, 15-pt window), Mean center	SG (1 st Derivative, 3 rd polynomial order, 21-pt window), Mean center
Cross-Validation	Leave-one out	Leave-one out

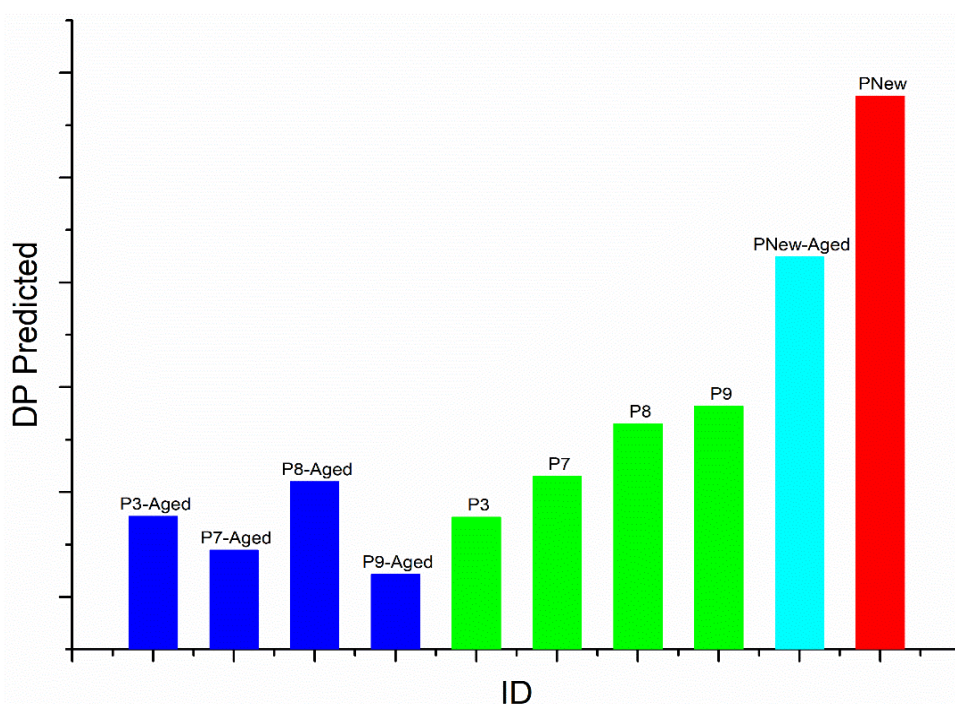


Figure 6-10. Predictions of cellulose DP of papyri samples before and after ageing based on the PLS regression model developed for determination of DP of cellulose in Islamic paper. The predictions are classified into more or less degraded state based on their predicted DP regardless of the numerical information. Colored bars represent the old samples before (green - naturally aged) and after ageing (blue – naturally/artificially aged) in addition to the new sample before (red – new) and after ageing (cyan – new/artificially aged) as well.

However, it was noticed while trying to check the repeatability of the results that the predictions are changing while using spectral data from different scans collected at different times for the same papyri samples. Figure 6-11 shows two examples of the predictions of DP of papyri samples scanned at two different times. The first example on the bottom is predicted using the same PLS model used in Table 6-6 (Model 1) where it correctly differentiates between the historic and new samples, but not between the

differently aged samples, as the aged samples have apparently higher DP values compared to their unaged counterparts.

I tried to compare the spectra of same sample from the different scans to get an idea of the causes of the variations in the predictions. Average spectra of a papyrus sample (P9) from different scans (4 scans) are plotted against each other after being treated with Savitzky-Golay (SG) derivation filter over a specific area (1450 – 2350 nm) (Figure 6-12). There are big differences between the scans, as seen in the figure for the 4 spectra, especially in the first part at shorter wavelengths less than about 1900 nm.

In order to verify that, Papyri samples were placed with the IP calibration target and both were scanned using the HSI at the same time (Figure 6-13) to assure similar acquisition environment and eliminate any possibility of variations. Then, a new PLS model was developed based on the spectral data of the IP calibration target samples using the spectral range 1900-2400 nm and DP values were predicted for the papyri samples based on that model. Specifications of the new model are shown in Table 6-6 (Model 2). The predictions (Figure 6-11, top) are very different compared to the above results. Although there is still reasonable classification of historic (P9, P8, P7, P3 and their aged version) and new samples (PNew and PNew-Aged), the DP of the new samples were predicted as the ones with the low values. Also, the historic samples before and after ageing are not classified correctly.

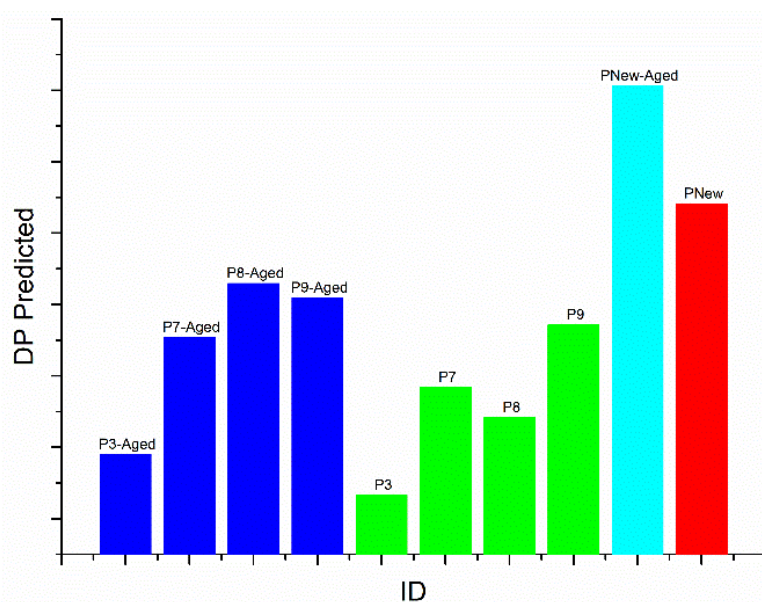
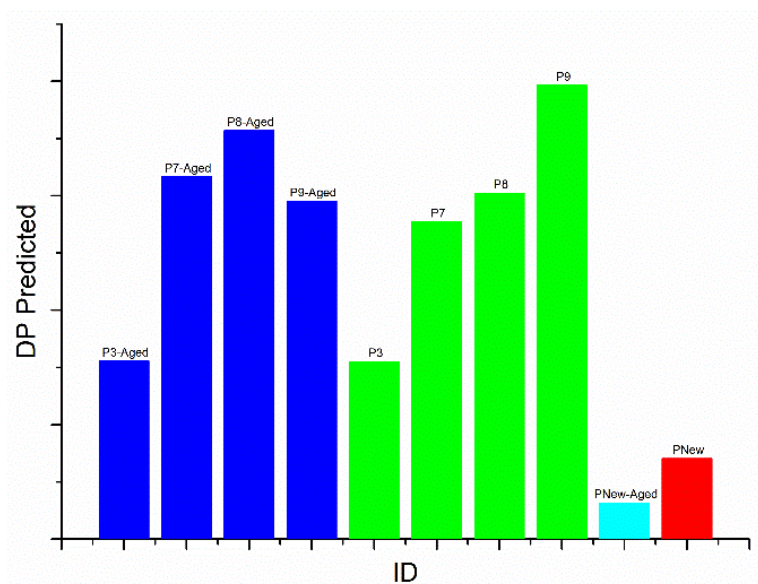


Figure 6-11. Predictions of DP of papyri samples before and after ageing based on two different PLS regression models developed for determination of DP of cellulose in Islamic paper. The predictions classify samples into more and less degraded based on their predicted DP regardless of the numerical information. Colored bars represent the historic samples before (green-naturally aged) and after degradation (blue – naturally/artificially aged) in addition to the new sample before (red) and after degradation (cyan – new/artificially aged) as well.

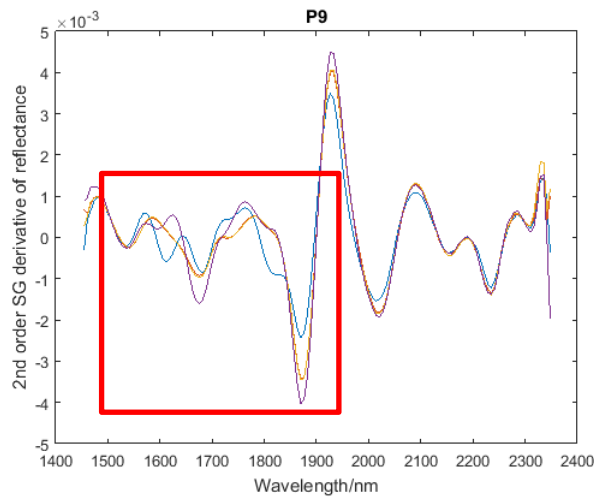


Figure 6-12. Four average reflectance spectra of a papyrus sample (P9) from different scans pre-processed by 2nd order Savitzky-Golay (SG) derivation over specific range 1450 – 2350 nm. Spectra were collected from different scans. The red square highlights the area with the most variations between spectra.



Figure 6-13. A grey image at 1750 nm of Islamic paper calibration target and 5 papyri samples before and after ageing scanned together using HSI system.

I also suspected that the position of the samples over the HSI stage during scanning might be the reason of such variations in their spectra (which was discussed earlier in Chapter 3 – Section 3.5.5), so I compared average spectra of a papyri sample located in three different positions on the stage (vertically from top to down) which are collected at same scanning time (session). The three average spectra were then pre-processed with Savtizky-Golay derivative filter from 1400 – 2500 nm. Figure 6-14 shows significant variation between spectra compared to each other, especially in the short wavelengths (less than 1900 nm), reflecting the effect of the sample's position on the spectra and could possibly verifying the detected variations in the DP predicted values. Unfortunately, due to time constraint, the influence of the position and the other causes of the variations in the spectra will need to be explored in the future.

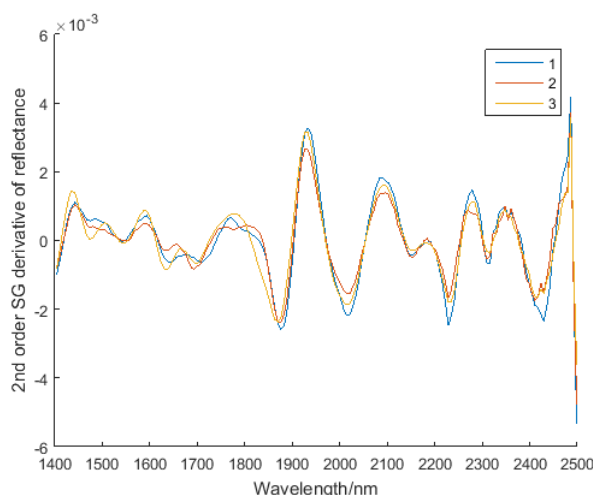


Figure 6-14. Three average reflectance spectra of a papyri sample located in different positions on the stage (changing vertically from top to down) collected using the HSI system in the same scanning time/session for the purpose of exploring the effect of sample position on the spectra. The spectra are pre-processed by 2nd order Savitzky-Golay (SG) derivation over specific range 1400 – 2500 nm.

In a trial to use the potential seen in applying the PLS regression model developed for prediction of cellulose DP of Islamic paper (Model 1) on papyri samples for the purpose of classification between its degradation levels, I applied the same model on a few examples (4 objects) from the Petrie museum collection where all were scanned through their glass frames using the HSI system. A DP map was generated for each object showing the estimated DP for each pixel in the object after excluding the background and inks as these will need another regression model to estimate their DP. Pixels with high DP values (indicating good degradation state) are colored in blue and the ones with the low DP values (bad degradation state) are colored in red as these are the areas that would need intervention. For the first object (ID=55861-blue cell in Table 6-4), 3 pieces of papyri from the Ptolemaic period, are placed in one glass frame. Visually, there is no clear conclusion about which one is in a better material state and whether within one piece if there are any variations. As shown in the DP map (Figure 6-15), we can visualize the change in the degradation level (material state) from the left to the right piece, showing that the left piece is in the least state compared to the others. Also, there are some variations spotted in the right piece at the bottom where the bottom-left part is in high degraded condition. The second object (ID=55898-blue cell in Table 6-4) shown is also from the Ptolemaic period, and in this example I applied the model on the front and back of the object to see any correlation in the results on both sides (Figure 6-16) . It can be seen that the upper part is less degraded. Generally, the distribution of the degradation level is not following the visual appearance of the object which is interesting from the conservation perspective.

The last example shows the same two objects (ID = 32069 and 32070 –blue cells in Table 6-4) that are placed in one glass frame and were proven above to have different supports where one is from the Roman period (right) and the other is from the Byzantine period

(left). The DP maps generated for both (Figure 6-17) are actually showing that both have similar degradation state and tend to have good degraded state.

Having such semi-quantitative maps from HSI scans of glass framed papyri objects where the material state can be classified somehow from more to less degraded within one object, even without knowing the value of the DP, is of great importance for the preservation of papyri collections especially when such information can only be assessed either visually or with destructive methods. Despite the problem with the effect of the position that needs further investigation, as an initial step towards quantitative results, the method could work as a guidance for conservators and researchers about areas that would need more attention/intervention.

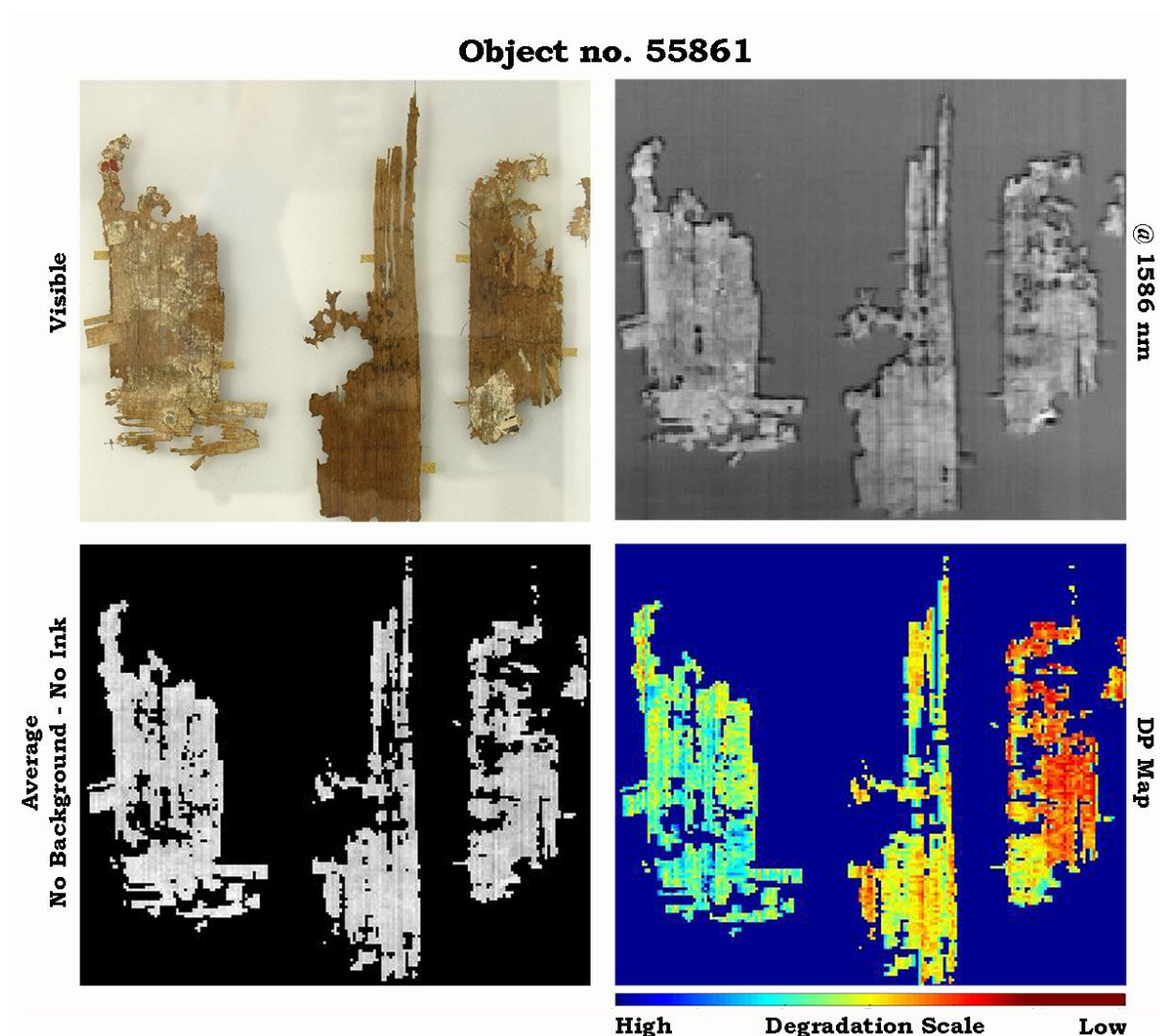


Figure 6-15. Semi-quantitative chemical map of the distribution of estimated DP values of a papyri object (ID=55861-blue cell in Table 6-4) from the Petrie museum collection, estimated based on the PLS regression model developed using the HSI spectral data of Islamic paper calibration target. The map visualizes the DP values according to the degradation state, from less (red pixels) to more (blue pixels) degraded. The figure shows the visible image of the object with a grey image at band 1586 nm in addition to an average image with a threshold to exclude inks and background.

Object no. 55898

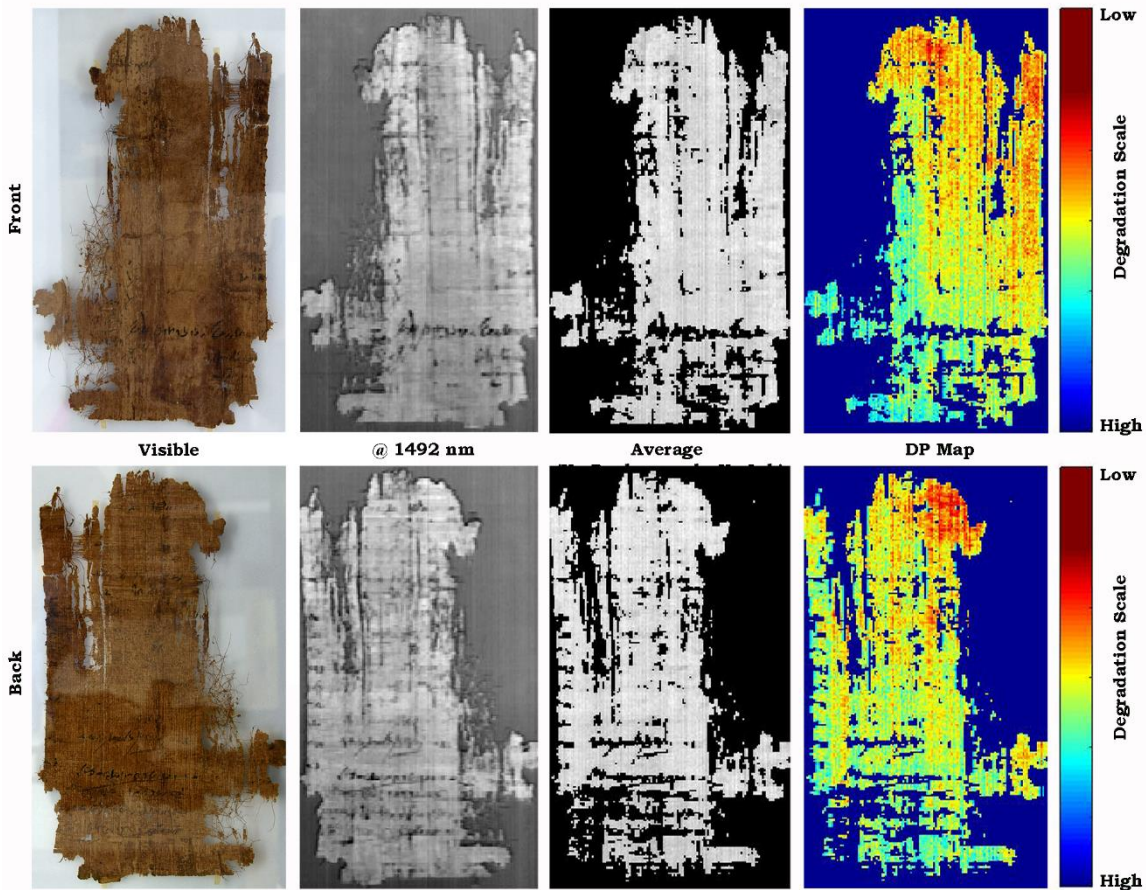


Figure 6-16. Semi-quantitative chemical maps of the distribution of estimated DP values of a papyri object (front and back sides) (ID=55898-blue cell in Table 6-4) from the Petrie museum collection, estimated based on the PLS regression model developed using the HSI spectral data of Islamic paper calibration target. The maps visualize the DP values according to the degradation state, from less (red pixels) to more (blue pixels) degraded. The figure shows the visible images of the object with grey images at band 1492 nm in addition to average images with a threshold to exclude inks and background.

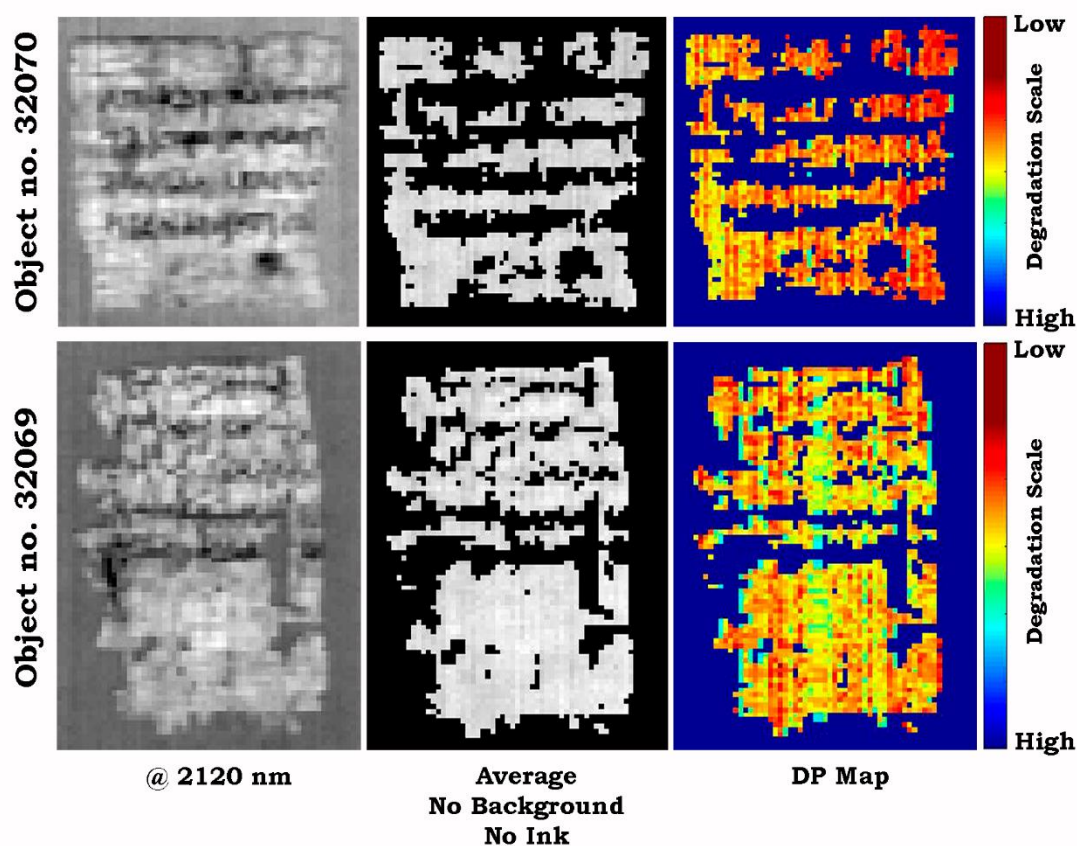


Figure 6-17. Semi-quantitative chemical maps of the distribution of estimated DP values of two papyri objects (ID=32069 (bottom) and 32070 (top) -blue cell in Table 6-4) from the Petrie museum collection, estimated based on the PLS regression model developed using the HSI spectral data of Islamic paper calibration target. The maps visualize the DP values according to the degradation state, from less (red pixels) to more (blue pixels) degraded. The figure shows the grey images of the two objects at band 2120 nm in addition to average images with a threshold to exclude inks and background. Visible image of the two objects can be seen in an earlier figure (**Figure 6-6**).

6.4 Summary of Results

Papyri as a cellulose-based material was explored using hyperspectral imaging in the SWIR region (1000 – 2500 nm). The main focus of the chapter is to investigate the effect of imaging through glass on the accuracy of the acquired information from the spatial and spectral perspectives in addition to the ability to extract chemical information that can be used to enrich our knowledge about papyri materials scientifically. Some of the goals were achieved, as summarized here:

- Spectral data can successfully be collected using HSI Imaging through glass in the SWIR region without influencing its accuracy.
- Glass layer acts only as a filter for the spectra where the intensity of the reflection is related to the thickness of the layer. The thicker the glass layer, the lower the intensity of the spectra is. This can be corrected if glass layer is taken into account in the calibration process.
- No significant variations in the calibration errors of the developed PLS regression models for determination of DP of Islamic paper samples were generated, based

on the spectral information of Islamic paper calibration target scanned with and without glass.

- A survey of 60 papyri objects (kept in glass frames) from Petrie museum was conducted using HSI system and their spectral information were analysed with the aid of multivariate data analysis methods.
- Two papyri objects from the survey mounted on the same paper backing were used as an example to qualitatively characterize their support material through the analysis of its spectral data. Each support has a spectral feature different from the other that can be detected at bands 1393 and 1879 nm. This might be an evidence of changing of the used raw materials through the different periods (from Roman to Byzantine).
- Iron-gall ink was detected in only one of the surveyed papyri objects from the 4th/5th century AD through the analysis of its spectral information.
- A good classification of papyri samples with different degradation level/material state was achieved based on their DP values predicted using the PLS regression model for determination of cellulose DP for Islamic paper.
- Semi-quantitative chemical (DP) maps were generated based on the suggested classification method with the ability to classify and visualize areas within a papyri object that are more degraded than the rest.
- An issue was detected regarding the repeatability of the DP prediction for spectral data of the same samples scanned with HSI in different times. Spectra were investigated where significant variations were spotted especially in the short wavelengths (less than 1900 nm). The position of samples over the HSI stage while scanning is one of the possible causes of the variations which was also investigated confirming its significant effect on the accuracy of the spectra which may lead to the uncertainty of the prediction of the DP values. Unfortunately, due to time constraint, the influence of the position and the other causes of the variations in the spectra will need to be explored in the future.

7. CONCLUSIONS

My PhD research dealt with the metrology of quantitative hyperspectral imaging in the SWIR region in relation to cellulose-based materials. It explores chemical properties of two historical materials: Islamic paper (starch sizing, polishing and distribution of acidity and cellulose degree of polymerization - DP) and painting canvas (pH and cellulose DP). Such information allowed for better understanding of the composition of the materials and their degradation processes, providing a measure of change in collections through imaging, which would reflect on the management and preservation plans of collections. The research also took another case study of cellulosic material: papyri to study the potential of using NIR HSI in the extraction of valuable information with the challenge of scanning the samples through their glass frames. Taking advantage of the new knowledge gained about the properties of Islamic paper and canvases in the research and putting into consideration that their durability is related to the materials and techniques used in the production, degradation study was carried out to understand the behaviour of the materials and its stability especially with the lack of enough information about the reference collections used in the research in terms of provenance, date and previous storage history.

7.1 Research Questions and Contribution to New Knowledge

This section answers the research questions raised in the introduction chapter reflecting the main conclusions achieved through the research and any contributions to new knowledge.

- **Can the spatial distribution of chemical properties (pH and cellulose DP) in cellulosic materials (Canvases and Islamic papers) be imaged?**

This was successfully achieved through generating for the first time quantitative chemical maps of Islamic paper and painting canvases for acidity and cellulose DP which could act as a tool to identify degradation variations across an object surface. This would improve our understanding of heritage surfaces as spatially resolved quantitative data could improve the interpretation and conservation of historic cellulose-based materials. To achieve that, new characterization models were developed and validated for calibration and prediction of the same properties of unknown samples using spectral data collected by the HSI system. New calibration targets from both materials based on well-characterized reference collections were also developed to be able to build such models. In order to put a level of confidence in the results obtained from the models, similar models were developed using same reference samples based on the spectral data collected with NIR spectroscopy where the calibration and prediction errors of the models from both techniques were compared, in addition to the comparison with the uncertainty of similar models from previous studies. The models from both techniques proved to be comparable based on the validation (RMSECV) and prediction (RMSEP) errors which suggesting its ability to be used in surveying collections especially for cellulose DP. The performance of

the pH models in general for both materials using both techniques are less satisfactory which an indication of the need for better reference samples. However, the model still can be used for classification of samples regarding their acidity.

Although the HSI calibration models are performing less satisfactory than the models using spectroscopic data in some cases, the HSI technique is still considered more advantageous due to its ability to produce chemical images visualizing the spatial distribution of chemical composition in non-homogeneous samples.

One issue was observed regarding the chemical maps, where some noise-like features can be observed, which needs further research to evaluate their causes in details. The cause of these noises could not be determined if it is originated from spectral noise or from the variations in material surface morphology, which could lead to minor differences in the spectra and the modelled values. However, the maps still could be of great use to conservators and researchers providing them with a tool that help them to take evidence-based conservation decisions for their collections or study the effect of some factors on the object in terms of handling or display such as exposure to a localized light source or how readers as an example handle a document in a library through investigating the deterioration locations on the object's surface.

Moreover, the experiments which were conducted to answer this question resulted in new contributions to the body of knowledge which are listed below;

- Development of a non-destructive characterization methodology of material properties of Islamic paper; Starch sizing, surface polishing, pH and cellulose degree of polymerization using NIR spectroscopy and HSI techniques with the aid of multivariate data analysis methods. This is achieved by conducting a scientific and systematic survey of a reference collection of Islamic paper samples from the 18th – 19th century where almost half of the samples were found to be starch-sized and more than 60% are polished. The current state of collection material was evaluated based on their pH and DP where ~36% have pH < 6 and more than half of the samples with DP < 1000, which indicates its suitability for handling. Polished samples are found to have better material state associated with high DP and pH values which highlights the need to study the effect of starch sizing and surface polishing on paper stability.
- Discovery of the inapplicability of calibration models developed for the characterization of European paper (SurveNIR project) on Islamic paper, highlighting the effect of starch in relation to that. However, an experiment showed that starch has no effect on cellulose degradation giving same degradation rate for samples (pure cotton) with and without starch.
- Validation of the developed methodology using NIR spectroscopy by surveying real historic Islamic collection in Wellcome Collection for better understanding of the

Islamic paper properties and getting an overview about its proportion among libraries collections and about the current state of the collection. As an example of the type of information what can be provided from the survey, 90% of the surveyed collection has the potential to be of Islamic origin based on estimated starch presence and polishing properties and most of the collection have a good condition and can be handled safely based on pH and DP estimated values.

- Development of a dating model to predict the date of Islamic paper sample from 1652 to 1880 AD using the spectral data of the surveyed samples from Wellcome collection, which shows the power and potential of the use of NIR spectral data with multivariate calibration techniques, especially when applied to reference samples with known provenance and date.
- Development of a new condition assessment tool for surveying painting canvas collections to predict non-destructively the pH and cellulose DP in canvases using HSI in the SWIR region (1000-2500 nm) and a well-characterized reference database of historic canvases which is performing similar to the results of similar models developed using NIR spectroscopy.
- **Do the measurement parameters (calibration, illuminant intensity and stability, material surface structure) affect the quantitative image data?**

The answer for this question was obtained through the development of new evaluation methodology not only based on the system performance but also taking into account its performance when it is applied to artworks. This was carried out by exploring the effect of different measurements conditions and acquisition parameters on the performance of the HSI system, focusing on the quality, stability and reproducibility of the collected data and highlighting the importance of the calibration process. Firstly, getting a deeper understanding of the capabilities and limitations of the instrumentation used by applying several tests, then studying the metrology of quantitative calibrations based on the spectral measurements collected by the HSI in the SWIR region using different acquisition parameters such as illumination intensity, lens and scanning background and different spectral treatment methods. Such information is of use to heritage scientists as it increases the reliability of the data in addition to better understanding the type of cultural heritage objects and the applications suitable for investigation using the current system, e.g. the need for acquiring fine details for the detection of underdrawings or characterizing materials where high spectral resolution is needed. The results showed that the used system is suitable for material characterization and mapping applications, but not for the detection of fine spatial details due to its low spatial resolution. Regarding the effect of the acquisition parameters, changing the illumination intensity did not show an effect on the quality of the spectra while the distribution of illumination on the scanning stage causes some variations on the spectra collected from different positions which may lead to

significant variations in any further quantitative analysis. This will need further research to verify such information. On the other hand, using lenses with different focal lengths showed a spectral change in the data, but this did not affect the performance of the quantitative calibrations. Moreover, changing some of the measurement conditions such as scanning background and the ROI size used to obtain average spectra in addition to the pre-treatments applied to the spectra during analysis were found to have no significant effect on the obtained calibrations as well. Of course, more measurement conditions and acquisition parameters would need to be assessed for better understanding of the system performance and to assure the robustness of the obtained data, such as the surface morphology of the objects and the influence of environmental conditions, e.g. heat and relative humidity on the quality of the spectral information.

- **Can further case studies be developed for other cellulosic materials such as papyri, contributing to their more successful conservation?**

Papyri was chosen as a case study in order to investigate the potential of using the HSI technique for such less explored material. Since most of the papyri collections are embedded in glass frames, so the first focus was to demonstrate the influence of imaging objects through glass using HSI system in the SWIR region on the accuracy of the spatial and spectral information in addition to the ability to extract chemical information that can be used for further analysis to enrich our scientific knowledge about papyri. Glass was found to have no influence on the accuracy of the collected spectra acting as a filter where the reflection correlates negatively with the thickness of the glass layer which can be compensated for through the calibration process. Moreover, no significant variations were found in the calibration errors when I tried to apply the developed PLS regression models for determination of DP of Islamic paper samples on papyri samples with and without glass. A successful extraction of useful information out of surveying papyri collection kept in glass frames from the UCL Petrie museum using the non-destructive imaging technique was made, e.g. detection of iron-gall ink in one of the surveyed samples from the 4th/5th century AD. Another trial also was conducted to show the potential of using regression modelling and HSI for the classification of the different degradation level or material state of objects based on their estimated pH and DP values through applying the Islamic paper regression model developed for the determination of cellulose DP on papyri samples that have different levels of degradation (naturally aged, naturally/artificially aged, new and new/artificially aged). The results of the trial showed the ability to correctly classify the samples using the predicted DP. However, the experimental trial opened a new research question about the influence of the position of the samples over the scanning stage while collecting the spectral data on the uncertainty / repeatability of the results. This will significantly contribute to Quantitative HSI imaging metrology.

- **What information of value to conservators, curators and scholars can be obtained using NIR hyperspectral imaging technique and accelerated degradation to study degradation behaviour of cellulosic materials?**

To achieve conclusion about this question, the degradation behaviour of Islamic paper and painting canvas was explored through a systematic degradation study of the materials at a combination of controlled environmental conditions (temperature and relative humidity) with the aid of both Ekenstam equation and the recently modelled dose-response function developed for European paper which proved their applicability to both materials. This information is very useful for simulating different scenarios of storage conditions and potential risks based on that for better evidence based preservation plans. Taking advantage of that, accompanied by the successful generation of pH and DP quantitative HSI chemical maps, data from both were used to generate lifetime maps to visualize the effect of the current state of an object (paper or canvas) on its lifetime under specific storage conditions. This showed the different spots with low expected lifetime, which would need more care from a conservation perspective. However, the results showed that although there is no correlation between pH and DP values, there is a reasonable equal one between lifetime and both properties which means that objects with higher DP and pH are expected to stay longer before it becomes unfit for handling. This highlights the need for further research to confirm such results.

7.2 Future Work

During the course of this PhD research, a number of topics on which further research would be valuable were highlighted. These include the following:

- Conducting further investigation on the reference collection of Islamic paper to study other characteristics of Islamic paper, e.g. fibre furnish of all the samples to verify the use of other fibres than bast and cotton in Islamic papermaking.
- Improving and further elaborating model analyses and development by investigating larger datasets with known provenance and date information representing the typical collections that can be found in heritage institutions.
- Investigating further the effect of starch on stability of cellulose degradation to verify the obtained results taking into consideration different starch sources and support samples, e.g. use of historic samples instead of pure cotton ones in addition to exploring the effect of polishing characteristic as well.
- Exploring the validity of the negative correlation between pH and DP estimated values obtained from the chemical maps of painting canvases.
- Studying and verifying the obtained information about the degradation behaviour of Islamic paper and canvas painting using modelled dose-response function of European paper. Future efforts can also focus on the development of dose-

response functions specifically modelled for both materials to assure the reliability of the results.

- Using the proposed imaging technique to survey more papyri collections with known provenance and date in a trial to deeply understand the development of the used materials in the production process of papyri. Moreover, it is worth trying to build calibration models using reference samples of historic papyri for the purpose of material characterization taking the glass layer into consideration.
- Investigating in depth the highlighted issue about the position of the sample on the scanning stage in relation to the variations in the illumination across the stage and how that could lead to significant variations in the calibration modelling results. Further research would also try to figure out a way to address that issue and compensate for it within the routinely calibration process.
- Exploring the possible causes of the problem of linear pattern appeared on the chemical maps which needs further investigation in addition to the development of methods to overcome the problem.

7.3 Dissemination

The results of the research project were disseminated to heritage and imaging scientists and researchers through poster and oral presentations at international conferences in addition to publications in peer-reviewed journals (Mahgoub et al. 2016; 2017).

I have published some results of this research in two peer-reviewed papers in Heritage Science and SPIE Optical Metrology journals, as well as six conferences.

Moreover, I am drafting three papers to disseminate the rest of the research results. The first paper is about the papyri study where I intend to publish it in the peer-reviewed journal, Angewandte Chemie. The second paper is about the results of the Islamic paper survey conducted on the Islamic collection of the Wellcome Collection. There is a potential to publish this paper as a chapter in a new book about the applications of near infrared spectroscopy but this still not confirmed. The last drafted one is about the quantitative imaging aspect from the two studies about Islamic paper and painting canvas but no plans yet about the publisher.

REFERENCES

1. AIC (1990). Paper conservation catalog. 7th edition. Washington, D.C.: *American Institute for Conservation of Historic and Artistic Works, Book and Paper Group*. Chapter 10: Spot tests. Retrieved from: http://cool.conservations.org/coolaic/sg/bpg/pcc/10_spot-tests.pdf.
2. Aikio, M. (2001). Hyperspectral Prism-Grating-Prism Imaging Spectrograph, *PhD thesis*, University of Oulu.
3. Akbari, H., Uto, K., Kosugi, Y., Kojima, K. and Tanaka, N. (2011). Cancer detection using infrared hyperspectral imaging, *Cancer science*, Vol.102, Issue 4, pp. 852-857, doi: 10.1111/j.1349-7006.2011.01849.x.
4. Al-Hassan, A. (2001). The different aspects of Islamic culture: science and technology in Islam, Part II: Technology and applied sciences, 4:155–8, *UNESCO*. Retrieved from: <https://unesdoc.unesco.org/ark:/48223/pf0000134503>.
5. Al-Sāmarrā'ī, Q. (2001). Arabic Islamic palaeography & codicology = 'Ilmal-iktināh al-'Arabī al-Islāmī', Riyadh: *King Faisal Centre for research and Islamic studies*.
6. ANONYMOUS (1997). Manual on the conservation of paintings, London: *Archetype*, reprint of the first edition in Paris 1940.
7. Antti, H., Sjöstrom, M. and Wallbacks, L. (1996). Multivariate calibration models using NIR spectroscopy on pulp and paper industrial applications, *Journal of Chemometrics*, Vol. 10, pp. 591-603.
8. ARNGREN, M. (2011). Hyperspectral NIR Camera, Technical note, version 1.2.
9. Arrhenius, S. (1889). Über die Reaktionsgeschwindigkeit bei der Inversion von Rohrzucker durch Säuren, *Z. Phys. Chem.*, 4, 226-248.
10. ASTM (2000). Standard practices for infrared multivariate quantitative analysis, Vol. E 1655-00, West Conshohocken PA: *ASTM International*.
11. Armstrong, P. R., Maghirang, E. B., Xie, F. and Dowell, F. E. (2006). Comparison of dispersive and Fourier-transform NIR instruments for measuring grain and flour attributes, *Appl. Eng. Agric.*, 22(3), 453-457, doi:10.13031/2013.20448.
12. ASTM-D778-97 (2002). Standard test methods for Hydrogen ion concentration (pH) of Paper extracts (Hot-extraction and Cold-extraction procedures), *ASTM International*, USA.
13. Au, C. and Thorn, I. (1995). Applications of wet-end paper chemistry, Glasgow: *Chapman & Hall*.

14. B&W TEK (2016). An Introduction to a Spectrometer: Spectral Resolution. Retrieved from: <https://www.azom.com/article.aspx?ArticleID=13369>.
15. B&W TEK (2019). Part 3b: The Detector. Retrieved from: <http://bwtek.com/spectrometer-part-3b-the-detector/>.
16. Baker, D. (1989). A note on the expression. A manuscript on oriental paper *Manuscripts of the Middle East*, Vol. 4, *Ter Lugt Press*, p. 67–8, Leiden, Netherlands.
17. Baker, D. (1991). Arab Papermaking, *The Paper Conservator*, Vol. 15, Issue 1, pp. 28-35.
18. Barker, M. and Rayens, W. (2003). Partial least squares for discrimination. *Journal of chemometrics*, 17, 166-173.
19. Barrow, W. J. (1974). Permanence/durability of the book-VII physical and chemical properties of book papers, Richmond: *W. J. Barrow Research Laboratory Inc*, p. 1507–949.
20. Bazar, G., Kovacs, Z., and Tsenkova, R. (2016). Evaluating Spectral Signals to Identify Spectral Error. *PloS one*, 11(1), e0146249. <https://doi.org/10.1371/journal.pone.0146249>
21. Beebe, K. R., Pell, R. J. and Seasholtz, M. B. (1998). *Chemometrics: A practical guide*. New York etc.: John Wiley & Sons.
22. Bhushan, B. (2001). *Modern tribology handbook*. Boca Raton: *CRC Press*. Chapter 2: Surface roughness analysis and measurement techniques.
23. Blanco, M. and Villarroya, I. (2002). NIR spectroscopy: a rapid-response analytical tool, *Trends in Analytical Chemistry*, Vol. 21, Issue 4, pp. 240-250.
24. Bloom, J. (2001). *Paper before print: the history and impact of paper in the Islamic world*. New Haven: *Yale University Press*.
25. Boersma, F., Brokerhof, A. W., Berg, S. V. D. and Tegelaers, J. (2007). *Unravelling textiles: A handbook for the preservation of textile collections*. London: *Archetype Publications Ltd*.
26. Boon, J. J., Hoogland, F. and Keune, K. (2007). *34th Annual meeting of the AIC of Historic & Artistic Works providence*, Rhode Island, 2006, postprints, Vol. 19, pp. 16–23.
27. Brereton, R. (2009). *Chemometrics for pattern recognition*, *John Wiley & son*, England.

28. Brereton, R. and Lloyd, G. (2014). Partial least squares discriminant analysis: taking the magic away, *Journal of chemometrics*, special issue – tutorial, 28(4), 213-225, doi: 10.1002/cem.2609,28;213-225.
29. Brown, N., Lichtblau, D., Fearn, T. and Strlič, M. (2017). Characterisation of 19th and 20th century Chinese paper. *Heritage Science*, 5, 47.
<https://doi.org/10.1186/s40494-017-0158-x>
30. BS-7463 (1991). Fibre furnish analysis of paper, board and pulps. London: *British Standardization Institute-BSI*.
31. BS-ISO-2470-1 (2009). Paper, board and pulps. Measurement of diffuse blue reflectance factor. Indoor daylight conditions (ISO brightness). London: *British Standardization Institute-BSI*.
32. BS-ISO-5351 (2010). Pulps - Determination of limiting viscosity number in cupriethylenediamine (CED) solution, *British Standardization Institute-BSI*, 2nd edition.
33. Bülow-Jacobsen, A. (2012). Writing materials in the Ancient world, *The Oxford Handbook of Papyrology*, doi: 10.1093/oxfordhb/9780199843695.013.0001.
34. Burger, J. and Geladi, P. (2005). Hyperspectral NIR image regression. Part I: Calibration and correction, *Journal of Chemometrics*, 19, 355–363, doi: 10.1002/cem.938.
35. Burger, J. and Geladi, P. (2006). Hyperspectral NIR image regression, part II: Dataset preprocessing diagnostics. *Journal of Chemometrics*, 20, 106-119, doi: 10.1002/cem.986.
36. Calvini, P. and Gorassini, A. (2006). On the rate of paper degradation: Lessons from the past. *Restaurator*, 27:275-290.
37. CCI (2002). Know your paintings - Structure, materials, and aspects of deterioration, CCI Notes 10/17. In *CCI Notes. Canadian Heritage*, Vol. 10/17, pp. 1-4.
38. CCI (2008). Textiles and the environment. CCI Notes 13/1. In *CCI Notes. Canadian Heritage*, Vol. 13/1, pp. 1-6.
39. Chang, C. (2007). Hyperspectral data exploitation: Theory and applications, chapter 1 and 2, *John Wiley & Sons*, doi: 10.1002/0470124628.
40. Cosentino, A. (2014). Identification of pigments by multispectral imaging; a flowchart method, *Heritage Science*, 2:8, doi:10.1186/2050-7445-2-8.

41. Cséfalvayová, L., Strlič, M. and Karjalainen, H. (2011). Quantitative NIR chemical imaging in heritage science, *Analytical Chemistry*, 83(13): 5101–6.
42. Cucci, C. (2014). Presentation: Introduction to 2D hyperspectral imaging devices and data acquisition, COSCH; *Color and Space in Cultural Heritage training school: Hyperspectral Imaging-Techniques applied to the investigation of 2D polychrome surfaces*, Florence, Italy.
43. Cucci, C., Casini, A., Picollo, M., Poggesi, M. and Stefani, L. (2011). Open Issues in hyperspectral imaging for diagnostics on paintings: when high-spectral and spatial resolution turns into data redundancy, Proceedings of SPIE 8084, O3A: Optics for Arts, Architecture, and Archaeology III, 808408. *SPIE Optical Metrology*, Munich, Germany. Retrieved from: <https://doi.org/10.1117/12.889460>.
44. Cucci, C., Webb, K., Casini, A., Ginanni, M., Prandi, E., Stefani, L., Vitorino, T. and Picollo, M. (2019). Short-wave infrared reflectance hyperspectral imaging for painting investigations: A methodological study, *Journal of the American Institute for Conservation*, 58:1-2, 16-36, doi:10.1080/01971360.2018.1543102.
45. Delaney, J.K., Walmsley, E., Berrie, B.H., and Fletcher, C.F. (2003). Multispectral imaging of paintings in the infrared to detect and map blue pigments, in Sackler NAS Colloquium, *Scientific Examination of Art: Modern Techniques in Conservation and Analysis*, Washington, 2003, Proceedings of the National Academy of Sciences, National Academies Press, Washington, D.C., PP. 120–136.
46. Déroche, F. (2005). Islamic codicology - an introduction to the study of manuscripts in Arabic script. London: *Al-Furqan Islamic Heritage Foundation*.
47. Derrick, M. R., Stulik, D., Landry, J. M. (1999). Infrared spectroscopy in conservation science, scientific tools for conservation, *the Getty Conservation Institute*, Los Angeles.
48. Dillon, C., Lindsay, W., Taylor, J., Fouseki, K., Bell, N. and Strlič, M. (2013). Collections Demography: Stakeholders' Views on the Lifetime of Collections, in: J. Ashley-Smith, A. Burmester & M. Eibl, eds. *Climate for Collections Conference*, Munich, Doerner Institut, 7–9 November 2012, Postprints. London: Archetype, pp. 45–58.
49. Dominguez Rubio, F. (2014). Preserving the unpreservable: docile and unruly objects at MoMA, UC San Diego. Retrieved from: <https://escholarship.org/uc/item/9qr4d9qx>.
50. Dooley, K., Lomax, S., Zeibel, J., Miliani, C., Ricciardi, P., Hoenigswald, A., Loewb, M. and Delaney, J. (2013). Mapping of egg yolk and animal skin glue

- paint binders in early renaissance paintings using near infrared reflectance imaging spectroscopy, *Analyst*, 138(17): 4838–48, doi:10.1039/c3an00926b.
51. Dupont, A. L. (2003). Gelatine sizing of paper and its impact on the degradation of cellulose during aging: aging: a study using size-exclusion chromatography. Amsterdam: University of Amsterdam.
 52. Ekenstam, A. (1936). Über das Verhalten der Cellulose in Mineralsäurelösungen, II. Mitteil: Kinetisches Studium des abbaus der Cellulose in Säurelösungen, *Berichte der deutschen chemischen Gesellschaft (A and B series)*, 69(3), pp. 553–559.
 53. Elmasry, G. and Sun, D. (2010). Principles of hyperspectral imaging technology. In *Hyperspectral imaging for food quality analysis and control*, 3–44, Burlington, MA: Elsevier.
 54. Elnaggar, A., Fitzsimons, P., Nevin, A., Watkins, K. and Strlič, M. (2015). Viability of laser cleaning of papyrus: Conservation and scientific assessment, *Studies in Conservation*, 60: S73-S81, doi:10.1179/0039363015Z.000000000211.
 55. EIGENVECTOR (2019). PLS Toolbox, Advanced Chemometrics Software for use with MATLAB. Eigenvector Research Incorporated, <https://eigenvector.com>.
 56. Erhardt, D. and Mecklenburg, M. (1995). Accelerated vs. natural aging: Effect of aging conditions on the aging process of cellulose. In Druzik, J. R., Galván van Madrid, J. L., Freestone, I.C. and Wheeler, G. S. (editors), Materials issues in art and archaeology IV: symposium, 16th -21st May, Mexico, *Materials Research Society (MRS) proceedings*, 352, pp247-270, doi:10.1557/PROC-352-247.
 57. Evans, R. and Wallis, A.F.A. (1987). Comparison of Cellulose molecular weights determined by high performance size exclusion chromatography and viscometry, *Fourth International symposium on Wood and Pulping Chemistry*, Vol. 1, pp. 201-205, Paris.
 58. Fearn, T. (2001). Standardisation and calibration transfer for Near Infrared instruments: A review. *Journal of Near Infrared Spectroscopy*, Vol. 9, Issue 4, PP. 229–244.
 59. Fearn, T. (2005). Chemometrics: an enabling tool for NIR. In *NIR News, International Council for Near Infrared Spectroscopy*, Vol. 16, pp. 17-19.
 60. Fenech, A., Strlič, M. and Cassar, M. (2012). The past and the future of chromogenic colour photographs: lifetime modelling using near-infrared spectroscopy & enhancement using hypoxia. *Applied Physics A*, 106, 411–417 (2012). <https://doi.org/10.1007/s00339-011-6688-2>

61. Fischer, C. and Kakoulli, I. (2006). Multispectral and hyperspectral imaging technologies in conservation: Current research and potential applications. *Reviews in Conservation*, 7: 3–16.
62. Flinn, P. (2005). An average day (or how near infrared affects daily life). In *NIR News, International Council for Near Infrared Spectroscopy*, Vol. 16, pp. 4-8.
63. Françoise, F. and Delange, E. (2001). Papyrus: The need for analysis. *Restaurator*, 22 (2):84-106.
64. Frösén, J. (2012). Conservation of ancient Papyrus materials, *The Oxford Handbook of Papyrology*, doi: 10.1093/oxfordhb/9780199843695.013.0004.
65. Gál, L., Čeppan, M., Reháková, M., Dvonka, V., Tarajčáková, J. and Hanus, J. (2013). Chemometric tool for identification of iron–gall inks by use of visible–near infrared fibre optic reflection spectroscopy, *Analytical and Bioanalytical Chemistry*, 405(28):9085–9091, Springer-Verlag Berlin Heidelberg, doi:10.1007/s00216-013-7333-z.
66. Garlick, K. (1986). A brief review of the history of sizing and resizing practices. The book and paper group-annual meeting, Vol.5. *The American Institute for Conservation of Art and Historic Artifacts*. Retrieved from: <http://cool.conservation-us.org/coolaic/sg/bpg/annual/v05/bp05-11.html>.
67. Garside, P. and Wyeth, P. (2006). Textiles. In May, E. and Jones, M. (eds.), *Conservation science: Heritage materials*, Cambridge: RSC Pub., pp.56-91.
68. Garside, P., Howard, S., Loubser, K. and Wyeth, P. (2011). On-site categorisation and condition assessment of silks in textile collections, Portugal: *ICOM-CC 16th triennial conference preprints*, 1–10.
69. Garthwaite, P.H. (1994). An interpretation of partial least squares, theory and methods, *Journal of the American Statistical Association*, Vol. 89, Issue 425, pp. 122-127.
70. Gibson, A., Piquette, K. E., Bergmann, U., Christens-Barry, W., Davis, G., Endrizzi, M., Fan, S., Farsiu, S., Fitzgerald, A., Griffiths, J., Jones, C., Li, G., Manning, P. L., Jones, C. M., Mazza, R., Mills, D., Modregger, P., Munro, P. R.T., Olivo, A., Stevenson, A., Venugopal, B., Wallace, V., Wogelius, R. A., Toth, M. B. and Terras, M. (2018). An assessment of multimodal imaging of subsurface text in mummy cartonnage using surrogate papyrus phantoms, *Heritage Science*, 6:7, doi:10.1186/s40494-018-0175-4.
71. Gorassini, A., Calvini, P., Baldin, A. (2008). Fourier transform infrared spectroscopy (FTIR) analysis of historic paper documents as a preliminary step

- for chemometrical analysis, Italy: *CMA4CH 2nd Mediterranean meeting on multivariate analysis and chemometry for cultural heritage and environment*, 2:47–8.
72. Gower, J., Lubbe, S. and Le Roux, N. (2011). *Understanding Biplots*. John Wiley & Sons.
73. Grasselli, J. G. (1983). The analytical approach: Papyrus; The paper of Ancient Egypt, *analytical chemistry, American chemical society*, vol. 55, no. 12, pp. 1220A, Washington DC.
74. Hackney, S. and Hedley, G. (1993). Linen canvas artificially aged. In Villers, C. (ed.), *Measured opinions. Collected papers on the conservation of paintings*. Gerry Hedley. London: *UKIC*, pp.70-75, (Initially published in 1984).
75. Havermans, J., Abdul Aziz, H. and Scholten, H. (2003). Non-destructive detection of Iron gall inks by means of multispectral imaging, Part 2: Application on original objects affected with iron-gall-ink corrosion, *Restaurator* 24, pp88–94, doi:10.1515/REST.2003.55.
76. Helman-Ważny, A. and Van-Schaik, S. (2012). Witnesses for Tibetan craftsmanship: bringing together paper analysis, palaeography and codicology in the examination of the earliest Tibetan manuscripts, *Archaeometry*, 55(4):707–41.
77. Hubbe, M. (2004). Acidic and alkaline sizings for printing, writing, and drawing papers, *The Book and Paper Group Annual*, 23:139–51.
78. Hubbe, M. A., Smith, R. D., Zou, X., Katuscak, S., Potthast, A. and Ahn, K. (2017). Deacidification of acidic books and paper by means of non-aqueous dispersions of alkaline particles: A review focusing on completeness of the reaction, *BioResources*, 12(2), 4410 – 4477.
79. Hunter, D. (1947). *Papermaking: the history and technique of an ancient craft*. New York: *Dover Publications*.
80. Ibn Bādīs, M. (Ca. 1025). The staff of the scribes and implement of the discerning with a description of the line, the pens, soot inks, Līq, gall inks, dyeing, and details of bookbinding = 'Umdat Al-kuttab Wa'uddat Dhawi Alalbab'. Iran: *Islamic Research Center*.
81. Ilvessalo-Pfäffli, M. (1995). *Fibre atlas: identification of papermaking fibres*, Germany: *Springer-Verlag*.
82. IRUG (2000). *Infrared and Raman Users Group, IRUG spectral database*. Retrieved from: <http://www.irug.org/>.

83. Isenberg, I. (1967). Pulp and paper microscopy, 3rd edition, Appleton: *Institute of Paper Chemistry*.
84. Karabacek, J. (2001). Arab Paper, translated by Baker, D. and Dittmar, S., London: *Don Baker Memorial Fund and Archetype Publications*.
85. Kolar, J., Strlič, M. and Havermans, J. B. G. A. (2004). Proceedings of the International Conference Durability of Paper and Writing, 16th – 19th November, *National and University Library*, Ljubljana, Slovenia.
86. Kolomiets, O. and Siesler, H. W. (2004). The influence of spectral resolution on the quantitative near-infrared spectroscopic determination of an active ingredient in a solid drug formulation, *Journal of Near Infrared Spectroscopy*, 12(1), 271-277, doi: [10.1255/jnirs.435](https://doi.org/10.1255/jnirs.435).
87. Kubik, M. (2007). Hyperspectral imaging: A new technique for the non-invasive study of artworks. In *Physical techniques in the study of art, archaeology and cultural heritage*, vol. 2, chapter 5, 199–259, doi: 10.1016/S1871-1731(07)80007-8.
88. Kumar, S. (2005). Optical and microwave remote sensing, chapter 3, *Basics of remote sensing and GIS*, University Science Press.
89. Lawrence, K., Park, B., Windham, W. and Mao, C. (2003). Calibration of a pushbroom hyperspectral imaging system for agricultural inspection. *Transactions of the American Society of Agricultural Engineers*, 46(2): 513–21.
90. Leach, B. and Tait, J. (2000). Papyrus. In: P.T. Nicholson, & I. Shaw, eds. *Ancient Egyptian Materials and Technology*. Cambridge: Cambridge University Press, pp. 227–53.
91. Lee, L. C., Liong, C. and Jemain, A., (2018). Partial least squares-discriminant analysis (PLS-DA) for classification of high-dimensional (HD) data: a review of contemporary practice strategies and knowledge gaps, *Analyst, Critical review*, Royal society of chemistry, 143, 3526–3539, doi: 10.1039/c8an00599k.
92. Leising, C. (2010). Paper surface roughness with 3D profilometry. Irvine, USA. Retrieved from: <http://nanovea.com/wp-content/themes/wp-nanovea/Application%20Notes/paperroughness.pdf>.
93. Levey, M. (1962). Mediaeval Arabic bookmaking and its relation to early chemistry and pharmacology, *Transactions of the American philosophical society*, 52(4):1–79.
94. Lewin, M. (2007). Handbook of fibre chemistry, 3rd edition, *CRC Press*, Taylor & Francis.

95. Liang, H. (2012). Advances in multispectral and hyperspectral imaging for archaeology and art conservation, *Applied Physics A: Materials science & processing*, 106(2): 309–23, doi 10.1007/s00339-011-6689-1.
96. Loveday, H. (2001). Islamic Paper: A Study of the Ancient Craft, *Don Baker Memorial Fund*, London.
97. Lu, R. and Chen, Y. (1999). Hyperspectral imaging for safety inspection of food and agricultural products. *Proceedings of the SPIE, Pathogen Detection and Remediation for Safe Eating*, 3544: 121–33, doi:10.1117/12.335771.
98. Lucas, A. (1922). The inks of Ancient and modern Egypt, *Analyst*, 47, 9-15, doi:10.1039/AN9224700009.
99. Lucas, A. and Harris, J. R. (1962). Ancient Egyptian materials and industries, Chapter XIV, London.
100. Macdonald, L. (2010). The limits of resolution. *Proceeding of EVA'10 international conference on electronic visualization and the arts*, pp. 149-156, British computer society - BCS learning & development Ltd., UK.
101. MacDonald, L., Vitorino, T., Picollo, M., Pillay, R., Obarzanowski, M., Sobczyk, J., Nascimento, S. and Linhares, J. (2017). Assessment of multispectral and hyperspectral imaging systems for digitisation of a Russian icon, *Heritage Science*, 5:41, doi:10.1186/s40494-017-0154-1.
102. Mahgoub, H., Bardon, T., Lichtblau, D., Fearn, T. and Strlič, M. (2016). Material properties of Islamic paper, *Heritage Science*, 4:34, doi: 10.1186/s40494-016-0103-4.
103. Mahgoub, H., Lichtblau, D. and Strlič, M. (2016). Scientific characterization of Islamic paper, *Icon Conference 2016*, 15th -17th June, Brimingham, UK.
104. Mahgoub, H., Signorello, S., Gilchrist, J. R. and Strlič, M. (2016). Islamic paper detective: survey of the wellcome library collection, *SEAHA 2nd International Conference on Science and Engineering in Arts, Heritage, and Archaeology*, 20th – 21st June, Oxford, UK.
105. Mahgoub, H., Gilchrist, J. R., Fearn, T. and Strlič, M. (2017). Analytical robustness of quantitative NIR chemical imaging of historic cellulosic materials characterization. *SEAHA 3rd International Conference on Science and Engineering in Arts, Heritage, and Archaeology*, 19th – 20th June, Brighton, UK.
106. Mahgoub, H., Gilchrist, J. R., Fearn, T. and Strlič, M. (2017). Analytical robustness of quantitative NIR chemical imaging for Islamic paper characterization. In *O3A: Optics for Arts, Architecture, and Archaeology VI - SPIE*

Optical Metrology, Proceedings. of SPIE, Vol. 10331, doi:10.1117/12.2271971.
Retrieved from: <http://proceedings.spiedigitallibrary.org/>.

107. Mahgoub, H., Chen, H., Gilchrist, J. R., Fearn, T. and Strlič, M. (2017). Quantitative chemical hyperspectral NIR imaging of Islamic paper, In ICOM-CC 18th Triennial Conference Preprints, 4th – 8th September, Copenhagen, ed. J. Bridgland, art. 1606. Paris: International Council of Museums. Retrieved from: <http://discovery.ucl.ac.uk/10041889/1/Mahgoub%20ICOM.pdf>.
108. Manley, M. (2014). Near-infrared spectroscopy and hyperspectral imaging: Non-destructive analysis of biological materials, *Chemical Society Reviews*, 43: 8200–214, doi: 10.1039/c4cs00062e.
109. Martins, A., Daffner, L.A., Fenech, A., McGlinchey, Ch. and Strlič, M. (2012). Non-destructive dating of fiber-based gelatin silver prints using near-infrared spectroscopy and multivariate analysis. *Analytical and Bioanalytical Chemistry*, volume 402, 1459–1469. <https://doi.org/10.1007/s00216-011-5566-2>
110. May, E. and Jones, M. (2006). *Conservation Science: Heritage Materials*, Chapter 3, Royal Society of Chemistry -RSC Publishing, Cambridge.
111. Menart, E., De Bruin, G. and Strlič, M. (2011). Dose-response functions for historic paper. *Polymer degradation and stability*, 96, 2029–2039, doi:10.1016/j.polymdegradstab.2011.09.002.
112. Menart, E., De Bruin, G. and Strlič, M. (2014). Effects of NO₂ and acetic acid on the stability of historic paper, *Cellulose*, 21:3701–13.
113. Mettler Toledo (2013). *A guide to pH measurement – the theory and practice of pH applications*, Mettler-Toledo AG, Switzerland. Retrieved from: www.mt.com/pro/.
114. Miller, J. N. and Miller, J. C. (2010). *Statistics and chemometrics for analytical chemistry*, 6th edition, Upper Saddle River: Prentice Hall/Pearson.
115. Mills, J. S. and White, R. (1987). *The organic chemistry of museum objects*. London: Butterworth-Heinemann.
116. Min, M., Lee, W. S., Burks, T. F., Jordan, J. D., Schumann, A. W., Schueller, J. K. and Xie, H. (2008). Design of a hyperspectral nitrogen sensing system for orange leaves, *Comput. Electron. Agric.*, 63(2), 215-226, doi: 10.1016/j.compag.2008.03.004.
117. Mitchell, C. A. and Hepworth, T. C., (1937). *Inks: their composition and manufacture*, London.

118. Moncrieff, A. and Weaver, G. (1992). *Science for conservators. An introduction to materials*. Vol.1. London: Routledge.
119. Montague, A. P. (1890). Writing Materials and Books among the Ancient Romans, *American Anthropologist*, Vol.3, No.4, pp.331-340.
120. Možir, A., Strlič, M., Trafela, T., Cigić, I. K., Kolar, J., Deselnicu, V. and De Bruin, G. (2011). On oxidative degradation of parchment and its non-destructive characterisation and dating. In *Applied Physics A: Materials Science & Processing*, Springer, Vol. 104, pp. 211-217.
121. Možir, A., Strlič, M., De Bruin, G., Trafela, T., Kralj Cigić, I., Kolar, J. and Deselnicu, V. (2011). Non-destructive characterisation and dating of historic parchment using Near Infrared spectroscopy, *International Conference on non-destructive investigations and microanalysis for the diagnostics and conservation of cultural and environmental heritage (ART 2011)*, Florence, Italy.
122. Næs, T., Isaksson, T., Fearn, T. and Davies, T. (2002). A user-friendly guide to multivariate calibration and classification, Chichester, UK: *NIR Publications*.
123. Neevel, J. G. (2006). The development of in-situ methods for identification of Iron–gall inks, In Kolar, J. and Strlič M. (editors) *Iron–gall inks: on manufacture, characterization, degradation and stabilization*, Ljubljana: National and University Library, pp 147–172.
124. Norton, P. (2003). Detector focal plane array technology, in *Encyclopedia of Optical Engineering*, ed. R. G. Driggers, Marcel Dekker, New York, 320–348.
125. Nouri, D., Lucas, Y. and Treuillet, S. (2013). Calibration and test of a hyperspectral imaging prototype for intra-operative surgical assistance, *Proceedings of SPIE 8676, Medical Imaging: Digital Pathology*, Florida, United States. pp. 86760P, doi:10/1117/12.2006620. hal-00837756.
126. Oriola, M. (2011). Thesis: Non-destructive condition assessment of painting canvases using NIR spectrometry, Barcelona, Spain. Retrieved from: https://www.tesisenred.net/bitstream/handle/10803/663091/MOF_PhD_THESIS.pdf?sequence=1&isAllowed=y.
127. Oriola, M., Strlič, M., Cséfalvayová, L., Možir, A., Odlyha, M. and Campo, G. (2011). Non-destructive condition assessment of painting canvases using near infrared spectroscopy, in *Proceedings of ICOM-CC 16th Triennial Conference*, Lisbon. Retrieved from: <https://www.icom-cc-publications-online.org/publicationDetail.aspx?cid=83b25db8-8983-4dac-af92-6c03e964bf50>

128. Oriola, M., Možir, A., Garside, P., Campo, G., Nualart-Torroja, A., Civil, I., Odlyha, M., Cassar, M. and Strlič, M. (2014). Looking beneath Dalí's paint: Non-destructive canvas analysis, *Analytical Methods*, 6: 86–96, doi:10.1039/c3ay41094c.
129. Padgett, R. and Kotre, C. J. (2004). Assessment of the effects of pixel loss on image quality in direct digital radiography, *Physics in Medicine & Biology*, 49, 977–986, Institute of Physics publishing, doi: 10.1088/0031-9155/49/6/008.
130. Paltakari, J. T. and Karlsson, M. A. (1996). Determination of specific heat for dry fibre material, in 82nd Annual Meeting, CPPA, Technical Section, pp. B117–B120.
131. Papyrus project, www.science4heritage.org/papyrus/.
132. PAS 198 (2012). Specification for managing environmental conditions for cultural collections, *British Standards Institution – BSI*.
133. Pearsall, J.(ed.) (1998). *The new Oxford dictionary of English*. Oxford: Oxford University Press.
134. Pedersen, J. (1984). *The Arabic book*. French G., translator. Hillenbrand R., editor. New Jersey: *Princeton University Press*.
135. PHOTOMETRICS (2010). Keep the noise down! Low noise: An integral part of high-performance CCD (HCCD) camera systems, Technical note. Retrieved from: <https://www.photometrics.com/resources/technotes/pdfs/snr.pdf>.
136. Picollo, M. (2014). Hyperspectral imaging techniques applied to the investigation of 2D polychrome surfaces: Introduction to 2D spectral imaging & artists' materials and their Vis-NIR spectral features. *PowerPoint presentation at COSCH Training School*, 12th -14th December, Florence, Italy.
137. Picollo, M. (2014). Limits and advantages of different 2D VIS-NIR spectral imaging systems in answering conservators questions. *PowerPoint presentation at 4th WG Meeting and Workshop (COSCH)*, September 15th - 17th, Belgrade, Serbia.
138. Polder, G. and Van Der Heijden, G. W., (2001). Calibration and characterization of spectral imaging systems, *Proceedings of SPIE 4548, Multispectral and Hyperspectral Image Acquisition and Processing, Multispectral Image Processing and Pattern Recognition*, pp.10-17, China, doi:10.1117/12.441362.
139. Porck, H. J. (2000). Rate of paper degradation. The predictive value of artificial aging tests. Amsterdam: *European Commission on Preservation and Access*.

140. Qin, J. (2010). Chapter 5: Hyperspectral imaging instruments. In *Hyperspectral Imaging for Food Quality Analysis and Control* (Ed. Da-Wen Sun), 127-172., San Diego, CA: Academic Press, Elsevier.
141. Quye, A. and Strlič, M. (2019). Ethical Sampling Guidance, Icon Heritage Science Group, ICON-The Institute of Conservation.
142. Rasti, B., Scheunders, P., Ghamisi, P., Licciardi, G. and Chanussot, J. (2018). Noise reduction in hyperspectral imagery: Overview and application, *Remote Sensing*, 3, 482; doi:10.3390/rs10030482.
143. Richardson, E. and Garside, P. (2009). The use of near infrared spectroscopy as a diagnostic tool for Historic silk artefacts, In *e-Preservation Science*, Morana RTD, Vol. 6, pp. 68-74.
144. Rizzo, A. and Burnstock, A. (2003). A review of the effectiveness and effects of de-acidification of linen, cotton and flax canvas after 17 years of natural ageing. In Bustin, M. and Caley, T. (eds.), *Alternatives to lining. The structural treatment of paintings on canvas without lining*, London: UKIC, pp.49-54.
145. Rogalski, A. (2004). Optical detectors for focal plane arrays, *Opto-Electronics Review*, 12(2), 221–245.
146. Rogalski, A. and Chrzanowski, K. (2002). Infrared devices and techniques', *Opto-Electronics Review*, 10(2), 111–136.
147. Rogass, C., Mielke, C., Scheffler, D., Boesche, N. K., Lausch, A., Lubitz, C., Brell, M., Spengler, D., Eisele, A., Karl Segl, A., and Guanter, L. (2014). Reduction of uncorrelated striping noise - Applications for hyperspectral pushbroom acquisitions, *Remote Sensing*, 6, 11082-11106, doi:10.3390/rs61111082.
148. Ruiz-Perez, D. and Narasimhan, G. (2017). So you think you can PLS-DA?, doi: <http://dx.doi.org/10.1101/207225>.
149. Savitzky, A. and Golay, M. J. E. (1964). Smoothing and differentiation of data by simplified least squares procedures, *Analytical Chemistry*, 36(8), pp. 1627–1639, doi: 10.1021/ac60214a047.
150. Sebera, D. K. (1994). Isoperms. An environmental management tool. Retrieved from: <https://cool.conservation-us.org/byauth/sebera/isoperm>.
151. Sizov, F. F. (2000). Infrared detectors: outlook and means, *Semiconductors Physics, Quantum Electronics & Optoelectronics*, 3(1), 52–58.
152. Small, G.W. (2006). Chemometrics and Near-Infrared spectroscopy: Avoiding the pitfalls, *Trends in analytical chemistry*, Vol. 25, Issue 11, pp. 1057-1066.

153. Specim (2008). ImSpector Imaging Spectrograph User Manual. Oulu, Finland: *Spectral Imaging Ltd.*, pp. 23-25.
154. Strlič, M. and Kolar, J. (2005). Ageing and stabilization of paper, Ljubljana, Slovenia: *National and University Library*.
155. Strlič, M. and Kolar, J. (2005). Degradation and stabilisation of cellulosic materials. In Janaway, R. and Wyeth, P. (eds.), *Scientific analysis of ancient and historic textiles: informing preservation, display and interpretation: postprints*, London: *Archetype Publications Ltd.*, pp.33-37.
156. Strlič, M., Kolar, J., Kočar, D., Drnovšek, T., Šelih, V.-S., Susič, R. and Pihlar B. (2004). What is the pH of Alkaline Paper?, *e-Preservation Science*, Issue 1, pp. 35-47, MORANA RTD. Retrieved from: <<http://www.morana-rtd.com/e-preservation-science/2004/Strlic-03-06-2004.pdf>>.
157. Strlič, M., Kolar, J. and Lichtblau, D. (2007). The SurveNIR project- A dedicated near Infrared instrument for paper characterization, *Museum Microclimates*, Edited by T. Padfield and K. Borchersen, National Museum of Denmark, pp. 81-84, Denmark.
158. Strlič, M., Cséfalvayová, L., Kolar, J., Menart, E., Kosek, J., Barry, C., Higgitt, C. and Cassar M. (2010). Non-destructive characterisation of iron gall ink drawings: Not such a galling problem, *Talanta*, 81, 412–417, Elsevier B.V., doi:10.1016/j.talanta.2009.12.017.
159. Strlič, M., Thickett, D., Taylor, J. and Cassar, M. (2013). Damage functions in heritage science, *Studies in Conservation*, 58, 80-87, doi:10.1179/2047058412Y.0000000073.
160. Strlič, M., Grossi-Sampedro, C., Dillon, C., Bell, N., Fouseki, K., Brimblecombe, P., Menart, E., Ntanos, K., Lindsay, W., Thickett, D., France, F. and De Bruin, G. (2015). Damage function for historic paper, Part I: fitness for use, *Heritage Science*, Springer International Publishing, 3:33.
161. Strlič, M., Grossi, C. M., Dillon, C., Bell, N., Fouseki, K., Brimblecombe, P., Menart, E., Ntanos, K., Lindsay, W., Thickett, D., France, F. and De Bruin, G. (2015). Damage Function for Historic Paper, Part II: Wear and tear. *Heritage Science*, Springer International Publishing, 3:36.
162. Strlič, M., Grossi, C. M., Dillon, C., Bell, N., Fouseki, K., Brimblecombe, P., Menart, E., Ntanos, K., Lindsay, W., Thickett, D., France, F. and De Bruin, G. (2015). Damage function for historic paper, Part III: isochrones and demography of collections, *Heritage Science*, Springer International Publishing, 3(40), PP. 1-12, doi:10.1186/s40494-015-0069-7.

163. Stuart, B. (2007). Analytical techniques in materials conservation, Chapter 4. Molecular spectroscopy. Chichester: *John Wiley & Sons*.
164. Sun, Y., Huang, T., Ma, T. and Chen, Y. (2019). Remote sensing image stripe detecting and destriping using the joint sparsity constraint with Iterative Support Detection, *Remote Sensing*, 11(6), 608. Retrieved from: <https://doi.org/10.3390/rs11060608>.
165. SurveNIR project, Available at : www.science4heritage.org/survenir/.
166. SVI (n.d.). Sampling and sampling density and The Nyquist rate, Scientific Volume Imaging. Retrieved from <https://svi.nl/SamplingRate> and <https://svi.nl/NyquistRate>.
167. TAPPI-452-om (1998). Brightness of pulp, paper and paperboard (Directional Reflectance at 457 nm).
168. Tímár-Balázsy, Á. and Eastop, D. (1998). Chemical principles of textile conservation. Oxford: *Butterworth-Heinemann*.
169. Trafela, T., Strlič, M., Kolar, J., Lichtblau, D., Anders, M., Pucko-Mencigar, D. and Pihlar, B. (2007). Non-destructive analysis and dating of historical paper based on IR spectroscopy and chemometric data evaluation, *Analytical Chemistry*, 79(16): 6319–23, doi: 10.1021/ac070392.
170. Tsai, F. and Chen, W. W. (2008). Striping noise detection and correction of remote sensing images, *IEEE Transactions on geoscience and remote sensing*, Vol. 46, No. 12.
171. Tse, S. (2007). Guidelines for pH Measurement in Conservation. Technical Bulletin, No. 28, *Canadian Conservation Institute-CSI*.
172. Vidal, M. and Amigo, J. M. (2012). Pre-processing of hyperspectral images. Essential steps before image analysis. *Chemometrics and Intelligent Laboratory Systems*, 117, 138-148. Doi: 10.1016/j.chemolab.2012.05.009.
173. Villers, C. (1981). Artist's canvases: A history. In *ICOM-CC (ed.), ICOM- CC 6th Triennial Meeting: Ottawa, 21st -25th September*. Paris; France: ICOM, pp.81/2/1-1-81/2/1-12.
174. Vitorino, T. (2014). Analysis of the round robin test data acquired at IFAC-CNR [STSM report online]. *Colour & Space in Cultural Heritage (COSCH)*. Ref: COST-STSM-ECOST-STSM TD1201-310814-048809. Retrieved from: <http://cosch.info/exchange-visits>.

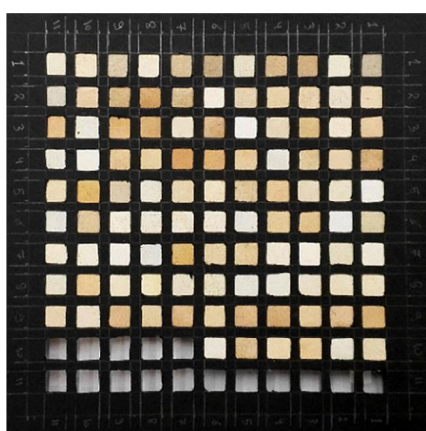
175. Wang, W. and Paliwal, J. (2007). Near-infrared spectroscopy and imaging in food quality and safety, *Sensing and Instrumentation for Food Quality and Safety*, 1(4): 193–207, doi: 10.1007/s11694-007-9022-0.
176. Wang, W., Li, C., Tollner, E., Rains, G. and Gitaitis, R. (2012). A liquid crystal tunable filter based shortwave infrared spectral imaging system: Calibration and characterization, *Computers and Electronics in Agriculture*, Vol. 80, 135-144.
177. Wang, Y., Huang, T., Liu, J., Lin, Z., Li, S., Wang, R. and Ge, Y. (2015). Soil pH value, organic matter, and macronutrients contents prediction using optical diffuse reflectance spectroscopy, *Comput. Electron. Agric.*, 111, 69-77, doi:10.1016/j.compag.2014.11.019.
178. Webb, K. (2015). Elaboration of hyperspectral image data from round robin test acquisition, *COSCH STSM Report, Short Term Scientific Mission, COST TD1201, COST-STSM-TD1201-25225*.
179. Westerhuis, J. A., Hoefsloot, H. C. J., Smit, S., Vis, D. J., Smilde, A. K., van Velzen, E. J. J., van Duijnhoven, J. P. M. and van Dorsten, F. A. (2008). Assessment of PLSDA cross validation, *Metabolomics*, 4:81–89, Springer, doi:10.1007/s11306-007-0099-6.
180. Wiesmüller, B. (2008-2012). The watermarks from the Refaiya library, *Trans. from the German by Steven Black*. Retrieved from: http://www.refaiya.uni-leipzig.de/texts/Watermarks_Refaiya.pdf.
181. Williams, P. (2013). The bounty of precision. *NIR news*, 24: 3. doi:10.1255/nirn.1360.
182. Workman, J., Schumann, B., Eilert, A., Persson, J. and Gajewski, R. (2014). *Near-Infrared spectrometers: a guide to evaluating instrument calibration and performance*, Unity scientific.
183. Xie, L. J., Wang, A. C., Xu, H. R., Fu, X. P. and Ying, Y. B. (2016). Applications of near-infrared systems for quality evaluation of fruits: a review, *Transactions of the ASABE, American Society of Agricultural and Biological Engineers*, Vol. 59(2): 399-419, doi:10.13031/trans.59.10655.
184. Yao, H. and Lewis, D. (2010). Spectral pre-processing and calibration techniques. In *Hyperspectral imaging for food quality analysis and control*, chapter 2, 45–78, Elsevier.
185. Zervos, S. (2007). Evaluating treatments of paper using statistically valid test methods. Part II: experimental setup and protocol, *Restaurator*, 28(4):256–88.

186. Zervos S. (2010). Natural and accelerated ageing of cellulose and paper: a literature review. In: Lejeune A, Deprez T, editors. Cellulose structure and properties, derivatives and industrial uses. Happaugue NY: Nova Science Publishers; p. 155–203.
187. Zervos, S. and Moropoulou, A. (2005). Cotton cellulose ageing in sealed vessels. Kinetic model of autocatalytic depolymerization. *Cellulose*. Springer Netherlands, Vol. 12, pp. 485-496.
188. Zou, X., Uesaka, T. and Gurnagul, N. (1996). Prediction of paper permanence by accelerated aging, Part I: Kinetic analysis of the aging process. *Cellulose*, Vol. 3, pp. 243-267, doi:10.1007/BF02228805.
189. Zou, X., Uesaka, T. and Gurnagul, N. (1996). Prediction of Paper Permanence by Accelerated Aging, Part II: Comparison of the Predictions with Natural Aging Results, *Cellulose*, Issue 3, pp. 269-279.

APPENDICES

Appendix I: Islamic Paper Reference Collection: Calibration Target / ISH Collection

The Islamic paper calibration target is devised of 105 out of 228 Islamic paper samples from the well-characterized reference database collected by visual and scientific examination. The samples are part of the UCL Institute for Sustainable Heritage (UCL-ISH) historic reference material collection, which were gathered from different sources in central Asia, Near East and North Africa mainly in the period from 15th to 19th century for material analysis purpose. The table below shows the properties of the selected samples as described below. Also the below figure demonstrates the distribution of the samples across the calibration target.



11	10	9	8	7	6	5	4	3	2	1	
56-3	55	45-3	42	36	26	6	5	3	56-1	45-2	1
131	125-1	121	114	108	97	91	85	84	83	74	2
43	18	10	9	8	29-2	127-2	133-2	17	44	125-2	3
126	116	115-1	113	107	100	98	72-4	69	49	29-1	4
2	129-2	129-1	16-1	25	35	37	115-3	133-1	128	127-1	5
109	38	39	40	41	47	48	63	65	75-T1	76	6
34	33	89	110	111	117	118	123	124	130	120	7
75-1	27-1	72-2	101	96	82-1	73-2	53	57	50	46	8
95	72-1	62-1	52	31	30-1	28-2	23	11-1	4	62-2	9
					72-3	24	132	106	104	103	10
											11

*Yellow cells represent the samples containing starch

*Grey cells are empty cells with no samples

Description of the table heads and list of abbreviations:

Y/N: Yes or No answer.

N/A: Not Applicable or Not Available.

DP: Degree of Polymerization.

WM: Watermark.

Thick: Thickness.

S: Sample contain starch.

P: Polished surface.

Provenance: Date (AD) and origin provided for each sample from the source.

Paper Type: The type of each paper according to the mould construction used in the production with information about the laid and chain lines spacing and grouping if exist and whether the paper is machine paper (M) or hand-made (H).

ID (AP#)	Size (mm)	Thick (mm)	WM	Paper Type	Text	Provenance	S	P	pH	DP
2	169X113	0.12	Y	Laid with chain lines , (H)	Arabic	1750 / 18th C.	N	Y	N/A	N/A
3	212X132	0.14	N	Laid with no chain lines, (H)	Arabic	N/A	Y	Y	6.1	627
4	143X225	0.14	N	Laid with no chain lines, (M)	Arabic	N/A	Y	N	6.6	591
5	275X182	0.14	N	Laid with chain lines, (H)	Arabic	N/A	Y	Y	7.2	667
6	149X106	0.12	Y	Laid with chain lines , (H)	Arabic	1750 / 18th C.	Y	Y	6.6	1152
8	195X144	0.12	N	Wove, (M)	Arabic	18-19th C., Middle East	N	N	N/A	N/A
9	189X117	0.13	N	Wove, (M)	Arabic	18 -19th C., Middle East	N	N	5.2	N/A
10	177X113	0.14	N	Wove, (M)	Arabic	18-19th C., Middle East	N	N	N/A	N/A
11-1	188X115 (236)	0.13	N	Wove, (M)	Arabic	18 -19th C., Middle East	Y	N	6.2	N/A
16-1	214X156	0.17	Y	Laid with chain lines , (H)	Arabic	18th C., Middle East	N	Y	6.9	N/A
17	169X106 (212)	0.13	Y	Laid with chain lines , (M)	Arabic	Middle East	Y*	Y	6.1	N/A
18	224X164	0.14	N	Laid with chain lines , (H)	Arabic	18th C., Middle East	N	N	7.2	1278
23	119X200	0.12	N	Laid with no chain lines, (H)	Arabic	N/A	Y	N	6.7	802
24	115X200	0.15	N	Laid with no chain lines, (H)	Arabic	N/A	Y	N	N/A	N/A
25	113X169	0.12	Y	Laid with chain lines , (H)	Arabic	N/A	N	Y	7.2	1105
26	118X192	0.13	N	Laid with no chain lines, (H)	Arabic	N/A	Y	Y	6.7	642
27-1	116X89 (177)	0.1	N	Wire-mesh, (M)	Arabic	Ethiopia / Harar	Y*	N	N/A	N/A
28-2	172X120 (237)	0.16	N	Laid with no chain lines, (H)	Not Arabic	N/A	Y	N	6.6	605
29-1	126X97 (195)	0.16	N	Laid with no chain lines, (H)	Not Arabic	N/A	N	N	7.3	723
29-2	130X97 (199)	0.15	N	Laid with no chain lines, (H)	Not Arabic	N/A	N	N	N/A	N/A
30-1	237X133 (265)	0.13	N	Laid with no chain lines, (H)	Arabic	N/A	Y	N	6.6	610
31	227X150	0.14	N	Wove, (M)	Not Arabic	N/A	Y	N	6.4	475
33	168X234	0.19	N	Laid with chain lines , (H)	Arabic	around 150 years old / 19th C., Middle East	N	Y	N/A	N/A
34	170X246	0.20	Y	Laid with chain lines , (H)	Arabic	1850 / 19th C., Middle East	N	Y	N/A	N/A
35	302X215	0.18	Y	Laid with chain lines , (H)	Arabic	around 200 years old / 18-19th C. (safavids era), Middle East / Persia	N	Y	7.2	1806
36	258X151	0.13	N	Laid with no chain lines + Zigzag, (H)	Arabic	>500 years / 15-16th C. (Mamluk era), Middle East	Y	Y	7.0	708
37	213X170	0.17	N	Laid with chain lines + Zigzag, (H)	Arabic	1792 / 18th C., Middle East / Kashmir (North India)	N	Y	6.6	891
38	162X212	0.21	N	Laid with chain lines (unclear) + Zigzag, (H)	Arabic	1792 / 18th C., Middle East / Kashmir (North India)	N	Y	N/A	N/A
39	168X234	0.24	Y	Laid with chain lines , (H)	Coptic & Arabic	around 250 years old / 18th C., Middle East / Egypt	N	Y	7.3	1576
40	147X197	0.15	N	Laid with chain lines , (H)	Arabic	1821 / 19th C., Middle East	N	Y	N/A	N/A
41	236X190	0.17	Y	Laid with chain lines , (H)	Arabic	around 200 years old / 18-19th C., Middle East (Maghreb)	N	Y	N/A	N/A

42	229X172	0.15	N	Wove, (M)	Arabic	1789 / 18th C., Middle East / Dagestan	Y	Y	N/A	N/A
43	115X120	0.13	N	Wire-mesh, (M)	Arabic	1868 / 19th C., Middle East / N.Africa (Maghreb)	N	N	6.2	405
44	200X289	0.23	Y	Laid with chain lines , (H)	Arabic	1713 / 18th C., Middle East	Y**	Y	6.8	1384
45-2	152X229	0.12	N	Laid with no chain lines, (H)	Arabic	1716 / 18th C., Middle East	Y	Y	N/A	N/A
45-3	161X234	0.13	N	Laid with no chain lines, (H)	Arabic	1716 / 18th C., Middle East	Y	Y	6.5	773
46	183X292	0.21	N	Laid with chain lines , (H)	Arabic	1615 / 17th C., Middle East	N	Y	N/A	N/A
47	210X302	0.19	N	Laid with chain lines , (H)	Arabic	1717 / 18th C., Middle East	N	Y	6.9	1449
48	157X230	0.12	Y	Laid with chain lines , (H)	Arabic	Middle East	N	Y	7.2	1391
49	181X234	0.15	N	Laid with chain lines , (M)	Arabic	around 80 years old / 20th C., Middle East	N	N	5.6	463
50	115X176	0.13	N	Laid with chain lines , (H)	Not Arabic	1870 / 19th C., Middle East	N	Y	N/A	N/A
52	164X218	0.18	N	Wire-mesh, (M)	Arabic	1849 / 19th C., Middle East / N.Africa (Maghreb)	Y	N	5.8	205
53	134X190	0.16	Y	Laid with chain lines , (H)	Arabic	around 200 years old / 18- 19th C., Middle East	N	Y	N/A	N/A
55	227X154 (311)	0.14	N	Wove, (M)	Arabic	18 -19th C., Middle East	Y	Y	6.4	681
56-1	191X118 (234)	0.11	N	Wire-mesh, (M)	Arabic	18-19th C., Middle East	Y	Y	N/A	N/A
56-3	195X121 (243)	0.11	N	Wove, (M)	Arabic	18 -19th C., Middle East	Y	Y	6.6	867
57	227X154 (311)	0.14	N	Wove, (M)	Arabic	18 -19th C., Middle East	Y	Y	6.4	681
62-1	191X118 (234)	0.11	N	Wire-mesh, (M)	Arabic	18-19th C., Middle East	Y	Y	N/A	N/A
62-2	119X185	0.13	N	Wire-mesh, (M)	Arabic	Middle East	Y	N	N/A	N/A
63	158X218	0.18	Y	Laid with chain lines , (H)	Arabic	Middle East	N	Y	7.0	461
65	152X213	0.20	Y	Laid with chain lines , (M)	Arabic	Middle East	N	Y	6.9	440
69	119X166	0.21	Y	Laid with chain lines , (H)	Arabic	Middle East	N	N	N/A	N/A
72-1	188X121 (242)	0.11	N	Wove, (M)	Arabic	N/A	Y	N	5.9	503
72-2	172X125	0.13	N	Wove, (M)	Arabic	N/A	Y	N	5.9	742
72-3	98X149	0.11	N	Wire-mesh, (M)	Arabic	N/A	Y	N	5.8	512
72-4	105X177	0.09	N	Wire-mesh, (M)	Arabic	N/A	N	N	5.6	726
73-2	160X110 (222)	0.11	Y	Laid with chain lines , (H)	Arabic	N/A	N	Y	N/A	N/A
74	181X116 (232)	0.11	N	Laid with chain lines , (M)	Arabic	1876 / 19th C.	Y	Y	5.7	N/A
75-1	182X120 (260)	0.13	N	Wove, (Handmade)	Arabic	N/A	Y	N	N/A	N/A
75- Type1	181X121 (242)	0.12	Y	Laid with chain lines , (H)	Arabic	N/A	N	Y	7.3	1815
76	183X252	0.11	Y	Laid with chain lines , (H)	Arabic	N/A	N	Y	7.2	1448
82-1	139X95 (191)	0.15	Y	Laid with chain lines , (H)	Not Arabic	N/A	N	Y	N/A	N/A
83	84X166	0.17	N	Laid with no chain lines, (H)	Arabic	N/A	Y	Y	6.8	797
84	188X127	0.22	N	Wove, (M)	Not Arabic	N/A	Y	Y	7.1	896
85	115X120	0.13	N	Wire-mesh, (M)	Arabic	1868 / 19th C., Middle East / N.Africa (Maghreb)	Y	Y	5.9	498

89	133X189	0.16	Y	Laid with chain lines , (H)	Arabic	N/A	N	Y	7.0	1413
91	151X249	0.14	N	Laid with no chain lines, (H)	Arabic	More than 500 years old / 15-16th C., Mamluk era, Middle East	Y	Y	7.1	853
95	163X220	0.15	N	Wire-mesh, (Mechanical-made)	Arabic	1849 / 19th C., Middle East / N.Africa (Maghreb)	Y	N	5.8	179
96	198X286	0.14	Y	Laid with chain lines , (H)	Arabic	1692 / 17th C., Middle East	N	Y	N/A	N/A
97	198X291	0.23	Y	Laid with chain lines , (H)	Arabic	1713 /18th C., Middle East / N.Africa	Y**	Y	7.0	1588
98	116X121	0.14	N	Wove, (M)	Arabic	1868 / 19th C., Middle East / N.Africa (Maghreb)	N	N	5.8	629
100	193X137 (273)	0.12	N	Wire-mesh, (M)	Arabic	ca.100 years / 20th C., Middle East	N	N	4.8	N/A
101	109X157	0.17	Y	Laid with chain lines , (H)	Not Arabic	1848 / 19th C., Middle East / Syriac	N	Y	N/A	N/A
103	66X152	0.13	N	Wove, (M)	Not Arabic	1850 / 19th C., Middle East	Y	N	N/A	N/A
104	109X110	0.11	N	Wire-mesh, (M)	Not Arabic	N/A	Y	N	N/A	N/A
106	112X117	0.13	N	Wire-mesh, (M)	Arabic	1868 / 19th C., Middle East / N.Africa (Maghreb)	Y*	N	5.4	504
107	120X81	0.14	N	Laid with chain lines , (M)	Arabic	1843 / 19th C., Middle East	N	N	5.0	244
108	83X119	0.10	N	Laid with no chain lines, (H)	Arabic	Before 1516 / 15-16th C., Mamluk era, Middle East	Y	Y	N/A	N/A
109	119X173	0.10	Y	Laid with chain lines , (H)	Arabic	1845 / 19th C., Middle East	N	Y	N/A	N/A
110	119X172	0.09	Y	Laid with chain lines , (H)	Arabic	1845 / 19th C., Middle East	N	Y	7.2	1111
111	110X172	0.09	N	Wire-mesh, (Handmade)	Arabic	around 1600/ 16-17th C., Middle East	N	Y	4.9	N/A
113	207X86	0.12	N	Wire-mesh, (M)	Not Arabic	around 150 years old / 19th C., Asian / Eastern Turk (kazakhstan and uzbeistan)	N	N	5.7	490
114	120X249	0.11	N	Laid with chain lines , (H)	Arabic	1799 / 18th C., Ottoman era, Middle East	Y	Y	6.6	309
115-1	187X119 (223)	0.11	N	Laid with chain lines , (M)	Arabic	1850 / 19th C., Middle East	N	N	5.2	N/A
115-3	187X120 (242)	0.11	N	Laid with chain lines and a wire-mesh base, (M)	Arabic	1850 / 19th C., Middle East	N	N	N/A	N/A
116	207X153 (306)	0.16	Y	Laid with chain lines , (H)	Arabic	1850 / 19th C., Middle East	N	N	6.9	1137
117	155X227	0.12	Y	Laid with chain lines , (H)	Arabic	around 300 years old, (seal) 1788 / 18th C., Ottoman era, Middle East / Egypt	N	Y	5.6	643
118	168X227	0.14	Y	Laid with chain lines , (H)	Arabic	1806 / 19th C., Ottoman era, Middle East	N	Y	6.5	750
120	152X218	0.16	N	Laid with chain lines , (H)	Arabic	1397(maybe) / 14th C., Middle East	N	Y	N/A	N/A
121	210X169	0.18	N	Laid with chain lines , (H)	Arabic	N/A	Y	Y	N/A	N/A

123	210X169	0.18	N	Laid with chain lines , (H)	Arabic	N/A	Y	Y	N/A	N/A
124	195X272	0.22	Y	Laid with chain lines , (H)	Arabic	1850 / 19th C., Middle East / N.Africa (Maghreb)	N	Y	6.7	1538
125-1	124X199	0.09	N	Wire-mesh, (H)	Arabic	N/A	Y	Y	4.6	300
125-2	120X199	0.10	N	Wire-mesh, (H)	Arabic	N/A	Y	Y	N/A	N/A
126	235X171 (343)	0.13	Y	Laid with chain lines , (H)	Arabic	1850 / 19th C., Middle East	N	N	5.7	N/A
127-1	231X164 (328)	0.18	Y	Laid with chain lines , (H)	Arabic	1850 / 19th C., Middle East	N	N	7.5	1305
127-2	230X163 (328)	0.17	Y	Laid with chain lines , (H)	Arabic	1850 / 19th C., Middle East	N	N	N/A	N/A
128	315X154	0.12	N	Wire-mesh, (M)	Arabic	1850 / 19th C. , Middle East	N	N	5.6	691
129-1	160X222	0.10	N	Laid with chain lines , (H)	Arabic	N/A	N	Y	N/A	N/A
129-2	160X222 (320)	0.13	Y	Laid with chain lines , (H)	Arabic	N/A	N	Y	N/A	N/A
130	284X209	0.13	Y	Laid with chain lines , (H)	Not Arabic	1763 / 18th C., Middle East	N	Y	7.0	1259
131	246X421	0.13	N	Laid with no chain lines, (H)	Not Arabic	17th C. (Safavids era), Middle East / Persia (Iran)	Y	Y	6.4	919
132	240X340	0.13	N	Wire-mesh, (M)	Turkish	N/A	Y*	N	5.7	N/A
133-1	180X116 (235)	0.10	N	Wire-mesh, (H)	Arabic	N/A	N	N	N/A	N/A
133-2	179X120 (238)	0.10	N	Wove, (M)	Arabic	N/A	N	N	5.8	N/A

* Result of starch test was dotted

** starch found in the paste only

Appendix II: Painting Canvases Reference Collection: Calibration Target

Canvas Calibration target with 72 well-characterized samples of historical painting canvases (16th – 20th C.) from UCL-ISH collection. The table is showing the ID of the samples as sorted in the figure.



141	96	80	58	57	49	43	30	22-1	13-2	6
119	94	72-3	59	56-2	48	41	29-O	21	10-3	5-2
118	92	72-2	60	56-1	47	37	28	19	10-2	4-2
100-1	91	75	65	55	46	36-3	27	17	10-1	4-1
	90	73-O	69	54	45	36-2	25	15-2	8-1	3-2
	89	71	70-1	53	44	35	24	15-1	7-1	3-1
	85-1	70-2		52		32	22-2	13-1		2-2
	83									

The below table is showing the properties of the Canvas Calibration target samples; ID, fibre type, source and date in addition to their current measured pH and DP.

ID	pH	DP	Fibres	Date	Source*
2-2	4.7	874	-	1900	MNAC
3-1	5.1	775	Linen & Hemp	1875	MNAC
3-2	5.5	918	Linen & Hemp	1875	MNAC
4-1	5.0	557	Linen	1900	MNAC
4-2	4.9	417	Linen	1900	MNAC
5-2	5.9	963	Linen?	1875	MNAC
6	5.5	1446	-	1925	MNAC
7-1	5.9	1321	Hemp	1925	MNAC
8-1	6.1	891	Linen	1875	MNAC
10-1	5.9	1590	Linen	1875	MNAC
10-2	5.1	1456	Linen	1875	MNAC
10-3	5.7	1466	Linen	1875	MNAC
13-1	5.9	975	Linen	1875	MNAC
13-2	4.9	698	Linen	1875	MNAC
15-1	5.1	741	Ramie?	1925	MNAC
15-2	5.0	1008	Ramie?	1925	MNAC
17	4.8	652	Linen? Hemp?	1925	MNAC

19	5.0	948	Linen	1925	MNAC
21	5.4	1090	Jute	1925	MNAC
22-1	5.3	2294	Ramie?	1925	MNAC
22-2	6.0	1589	Ramie?	1925	MNAC
24	5.3	699	Linen	1875	MNAC
25	4.9	1010	linen? Ramie?	1900	MNAC
27	4.9	1174	Linen	1875	MNAC
28	5.6	1119	Linen & hemp	1875	MNAC
29-O	4.7	415	-	1650	MNAC
30	6.9	942	Linen?	1850	MNAC
32	6.5	436	Linen	1900	MNAC
35	5.2	1149	Linen	1850	MNAC
36-2	5.7	897	Linen	1900	MNAC
36-3	5.6	728	Linen	1900	MNAC
37	5.5	2135	Linen	1925	MNAC
41	5.8	901	Linen & Cotton	1925	MNAC
43	5.7	985	Cotton	1875	MNAC
44	5.3	1174	Linen	1925	MNAC
45	4.8	457	Cotton	1850	MNAC
46	4.8	898	Linen	1875	MNAC
47	5.8	1027	Linen	1875	MNAC
48	4.7	535	Jute	1925	MNAC
49	5.7	766	Linen	1925	MNAC
52	5.0	845	Cotton	1925	UB
53	5.0	663	Cotton	1925	UB
54	5.3	1981	Linen?	1925	UB
55	6.2	859	Cotton	1925	UB
56-1	5.6	1067	Cotton	1975	UB
56-2	5.2	969	Cotton	1975	UB
57	6.1	784	Cotton	1975	UB
58	6.3	1172	Cotton	1975	UB
59	5.3	1067	Cotton	1975	UB
60	4.8	1095	Jute	1975	UB
65	5.1	2333	Linen	1975	UB
69	5.9	577	-	1925	UB
70-1	4.7	426	Linen	1650	UB
70-2	5.5	809	Linen	1650	UB
71	4.9	614	-	1750	UB
73-O	5.4	608	Linen?	1875	UB
75	4.7	805	-	1975	UB
77-2	6.5	1136	Mostly linen (with a few hemp)	1875	CRBMC
77-3	5.0	736	Mostly linen (with a few hemp)	1875	CRBMC
80	6.6	1687	-	1700	CRBMC
83	5.2	1345	-	1925	MNAC
85-1	5.1	1936	Linen	1925	MNAC
89	5.0	942	Linen	1925	MNAC
90	5.4	1357	Cotton	1925	MNAC

91	5.3	1655	Linen	1925	MNAC
92	4.8	749	Cotton	1975	MNAC
94	7.4	1512	Linen & hemp	1550	Private Owner
96	5.5	1711	Linen	1875	Private Owner
100-1	6.0	799	Linen?	1650	Private Owner
118	4.8	1303	Cotton	1925	Private Owner
119	5.8	837	-	1750	Private Owner
141	5.0	760	Linen	1875	MMB

*

MNAC : Museu Nacional d'Art de Catalunya (Barcelona)

CRBMC : Restoration Center for Movable Property of Catalonia (Centre de Restauració de Béns M obles de Catalunya).

MMB : Maritime Museum of Barcelona (Museu Marítim de Barcelona).

UB: Collection of the Faculty of Fine Arts, University of Barcelona (Col.lecció de la Facultat de Belles Arts).

Appendix III: HSI Penetration Experiment

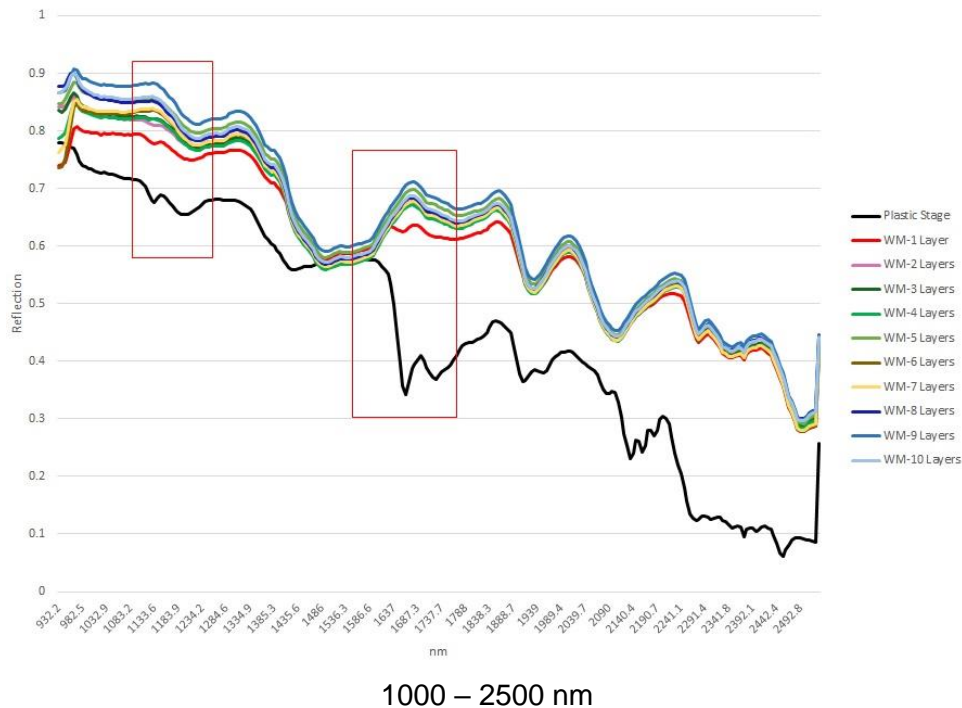
The aim of this experiment is to explore how many Whatman No. 1 filter paper sheets/layers (Maidstone) are required to be used as background for the materials while scanning with HSI system in the SWIR region. Different layers of Whatman sheets were scanned (adding one layer/sheet per scan, up to 10 sheets) in addition to a scan for the plastic stage of HSI without any sheets.

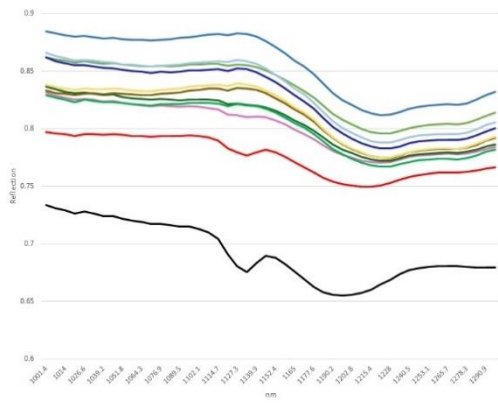
Scanning Parameters:

Exposure	5.5 ms	Lens	30 mm
Gain	1	Scan Speed	54.83 fps
Saturation Level	10% – 90%	Light	500 Watt

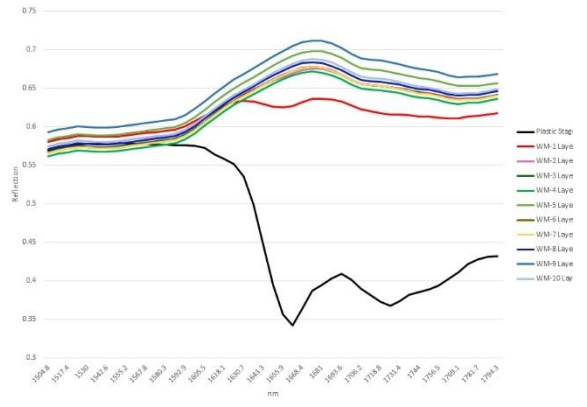
Results:

The below figures are showing an average spectrum per each scan to represent the different number of Whatman sheets used. As seen, the spectra reflect the penetration level by showing the characteristics of the plastic stage within the spectra of Whatman sheets. The first figure demonstrates the full range from 1000 – 2500 nm following by two close-up figures on two areas; 1000 – 1300 nm and 1500 – 1800 nm. The characteristics are fading with the increment of number of the sheets. After approx. two sheets there is no influence from the stage.





1000 – 1300 nm



1500 – 1800 nm

Appendix IV: UCL-ISH Painting Canvases Collection (10 Oil Paintings)

ID	Front and Back sides	Date	pH	DP	Fibres	Dimensions (cm)
P1		1908	4.9	1229	Linen	37 x 27
P2		Pre-1900	6.0	3289	Linen	76 x 52
P3		-	4.9	1207	Linen	50 x 37.7
P4		1950–1969	6.4	1834	Cotton	93 x 65

						
P5	 	1841	4.5	888	<i>Linen</i>	55 x 34.7
P6	 	1885	5.0	1032	<i>Linen</i>	35.6 x 45.7
P7		1900–1949	5.4	1397	<i>Linen</i>	46 x 34.9

						
P8		1909	4.9	899	Linen	37 x 25.4
						
P9		1900–1949	5.8	3826	Linen	28.7 x 36
						
P10		1900–1949	4.7	1166	Cotton (Probably mercerized)	38 x 25.4
						